Characterization of the Phase Behavior of CO_2 Containing Nonionic Surfactants

vorgelegt von

M. Sc.

Vivian Jeannette Spiering

an der Fakultät II - Mathematik und Naturwissenschaften

der Technischen Universität Berlin

zur Erlangung des akademischen Grades

Doktor der Naturwissenschaften

Dr. rer. nat.

genehmigte Dissertation

Promotionsausschuss

Vorsitzender:	Prof. Dr. Peter Strasser (Technische Universität Berlin)
1. Gutachter:	Prof. Dr. Michael Gradzielski (Technische Universität Berlin)
2. Gutachter:	Prof. Dr. Werner Kunz (Universität Regensburg)

Tag der wissenschaftlichen Aussprache: 23. November 2020

Berlin 2021

Diese Arbeit widme ich meinen Eltern, die immer an mich glauben und mich unterstützen!

Acknowledgments

Ich möchte nun diese Zeilen nutzen, um meinen Dank auszusprechen. An erster Stelle möchte ich mich bei meinem Doktorvater Prof. Dr. Michael Gradzielski für die Ausgabe des Themas und für die Betreuung während dieser Doktorarbeit bedanken. Die Bearbeitung des Themas hat mir außerordentlich Spaß gemacht und mir gezeigt wieviel Freude es mir bereitet an einem anwendungsnahen, nachhaltigen Thema zu arbeiten. Ich möchte mich auch dafür bedanken, dass stets ein großer Arbeitsfreiraum gefördert wurde, wodurch es mir möglich war eigene Ideen und Konzepte zu entwickeln und zu verfolgen, wobei ich stets auf Unterstützung und Rat zählen konnte. Ich möchte mich auch bei Prof. Dr. Werner Kunz für die Übernahme des Zweitgutachters meiner Doktorarbeit bedanken.

An dieser Stelle möchte ich mich auch bei dem BMBF für die Förderung des Projektes "Dream Resource" bedanken. Natürlich gilt mein Dank auch der Covestro Deutschland AG für die Projektleitung und für die Herstellung der Tenside. Einen Besonderen dank gilt dabei den Projektleitern Annika Stute, Michael Weinkraut und Marina Sebastian. Es war immer eine große Freude sich auf dem Projekttreffen auszutauschen und so das Projekt bestmöglich und erfolgreich voranzubringen. Ich möchte mich auch bei dem DAAD für die Finanzierung meiner Forschungsaufenthalte in Prag/Tschechien an der Charles University und in Fukuoka/Japan an der Kyushu University bedanken. Ich möchte mich auch noch einmal besonders bei Prof. Dr. Hiroki Matsubara bedanken, für die außerordentliche Gastfreundschaft, die mir in Japan entgegengebracht wurde.

Außerdem einen riesigen Dank an das gesamte Stranski-Team, welches stets für eine Wohlfühlatmosphäre im Pausenraum sorgte und durch einen angeregten kollegialen Austausch, einem mit Rat und Tat zur Seite standen und unterstützten. Diese Atmosphäre führte zu einer ausgezeichneten Arbeitsgrundlage während dieser Doktorarbeit. Ein besonderer Dank geht dabei an meine Bürokolleginnen Sarah Schatte, Kathrin Siegl und Rahel Marschall und auch an Albert Prause und den Rest des Arbeitskreises. Danke, dass ihr da seid und mir allerlei Fragen beantwortet habt und mich in vielerlei Dingen unterstützt habt. Vielen Dank Sarah, Rahel, Albert, Sebastian für das Korrekturlesen meiner Arbeit. Albert, vielen Dank für das Formfaktor Modell und deine Unterstützung bei vielen kleinen Fragen und Problemen. Einfach danke für eure Unterstützung und danke für eure Freundschaft. Ein besonderer Dank geht auch an Jana Lutzki für die Unterstützung bei den ITC Messungen und bei den vielen kleinen Fragen und Messungen. Ich möchte mich auch bei meiner studentischen Hilfskraft und bei meinen Masterstudentinnen

bedanken. Vielen Dank Rahel, Björn und Aurora, vielen Dank für eure Unterstützung. Es hat sehr viel Spaß gemacht mit euch zu arbeiten.

Zuletzt möchte ich mich an dieser Stelle bei meiner Familie und Freunden bedanken, die mich in dieser Zeit der Doktorarbeit unterstützt haben und ohne deren Rückhalt ich nicht so weit gekommen wäre. Meinen Eltern verdanke ich es mir während des Studiums den Rücken freigehalten zu haben und mir somit den Weg geebnet haben, den ich eingeschlagen habe. Meinen Freunden danke ich für ihre Bereicherung in vielerlei Hinsicht und ihrer Unterstützung.

Abstract

Carbon dioxide (CO_2) is one of the most abundant greenhouse gases in the earth´s atmosphere and a waste product from all combustion processes. Therefore, one can use CO_2 as a raw material to produce CO_2-based nonionic surfactants, which are a sustainable alternative to conventional fossil-based nonionic surfactants. The aim of this work is to gain a comprehensive picture of the influence of the CO_2 moiety on the physico-chemical properties. Accordingly, we characterized the phase behavior of the CO_2 containing nonionic surfactants to obtain a comprehensive picture of their physical-chemical properties and their application potential.

In this work, we studied the influence of the incorporated CO_2 moiety in the hydrophilic head group on the micellization behavior. For that purpose, we analyzed the surface activity and the influence on the thermodynamic parameters of micellization in terms of CO_2 content and temperature. Based on a thorough investigation we observed that the incorporation of CO_2 units renders the surfactants somewhat more efficient and effective by a reduced cmc and surface tension. Moreover, the analysis of the thermodynamic parameters of micellization provides information about a reduced hydration affinity, due to CO_2 incorporation.

The phase behavior at the low and high concentration regime and the temperature effects were studied by light and neutron scattering and rheology measurements. The detailed structural characterization was provided by a model of the small-angle scattering data. By this interpretation, a comprehensive picture of the formed micellar aggregates could be drawn. It could be shown, that ellipsoidal core-shell micelles are formed, which are slightly increasing with increasing CO_2 content, thereby reducing the water content in the hydrophilic head group. This study also shows that the formation of liquid crystalline phases at high concentrations is suppressed by the incorporation of CO_2 moieties. Even the incorporation of one CO_2 group leads to a disappearance of gel-like liquid-crystalline phases. Scattering experiments show that the origin of this constant behavior is controlled dehydration of the head groups and reduced repulsive interaction between the head groups. This results in an interpenetration of the aggregates, which allows Newtonian flow behavior. This means that the incorporation of CO_2 units results in an adjusted phase behavior rendering the CO_2 content as a further tuning- parameter to obtain desired properties for a variety of applications.

Additionally, the potential application as solubilizers of hydrophobic active ingredients was investigated. From these studies, the factor of solubility enhancement was obtained. This indicates comparable results for all surfactants, and the CO_2 incorporation leads to a slight decrease of solubilization. However, it can be stated that the CO_2 surfactants show comparable results, and

combined with better biodegradability, the CO_2 surfactants are a suitable alternative to conventional nonionic surfactants for hydrophobic compound solubilization. Finally, the adsorption at the oil/water interface was investigated to analyze the influence of the CO_2 moiety on the adsorption properties. These findings are quite interesting because the incorporation of a CO_2 unit renders the adsorption at the oil/water interface less favored. These results are relevant for a better understanding for further investigations such as emulsion and microemulsion formation.

This thesis provides a thorough understanding of the physico-chemical properties of the CO_2 surfactants. These fundamental studies are an interesting example where an understanding of the phase behavior and structural behavior of a surfactant system enables a systematic understanding based on the molecular architecture. The incorporation of CO_2 enables the ability to tune the properties in terms of the CO_2 content which indicates a further tuning parameter. Thereby, one can achieve desired properties that would not be easily achievable for conventional nonionic EO surfactants without the addition of additives. These CO_2-containing surfactants contribute to the goal of more sustainable chemistry, as the fossil-based EO units are replaced by CO_2 (up to 20%). For all these reasons, it is to be expected that CO_2-containing nonionic surfactants will become a promising alternative to the surfactant market.

Zusammenfassung

Kohlenstoffdioxid (CO_2) ist eines der am häufigsten vorkommenden Treibhausgase in der Erdatmosphäre und ein Abfallprodukt aus allen Verbrennungsprozessen. CO_2 besitzt das Potenzial als alternatives Kohlenstoff Rohmaterial zu fungieren. Daher kann man CO_2 als Rohstoff zur Herstellung von CO_2 basierten nichtionischen Tensiden verwenden, die eine nachhaltige Alternative zu herkömmlichen nichtionischen Tensiden auf fossiler Basis darstellen. Ziel dieser Arbeit ist es, ein umfassendes Bild des Einflusses der CO_2 Einheit auf die physikalisch-chemischen Eigenschaften zu erhalten. Dementsprechend haben wir das Phasenverhalten der CO_2 enthaltenden nichtionischen Tenside charakterisiert, um ein umfassendes Bild über ihre physikalisch-chemischen Eigenschaften und ihr Anwendungspotential zu erhalten.

In dieser Arbeit untersuchten wir den Einfluss der eingebauten Einheit in der hydrophilen Kopfgruppe auf das Mizellisierungsverhalten. Dazu analysierten wir die Oberflächenaktivität und den Einfluss auf die thermodynamischen Parameter der Mizellbildung in Bezug auf den CO_2 Gehalt und Temperatur. Basierend auf diesen gründlichen Untersuchungen hat sich herausgestellt, dass der Einbau von CO_2 Einheiten die Tenside durch eine verringerte cmc- und Oberflächenspannung etwas effizienter und effektiver macht. Darüber hinaus liefert die Analyse der thermodynamischen Parameter der Mizellisierung Informationen über eine verringerte Hydratationsaffinität aufgrund des Einbaus von CO_2.

Das Phasenverhalten im niedrigen und hohen Konzentrationsbereich und die Temperatureffekte wurden durch Licht- und Neutronenstreuungs und Rheologiemessungen untersucht. Die detaillierte strukturelle Charakterisierung wurde durch ein Modell der Kleinwinkeldaten beschrieben. Durch diese Interpretation konnte ein umfassendes Bild der gebildeten Mizellenaggregate gezeichnet werden. Es konnte gezeigt werden, dass ellipsoidale Kernschalemizellen gebildet werden, die mit zunehmendem CO_2 Gehalt größer werden, dabei verringert sich der Wassergehalt in der hydrophilen Kopfgruppe. Diese Arbeit zeigt auch, dass die Bildung flüssigkristalliner Phasen bei hohen Konzentrationen durch den Einbau von CO_2 unterdrückt werden kann. Selbst der Einbau einer einzigen Gruppe unterdrückt schon die Bildung gelartiger flüssigkristalliner Phasen. Streuexperimente zeigen, dass der Ursprung dieses Verhaltens eine kontrollierte Dehydratisierung der Kopfgruppen und eine verringerte abstoßende Wechselwirkung zwischen den Kopfgruppen ist. Dies führt zu einer gegenseitigen Durchdringung der Aggregate, was ein Newtonsches Fließverhalten ermöglicht. Dies bedeutet, dass der Einbau von CO_2 Einheiten zu einem veränderten Phasenverhalten führt, wobei der CO_2 Gehalt als weiterer “tuning parameter”

eingebaut werden kann, wodurch gewünschte Eigenschaften für eine Vielzahl von Anwendungen erreicht werden können.

Zusätzlich wurde die mögliche Anwendung als Lösungsvermittler von hydrophoben Wirkstoffen untersucht. Aus diesen Studien wurde die Löslichkeitsverbesserung ermittelt. Hier zeigten sich vergleichbare Ergebnisse für alle Tenside, wobei der Einbau von CO_2 zu einer leichten Abnahme der Solubilisierung führt. Es kann jedoch festgestellt werden, dass die Tenside vergleichbare Ergebnisse zeigen und in Kombination mit einer besseren biologischen Abbaubarkeit, stellen diese Tenside eine geeignete Alternative zu herkömmlichen nichtionischen Tensiden für die Solubilisierung hydrophober Verbindungen dar. Schließlich wurde die Adsorption an der Öl/Wasser-Grenzfläche untersucht, um den Einfluss der Einheit auf die Adsorptionseigenschaften zu analysieren. Diese Ergebnisse sind sehr interessant, da der Einbau einer CO_2 Einheit die Adsorption an der Öl/Wasser-Grenzfläche weniger begünstigt. Diese Ergebnisse liefern somit eine basis für ein besseres Verständnis für weitere Untersuchungen zum Emulsions- und Mikroemulsionsverhalten.

Diese Arbeit liefert ein gründliches Verständnis der physikalisch-chemischen Eigenschaften der CO_2 haltigen nichtionischen Tenside. Diese grundlegenden Studien sind ein interessantes Beispiel, bei dem ein Verständnis des Phasenverhaltens und des Strukturverhaltens eines Tensidsystems ein systematisches Verständnis auf der Grundlage der molekularen Architektur ermöglicht. Die Einbeziehung von CO_2 ermöglicht die Einstellung der Eigenschaften in Bezug auf den CO_2-Gehalt, als einen weiteren “tuning parameter”. Dadurch kann man gewünschte Eigenschaften erzielen, die für herkömmliche nichtionische EO-Tenside ohne Zusatz von Additiven nicht leicht erreichbar wären. Diese CO_2-haltigen Tenside tragen zum Ziel einer nachhaltigeren Chemie bei, da die fossilen EO-Einheiten durch CO_2 (bis zu 20%) ersetzt werden. Aus all diesen Gründen ist zu erwarten, dass CO_2-haltige nichtionische Tenside eine vielversprechende Alternative für den Tensidmarkt werden.

Publications

Main parts of this dissertation have been or will be published in:

◊ Patent: A. M. I. Stute, M. Meuresch, C. Gürtler, A. Wolf, R. Schomäcker, M. Gradzielski, M. Tupinamba Lima, *V. J. Spiering* (Covestro AG, Leverkusen, Germany), *WO2019076862*, **2018**.

◊ M. Tupinamba Lima, *V. J. Spiering*, S. N. Kurt-Zerdeli, D. Ch. Brüggemann, M. Gradzielski, R. Schomäcker: "The hydrophilic-lipophilic balance of carboxylate and carbonate modified nonionic surfactants", *Colloids and Surfaces A: Physicochemical and Engineering Aspects*, **2019**, *569*, 156-163, DOI https://doi.org/10.1016/j.colsurfa.2019.03.001.

◊ *V. J. Spiering*, A. Ciapetti, M. Tupinamba Lima, D. W. Hayward, L. Noirez, M.-S. Appavou, R. Schomäcker, M. Gradzielski: "Changes in Phase Behavior from the Substitution of Ethylene Oxide with Carbon Dioxide in the Head Group of Nonionic Surfactants", *ChemSusChem*, **2020**, *13*, 601-607, DOI https://doi.org/10.1002/cssc.201902855.

◊ M. Tupinamba Lima, S. N. Kurt-Zerdeli, D. Ch. Brüggemann, *V. J. Spiering*, M. Gradzielski, R. Schomäcker: "The dynamics of surface adsorption and foam formation of carbonate modified nonionic surfactants": *Colloids and Surfaces A: Physicochemical and Engineering Aspects*, **2020**, *588*, 124386, DOI https://doi.org/10.1016/j.colsurfa.2019.124386.

◊ *V. J. Spiering*, J. Lutzki, M. Gradzielski: "Thermodynamics of Micellization of Nonionic Surfactants – The Effect of Incorporating CO_2 Moieties into the Head Group", *Journal of Colloid and Interface Science*, **2020**, *581*, 794-805, DOI https://doi.org/10.1016/j.jcis.2020.07.141.

◊ *V. J. Spiering*, A. Prause, L. Noirez, M.-S. Appavou, M. Gradzielski: "Structural Characterization of Nonionic Surfactant Micelles with CO_2/EO Head Groups and their Temperature Dependence", *Langmuir*, **2021**, DOI https://doi.org/10.1021/acs.langmuir.1c01737.

◊ *V. J. Spiering*, B. Hanf, M. Tupinamba Lima, L. Noirez, M.-S. Appavou, R. Schomäcker, M. Gradzielski: "Solubilization Potential of Hydrophobic Compounds by CO_2 Containing Surfactants", *Journal to come*, **in Preparation**.

◊ *V. J. Spiering*, R. Marschall, H. Matsubara, M. Gradzielski: "Temperature Dependent Adsorption Behaviour of Nonionic CO_2/EO Surfactants at the Oil/water Interface", *Journal To Come*, **in Preparation**.

Table of Content

Chapter 1

General Introduction

1.1. CO_2-based Polymers

In this introduction, a general overview of the utilization of carbon dioxide (CO_2) and the use as a chemical building block for copolymerization will be given. The use of CO_2 as a sustainable feedstock for chemical synthesis has the potential to reduce the overall environmental impact of production processes and contributes to a more sustainable chemical industry by substituting fossil-based raw materials. After water vapor, CO_2 is the second most abundant greenhouse gas in earth's atmosphere; which mainly contributes to global warming.[1] Moreover, CO_2 is a potential alternative carbon feedstock because it is a waste product from all combustion processes.[2, 3] Therefore, CO_2 is a fundamental C1 carbon building block which is inexpensive and non-toxic, which renders it as an ideal raw material for the preparation of a variety of useful organic compounds including MeOH,[4] dimethyl ether,[5] urea,[3] lactones,[6] cyclic carbonates[7] and biodegradable polymers.[8, 9]

The use of CO_2 as a feedstock for chemical synthesis has the potential to reduce the overall environmental impact of production processes, saving valuable fossil resources, and paving the way towards a circular economy.[10, 11] Due to these economic and environmental benefits, the catalytic transformation of CO_2 into value-added chemicals has attracted a lot of attention in academic and industrial research.[12, 13] Although, the true environmental benefits of CO_2 capture and utilization (CCU) will only become clear after a full life cycle assessment (LCA). LCA is used to determine the impact reductions for greenhouse gas emission and fossil resource depletion for the production by using CO_2 as feedstock. CCU has a role to play in reducing the environmental impact of copolymer synthesis, particularly with regards to global warming and fossil resource depletion.[14–16]

One very important part of CO_2 utilization is the preparation of polycarbonates, poly-(ether)carbonates and polyurethanes. Therefore, it is of major interest to use CO_2 as a viable monomer to access novel tailor-made CO_2-based polymers.[17] The copolymerization of epoxides and CO_2 was discovered by Inoue *et al.*[18] in 1969. Since then it has become an important and useful technology for the large-scale utilization of CO_2 in chemical synthesis. The development of methods to activate and use CO_2 to prepare chemicals and materials is a major task of nowadays research. The activation of CO_2, which is a highly oxidized, nonactive, and thermodynamically stable compound, renders its utilization in redox reactions difficult. The activation requires high-energy substances or catalytic reactions. The alternating copolymerization of CO_2 and

epoxides can give access to highly valuable polymeric materials such as polyurethanes and polycarbonates and therefore the research on specific catalysts and epoxides is essential for copolymer production.[19]

Polyurethane, firstly established by Otto Bayer in 1937, has become an important polymer, which is widely used in coatings, elastomers, adhesives, foams, etc.[20] Polyurethanes mainly consists of a fossil-based oligomer. Therefore, it is of major interest to substitute fossil-based materials by CO_2. From the coupling of epoxides and CO_2, polycarbonates can be synthesized which are of major interest for industrial applications.[9] Polycarbonates have outstanding properties such as strength, durability and heat resistance.[21] The properties of the resulting polymer depend on the catalyst and the epoxide used in the coupling of epoxides and CO_2. The copolymerization of propylene oxide and CO_2 were firstly homogenous catalyzed by tetraphenylporphyrin aluminum derivatives. The use of various catalysts and the influence on the synthesis is summarized by Klaus *et al.*[22] and Kember *et al.*[23].

Darensbourg *et al.* investigated the use of chromium-salen derivatives as a catalyst for the copolymerization. This catalyst was widely investigated for the selective formation of CO_2 copolymers from both alicyclic and aliphatic epoxides by systematically altering ligand structure, cocatalyst and reaction conditions.[24] They also investigated in thorough detail the utilization of CO_2 and the copolymerization with various epoxides.[21, 24–26] Another widely used catalysts for the copolymerization are double metal cyanide (DMC) catalysts, i.e. $Zn_3[M(CN)_6]_2$, where M is Fe(III) or Co(III).[23, 27] Amorphous DMC catalysts are well known for their performance in the industrial copolymerization of CO_2/epoxide resulting in versatile properties of polyether carbonates.[9] With the use of various catalysts and epoxides as monomers copolymers with divers properties can become available.[8, 23] Besides metal catalysts, Fiorani *et al.*[28] discussed in thorough detail the organo-metal conversion for CO_2 catalysis, which is a viable green alternative for CO_2 catalysis conversion. Another interesting approach is the direct polymerization of CO_2 and diols as a simple method to produce sustainable polycarbonates from various diols.[29]

From the coupling of CO_2 with epoxides, many functional materials and copolymers can be obtained. From that approach, the CO_2 utilization opens a new approach to sustainable products for many applications. CO_2 based copolymers with different functionality gain more interest over the last years. Wang *et al.*[30] demonstrates the use of CO_2 as a building block for polyurethanes with excellent mechanical properties like hydrolysis and oxidation stability. It is also possible to produce CO_2-based block polycarbonates with different functionalities and charges to construct versatile and new functional nanostructures as shown by Wang *et al.*[31] Moreover, Xu *et al.*[17] demonstrated the production of biodegradable plastics from CO_2. Besides the use of CO_2 as a sustainable feedstock, Geschwind and co-workers [32] were also reporting the synthetic approach of poly(1,2-glycerol carbonate) as degradable materials. Scharfenberg *et al.*[33] reviewed functional polycarbonates from CO_2 and are giving a detailed overview of the wide functionalities, which are giving access to different applications. Among other things, drug encapsulation by polymersomes and micelles based on polycarbonates were demonstrated. This approach highlights the advantage of the two key features of aliphatic polycarbonates which are their (bio)degradability and good biocompatibility which allows them to be used in biomedical applications.[34]

Scharfenberg *et al.*[35] also established the first example of hyperbranched polycarbonates prepared from CO_2. The polymers were synthesized within a two-step process, where firstly the

glycerol branching core was synthesized, and the polyether carbonate arms were synthesized in a second copolymerization with CO_2. The multiarm star copolymers were investigated with respect to their thermal properties, viscosity, and potential application as polyols for polyurethane synthesis.[35] Frey *et al.*[36] investigated the synthesis of diblock nonionic aliphatic polycarbonate with a hydrophilic ethylene oxide based head group and a hydrophobic propylene oxide tail which is functionalized with CO_2. Surface tension measurements show that the amphiphilic polymers are surface-active and form micelles above the critical micelle concentration, whereby small-angle neutron scattering measurements show that they are nearly spherical. The hydrophilic-lipophilic balance (HLB) value of these polycarbonates renders them suitable for oil-in-water emulsion stabilization or for applications as degradable foam-stabilizers. The German Federal Ministry of Education and Research (BMBF) has funded several projects to support the research for a "green economy". In this framework, the program CO_2Plus is founded to enhance the research on innovative ideas for the use of CO_2 as a green resource. One project within this program is "Dream Resource" which uses CO_2 as a resource for the synthesis of surfactants.[37–39]

The full potential of the utilization of CO_2 and its use as a C1 building block for polycarbonates bears enormous potential for future applications. The physical and chemical properties can be adjusted by varying the types of monomers, catalysts and synthesis conditions. Thus, a much broader scope of applications is possible. The CO_2 units provides a further tuning parameter to achieve the desired properties. Polycarbonate based on carbon dioxide and tailored epoxide building blocks constitute a resource-saving possibility for a broad variety of materials and applications that require both biodegradability and biocompatibility. They provide opportunities for example drug delivery, tissue engineering, surface coatings and are also interesting for agricultural applications due to their biodegradability.

The main subject of this work is the characterization of the phase behavior of CO_2 based surfactants which were produced by the company Covestro Deutschland AG within the BMBF project "Dream Resource".[40] Therefore, in the next section a general overview about the properties and the phase behavior of surfactants will be given to obtain a fundamental understanding.

1.2. Surfactants

Surfactants are surface-active organic molecules which have a amphiphilic character. The term amphiphile means that surfactants generally have an unpolar and a polar character.[41] This is derived by their structure which contains a hydrophilic head group and a hydrophobic tail. Surfactants are classified by their head group which can be anionic, cationic, nonionic and zwitterionic. The hydrophobic tail of the surfactant can be branched, linear or cyclic, usually it is an alkyl chain. Thereby the characteristic properties of the surfactant mainly depends on the kind of the head group as well the length of the tail.[42]

Surfactants can either be natural based or fossil based chemicals.[41] Nature based surfactants which are usually known as lipids are abundant in all living organisms. Surface-activity is essential for organisms for example to overcome solubility issues or work as emulsifier, as dispersant or to modify surfaces. For many commercial applications in our everyday household "natural based" surfactants are manufactured by organic synthesis. Even alkyl glucoside which are usually referred to as "green surfactants" are made by a several step synthesis. However, industrial products can also be based on oleochemicals which are made from renewable raw materials like vegetable oils. These raw materials lead to identical products and can also be used in very large scale productions.

As already mentioned surfactants are primary classified based on their head group into three main groups (Table 1.1). The largest group of surfactants which are commonly used in many applications are anionic surfactants. Carboxylates, sulfates, sulfonates, and phosphates are the polar groups found in anionic surfactants.[43] Anionic surfactants are the largest class of surfactants and used in a wide range of everyday applications such as detergents, soaps, emulsifier, shampoos and many more. They properties can easily be varied by changing the head group, adapting the hydrophobic tail or adding a short polyethylene oxide unit between the head group and the alkyl chain which enhance the hard water tolerance. Another category of ionic surfactants are cationic surfactants. These surface-active moieties have a positive charge, which adsorbs strongly onto most solid surfaces (usually negatively charged), and can add special characteristics to the substrate. A majority of cationic surfactants are based on nitrogen, amine and quaternary ammonium-based products are common. Cationic surfactant show higher aquatic toxicity than other classes of surfactants.[41]

Table 1.1: Overview of the classification of surfactants with some examples of this class and their application.

Classification	Name	Examples
Anionics	alkyl ether carboxylate, alky sulfates/ alky ether sulfates, alky phosphate/ alkyl ether phosphate	detergents, soaps, emulsifying agents, shampoos, wetting agents
Cationics	fatty amine salt, quaternary ammonium salts	dispersant, hair conditioner, adhesion promoter, fabric softeners
Nonionics	alkylphenols, alkyl ethoxylates, glyceryl esters	emulsifier, detergents, soaps, dispersant, cosmetic, food and pharmaceutical emulsifier, foam stabilizer
Zwitterionics	betaine, amindobetaine, amine oxide	cosmetic products, shampoos , detergents

The second largest class of surfactants are nonionic surfactants which have usually a polyether unit as hydrophilic head group. Polyether-based surfactants are made by polymerization of ethylene oxide (EO) and have the advantage that they are compatible with any kind of other surfactants and they usually come as 100% active materials. Their physico-chemical properties can mainly be adjusted by the length of the hydrophilic head group. They are very temperature sensitive and become more hydrophobic with increasing temperature. The main application of nonionic surfactants is as detergents, soaps and in cosmetics. A small class of surfactants are zwitterionic surfactants which have a positive and a negative charge in the head group. Zwitterionic surfactants are in characterized by having excellent dermatological properties. They also exhibit low eye irritation and are frequently used in shampoos and other cosmetic products.[41]

1.3. Surface Activity of Surfactants

The previous section gives an overview of the different types of the surfactants. The fundamental characteristic of surfactants is their surface-active behavior, therefore they adsorb at interfaces due to their amphiphilic character. From this essential characteristic many properties can be determined such as their efficiency how much they reduce the surface tension, σ, the surface excess concentration, Γ, which describes the surface coverage and gives information about the surfactants head group area and the critical micelle concentration (cmc) at which micellar aggregates are formed. Moreover, information about the Gibbs free energy ΔG_{mic} of the system can be observed. These properties provide information of the surfactant at the interface and the efficiency and effectiveness as a surface-active material.[43]

The surface tension of liquids is related to the attractive forces between the molecules. The forces are all equal for a molecule in the bulk. Whereas, for molecules at the surface (e.g. at interfaces) the forces are asymmetric. This force distribution is the reason for the surface energy and results in the surface tension.[43] Therefore, the surface tension represents the cohesive forces in a liquid.[44] In aqueous systems, the addition of surfactants influences the surface tension. Already at very low concentrations the surfactants reduce the surface tension up to the cmc, above which the surface tension is reaching a constant value. Above the cmc, all additional surfactants form new micelles, thereby the surfactant unimer concentration remains constant in solution. Resulting in a constant surface tension above the cmc.[44]

A typical curve of the surface tension as a function of the logarithmic surfactant concentration is depicted in Fig. 1.1. The curve generally can be deviated into three regimes. Firstly, the surfactant molecules start to adsorb at the air/water interface which results in a large reduction in surface tension. Followed by the saturation of the interface. The surface tension is decreasing proportionally to the logarithmic concentration which indicates a constant adsorption. The adsorption of the surfactant molecules can be described by the Gibbs isotherm relating the adsorption to the surface tension.

$$\Gamma = -\frac{1}{nRT}\frac{d\sigma}{d\ln a} \tag{1.1}$$

where σ is the surface tension, a is the activity of the surfactant in the bulk solution and n is a constant. Other parameters are R the ideal gas constant (8.314 J/K·mol), T the temperature and Γ the surface excess concentration. The surfactant concentration below the cmc is normally very low, therefore the surfactant activity can be replaced by the surfactant concentration (c). The factor n

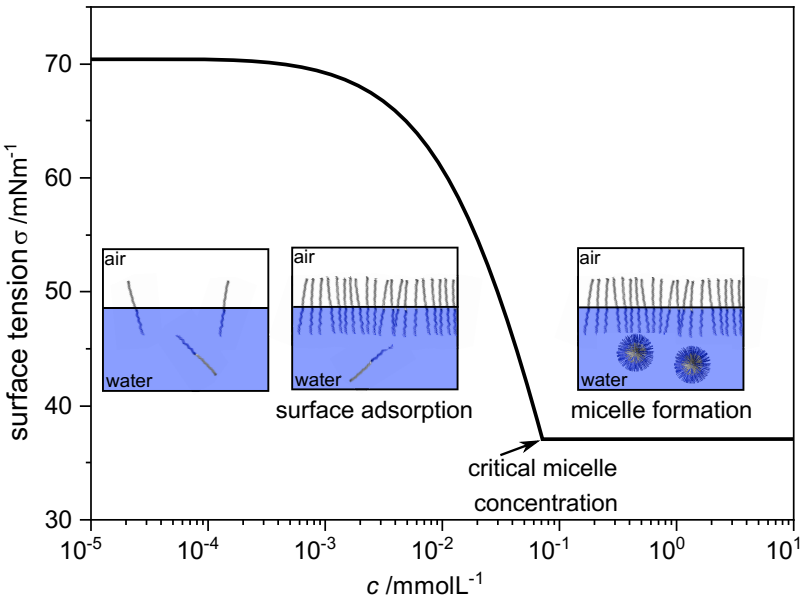

Figure 1.1: Schematic description of a typical curve of the surface tension, σ, as a function of the surfactant concentration, c. The slope describes the surface adsorption of the surfactant molecules until a certain saturation is achieved. Depicted is the critical micelle concentration (cmc) at which micelles are present in solution and the surface tension remains.

has a value of one for nonionic surfactants. In addition to the Gibbs Isotherm the adsorption at the air/liquid interface can also be described using the Langmuir-Szyszkowski isotherm: [45]

$$\sigma = \sigma_0 - RT\Gamma ln(1 + K_{ad} \cdot c) \tag{1.2}$$

σ_0 is the surface tension of water (72.8 mN/m at 298 K), K_{ad} the absorption constant, and c is the surfactant concentration. This equation relates the surface concentration to the bulk concentration, from which the surface excess concentration, Γ, and the head group area a_0 can be obtained. The head group area a_0 is related to the surface excess concentration Γ by the Avogadro constant, N_A, by:

$$a_0 = \frac{1}{\Gamma \cdot N_A} \tag{1.3}$$

The cmc can be derived by the change from the adsorption regime (decreasing slope) to the plateau regime.

1.3.1. Critical Micelle Concentration of Surfactants

The cmc is the most important characteristic of a surfactant. The cmc can be determined by surface tension measurements at the concentration at which the surface tension remains constant. But not only the surface tension is influenced by the presence of micelles. Many other physical properties changes with the presence of micelles such as osmotic pressure, turbidity, solubilization and many more. This change in properties occurs from the micelle formation (micellization). A number of important surface active application, such as detergency and solubilization, depend on the existence of micelles in solution.[43] Besides surface tension measurements, the cmc can also be determined by ITC and other methods. The surface tension measurements and the ITC method are generically described in the following chapter 2.

In general, the cmc can be influenced by the chemical structure of the surfactant molecule and by environmental changes. The cmc of nonionic surfactants is markedly changed by alkyl chain length, temperature of the solution, length of the head group and addition of salts or organic solvents.[46]

The cmc decreases strongly with increasing alkyl chain length.[47, 48] The cmc value decreases linearly with increasing carbon numbers in the alkyl chain n, which can be described for nonionc surfactants by the following equation:

$$\log(cmc) = -0.5 \cdot n + 1.89 \tag{1.4}$$

For nonionic surfactants, the cmc also depends on the length of the head group, which typically are ethylene oxide (EO) units. The cmc moderately increases with increasing EO units, due to the hydrophilic influence of the head group, which reduces the tendency to form micelles.

Temperature effects

For nonionic surfactants, the temperature plays also a major role. The cmc decreases with increasing temperature due to the fact that at higher temperatures the EO units become more hydrophobic thereby favoring micellization. For EO surfactants water becomes a less good solvent at higher temperatures. As the temperature is raised large aggregates precipitate out into a distinct phase. This phenomenon is called the cloud point (CP) and is caused by the configuration change of the ethylene oxide unit. At lower temperatures, the polar configuration (a-g-a) of the EO unit is the energetically favored configuration. With increasing temperature, the energetically unpolar configuration (a-a-a) becomes statistically more pronounces. Therefore, the EO unit becomes hydrophobic and unpolar which results in phase separation at higher temperatures.[48]

Considering temperature effects one also needs to explain the Krafft temperature T_K (or Krafft point). Below a certain temperature the surfactant precipitate into a different phase. At the Krafft temperature surfactant solubility is equivalent to the cmc. Below the Krafft temperature, the solubility is quite low and the solution does not contain any micelles. Therefore, also the effectivity of the surfactants is usually drastically reduced in most applications below the Krafft temperature. Above the Krafft temperature, micelle formation occurs and solubility increases rapidly.[49]

1.4. Thermodynamics of Micellization and Driving Force

The fundamental thermodynamic value is the free energy which can be obtained in therms of micellization by the cmc from the Gibbs equation.

$$\Delta G_{mic} = RT \cdot \ln x_{cmc} \tag{1.5}$$

where x_{cmc} is the mole fraction of surfactant in aqueous solution at the cmc (assuming ideal behavior). Here ΔG_{mic} represents the free energy between the unimers in the micelle and the micelles. The Gibbs-Helmholtz equation considers the relation between the enthalpy ΔH_{mic} and entropy term ΔS_{mic} with the free Gibbs energy.

$$\Delta G_{mic} = \Delta H_{mic} - T\Delta S_{mic} \tag{1.6}$$

Different models can be used to determine the thermodynamics of micellization. Here two commonly used models to describe the micellization process are presented.[47]

1.4.1. Phase Separation Model

The phase separation model considers the fact, that that micellization is comparable with the formation of a separate liquid phase. Micelle formation can be considered as phase separation, with the micelles being the separated phase and the cmc is the saturation concentration of surfactant in the monomer state. Hence, an increase in concentration above the cmc would only influence the micelle concentration and not the surfactant monomer concentration.[49] At low concentrations, the chemical potential of the surfactant monomer can be described by:

$$\mu_{sur}(solvent) = \mu^{\circ}_{sur} + RT \ln [S] \tag{1.7}$$

where μ°_{sur} is the effective standard chemical potential at dilute solution and [S] is the concentration of surfactants. At [S] = cmc the chemical potential of a surfactant in a micelle $\mu_{sur}(micelle)$ is equal to the chemical potential of a dissolved surfactant. This directly leads to

$$\mu_{sur}(micelle) = \mu^{\circ}_{sur} + RT \ln x_{cmc} \tag{1.8}$$

The phase separation model is a relative simple model which is easy to apply and sufficient for many systems with high aggregation numbers N_{agg}.[47, 49]

1.4.2. Mass Action Model

The mass-action model assumes that the surfactant molecules are in association-dissociation equilibrium and micellization is considered as reversible process.[47] The mass-action model was originally applied to ionic surfactants but later it was also applied to nonionic surfactants.

$$N_{\text{agg}}[S] \rightleftharpoons [S]_{N_{\text{agg}}} \; ; \; K = \frac{[S_{N_{\text{agg}}}]}{[S^{N_{\text{agg}}}]} \tag{1.9}$$

It is most valid for systems with a low aggregation number N_{agg} and it is also used to calculate thermodynamic parameters such as ΔG_{mic}.

1.4.3. Hydrophobic Effect

The fundamental driving force for the micelle formation is the hydrophobic effect.[47, 49, 50] The reason for this effect is the amphiphilic characteristic of surfactants. The water favoring polar hydrophilic head group and the water unfavored unpolar hydrophobic part. The water molecules can not form hydrogen bonds with the hydrophobic alkyl chain in water. Therefore, the alkyl chains try to avoid the water interaction and are expelled from the aqueous environment. This is achieved by a macroscopic phase separation or by self-aggregation, where the hydrophobic alkyl chains are hidden in the micellar core. The hydrophobic effect is an entropic effect. The highly oriented and structured water molecules are interacting by hydrogen bonds. The hydrophobic chains are disrupting the existing hydrogen bonds and the restructuring of water molecules is entropically very unfavorable. During micellization, the reoriented water molecules around the alkyl chains are released which results in an increase in entropy.

1.5. Surfactant Structure and Micellar Shape

As explained previously, the main driving force for micelle formation is the reduction of the contact of the alkyl chains with the water. At the cmc, the surfactant molecules self-aggregate into micellar structures. The shape and structures of the formed micelles depend mainly on the geometrical structure of the surfactant molecule. The shape of the micelles also determines the physical properties of the surfactants in water such as its viscosity, its capacity to solubilize hydrophobic material, and its cloud point.[43]

The aggregation number N_{agg} defines the number of surfactant molecules which form a micelle. It should be mentioned here, that in reality, a distribution of aggregation numbers are describing the micelle. Slightly below the cmc, most surfactants are present as monomers or low number aggregates and a small number of micelles already exist. At the cmc, the monomer concentration is almost saturated and constant, which results in a new micelle formation by addition of a new surfactant molecule. The distribution of aggregation numbers is almost Gaussian with a standard deviation ΔN_{agg}: $\Delta N_{agg} \approx N_{agg}$.[49, 50] A micelle is a dynamic structure; surfactants are in a associate and dissociate equilibrium. The detailed correlation of the surfactant structure and the corresponding micellar shape is discussed in the following section.

1.5.1. Packing Parameter

The structure of the surfactant can be explained by simple geometrical approaches.[49, 51] The alkyl chain length l_c and volume v occupied by the alkyl chains in the micellar core are considered, as well as the head group area a_0 which is occupied by the hydrophilic group at the micelle-solution interface. This value is called the packing parameter P and defines the ratio between the hydrocarbon volume and the head group area:

$$P = \frac{v}{l_c \cdot a_0} \tag{1.10}$$

The theory of micellar structure, based upon the geometry of the hydrophilic and hydrophobic groups of the surfactant molecules, has been developed by Israelachvili.[52]

From Tanfords rule, where n is the number of carbon atoms in the micellar core, one can determine the length of the alkyl chain, assuming fully extended chains.[53] The volume of the alkyl chain is also described by Tanford:

$$l_c \leq l_{max} = (0.154 + 0.1265 \cdot \mathrm{n})\, nm \tag{1.11}$$

$$v \approx (0.0274 + 0.0269 \cdot \mathrm{n})\, nm^3 \tag{1.12}$$

From a simple geometrical approach, the aggregation number of spherical micelles can also be theoretically determined, considering the micellar radius R ($R = 3v/a_0$).

$$N_{\mathrm{agg}} = \frac{4\pi R^2}{a_0} \tag{1.13}$$

The packing parameter illustrates which shape the molecules can adapt into their self-assembled structure. It should be mentioned that these values indicating limiting shapes determined by the molecular structure. As shown in Fig. 1.2 the packing parameter and the corresponding structures are shown. The preferred structure, with increasing P, would be spherical micelles ($P \leq \frac{1}{3}$) to ellipsoidal

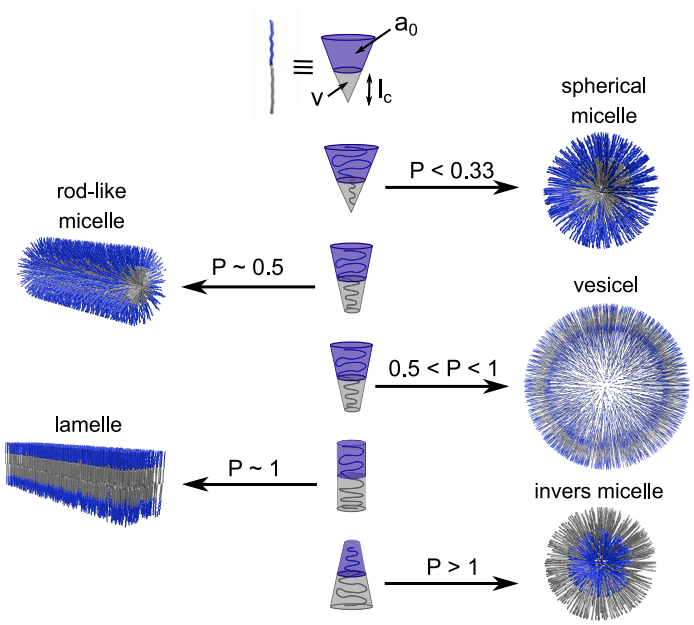

Figure 1.2: Schematic description of the packing parameter and the corresponding preferred structures formed by surfactants. Adapted from [50].

micelles ($\frac{1}{3} \leq P \leq \frac{1}{2}$) to cylindrical or rod-like micelles ($P \approx \frac{1}{2}$) to vesicles ($\frac{1}{2} \leq P \leq 1$) and bilayers or lamellar structures ($P \approx 1$) and finally to a "inverted" structures (P > 1). Changes in temperature, the concentration of surfactant, additives in the liquid phase, and structural groups in the surfactant can all cause a change in the size, shape, and aggregation number of the micelles.[43]

1.5.2. Phase Behavior and Liquid Crystalline Phases

The micellar structure is given by the geometrical structure of the surfactant molecule. With increasing concentration the micellar concentration is increasing, therefore they start to pack together in a densely packed geometric structures, depending on the shape of the individual micelles. These packing arrangements are known as *liquid crystals* (LC). Liquid crystals are a state in which properties are between conventional liquids and solid crystals. The micellar aggregates are highly packed in a crystal-like way, however, they can flow like a liquid. Because of this ordered arrangement of the molecules, they increase the viscosity, under some circumstances very drastically. There are different types of liquid crystalline phases which usually can be distinguished by their optical properties. Liquid crystalline phases of spherical micelles are usually cubic liquid crystals, cylindrical micelles pack to form hexagonal liquid crystals and lamellar micelles form lamellar liquid crystals. With an increase in surfactant concentration, a transition can occur from cylindrical micelles to branched micelles which are leading to a bicontinuous liquid crystalline phase.[43] Cubic LC phases (l_1) are isotropic and cannot be observed under the polarizing microscope. They also are highly viscous because of their highly ordered structure. Hexagonal phases (H_1) are more viscous than lamellar phases (L_α), however they are more viscous than ordinary solutions. Hexagonal and lamellar phases are anisotropic and can be detected under the polarizing microscope. Liquid crystal structures are important for viscosity modification, various applications such as detergency, emulsions, stabilization of foams and other applications.[43]

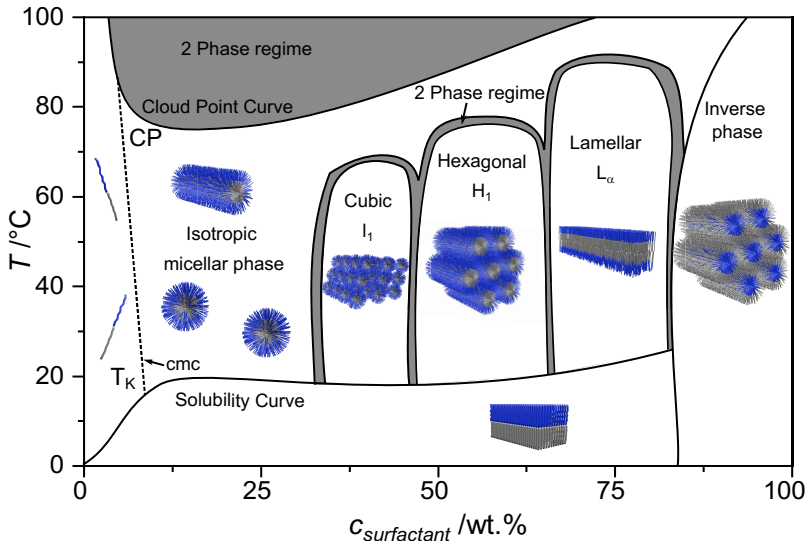

Figure 1.3: Schematic phase diagram of a nonionic surfactant with the temperature as a function of the concentration. The dashed line indicates the cmc. The Krafft temperature T_K and the cloud point CP indicating the lowest critical solution temperature (LCST). The grey area represent a two phase regime. Adapted from [46].

At higher concentrations, structural transitions can also occur from cubic phases into hexagonal, bicontinuous cubic, and lamellar. This type of behavior is illustrated in a schematic phase diagram depicted in Fig 1.3. Phase diagrams typically show the structural properties or phases of a system under certain conditions (temperature, composition).[51] The concentration is not the only parameter that can influence the phase behavior and the formation of higher-ordered phases. For nonionic surfactants, the aggregation number increases progressively with increasing temperature. The structural transition from spheres to rod-like structures can be described in terms of a decreasing head group area at higher temperatures. The change in the configuration of the EO unit is already described in a previous section. Therefore, it appears that there is a closer packing of polar head groups at the aggregate surface at higher temperatures.[48] With further temperature increase, typical behavior for nonionic surfactants occurs. One can observe the phase separation of the system due to the configuration change of the EO unit. This temperature is called cloud point (CP). With increasing temperature the configuration of the EO chains changes from the polar a-a-a to the apolar a-g-a configuration. This results in a decrease of the hydrophilic of the molecule and dehydration. At the cloud point phase separation occurs and very large aggregates are formed.

1.6. Micellar Solubilization

One of the most important properties of surfactant micelles is their potential for the solubilization of hydrophobic compounds. The term solubilization describes the dissolving of substances which are usually water-insoluble. Solubilization is defined as “the spontaneous dissolving of a substance (solid, liquid, or gas) by reversible interaction with the micelles of a surfactant in a solvent to form a thermodynamically stable isotropic solution with reduced thermodynamic activity of the solubilized material.”[43]

Solubilization is one of the most important phenomena for surfactant solutions, with major practical importance for many applications where water-insoluble compounds are involved.[43] Micellar systems can replace the use of organic solvents or cosolvents; they can be used in detergency, micellar catalysis, and in enhanced oil recovery, where solubilization produces the

ultralow interfacial tension required for mobilization of the oil. Solubilization of hydrophobic drugs is of major importance for pharmaceutical applications.[43, 46]

Typically the solubility stays very low until the cmc is reached, while above the cmc it increases rapidly and almost linearly with the surfactant concentration. The efficiency of solubilization by a surfactant can be described by the solubilization capacity, which describes the ratio of solubilized molecules S_{tot} and surfactant molecules c_{surf}:

$$\chi = \frac{S_{tot} - S_w}{c_{surf} - cmc} \tag{1.14}$$

considering the water solubility S_w of the compound and the cmc of the surfactant.

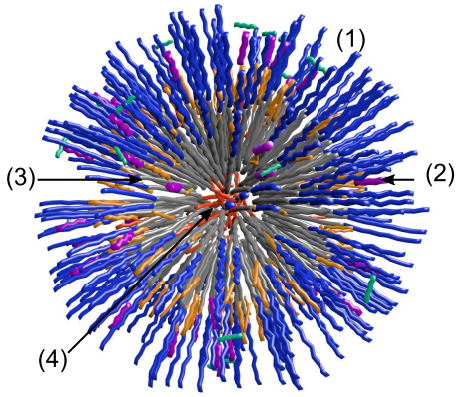

Figure 1.4: Schematic description of the possible locus of solubilizate: (1, turquoise) at the water/head group interface, (2, purple) penetration of the head group, (3, orange) at the palisade layer or in the micellar core (4, red). Depicted from [46].

The location of the hydrophobic compounds highly depends on the structure of the solubilized compound and the interaction with the surfactant molecules. Therefore the locus of the solubilizate can occur at different sites of the micelles as depicted in Fig. 1.4. The two major sites are the hydrophobic core and the hydrophilic head group. Moreover, the solubilizate can adsorb at the water/head group interface (1), or it can penetrate the EO chains in the hydrophilic head group (2). Penetration at the interface between the head group area and alkyl chain (palisade layer) (3) or dissolution in the hydrophobic core can occur (4). It should be noted, that the locus of the solubilizate can not only vary with the structure of the surfactant or solubilizate but also with an increasing amount of solubilizate.

The effect of the solubilization also reflects on the micellar size. An increase of the micellar weight can occur during solubilization by rearrangement of the surfactant molecules when solubilizate is present.

1.6.1. Microemulsions

The solubilization of oil by micellar aggregates can lead to a formation of microemulsion in the size range of 10-100 μm. Microemulsions are homogeneous mixtures of oil, water, and surfactant, which consist of individual aggregates of oil which are separated by a surfactant monolayer from the aqueous solvent. Microemulsions are thermodynamically stable, isotropic, and homogenous. The unique behavior of microemulsions is that they form spontaneously and reversibly to change such as temperature or composition. This mainly indicates the difference to emulsions or nanoemulsions, which are unstable systems in which the droplets coagulate over time. Even though one consider a ternary system of surfactant, oil, and water as microemulsion usually an addition of cosurfactants is used to enhance the oil solubilization.[54–57]

The phase behavior of microemulsions is classified into three different phases so-called Windsor Types I, II, and III. Type I describes an aqueous phase containing surfactant and solubilized oil in equilibrium with excess oil (o/w microemulsion). Type II describes an upper phase microemulsion, where water solubilizes into the oil phase by the surfactant micelles to form w/o microemulsions. Type III is a three-phase system with both excess phases and a microemulsion phase in the middle

consisting of the excess oil and water phase. For nonionic surfactants, the I–III–II transition from the upper to the lower microemulsion may occur by raising the temperature.[48]

Almost 20 years ago, Jakobs et al.[58] found that small amounts of amphiphilic poly(ethylene propylene)-co-poly-(ethylene oxide) polymers are able to considerably increase the efficiency of medium-chain surfactants in forming microemulsions. As a consequence, these block copolymers boost the efficiency of medium-chain surfactants, increase the length scales of the microstructure and decrease the oil/water interfacial tension.[59]

For interested readers, fundamental information of surfactants and the physical properties of surfactants is described in thorough detail in the book "Intermolecular and Surface Forces" by J. Israelachvili.[50] A very good overview of many physical parameters of surfactants and their properties is given in the book of M. Rosen "Surfactants and Interfacial Phenomena".[43] Moreover, surfactants and polymers are depicted by K. Holmberg and B. Kronberg *et al.*[48] in the book "Surfactants and Polymers in Aqueous Solution". The last to be mentioned is a specific book about the fundamentals of nonionic surfactants written by M. Schick.[46] These references give detailed insights into the properties of surfactants and self-aggregation behavior. They also served as the basis for this chapter.

1.7. Motivation and Aim of This Work

Carbon dioxide is one of the most abundant greenhouse gases in the earth´s atmosphere and a waste product from all combustion processes, which represent a potential as an alternative carbon feedstock. Using CO_2 as a resource opens up many opportunities for a circular economy. By this approach, one can use CO_2 to produce CO_2-based nonionic surfactants by substituting parts of the hydrophilic head group which are usually based on fossil-based resources. These CO_2 surfactants are a sustainable alternative to conventional petroleum-based nonionic surfactants. The approach to use CO_2 as a resource and use it to synthesis CO_2-based nonionic surfactants is a project called "Dream Resource" within the framework of a BMBF project.[40] The CO_2 based nonionic surfactants were developed by Covestro Deutschland AG to aim for CO_2 contents of 20 %.

This thesis was performed within the project "Dream Resource" and the aim of this work is to gain a comprehensive picture of the physical-chemical properties of these new sustainable CO_2 surfactants. The characterization of the surface activity, the micellization process, and the phase behavior in the low and high concentration regime of the CO_2 surfactants are crucial for a thorough fundamental understanding of such systems. For nonionic surfactants, the temperature plays also an important part therefore the micellization and phase behavior was also studied dependent on the temperature, which is also important for certain applications such as detergency. The main research question is to understand the impact of the CO_2 moiety in the hydrophilic head group on the properties and the phase behavior of the nonionic surfactants. With the obtained knowledge the CO_2 content is a further tuning parameter to achieve especially designed properties and opens up a wide range of potential applications.

Furthermore, the solubilization of hydrophobic compounds by the CO_2 surfactants was investigated to get insights into the application potential. Enhancing the bioavailability by an enhanced solubility of hydrophobic compounds such as pharmaceuticals, herbicides or oils is a common application for nonionic surfactants. Whereby the incorporated CO_2 moiety can be an attractive further interaction position and thereby enhancing the solubility of hydrophobic compounds. The understanding of the surface activity at the air/water interface was also transferred to the water/oil interface. Obtaining knowledge about the temperature dependent adsorption properties of these types of nonionic surfactants improves the understanding of further properties such as emulsion and microemulsion formation which opens up opportunities for several further applications.

The characterization of the physical-chemical properties of the CO_2 surfactants was performed with several techniques. The main methods to characterize the surface activity and the micellization process were surface tension measurements and isothermal titration calorimetry (ITC). The phase behavior was characterized by rheology measurements and a comprehensive picture of the structure of the formed aggregates and the interaction could be given by scattering techniques such as light and small-angle neutron scattering. The solubilization of hydrophobic compounds could be studied by UV-Vis measurements and NMR measurements and the adsorption at the water/oil interface was studied by pendant drop measurements. The fundamental basics of the main methods will be given in the next chapter.

Chapter 2

Instrumentation Techniques

The following chapter will give a short introduction and description of the instrumentation techniques which have been used to investigate the phase behavior of surfactants. To obtain more detailed information about the different methods the following references are recommended. For surface tension measurements a general basis is obtained by “Fundamentals of Interface and Colloid Science: Liquid-Fluid Interfaces“ by Lyklema[60] and isothermal titration calorimetry is well explained by the review article of Loh *et al.*[61] and the article of Bouchemal *et al.*[62] Followed by the section rheology which is based on the book “Handbook Of Rheology“ by Barnes.[63] For the scattering techniques, a good overview of light scattering techniques is given by Berne & Pecora[64] “Dynamic Light Scattering“ and for small-angle neutron scattering a general overview is given by the book of MLZ “Neutron Scattering“ written by Brückel *et al.*[65] and the chapter “Scattering Techniques“ in the book “Fluids, Colloids and Soft Materials: An Introduction to Soft Matter Physics“ by Cipelletti *et al.*[66]. These references also serve as a general basis for the following chapter.

2.1. Surface Tension Measurements

The surface tension is the tendency of liquids to reduce the surface area as much as possible. At the air-water interface, the surface tension results from the greater cohesive forces of the liquid molecules in the bulk to each other than to the molecules at the interface. The surface tension σ is an inward force which is defined as a force per unit length. In terms of energy, it can be described as the ratio of the change in energy of the liquid and the surface area of the liquid. This means that the energy of the film is increasing with increasing surface area. The surface tension of water is 72.8 mN/m and high in comparison to other liquids which is mainly caused by the hydrogen bonds which implies a strong network of water molecules.

Surfactants are known to be surface active, caused by their amphiphilic character, which results in reduce surface tension. The decrease of the surface tension caused by surfactants becomes stronger with increasing adsorption at the interface. Characteristic parameters of surfactants can be determined by a typical surface tension as a function of the equilibration concentration curve as described in chapter 1.3. To determine these values one needs to measure the surface tension of a surfactant in water at different concentrations. The used method is the Du Noüy ring method. This technique is similar to the Wilhelmy plate method and involves a platinum ring. A force tensiometer measures the excess of force needed to pull up the liquid. The Du Noüy ring method is

often employed in the detachment mode where the ring is completely wetted and the maximum pull is obtained beyond which the liquid constricts spontaneously.[60]

The maximum force is used for the calculations, considering a empirically determined correction factors for the correction of the finite ring diameter:

$$F(max) = w_{(ring)} + 4\pi R\sigma f \tag{2.1}$$

$w_{(ring)}$ is the weight of the ring and its wires. f implies a correction factor and a function of the ring geometry and it is usually taken into account by the tensiometer software. R is the radius of the ring which is simplified by the assumption that the ring thickness is much smaller than the ring diameter.

2.2. Isothermal Titration Calorimetry

Isothermal titration calorimetry (ITC) is a technique that allows highly precise and sensitive measurements. It allows to measure accurately the thermodynamic information of an association process in colloidal systems. The measurements provides information about the cmc for surfactants, the Gibbs energy, enthalpy and entropy of the system. Moreover, the binding constant and binding number can be determined by ITC. Titration calorimetry is becoming one of the most used techniques for acquiring information on the self-organization of surfactants into micelles. A good overview of the technique ITC and what information can be obtained by it is given by Bouchemal *et al.*[62] and an interesting overview of ITC for studies of surfactant to form micelles, with emphasis on the thermodynamic studies of homologous surfactant series is given by the review of Loh *et al.*[61] In the following section an overview will be given on the analysis of the thermodynamic parameters obtained from ITC for the concise analysis of micellar systems. It will start with a short introduction on the instrumental set up and will be followed by a description of the analysis of the enthalpogram to obtained the desired thermodynamic parameters.

2.2.1. Instrumental Set Up

From a technical point of view, ITC experiments are relatively simple. The basic principle is to inject defined small volumes of an aqueous micellar solution of surfactants from the stirring syringe into the water which is contained in the measurement cell. The solvent does not need to be water it can also be puffer solution or other dispersing medium. The basic set up is shown in Fig. 2.1. The measurement cell is maintained at a constant temperature and the heat which occurs during dilution is detected for each injection and plotted as a function of surfactant concentration. In commercial ITC instruments, the experimentally temperature range is between 2 and 80 °C. It is important that, the surfactant concentration in the syringe has to be chosen in such a way that the increase in surfactant concentration in the measurement cell has to reach slowly the cmc during the experiment. Usually the syringe concentration needs to be 10 times higher than the cmc.[67]

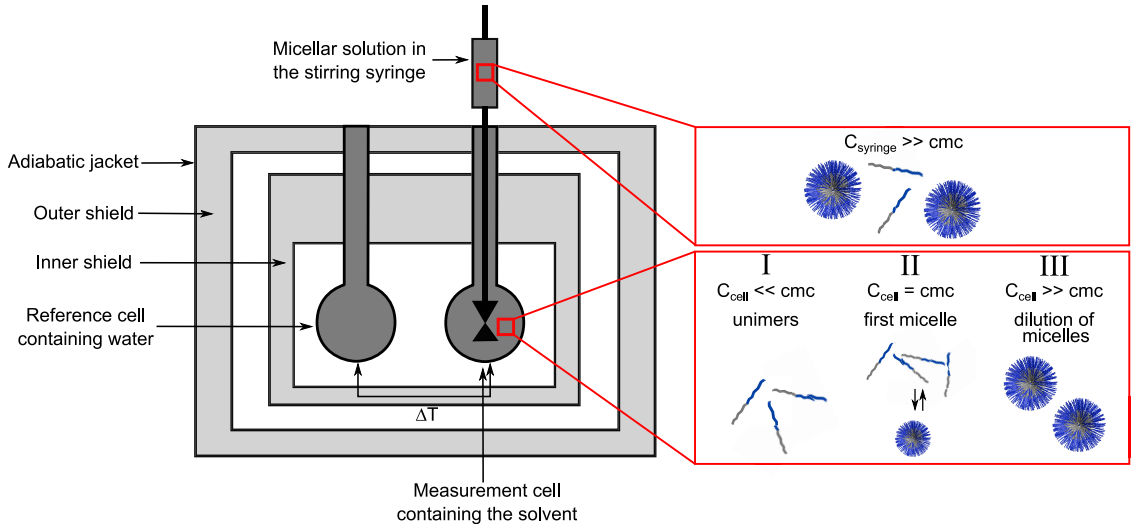

Figure 2.1: Schematic representation of the ITC set up with a schematic representation of the events in the measurement cell during the ITC experiment. The enthalpy of unimer dilution ΔH_I, the enthalpy of micellization ΔH_{mic} (ΔH_{II}), the enthalpy of micelle dilution ΔH_{III}. (Adapted from Bouchemal *et al.*[67])

2.2.2. Critical Micellization Concentration and Enthalpy of Micellization

In the case of surfactant self-aggregation the surfactant concentration is increased in the measurement cell during ITC measurements. Increasing the surfactant concentration in the measurement cell by each injection results in micelle formation once the critical micellization concentration (cmc) is reached (as visualized in Fig. 2.1). A typical enthalpogram is shown in Fig. 2.2 where each injection corresponds to a heat release in the enthalpogram. The measured heat rate (µJ/s) is plotted against the time (s) at an ITC measurement. The obtained enthalpogram needs do be corrected in terms of a baseline correction and the used solvent at the corresponding temperature needs to be subtracted. A typical enthalpogram of the demicellization process is shown in Fig. 2.2A. The measured heat flow can be calculated into the enthalpy by integrating the titration peaks:

$$\int_{i}^{i+1} q = \Delta H_i \tag{2.2}$$

The obtained enthalpy ΔH_i is related to the amount of molecules which are titrated into the measurement cell per injection:

$$\Delta H_{m,i} = \frac{\Delta H_i}{n} \tag{2.3}$$

The enthalpy per injection can be plotted against the surfactant concentration resulting in a usual calorimetry titration curve (Fig. 2.2B) ITC curves were analyzed using the mass-action model.[61, 68–70] It is a simple approximation model assuming an existing equilibrium between the surfactant unimers and the micelles at the cmc.

$$N_{\mathrm{agg}}[S] \rightleftharpoons [S]_{N_{\mathrm{agg}}} \; ; \; K = \frac{[S_{N_{\mathrm{agg}}}]}{[S^{N_{\mathrm{agg}}}]} \tag{2.4}$$

It is valid for systems with low aggregation number N_{agg} and is also used to calculate the thermodynamic parameters (ΔG_{mic}, ΔS_{mic}). The resulting curves change the shape and the profile depending on various factors, thereby the main influence has the surfactant concentrations, and the shape and aggregation number of the formed aggregates, also the solvation–desolvation process and the temperature effect the titration curve. A typical shape of the titration curve can be

described by three different regimes: (I) the pre-micellar region at low surfactant concentrations, the measured enthalpy represents demicellization and the dilution of monomers added into the cell; (II) transition concentration region from which the cmc can be obtained, where only a fraction of micelles is dissociated into unimers, while the rest remain in the micellar form; (III) a post-micellar region at high surfactant concentration, where the measured enthalpy is related to the dilution of both micelles and monomers (Fig. 2.2).

The micellization enthalpy ΔH_{mic} was obtained by the pre-micellar region ST (start of transition I) and of the post micellar region ET (end of transition III). By taking the difference of these values one obtains ΔH_{mic} (an example for such a determination is shown in Fig. 2.2B).[71]

$$\Delta H_{mic} = ET - ST = -\Delta H_{demic} \tag{2.5}$$

The cmc was determined by the inflection point and can be described by the first derivative method as described from the mass-action model (Fig. 2.2C). From the mass-action model the Gibbs energy for nonionic micelles is given as described previously (Eq. 1.5). This allows one to determine also the entropy of micellization by the Gibbs Helmholtz equation (Eq. 1.6). As shown in this section ITC is a powerful technique to determine simultaneously ΔH_{mic} and the cmc values. Moreover, these values can be determined at desired conditions such as temperature.

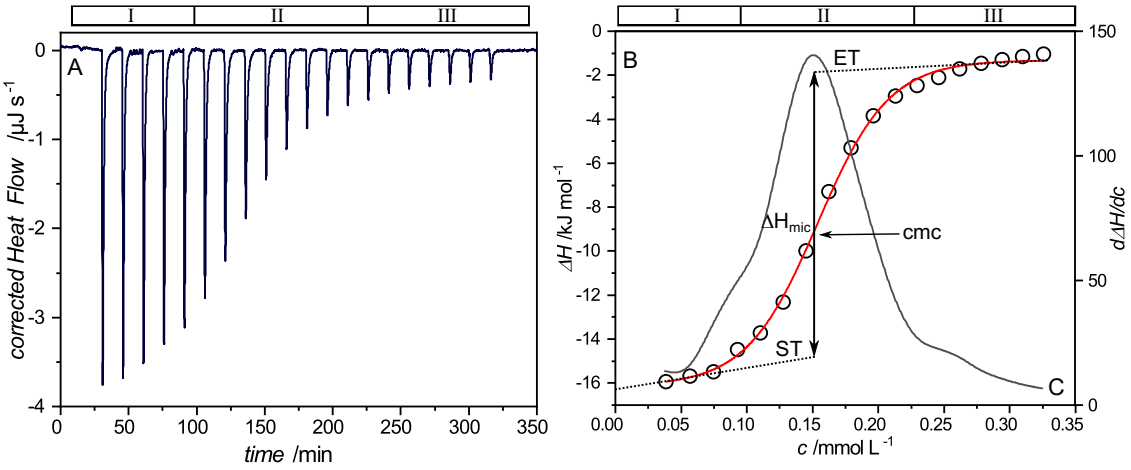

Figure 2.2: Typical data of the demicellization of surfactant obtained from ITC measurements. (A) Exothermic heat flow at each injection of surfactant solution (corrected by baseline). (B) Integration of the heat flow data results in a sigmoidal curve of the enthalpy ΔH. The cmc is defined as the concentration where the first derivative of the curve (B) reaches maximum (C). (Adapted from ref. [71])

2.3. Rheology

2.3.1. Flow Behavior and Viscosity

Rheology is defined as the study of flow and deformation of matter and it plays an important role in our everyday lives. For numerous applications understanding and controlling the flow behavior is crucial to obtain the desired properties for application. Rheology usually observes the fluid behavior of matter with a time-dependent response to stress. Accordingly, the term flow needs to be defined in the first place. Flow is defined as the deformation of the elements of the liquid. The molecules of the liquid are moving parallel to one another. One differentiates between two types of flow, the

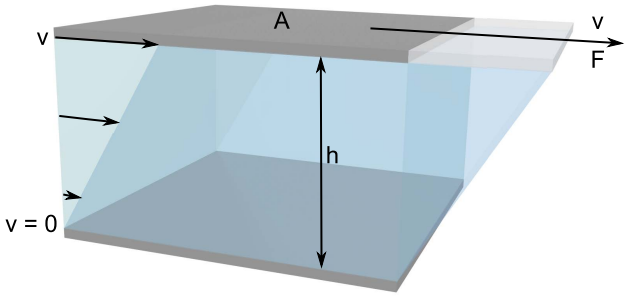

Figure 2.3: Calculation of shear stress and shear rate using the two-plates model with shear area A, gap width h, shear force F, and velocity v. (Adapted from ref. [72])

shear flow, and the extensional flow. In shear flow, the liquid molecules flow over or past each other, and in extensional flow, the molecules flow towards or away from another.[63] The resisting force influencing the flow of a liquid is the viscosity.

Shear Rate and Shear Stress

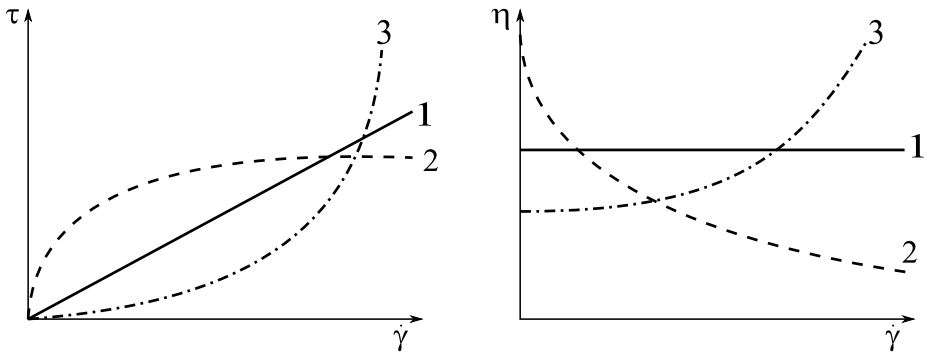

Figure 2.4: Flow curves (left) and viscosity curves (right) for (1) ideally viscous, (2) shear-thinning, and (3) shear-thickening flow behavior. (Adapted from ref. [72])

The flow is typically measured using shear rate ($\dot{\gamma}$) and shear stress (τ). To understand these terms it is easier to visualize a liquid as the movement of hypothetical parallel layers sliding over each other between two plates. In the simplest case, the velocity of each layer increases linearly with respect to its neighbor below. The shear rate ($\dot{\gamma} = v/h$) is defined as the velocity v per shear gap h and has the unit $1/s = s^{-1}$. The shear stress ($\tau = F/A$) is defined by the force per unit area and has the unit of N/m^2. A rheometer records the shear force F by the torque at each measuring point.

Viscosity

Viscosity (η) is defined as the shear stress divided by the shear rate ($\eta = \tau/\dot{\gamma}$). The viscosity values are not constant parameters; they are affected by several conditions such as temperature. Several types of flow behavior generally exist and are depending on the molecular structures. The simplest is Newtonian behavior, with a linear relationship between shear stress and the shear rate. Accordingly, the viscosity is independent of the shear rate. Typical example liquids are water, mineral oil, or acetone.[72]

Most common colloidal suspensions are shear-thinning (pseudo-plasticity), which means the viscosity decreases as the shear rate increases. Typical materials with this flow behavior are coatings, glues or shampoos and the shear-thinning behavior is related to the internal molecular structure of the liquid.[72]

Shear-thickening (dilatant flow behavior) means increasing viscosity with increasing shear rates. Materials that typically display such behavior are highly filled dispersions; a commonly known example is a starch dispersions.[72] Measuring the viscosity with a rheometer can be carried out by rotational test. A measuring system would be for instants the plate-plate system or the cone plate system as depicted in Fig. 2.5. Thereby is it important to consider the correct filling of the measuring system to obtain absolute values that are comparable and not dependent on the size of the measuring system. All parameters can only be precisely measured if a laminar flow (which means uniform flow) occurs without any turbulent flow behavior.

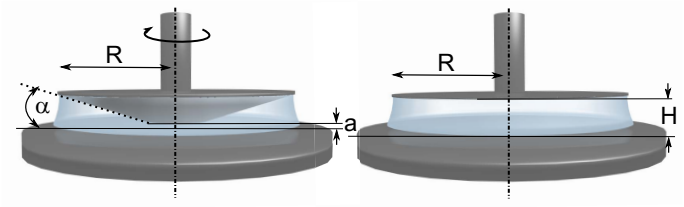

Figure 2.5: Measuring systems (left) cone-plate (with radius R, cone angle α, truncation a) and (right) plate-plate (with radius R, the distance between plates H). Additionally, the filling of the measuring system after the gap setting is shown. (Adapted from ref. [72])

2.3.2. Viscoelastic Behavior

Many materials are viscoelastic which means their behavior display a mixture of viscous and elastic behavior. Considering a highly concentrated suspension it can have viscous liquid-like behavior as well as elastic solid-like behavior depending on the timescale. On a short timescale, the system behaves as a solid (elastic response) but at a longer time scale the system behaves like a liquid (viscous response).[72] Viscoelasticity can be described by mechanical models, whereby the viscous behavior is represented by a dashpot and the elastic behavior by a spring. The spring represents the linear elastic behavior by Hooke´s law.[73] Thereby applying deformation γ to a system results in a proportionally applied stress τ. The shear deformation ($\gamma = s/h$) is thereby a dimensionless number, depending on the deflection path s and the shear gap h. The shear modulus G is the proportionality factor for the deformation and the shear stress:

$$G = \frac{\tau}{\gamma} \tag{2.6}$$

Notice that this behavior described by Hook´s law is time-independent. The deformation results suddenly after stress application. Again a similar simple mechanic model can be used to describe a viscous response, a dashpot. The Newtonian liquid-like behavior can be described by a shear stress τ proportional to the shear rate $\dot{\gamma}$. The viscosity η is the proportionality factor.

$$\tau = \eta \cdot \dot{\gamma} \tag{2.7}$$

If a stress is applied to a dashpot it imminently starts to deform with a constant deformation rate. The connection of a spring and a dashpot in series is the simplest representation of a viscoelastic

liquid, which is called a Maxwell model. Of course, these are only simple mechanical properties to describe viscoelastic behavior.

Oscillatory measurements – Viscoelastic Properties

Viscoelasticity can also be measured by means of forced oscillation methods (also known as dynamic measurements). In dynamic tests, a small oscillatory shear is applied to a sample and the response is measured. By that, the sample is slightly deformed from its original structure at rest, but not completely destroyed. By oscillatory measurements the elastic response of the system is measured and can be correlated to the structure of the suspension. A viscoelastic fluid is then characterized by a phase angle δ, which is the time lag between the preset and the resulting sinusoidal oscillation. This angle is always between $0° < \delta > 90°$.[72] In oscillatory shear, the so-called complex shear modulus G^* is defined as:

$$G^* = \frac{\tau_A(t)}{\gamma_A(t)} = G' + iG'' \tag{2.8}$$

and describes the entire viscoelastic behavior of the sample. Where τ_A is described as the shear-stress amplitude and γ_A as the deformation amplitude. Both G^* and δ depends on the frequency. The storage modulus G' represents the elastic properties of the viscoelastic behavior. It describes the storage of energy by the deformed material. This energy is stored by the material by extending or stretching the sample without destruction. It is immediately restored afterward. The loss modulus G" characterizes the viscous properties of the viscoelastic behavior, which can be seen as the liquid-state behavior of the sample. It describes the energy which is required to flow and it is irreversibly lost as shear heat.[72] Viscoelastic solids have a higher contribution of the storage modulus as a result of intermolecular interactions such as cross linking inside the material as chemical bonds or physical-chemical interactions. In contrast, viscoelastic liquids have a higher contribution of the loss modulus. As a result of weak interactions between the individual molecules of the material.[72]

2.4. Scattering Techniques

In soft matter science, the fundamental question is the understanding of the microscopic structure of matter employing its size and shape. Methods to investigate the samples by their structure and shape can be divided into two categories: direct methods such as optical, electron or atomic force microscopes which obtain information by real-space images. The second category are scattering techniques, such as light, neutron or X-Ray scattering, which measure the Fourier transformation of the structures being investigated. The main advantage of scattering techniques is the higher statistics of obtained data than derived from imaging methods. Scattering techniques often provide much better quantitative measurements of the average structural and dynamical properties of materials. Moreover, scattering techniques are more readily adapted to measure fully three-dimensional information and they are mostly nondestructive which is a major advantage in comparison to imaging methods.

Using scattering techniques for structural analysis one can investigate a broad size range depending on the wavelength and correspondingly on the frequency. Thereby the choice of methods is generally set by the length scale which wants to be observed. A general approach by the choice of scattering technique is the radiation wavelength, which needs to be about the same size as

the structures that scatters the radiation. For X-ray and neutron scattering, the wavelength of the radiation is approximately 0.1 nm, making X-rays and neutrons ideal for probing the structure of materials on molecular and structural length scales. For light scattering, the wavelength is about 500 nm, making light scattering ideal for probing the size of soft materials such as colloids, emulsions, polymer solutions, and surfactant solutions, all of which have structures on length scales from a few nm to a few hundred nm. Whereas, neutron scattering is best suited where light scattering measurements fail when it comes to turbid solutions such as micellar suspensions in which multiple light-scattering can occur. Moreover, small-angle neutron scattering provides information about the structure and shape of the formed aggregates in a larger q range than light scattering, therefore provides information about smaller sizes.

2.4.1. Short Scattering Theory

First, the fundamental description of scattering will be shortly given. The scattering mechanism applies to light and neutron scattering and is briefly discussed in this section. Light rays and X-rays are photons of electromagnetic radiation except for the wavelength difference and exhibit quantum mechanical wave nature. Whereas a neutron is an electrically neutral particle that has its own mass. The neutron also satisfies the wave nature since its de Broglie wavelength is $\lambda = \frac{h}{p}$, where h is the Planck's constant and p is the momentum of the neutron. For materials structure studies, λ must be equal to 1 Å and this corresponds to neutron energy of 0.08 eV. However, unlike X-ray and light rays in which scattering is entirely due to atomic electrons, neutrons are scattered entirely by the atomic nuclei. Scattering events arise radiation interaction with matter. Scattering can thereby be described as an interference phenomenon. In general, one can differentiate between elastic and inelastic scattering. In the simplest approximation assumes that atoms in the sample are in an equilibrium state and are fixed in position. Moreover, one assumes elastic scattering, where the energy remains constant by the scattering process and no energy loss occurs. Additionally, the source emits monochromatic light which means radiation with a given energy. By these assumptions, we can define the scattering vector $\vec{q}$ as the difference between the scattered light vector k_s and the incident light vector k_I. Where the refractive index is n, the wavelength is λ and the scattering angle is θ.

$$|\vec{q}| = \frac{4\pi n}{\lambda} \cdot \sin\frac{\theta}{2} \tag{2.9}$$

The scattering vector q describes a reciprocal length, respectively large structure scatters at low q and small structure scatter at high q. A scattering experiment is usually measured in terms of its intensity as a function of the scattering vector I(q). The scattering intensity is proportional to the

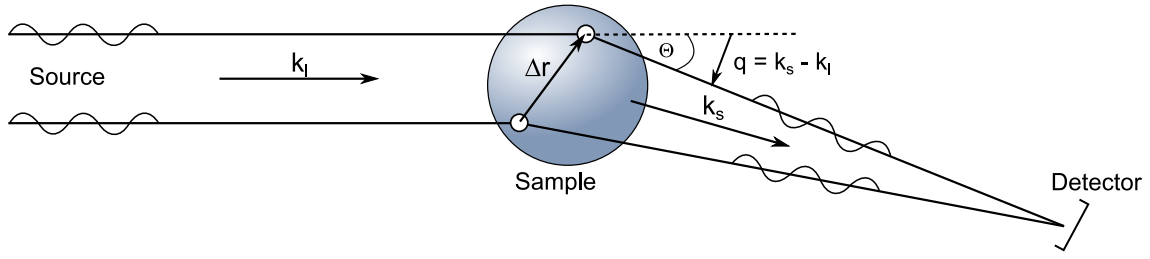

Figure 2.6: Geometrical relationship in scattering experiments. Scattering of two point scatterers in a sample with a distance Δr. The incident $\vec{k_I}$ and scattered vector $\vec{k_s}$ resulting in the scattering vector $\vec{q}$.

cross-section. It is defined as the number of radiated waves which are scattered into the angel Ω in the scattering direction 2Θ. For a three dimensional assembled system the scattering intensity (macroscopic cross-section) is defined by:

$$I(q) = \frac{d\sum_c(q)}{d\Omega} = {}^1N \cdot V_p^2 \cdot \Delta SLD^2 \cdot P(q) \cdot S(q) \tag{2.10}$$

with ^{1}N being the particle number density, V_p being the particle volume, ΔSLD the contrast of the scattering length density, and P(q) is the form factor and S(q) is the structure factor. In the following, a summary of light and neutron scattering theory and analysis is given.

2.4.2. Light Scattering

Light scattering is powerful technique when it comes to dilute systems. The scattering of light is typically 4-5 orders of magnitude stronger than the scattering of X-Rays. Moreover, light scattering is a technique usually more easy accessible than neutron or X-ray scattering which usually requires beamtime at a neutron or X-ray facility. Therefore, light scattering provides comparable information about a samples structure and therefore is a useful technique complementary to neutron or X-Ray scattering. Considering the required conditions such as low concentrations, low turbidity, and no multiscattering events.

Static Light Scattering

From static light scattering measurements an average scattering intensity can be obtained from which an average molecular weight M_w of the measured aggregates can be determined. Measurements of the scattering intensity at different angles allows us to determine the radius of gyration. The scattering intensity as a function of q can be determined by (Eq. 2.11) using the known Rayleigh ratio of toluene.

$$I(q) = \frac{\left(\frac{CR_1}{I_{mon}}\right)_{Probe} - \left(\frac{CR_1}{I_{mon}}\right)_{LM}}{\left(\frac{CR_1}{I_{mon}}\right)_{toluene}} \cdot R_{toluene} \tag{2.11}$$

The Rayleigh ratio of toluene is $R_{toluene} = 1.34 \cdot 10^{-5} cm^{-1}$. I_{mon} is the intensity of the monitor diode. The number of the count rate (CR/Imon) was measured for water. The molecular weight M_w can be calculated from the forward scattering intensity I(0), the concentration c_g and the optical constant K_L (Eq. 2.12).

$$K_L = \frac{4\pi^2}{\lambda^4 \cdot N_A} \cdot n_{solv}^2 \cdot \left(\frac{dn}{dc}\right)^2 \tag{2.12}$$

$$M_W = \frac{I(0)}{K_L \cdot c_g} \tag{2.13}$$

Where n_{solv} is the refractive index of the solvent, which for water at 25 °C is 1.33258. N_A is the Avogadro constant and λ the wavelength which is 632.8 nm for the used He-Ne laser. The refractive index increment (dn/dc) gives information about the change of the refractive index n with the concentration.

Dynamic Light Scattering

Dynamic light scattering (DLS) describes the collective diffusion of particles or aggregates in terms of intensity fluctuations. Particles or aggregates move in terms of density fluctuations (Brownian motion). These fluctuations lead to changed interferences of the scattering centers. Over time the intensity fluctuates around an average $\langle \mathrm{I} \rangle$. The intensity fluctuations can be analyzed by an auto correlation function $\mathrm{g}^2(\tau)$ of the scattered light:

$$g^2(\tau) = \frac{\langle I(t) \cdot I(t+\tau) \rangle}{\langle I(t) \rangle^2} \tag{2.14}$$

The sum of the intensities at a certain time and the intensities at a certain time plus the correlation time τ are described by the auto correlation function $g(\tau)$. For very small values of τ, $\mathrm{g}^2(\tau)$ matches $\langle \mathrm{I}^2(\mathrm{t}) \rangle$. For very large values of τ, the correlation function matches $\langle \mathrm{I}(\mathrm{t}) \rangle^2$. The normalized field auto-correlation function $g^1(\tau)$ is used, which is defined as:

$$g^1(\tau) = \frac{\langle E(t) \cdot E^*(t+\tau) \rangle}{\langle E(t) \cdot E^*(t) \rangle^2} \tag{2.15}$$

And connected to the intensity auto-correlation function by the Siegert relation[64]:

$$g^2(\tau) = B + ß \cdot g^1(\tau)^2 \tag{2.16}$$

The Siegert relation is typically used to relate the field auto-correlation function, which is generally what is calculated from theory. This can be related to the intensity auto-correlation function, which is generally what is measured experimentally. Herein lays the power of DLS because the function of the decay depends on the dynamic of the scatterers. This function can be fitted by an exponential function, depending on the system and the distribution of the particle size. Auto-correlation functions are shown in Fig. 2.7 (a). The cumulant fit function can be described as an extended exponential function, where the decay depends on the size and size distribution of the particles.

$$g^1(\tau) = e^{(-\Gamma\tau)}(1 + \frac{\mu_2}{2!}\tau^2 - \frac{\mu_3}{3!}\tau^3) \tag{2.17}$$

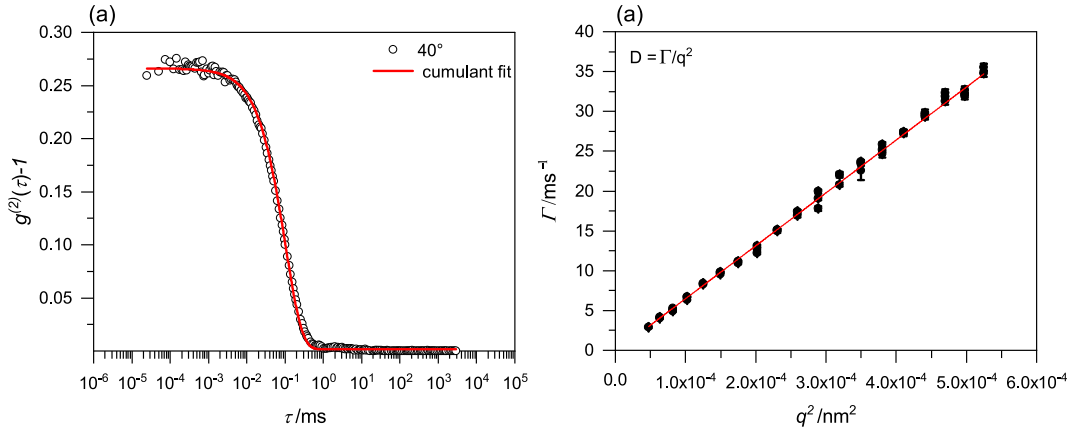

Figure 2.7: (a) Autocorrelation function of spherical micelles at an angle of 40°. $g(2)(\tau) - 1$ is plotted vs. the correlation time, τ, and fitted by a cumulant exponential fit. (b) Relaxation times Γ vs q^2 to determine the collective diffusion coefficient.

with μ_i being the ith momentum. The decay time Γ, of the fit function can be calculated for all measured angles. From Γ and q^2 the collective diffusion coefficient D_{col} can be calculated (Fig. 2.7 (b)):

$$D_{col} = \frac{\langle \Gamma \rangle}{q^2} \tag{2.18}$$

The Stokes-Einstein equation describes the relation of the hydrodynamic radius R_H and the diffusion coefficient D:

$$R_H = \frac{k_B \cdot T}{6\pi \cdot \eta_0 \cdot D} \tag{2.19}$$

The polydispersity index (PDI) can be calculated by dividing the second momentum $\langle \mu_2^2 \rangle$ by the square of the first momentum $\langle \Gamma \rangle^2$ of the distribution.

$$PDI = \frac{\langle \mu_2^2 \rangle}{\langle \Gamma \rangle^2} \tag{2.20}$$

2.4.3. Small-Angle Neutron Scattering

At the beginning of the section, a short introduction into small-angle neutron scattering (SANS) is given. This technique has become a powerful tool for structural studies. The typical length scale covered by SANS ranges from pm to µm This length scale typically represents mesoscale properties like self-assembly. In comparison to light scattering, the experiments are not easily available. They are only accessible at neutron sources or beam facilities. To mention a few: NIST (National Institute of Standards and Technology - Center for Neutron Research; USA), ISIS (UK), ILL (Institut Laue-Langevin; France), MLZ (Heinz Maier-Leibnitz Zentrum; Germany) and HZB (Helmholtz Zentrum Berlin; Germany) and LLB (Laboratoire Léon Brillouin; France) which were closed in 2019. Nevertheless, SANS is a strong method especially when light scattering techniques fail - for instance for turbid systems, or to obtain 3-D information about the shape and it is useful for contrast variation.

Neutron Properties

Neutrons are used for structural characterization because of their very specific properties which render them useful for structural studies. Neutrons are uncharged subatomic particles with a mass of $1.675 \cdot 10^{-27}$ kg. [65] Caused by their electrical neutrality they are highly penetrating, resulting in a nondestructive method to investigate three-dimensional structures. They have a wavelength of a few Å resulting in high resolutions. They can provide information in the size range of several pm up to 100 μm. Moreover, neutrons are scattered from material by interacting with the nucleus of an atom. This means that the scattering of neutrons is not strongly related to its atomic number, unlike X-rays and electrons where the scattering power increases with increasing atomic number. This results in an additional advantage, the contrast variation. By substituting some atoms by their isotope one can determine the structure of these functional groups on the background of the other molecules. Considering neutron scattering one also needs to explain coherent and incoherent scattering events. At coherent scattering, the incident neutrons are interacting with all nuclei in a sample in a coordinated fashion. Coherent scattering also contains structural information. Whereas incoherent scattering results from random events and provides information about collective

motions. The scattering of neutrons by different nuclei depends on the scattering length density (SLD) of the atoms which is isotope dependent. It quantifies the different scattering properties of the atoms in a sample. This SLD is directly proportional to the interaction potential and by that on the scattering intensity. The SLD represents the scattering length per unit volume of substance and is the sum over all atomic contributions in the molecular volume V_m.

$$SLD_{coherent} = \frac{1}{V_m} \sum_i b_{i,coherent} \tag{2.21}$$

where $b_{i,coherent}$ is the coherent scattering length of the i_{th} atom in the molecule.

SANS instruments

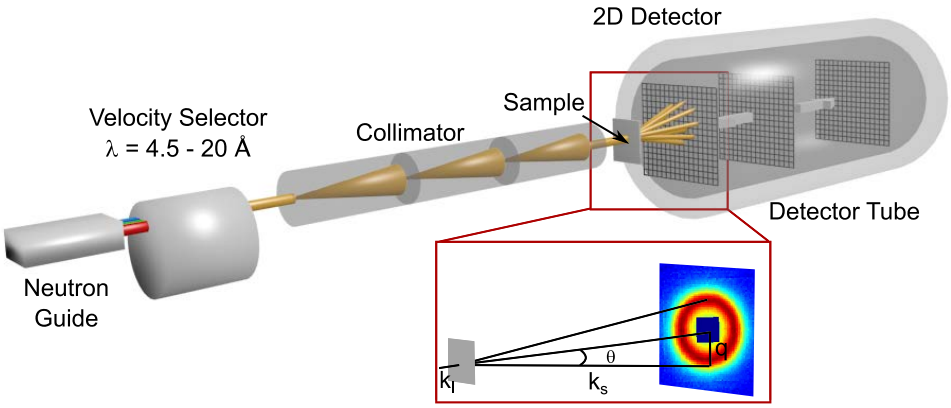

Figure 2.8: Scheme of the small-angle neutron scattering instrument. The neutrons pass from left to right. Figure is altered from [74].

In neutron scattering experiments instruments count the number of scattered neutrons as a function of scattering vector $\vec{q}$, which depends on the scattering angle Θ and wavelength λ which was already described in section 2.4.1 in Eq. 2.9. As shown in Fig. 2.8, a neutron beam is monochromated and collimated before it hits the sample. The scattered neutrons are collected in an area-sensitive detector placed at an adjustable distance from the sample. In more detail, the neurons are released from a reactor, where a nucleus chain reaction takes place. Only one part of the neutrons can be used for the scattering experiment. Cold neutrons are produced by thermalization resulting in easy transportability of neutrons which can be used for the experiment. The neutron velocity selector works mechanically and results in a monochromatic beam. The collimation determines the divergence of the beam and it usually consists of a set of apertures that converge onto the detector. A flight path contains the beam collimation system before the sample. Typical adjustable flight path distances are from 1 m to 20 m depending on resolution and intensity considerations. The sample or sample holder is placed directly behind the sample aperture and it usually can hold several samples and contains a heating and/or cooling system. The beam stop is an absorber which blocks all the unscattered neutrons which leave the sample to prevent detector damage. Only the scattered neutrons are detected by the detector at an adjustable distance depending to the q range which is wanted to be covered. The sensitive detector detects about 93% of the scattered neutrons.

2.4.4. Simple SANS Data Interpretation

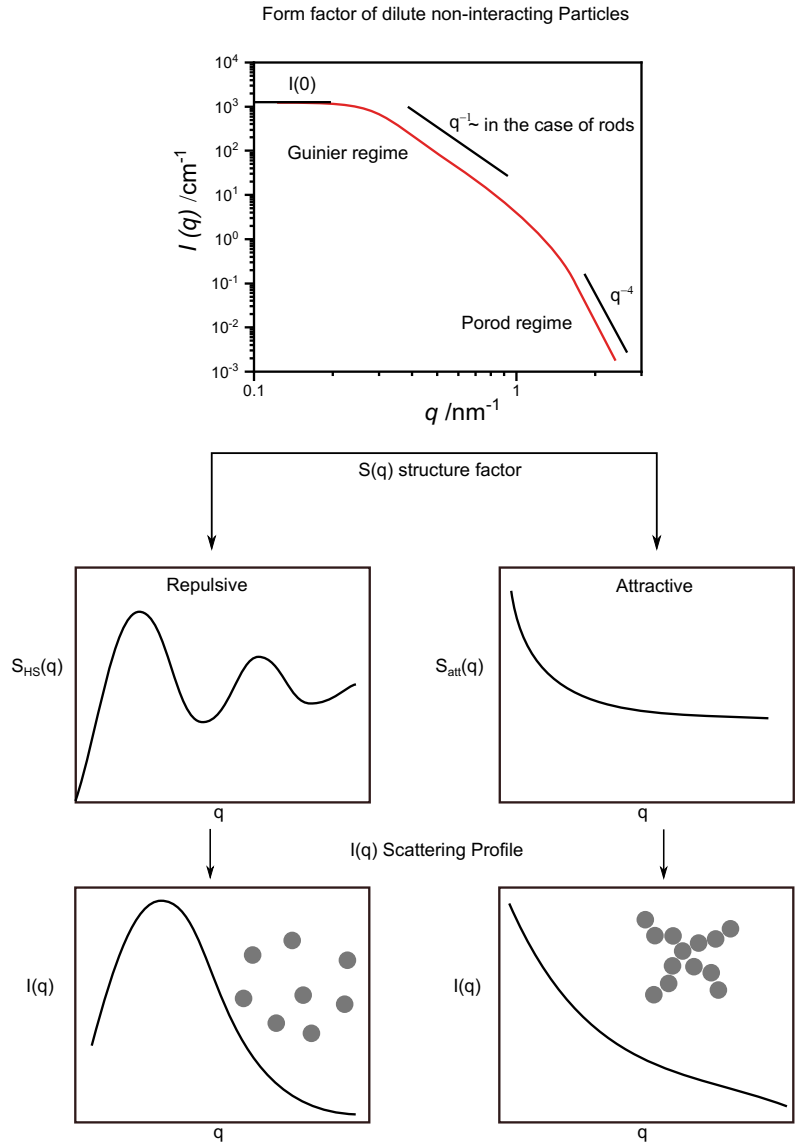

Figure 2.9: Schematic representation of the intensity I(q) and structure S(q) factors for attractive and repulsive homogeneous spheres, and their contribution to the scattered intensity I(q). Moreover, the low-q Guinier region and the high-q Porod region is shown (adapted from [66] & [75]).

In this section, the scattering of spherical micellar aggregates is shown to obtain a basic understanding of the information which can be derived from SANS data. For homogenous spherical colloidal particles with the radius R, the scattering intensity I(q) can be described as the sum of the particle number density ${}^1N$, the difference of the scattering length density of the scatterer and the solvent ($\Delta SLD = |SLD_{scatterer} - SLD_{solvent}|$), the volume of the particle V_p, and the structural depending form P(q) and structure factor S(q).

$$I(q) = {}^1N \cdot (\Delta SLD)^2 \cdot V_p^2 \cdot P(q) \cdot S(q) \tag{2.22}$$

The q independent factor in this equation can be described as the scaling factor and is based on the sample composition. The factor can also be described by the volume fraction ϕ_p of the sample and the scattering length density ${}^1N \cdot (\Delta SLD)^2 \cdot V_p^2 = \phi_p \cdot (\Delta SLD)^2 \cdot V_p$. The q dependent factors in this equation are the form factor F(q) and the structure factor S(q). These two values are dependent on the size, shape, and interaction potential of the colloidal particles. The form factor P(q) is derived

from intra-particle scattering, and the structure factor S(q) describes the inter-particle interactions. For further understanding, the factors are described in further detail in the following sections.

The first estimation of the size and shape of particles can be obtained from simple relations between I(q) and the particle radius. For forward scattering ($q \to 0$) the form factor is normalized to one. The scattering intensity $I(q \to 0)$ contains information about the effective molecular weight of the aggregates:

$$M_p = \frac{I(0) \cdot N_A \cdot \rho}{\phi_p \cdot (\Delta SLD)^2} \tag{2.23}$$

The slope of a log-log plot in the mid q regime (q^{-x}) gives information about the fractal dimension of the sample, which correlates with the shape of the particle. A power law of q^{-1} represents a rod-like structure, whereas q^{-2} represent large plane-like structures.

At the low q of the scattering plot (Fig. 2.9) the **Guinier-Approximation** is valid. It contains information about the specific particle shape and it relates to the radius of gyration R_g. For dilute systems ($S(q) \to 1$) at low q, the form factor simplifies to:

$$P(q \to 0) = 1 - \frac{1}{3} q^2 R_g^2 \tag{2.24}$$

The radius of gyration R_g is the distance of the centered mass of a particle without changed momentum of gravity. It is described by the root mean square value of the radius averaged over the particle volume, which relates to the shape of the particle. The Guinier approximation is defined as follows and varies depending on the shape of the particles:

$$I(q) = \frac{I(0)}{q^\alpha} \exp\left(-\frac{q^2 R_g^2}{3-\alpha}\right) \tag{2.25}$$

The radius of gyration represents the effective size of the scattering particle whether it is a polymer chain, a micelle or a domain in a multiphase system. The main advantage of this approximation is the independence of the static intensity I(0) and of any model. Therefore, $R_g$provides basic information of a system without any further knowledge.

• For spheres:

$$R = R_g, \alpha = 0 \tag{2.26}$$

• For rods:

$$R = \sqrt{2} R_g \;\&\; L = \sqrt{12} R_g, \alpha = 1 \tag{2.27}$$

• For planes:

$$t = \sqrt{12} R_g, \alpha = 2 \tag{2.28}$$

R is the radius of spheres or cylinders, or disc thickness t, and L is the rod length. The Guinier plot – i.e., $\ln(I(q))$ vs. q^2 (for spheres)– should includes a linear section up to the limit $qR_g < 1$. From the corresponding slope $-\frac{R_g^2}{3-\alpha}$, R_g can be determined for any isometric particles. Where the Guinier plot for rods would be $\ln(I(q) \cdot q)$ vs. q^2 and for planes $\ln(I(q) \cdot q^2)$ vs. q^2.

At high q values (Fig. 2.9), the SANS intensity is sensitive to scattering from local interfaces and intra-particle scattering. At high q one usually observes an average intensity, representing the scattering at the interface of the polymer chains for micellar aggregate for instants. One usually

observes a power law of $q^{-n_{frac}}$ depending on the interface at high q. This law is called the **Porod approximation**. For sharp interfaces the porod formula can be described as $n_{frac} = 4$:

$$I(q) = 2\pi(\Delta SLD)^2 \left(\frac{S}{V}\right) \cdot q^{-4} \tag{2.29}$$

where S/V is the interfacial area per unit volume of solution.

The porod regime can also be used to determine the incoherent background I_{bkg}.

$$I(q) = A \cdot q^{n_{frac}} + I_{bkg} \tag{2.30}$$

From the Porod slope, the probed local structure can be estimated. A slope $n_{frac} = 1$ is obtained for scattering from rigid rods; a slope $n_{frac} = 4$ represents a smooth surface for the scattering particle; whereas a slope n_{frac} between 3 and 4 characterizes rough interfaces of fractal dimension D with n_{frac} = 6-D. This is called a surface fractal. Moreover, in the case of polymer coils, the fractal exponent of the Porod regime n_{frac} is related to the excluded volume parameter ν as its inverse $n = 1/\nu$. A slope $n_{frac} = 2$ is a signature of Gaussian chains in a dilute environment, a slope $n_{frac} = 5/3$ is for fully swollen coils, and a slope $n_{frac} = 3$ is for collapsed polymer coils.[75]

The non-model approaches allow a first estimation of size and shape for dilute systems. However, these assumptions only hold for systems without interaction and if one observes a forward scattering intensity I(0). For a more advanced analysis, information about the size and shape of aggregates are obtained by fitting SANS experimental data to more complex mathematical models. This can be necessary for sample that might be unstable to dilution, or also the addition of salt may introduce structural changes.

Single Particle Form Factor P(q)

The form factor for independent spherical colloids describes the size and shape of the particles and is defined as followed:

$$P(q) = \left(3 \cdot \frac{\sin(qR) - qR\cos(qR)}{(qR)^3}\right)^2 \tag{2.31}$$

The first minimum of the form factor correlates with the radius of the spheres $q = 4.493/R$. The form factor can be simulated by different approaches depending on the observed system.

Structure factor S(q)

The inter-particle structure factor S(q) depends on the interactions in the system, i.e. attractive, repulsive interactions or excluded volume. The systematic impact of the structure factor on the scattering curve is schematically shown in Fig. 2.9. Repulsive interaction leads to an decrease of the intensity I(0) and attractive interaction can lead to an increase of I(0) which is caused by the potential. For spherical particles with low attractive interactions, a first approximation can be given by a hard-sphere potential, S_{hs}(q):

$$S_{hs}(q) = \frac{1}{1 - n_f \cdot f(R_{hs} \cdot \phi_{hs})} \tag{2.32}$$

where R_{hs} is the hard-sphere radius and $\phi_{hs} = \frac{4}{3}\pi R_{hs}^3\, ^1N$ is the hard-sphere volume fraction. The structure factor S(q) plays a major role for low and mid q values where it reduces or increases the static intensity I(0) and produces a correlation peak depending on the particle interactions.

Chapter 3

The CO_2 Surfactants

The CO_2 surfactants, whose phase behavior is the matter of this dissertation, were synthesized by the company Covestro Deutschland AG within the framework of a BMBF project called "Dream Resource" (033RC002C).[37–39] The motivation of this project is the usage of CO_2 as a resource to obtain sustainable alternatives to conventional fossil-based materials like ethylene oxide. In the following chapter, the synthesis of the CO_2 surfactants will be shortly described and an overview of the characteristic properties of the CO_2 surfactants and their reference surfactants will be given. The analysis of the CO_2 content is described, as well as the resulting composition and structure of the CO_2 surfactants. Furthermore, the application potential of the CO_2 surfactants will be discussed shortly. This chapter will provide the fundamental molecular details of the CO_2 surfactants, which will be needed for the analysis in the following chapters. The analyses of the application potential of the CO_2 surfactants, which are shown in this chapter, are mainly performed by Tupinamba Lima *et al.* and reported in the following publications.

The synthesis of the CO_2 surfactants was done by Covestro Deutschland AG. The synthesis and the main properties of the CO_2 surfactant are successfully patented:

◊ A. M. I. Stute, M. Meuresch, C. Gürtler, A. Wolf, R. Schomäcker, M. Gradzielski, M. Tupinamba Lima, V. J. Spiering (Covestro AG, Leverkusen, Germany), *WO2019076862*, **2018**.

The analyses of the structure and the application potential of the CO_2 surfactants were mainly done by Tupinamba Lima et al. and are published in the following publications:

◊ M. Tupinamba Lima, V. J. Spiering, S. N. Kurt-Zerdeli, D. Ch. Brüggemann, M. Gradzielski, R. Schomäcker: "The hydrophilic-lipophilic balance of carboxylate and carbonate modified nonionic surfactants", *Colloids and Surfaces A: Physicochemical and Engineering Aspects*, **2019**, *569*, 156-163, DOI https://doi.org/10.1016/j.colsurfa.2019.03.001.

◊ M. Tupinamba Lima, S. N. Kurt-Zerdeli, D. Ch. Brüggemann, V. J. Spiering, M. Gradzielski, R. Schomäcker: "The dynamics of surface adsorption and foam formation of carbonate modified nonionic surfactants": *Colloids and Surfaces A: Physicochemical and Engineering Aspects*, **2020**, *588*, 124386, DOI https://doi.org/10.1016/j.colsurfa.2019.124386.

3.1. Synthesis of CO_2 Surfactants

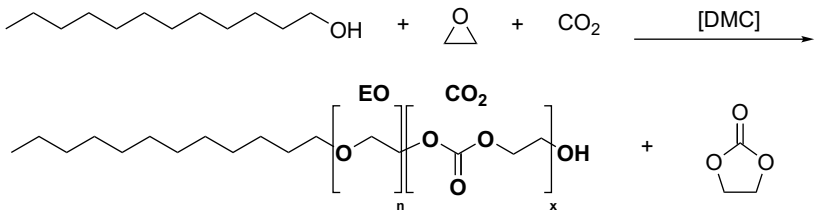

Figure 3.1: Sythesis of the CO_2 containing nonionic surfactants with a monofunctional alkyl starter, epoxide and CO_2, which react to the CO_2 surfactant by a DMC catalyst. Cyclic ethylene carbonate is a sideproduct.

The tailor-made nonionic CO_2 surfactants were produced by Covestro Deutschland AG via a double metal cyanide (DMC) catalyzed copolymerization of ethylene oxide (EO) with CO_2. A monofunctional alcohol starter with the desired n-alkyl chain length was used and the final molecular composition was controlled by the initially added amounts of EO and CO_2.[9] Dried DMC-catalyst (synthesized as described in the patent WO2012059550A1[76] and WO2019076862[77]) and 1-dodecanol (or 1-hexadecanol) were charged into a 2-L pressure reactor. The reactor was heated to 130 °C under reduced pressure (N_2, 100 mbar) for 30 minutes. Subsequently, the reactor was pressurized to 50 bar CO_2 and a defined amount of ethylene oxide was introduced. The activation of the catalyst can be observed by a temperature increase and pressure decrease. This procedure was repeated one more time. After the catalyst activation, the reactor was cooled to 100 °C and EO was introduced for 3 hours. The reaction progress was observed by the corresponding CO_2-consumption, whereas the reactor pressure was balanced to 50 bar. After completion of epoxide addition, the reactor was stirred one hour at 100 °C. Epoxide residues were removed at low pressure (10 mbar) and a colorless liquid was obtained.

Table 3.1: Summary of the M_n, unit content in %, CP (cloud point temperature) and HLB values for all surfactants for all CO_2 surfactants and the reference samples. *reported in[78]

Surfactants	Name	Supplier	M_n /g/mol	Unit /%	CP /°C	T_K /°C	HLB
$C_{12}EO_{8.2}(CO_2)_{3.1}-OH^*$	-	Covestro AG	680	19.6	69	<25	14.3
$C_{12}EO_{11.6}(CO_2)_{1.5}-OH^*$	-	Covestro AG	762	8.8	85	<25	14.9
$C_{12}EO_{11.4}(CO_2)_{1.3}-OH^*$	-	Covestro AG	744	7.8	88	<25	14.4
$C_{12}EO_{13.3}(CO_2)_{0.6}-OH^*$	-	Covestro AG	792	3.2	>100	<25	16.5
$C_{12}EO_{13.2}(PO)_{1.1}-OH$	-	Covestro AG	821	10.0	-	<25	-
$C_{12}EO_{14.7}(PO)_{0.6}-OH$	-	Covestro AG	859	5.0	-	<25	-
$C_{12}EO_{10.3}(PL)_{1.0}-OH$	-	Covestro AG	686	6.5	-	<25	-
$C_{12}EO_{14.0}-OH^*$	-	Covestro AG	802	0	>100	<25	16.4
$C_{12/14}EO_9-OH$	Marlipal 24/90	Sasol	618	0	82[1]	<25	13.4[1]
$C_{16}EO_{7.8}(CO_2)_{2.8}-OH^*$	-	Covestro AG	709	16.7	57	37	11.4
$C_{16}EO_{9.3}(CO_2)_{1.5}-OH^*$	-	Covestro AG	707	9.0	60	37	12.2
$C_{16}EO_{5.5}(CO_2)_{1.2}-OH^*$	-	Covestro AG	544	9.3	-	-	8.6
$C_{16}EO_{12.5}(PL)_{1.1}-OH$	-	Covestro AG	856	5.5	-	-	-
$C_{16}EO_{14.6}-OH^*$	-	Covestro AG	825	0	-	>100	14.5
$C_{16/18}EO_{13}-OH$	LutensolAT13	BASF	830	0	92[2]	46	12.0

[1] *Sasol* [2] *BASF*

(Description of the synthesis process by Covestro Deutschland AG as published in the supplementary information of ref. [79]) All surfactants were purified to remove other side products from the synthesis. This provides the best comparability of all surfactants. [77]

Moreover, two different types of triblock polyether carbonate polyols were produced by Covestro Deutschland AG via the same copolymerization process as described in the previous paragraph. On the one hand the triblock polyols have a PPO starter with 2000 g/mol and containing CO_2 units in their hydrophilic EO head group (EO/CO_2-PO/CO_2-EO/CO_2) or only EO in their hydrophilic head group (EO/CO_2-PO-EO/CO_2). On the other hand a PPO/CO_2 starter was used, with a molecular weight of 2000 g/mol and a CO_2 content of 18 wt% in the PPO starter block. Furthermore, a reference without CO_2 was synthesized. The starter is pure PPO with a molecular weight of 2000 g/mol and the hydrophilic head group consists only of EO (EO-PO-EO).

Table 3.2: Summary of the M_n and the CO_2 content for all surfactants for all triblock polyols and the reference samples without CO_2. *Supplier is Covestro Deutschland AG. ** Supplier is BASF.

Surfactants	Name	M_n /g/mol	Unit /%
$(CO_2)_{0.3}EO_{10.6}-PO_{30.4}(CO_2)_{8.2}-EO_{10.6}(CO_2)_{0.3}$*	EO/CO_2-PO/CO_2-EO/CO_2	2956	13.13
$(CO_2)_{3.4}EO_{31.2}-PO_{17.2}-EO_{31.2}(CO_2)_{3.4}$*	EO/CO_2-PO-EO/CO_2	4041	7.39
$EO_{27.8}-PO_{17.2}-EO_{27.8}$*	EO-PO-EO	3446	0
$EO_{43}-PO_{16}-EO_{43}$**	Pluronic F38	4700	0

3.2. Structure of CO_2 Surfactants

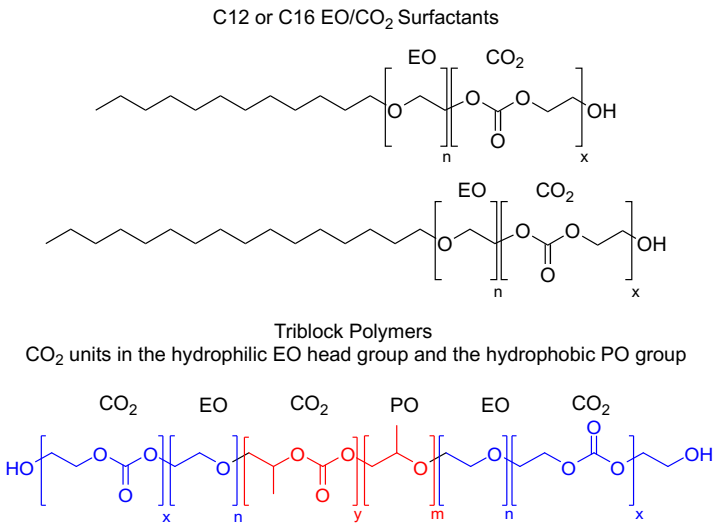

Figure 3.2: Schematic description of the structural formula of the CO_2 containing nonionic surfactants and triblock polymers.

To obtain the structural composition of the CO_2 surfactants, the CO_2 content and the molecular weight were determined. From these values the chemical structure can be obtained. Molecular weight and the CO_2 content was analyzed by Tupinamba Lima *et al.*[78] as described in the following. The molecular weight was determined by electron-spray ionization mass spectrometry (ESI-MS) measurements. The CO_2 content of the modified surfactants was determined by ATR-Infrared spectroscopy. A calibration curve was derived from mixtures of the reference

surfactant $C_{12/14}EO_9-OH$ and diethyl carbonate (DEC). The absorption at 1750 cm^{-1} was determined as a function of the carbonate weight fraction in these mixtures. The CO_2 weight fraction was calculated from the mass fraction of DEC and the ratio of the molecular weight of CO_2 (44g/mol) and DEC (118.3 g/mol). From these measurements the structure of the CO_2 surfactants was obtained as shown in table 3.1 & 3.2 and schematically depicted in Fig. 3.2. It should be mentioned here that the CO_2 units in the hydrophilic head group are arranged statistically with EO and not as blocks.

In this thesis the different C_{12} CO_2-based nonionic surfactants with varying CO_2 content in the hydrophilic head group ($C_{12}(EO)_n(CO_2)_x$-OH, called CO_2 surfactants) are studied in thorough detail and compared to surfactants with other hydrophobic units, such as propylene oxide (PO) or propiolactone ($C_{12}(EO)_n(PO)_x$-OH and $C_{12}(EO)_n(PL)_x$-OH so called PO and PL surfactants). A reference EO surfactant (only containing EO in the head group), the PL surfactant and the PO surfactants were synthesized by the same semi-batch process to compare directly the influence of the incorporated unit on the micellization properties. The characteristics of these surfactants are also summarized in Table 3.1.

The surfactants are stable against hydrolysis for a relatively long time as confirmed by corresponding experiments, where the hydrolysis stability of one CO_2 surfactant ($C_{12}EO_{11.4}(CO_2)_{1.3}-OH$) at a pH of 4, 7 and 11 was tested over 10 weeks at 25 and 60 °C, was determined by regularly measuring the surface tension and the cloud point temperature. This confirmed that at 25 °C no degradation occurs, while at 60 °C it apparently hydrolyzes to some extent and one observes larger changes than for a classical nonionic surfactant (Marlipal13/100).

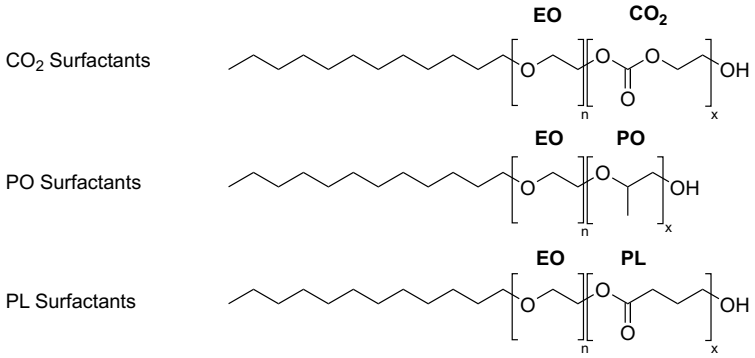

Figure 3.3: : Schematic description of the structural formula of the nonionic dodecyl surfactants. Figure adapted from Spiering *et al.*[71]

3.3. Application Potential of CO_2 Surfactants

The HLB (hydrophilic-lipophilic balance) value is an empirical parameter for nonionic surfactants established by Griffin. This parameter gives the molecular mass ratio between the hydrophilic head group containing EO units and the lipophilic alkyl chain. The resulting parameter is in the range between 0 up to 20 and classifies the nonionic surfactant for their application potential. Surfactants with an application potential in the range between 13 and 16 can be used as detergents.[80]

The HLB values of the CO_2 surfactants were analyzed and discussed in detail by Tupinamba Lima *et al.*[78] The HLB values of the CO_2 surfactants was determined by an experimental method because the HLB values from Griffin's equation only consider the EO units in the hydrophilic head

group. An experimental method was used to determine the HLB values of the CO_2 surfactants by the phase inversion temperature with a calibration by a reference surfactant with known HLB value. From an application point of view, the CO_2 modified surfactant can be considered almost as stable as the unmodified ones. The experimentally determined values are slightly higher than the values from the Griffin's method, indicating a contribution of the CO_2 unit to the hydrophilicity of the surfactants. This means the additional CO_2 units contributes to the hydrophilic head group which renders the surfactants somewhat more hydrophilic in comparison to a reference surfactant with the same numbers of EO units without CO_2. The C_{12} CO_2 surfactants show HLB value between 14 and 16.5, which renders the C_{12} CO_2 surfactants perfectly for applications as detergents. The C_{16} CO_2 surfactants are more hydrophobic, thus have HLB values between 8.6 and 12.2, which are caused by a longer alkyl chain and a reduced head group.[78] Furthermore, another important aspect of the application potential of the CO_2 surfactants is the reduced cloud point (CP). By incorporating CO_2 units in the hydrophilic head group the CP is reduced by $\approx 10\ ^{\circ}C$ per CO_2 unit.[78] This is a major advantage considering the application as detergent. Reducing the CP increases solubility at a lower temperature significantly.

To obtain a better understanding of the application potential of the CO_2 surfactants as detergent the adsorption dynamics at the water/air surface were investigated by Tupinamba Lima *et al.*[81] The dynamic surface tension was measured using the maximum bubble pressure technique. From the apparent diffusion coefficients at different concentrations, the diffusion coefficients of surfactant monomers and micelles were deduced and compared to conventional nonionic surfactants. These transport properties were correlated with results from foamability studies. The dynamic surface tension studies show that the diffusion coefficients of the CO_2 surfactants is only weakly influenced by the incorporation of CO_2 units. The obtained foam volumes show a good correlation with the diffusion coefficients of the surfactant monomers, thereby show comparable faomability. However, the stability varies significantly. The stability is drastically increased by a higher monomer diffusion coefficient introduced by a reduced head group area due to a smaller head group hydration by CO_2 incorporation.

Chapter 4

Surface Activity and Micellization Behavior of CO_2 Containing Nonionic Surfactants

The surface activity of surfactants is one of their major properties, which mainly defines their application potential. Therefore, knowledge about the surface activity of this type of surfactant is an important aspect for a complete understanding of the phase behavior. The properties of the surface activity and the thermodynamic aspect of micellization will be discussed in thorough detail in this chapter and compared in a systematic fashion to other incorporated units in the hydrophilic head group. In this chapter, surface tension measurements and isothermal titration calorimetry (ITC) were used to describe effects on the thermodynamics of micellization by substituting EO units by CO_2, polypropylene oxide (PO), or propiolactone (PL). This study was done over the temperature range of 25 to 50 °C. The critical micellization concentration (cmc) was obtained from surface tension measurements and compared in a systematic fashion to the other incorporated moieties. ITC measurements allowed to determine simultaneously the thermodynamic parameters associated with micelle formation: Gibbs energy, enthalpy, and entropy, which were compared to the values determined from the van't Hoff relation. The studies in this chapter will give an overview of the surface activity of the CO_2 surfactants and will highlight the advantages in their properties, combined with the use of CO_2 as a renewable resource.

Main parts of this chapter are based on the following publications:

◊ V. J. Spiering, A. Ciapetti, M. Tupinamba Lima, D. W. Hayward, L. Noirez, M.-S. Appavou, R. Schomäcker, M. Gradzielski: "Changes in Phase Behavior from the Substitution of Ethylene Oxide with Carbon Dioxide in the Head Group of Nonionic Surfactants", *ChemSusChem*, **2020**, *13*, 601-607, DOI https://doi.org/10.1002/cssc.201902855.

◊ V. J. Spiering, J. Lutzki, M. Gradzielski: "Thermodynamics of Micellization of Nonionic Surfactants – The Effect of Incorporating CO_2 Moieties into the Head Group", *Journal of Colloid and Interface Science*, **2020**, *581*, 794-805, DOI https://doi.org/10.1016/j.jcis.2020.07.141.

4.1. Introduction

Nonionic surfactants are widely used with their main general applications in the household industry. Therefore, they are used in a wide range of applications and are large scale commodity products. Alkyl oligoethyleneoxide ether type (C_iE_j) surfactants, also known as alkyl ethoxylates, are employed in a wide range of applications, like detergency and formulations in cosmetics or pharmacy.[46] The hydrophilic head group is based on fossil-based raw material. Typical nonionic surfactants include alkyl oligoglycol ethers and ethoxy-/propoxylates, which form so-called niosomes.[82] Their physical properties can be varied by the length of the alkyl and the EO chain and temperature, thereby the corresponding HLB value indicates their potential applications (e.g. detergency, emulsion stabilizers).[46, 83] Thus, much research has been dedicated toward the design, development, and analysis of novel surfactant structures with improved properties and functionalities. In order to modify the properties (e.g. the hydrophilic-lipophilic balance, HLB), other units such as propylene oxide (PO) or 1,2-butylene oxide (BO) can be included in the ethylene oxide (EO) chain.[84, 85]

In the context of promoting more sustainable chemistry and employing more 'eco-friendly' products, it is interesting to substitute at least parts of the hydrophilic head group with ones derived from a non-oil-based resource. Options include alkyl polyglycosides, alkylglucuronamides[86, 87] or alkyl oligoglycerides[88, 89], which are much less temperature sensitive than alkyl ethoxylates and have already been employed in applications based on their ability for solubilization.[90–92] Additionally, introducing chemical moieties into the chemical surfactant structure can result in a substantial variation of the physico-chemical properties and thereby modify the application spectrum. For instance, nonionic alkyl-N-methylglucamines (MEGA-n) which have an amide group between the hydrophobic alkyl chain and the hydrophilic head group show distinct features, as observed by Okawauchi *et al.*[93]. Due to this structural feature, MEGA-n surfactants do not have a cloud point even if the solutions are heated up to the boiling point and large amounts of salt are added. This shows an adjustment of the properties by the change of chemical structure of a surfactant.

As explained in the previous chapter, a technology was developed to copolymerize fossil-based alkylene oxides with the abundant resource CO_2.[17, 94] The technique has also been used to investigate the copolymerization of ethylene oxide and CO_2, giving rise to compounds such as CO_2-containing fatty alcohol surfactants. Based on this new method, different CO_2-containing dodecyl ethoxylate surfactants were synthesized.[77] The application potential of these nonionic surfactants was already investigated with respect to their HLB values by Tupinamba Lima *et al.* and they were found to be suitable for detergency as shown in the previous chapter.[78, 81] Frey *et al.*[36] also developed a method to use CO_2 as a carbon feedstock and copolymerized degradable aliphatic polycarbonate diblock copolymers (mPEG-b-PBC). CO_2 is incorporated into the PBC block, which is influencing the physical properties of the block copolymers and thereby increasing their efficiency. The HLB values of these types of surfactants are in the range between 9 and 16, indicating a suitable application as emulsifier or foam stabilizer. This study shows, that the abundant resource CO_2 can be used in various polymer systems to obtain sustainable alternatives for a broad range of applications.

In this chapter, the main focus will be on the direct impact of the modification of the hydrophilic head group by hydrophobic units on the thermodynamic details of micellization. For that purpose, the effect of the CO_2 unit on the micellization process was compared to that of PO or PL units. Their surface tension was measured to derive the surface activity and the cmc. Moreover, from temperature dependent surface tension measurements thermodynamic properties (van't Hoff enthalpies) of the micellization process in aqueous solution can be obtained and compared systematically to a conventional C_iE_j surfactant. To enhance the understanding of the micellization process, ITC measurements were performed, which yield direct thermodynamic information on the micellization behavior. The outcome of both approaches is compared critically and discussed in detail with respect to the impact of different units incorporated into the EO head group on the micellization process.

4.2. Experimental Section

4.2.1. Surface tension measurements

The theoretical background of this technique and the surface activity of surfactants is given in previous chapters 1.3 and 2.1. Surface tension measurements were done using a Du Noüy ring on a DCAT tensiometer (Data Physics) at 25, 30, 40 and 50 °C. The temperature was maintained by a circulating thermostat with prior heating of the surfactant solution in an oven and an equilibration time of 20 min. The surface tension was measured until the value remained constant for a given period, as defined by the measurement software (typically 350 s). The measured average surface tension was determined for each sample in a concentration range from 10^{-5} *wt%* up to 0.2 *wt%* and plotted as a function of logarithmic concentration. The critical micelle concentration (cmc) was determined by calculating the point at which the surface tension reaches a constant plateau value. In addition, the surface tension measurements were used to determine the surface excess concentration, Γ, and the head group area a_0, using the Langmuir-Szyszkowski isotherm: [45]

$$\sigma = \sigma_0 - RT\Gamma \cdot \ln(1 + K \cdot c) \tag{4.1}$$

where σ is the surface tension, σ_0 the surface tension of water (72.8 mN/m at 298 K), R the ideal gas constant (8.314 J/K·mol), T the temperature, Γ the surface excess concentration, K the absorption constant, and c is the concentration. The head group area a_0 is related to the surface excess concentration Γ by the Avogadro constant, N_A, by:

$$a_0 = \frac{1}{\Gamma \cdot N_A} \tag{4.2}$$

According to the phase separation model[95] and the mass action model[96], the standard Gibbs free energy of micellization per mole of monomer ΔG_{mic} is given by:

$$\Delta G_{mic} = RT \cdot \ln x_{cmc} \tag{4.3}$$

where x_{cmc} is the mole fraction of surfactant in aqueous solution at the cmc (assuming ideal behavior). From the temperature dependence of the cmc, the enthalpy ΔH_{mic} of the micellization

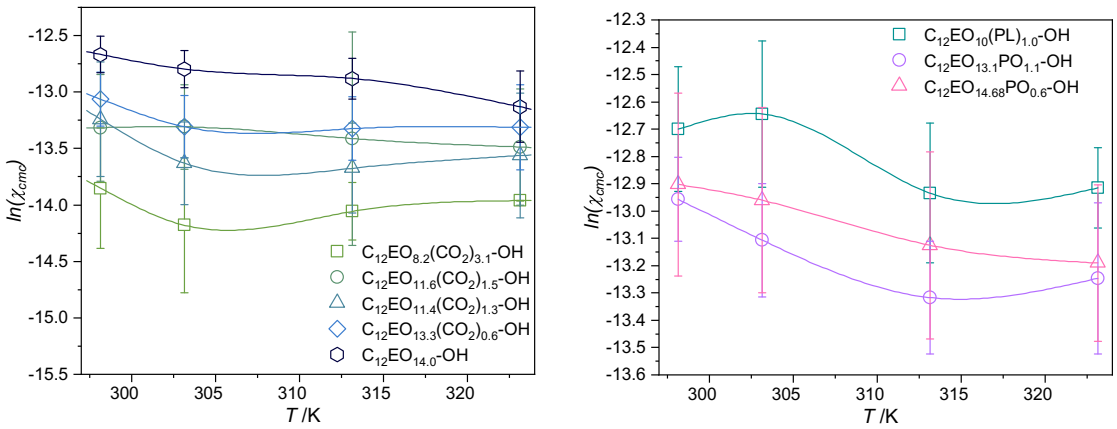

Figure 4.1: Spline function of the logarithm of the mole fraction of the cmc $ln(\chi_{cmc})$ as a function of the temperature for the CO_2 surfactants (a) and the PL and PO surfactants (b).

can be obtained. Therefore, the $\ln(x_{cmc})$ vs. T curve was fitted by a spline function of third order (see Fig. 4.1) and the first derivative of it gave ΔH_{mic}.

$$\Delta H_{mic} = -T^2 \frac{\delta(\Delta G_{mic}/T)}{\delta T} = -RT^2 \frac{\delta \ln(x_{cmc})}{\delta T} \tag{4.4}$$

Once ΔG_{mic} and ΔH_{mic} are known, the entropy of micellization ΔS_{mic} can be determined by the Gibbs-Helmholtz equation:

$$\Delta S_{mic} = \frac{1}{T}(\Delta H_{mic} - \Delta G_{mic}) \tag{4.5}$$

4.2.2. Isothermal titration calorimetry (ITC)

Isothermal titration calorimetry (ITC) measurements were done with a NanoITC 2G (TAinstruments) at 25, 30, 40 and 50 °C. The surfactants syringe concentration was 10 x cmc and was injected into the cell, containing degassed and filtered milliQ water (initial cell volume 950 µL) under continuous stirring of 150 RPM. The system was equilibrated for up to 9000 s. The surfactant solution was injected into the cell with a total number of 22 injections with an injection volume of 10.01 µL (first and last injection 2.01 µL). The reference cell was filled with degassed filtered milliQ water. The resulting heat rate (μJ/s) per time (s) was evaluated with the program NanoAnalyze Data Analysis version 3.11.022 taking into account the water file and baseline subtraction. For each temperature, degassed milliQ water was measured to subtract the heat rate from the water titration. Furthermore, for each file the baseline was subtracted individually and the water correction was done by area correction with the program NanoAnalyze. The measured heat flow caused by the injection of the surfactant was obtained by integrating the titration peaks as already described in chapter 2.2 (detailed visualization of the data treatment is shown in the Appendix Chapter 4 Fig: 10.2):

$$\int_i^{i+1} q = \Delta H_i \tag{4.6}$$

ΔH is related to the amount of molecules n, titrated into the sample cell per injection:

$$\Delta H_{m,i} = \frac{\Delta H_i}{n} \tag{4.7}$$

Plotting $\Delta H_{m,i}$ vs. the surfactant concentration, a typical calorimetry titration curve was obtained as already shown in chapter 2 Fig. 2.2B. ITC curves were analyzed using the mass-action model,[61, 68–70] It is valid for systems with low aggregation number N_{agg} and is also used to calculate the thermodynamic parameters (ΔG_{mic}, ΔS_{mic}). The shape and profile of the curves are dependent on different factors such as, surfactant concentration, aggregation number, counter ion binding, solvation–desolvation, temperature, and micellar shape. The titration curve can be divided into three different regimes which were described in the theoretical chapter 2.2 of this thesis. As shown there, the micellization enthalpy ΔH_{mic} was obtained by the pre-micellar region ST (start of transition I) and of the post micellar region ET (end of transition III). By taking the difference of these values one obtains ΔH_{mic}:

$$\Delta H_{mic} = ET - ST = -\Delta H_{demic} \tag{4.8}$$

The enthalpy of micellization according to Eq. 4.8 was determined by two different methods depending of the shape of the enthalpogram. The first method was used for curves following a sigmoidal curve. This was observed for lower temperatures for the CO_2 surfactants, and always for the PO/PL surfactants and the reference surfactant ($C_{12}EO_{14.0}-OH$). These curves were fitted with a sigmoidal logistic function, written as:

$$\Delta H = \frac{ST - ET}{1 + e^{(c-cmc)/\Delta cmc}} + ET \tag{4.9}$$

with the start of transition ST and end of transition ET, from which the enthalpy of micellization ΔH_{mic} was calculated by Eq. 4.9, and Δcmc giving the width of the micellar transition. The second method was applied for enthalpograms, which do not show a typical sigmoidal curve. In this chase, a different approach was used to analyze the data as described in the following. Linear fits of the data sets in the lower and upper concentration regime were performed (Fig. 2.2B: ET and ST dotted lines). ΔH_{mic} can be determined by the difference of the interpolated linear fits of the pre-micellar region ST (start of transition I) and in the post micellar region ET (end of transition III) at the cmc. This data treatment is analogous to the one suggested by Loh *et al.*[61]. Cmc values were determined by the maximum value of the first derivative of the titration curve Fig. 2.2C.

4.3. Results & Discussion

4.3.1. Surface Activity of CO_2 Containing Nonionic Surfactants

Starting with the characterization of surfactants, one of the main properties is their surface activity and the critical micelle concentration (cmc), which can both be determined from surface tension measurements. The surface tension as a function of the concentration of all four CO_2-containing surfactants was measured with a ring tensiometer. The obtained curves are shown in Fig. 4.2 and have a similar shape with a small shift of the CO_2 surfactants towards lower concentrations. The CO_2 surfactant with the highest CO_2 content ($C_{12}EO_{8.2}(CO_2)_{3.1}-OH$) has a cmc value of 0.053 mmol/L and in comparison the reference surfactant ($C_{12}EO_{14.0}-OH$) without CO_2 has a cmc of 0.175 mmol/L. This shift to lower cmc values indicates an increase in hydrophobicity with increasing CO_2 content. This finding indicates already a further introduction of a tuning parameter by introducing CO_2 units in the hydrophilic head group. The cmc, the headgroup areas a_0

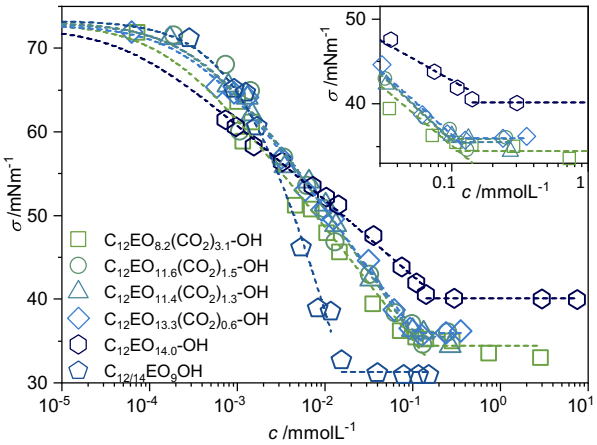

Figure 4.2: Surface tension σ as a function of concentration for the CO_2 surfactants: $C_{12}EO_{8.2}(CO_2)_{3.1}-OH$, $C_{12}EO_{11.6}(CO_2)_{1.5}-OH$, $C_{12}EO_{11.4}(CO_2)_{1.3}-OH$, $C_{12}EO_{13.3}(CO_2)_{0.6}-OH$ and the reference sample $C_{12}EO_{14.0}-OH$and Marlipal 24/90 $C_{12/14}EO_9-OH$ at 25 °C. Inset shows the regime of the surface tension vs. the concentration at the cmc. Where the slope changes from the decreasing regime to the plateau regime. Figure is reproduced from ref. [79].

(calculated from Eq. 4.2) and the free energy of micellization, ΔG_{mic} (calculated from Eq. 4.3) of the different surfactants are summarized in Table 4.1.

The obtained cmc values of the CO_2 surfactant are lower compared to other nonionic C_{12}-surfactants with the same monomer units in the head group at 25 °C. As a comparison, $C_{12}EO_5$ has a cmc of 0.064 mmol/L[97] and with increasing EO units the cmc is also increasing, so $C_{12}EO_8$ has a cmc of 0.109 mmol/L.[97] Also other nonionic surfactants such as n-dodecyl-β-D-glucoside have cmcs, which are slightly higher, with 0.19 mmol/L.[98] The lowering of the cmc for the CO_2 surfactants in comparison to reference nonionic surfactant indicates an increase of hydrophobicity.

The surface tension of the CO_2 surfactants at 25 °C at the cmc was found to be between 34.4 up to 35.9 mN. This is in the expected range for $C_{12}EO_j$ nonionic surfactants.[99–101] It should be mentioned, that there is a systematic decrease in surface tension with increasing CO_2 content, which indicates an increase in efficiency. The properties of the CO_2 surfactants were also compared to a commercial reference sample, which is already used in applications such as Marlipal 24/90 from Sasol ($C_{12/14}EO_9$-OH; properties summarized in Table 3.1).

Table 4.1: Summary of the surface tension measurements: critical micelle concentration cmc, surface tension σ_{cmc} at the cmc, head group area a_0, and Gibbs free energy of micellization ΔG_{mic}.

Surfactants 25 ° C	**cmc** /mmol/L	σ_{cmc} /mN/m	a_0 /nm^2	ΔG_{mic} /kJ/mol
$C_{12}EO_{8.2}(CO_2)_{3.1}-OH$	0.053	34.4	0.55	-34.3
$C_{12}EO_{11.6}(CO_2)_{1.5}-OH$	0.091	35.9	0.65	-33.0
$C_{12}EO_{11.4}(CO_2)_{1.3}-OH$	0.099	35.5	0.67	-32.8
$C_{12}EO_{13.3}(CO_2)_{0.6}-OH$	0.118	35.9	0.69	-32.4
$C_{12}EO_{10.3}(PL)_{1.0}-OH$	0.169	36.2	0.68	-31.5
$C_{12}EO_{13.2}(PO)_{1.1}-OH$	0.131	37.6	0.90	-32.1
$C_{12}EO_{14.7}(PO)_{0.6}-OH$	0.138	38.8	1.02	-32.0
$C_{12}EO_{14.0}-OH$	0.175	40.1	1.07	-31.4
$C_{12/14}EO_9$-OH	0.028	32.8	0.39	-35.9

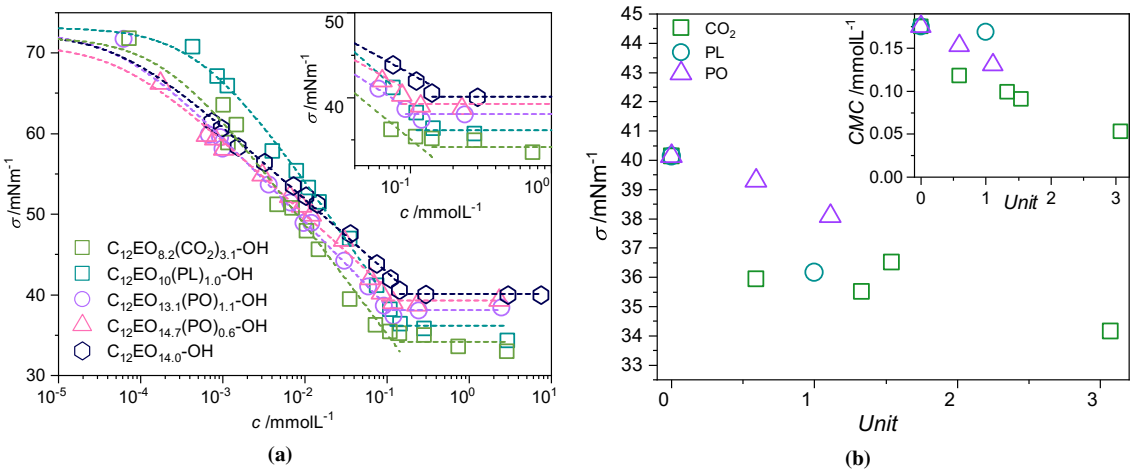

Figure 4.3: (a) Surface tension σ as a function of concentration: $C_{12}EO_{8.2}(CO_2)_{3.1}-OH$, $C_{12}EO_{10.3}(PL)_{1.0}-OH$, $C_{12}EO_{13.2}(PO)_{1.1}-OH$, $C_{12}EO_{14.7}(PO)_{0.6}-OH$ and the reference sample $C_{12}EO_{14.0}-OH$ at 25 °C. Inset shows the regime of the surface tension vs. the concentration at the cmc. The slope changes from the decreasing regime to the plateau regime, indicating the cmc. (b) The surface tension σ at the cmc in dependency on the number of incorporated units. Inset shows the decreasing cmc per incorporated unit. Figure is reproduced from ref. [71].

The commercial reference surfactant shows also a reduced surface tension value with 33 mN/m and a cmc of 0.028 mmol/l as shown in Table 4.1. This reduction of the surface tension and the lower cmc also indicate a higher effectivity and efficiency such as the CO_2 surfactants. This phenomenon may be explained by the fact that this surfactant contains a mixture of C_{12} and C_{14} chains, as opposed to the other surfactants that contain only C_{12}. This mix of alkyl chains could also explain the lower head group area. As explained by Folmer *et al.*, the higher the polydispersity of the hydrophobic and hydrophilic tail, the lower the head group area.[102] For example, the head group area of $C_{12/15}EO_7$-OH was found to be 32 Å^2, whereas that for pure $C_{12}EO_7-OH$ is 57 Å^2.[97] In summary, the CO_2 containing surfactants are having a lower cmc, which means for many applications that one can reduce the required amount, and they also show lower surface tension values above the cmc, as typically desired for surfactants.

Furthermore, the influence of the incorporated CO_2 moiety was compared to other incorporated units to obtain a deeper understanding of the influence of an additional moiety in the hydrophilic head group on the surface active behavior of the surfactants. This study is mainly discussed in an article, which is published in the *Journal of Colloid and Interface Science*.[71] The incorporation of CO_2 units leads to a reduced cmc and lower values of the surface tension above the cmc, as already discussed above. For a comparison to the CO_2 surfactants, the surface tension curves of the surfactants with PO and PL incorporated in the hydrophilic head group are shown in Fig. 4.3a. One can observe that the surface tension at the cmc is lowered by the incorporation of PO or PL units but the impact is smaller than for the incorporation of CO_2 units. This trend becomes more clearer in Fig. 4.3b. The surface tension σ is linearly reduced by the number of incorporated units of the hydrophobic moieties. The incorporation of CO_2 has the highest influence. The presence of one CO_2 or PL unit in the head group reduces the surface tension by ~ 4 mN/m, whereas the incorporation of one PO units leads only to a reduction by ~ 2 mN/m. Interestingly, the effect is independent of the number of CO_2 units incorporated and only for the highest CO_2 content a lower value is observed. In general, all modifications lead to a reduction of surface tension compared to the reference surfactant ($C_{12}EO_{14.0}-OH$), but clearly, a higher efficiency is observed for the CO_2 and PL surfactants in comparison to the PO surfactants.

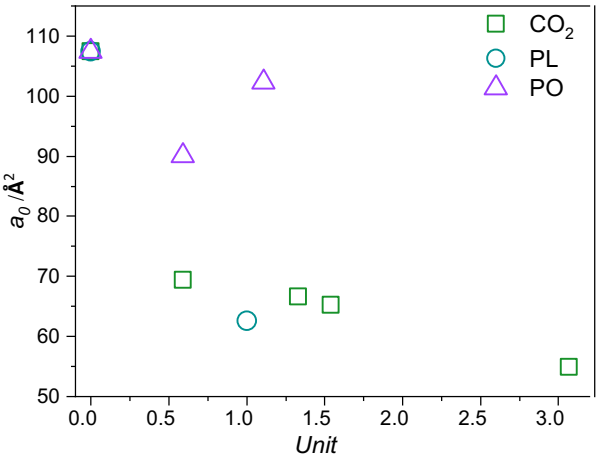

Figure 4.4: Head group area a_0 as a function of the incorporated unit fur the CO_2 ,PL and PO surfactants at 25°C. Figure is reproduced from ref. [71].

Besides the surface tension, also the cmc is lowered for all surfactants with incorporated units in the hydrophilic head group. However, the surfactant with the highest PO content ($C_{12}EO_{13.2}(PO)_{1.1}-OH$) has a cmc of 0.138 mmol/L, just slightly lower than that of the reference surfactant ($C_{12}EO_{14.0}-OH$) with 0.175 mmol/L (Fig. 4.3a). Yada *et al.*[85, 103] have reported, that alkyl ether type nonionic surfactants with a PO unit added at the end of the hydrophilic head group have a prominent effect of lowering the cmc and increase the surface activity as well as modify the aggregation behavior. By adding only one PO unit at the EO end of a $C_{12}EO_8$ surfactant, the cmc is already reduced drastically ($C_{12}EO_8PO_1$: 0.031 mM; $C_{12}EO_8$: 0.102 mM).[85] This impact is much larger than in the case of this work, where the PO group is randomly contained in the EO block, which demonstrates that the precise molecular architecture of the surfactant head group is very important for the cmc value. In comparison, the incorporation of the PL unit has only little effect on the cmc. In contrast, the CO_2 incorporation has a very prominent effect on the cmc and lowers it systematically with increasing CO_2 content, which is shown in Fig. 4.3b. The cmc values, the head group areas, a_0, and the free energy of micellization, ΔG_{mic} of the different surfactants are also summarized in Table 4.1.

Moreover, the head group area a_0 of the surfactants are also changing systematically with the type and number of the incorporated moiety. It was observed that the head group area decreases with increasing content, thereby rather jump-wise once CO_2 is present (see Fig. 4.4). This decrease can be explained by an enhanced hydrophobicity and a reduced hydration. The head group area a_0 decreases substantially with increasing CO_2 content. This decrease can be explained by a reduced hydration of the head groups. A similarly reduced head group area is seen for PL incorporation while the PO unit leads only to a small decrease. This phenomenon indicates a similar reduced hydration behavior of the head groups. Therefore, the CO_2 unit and the PL unit renders the surfactants less hydrated and reducing the head group area prominently, while PO is only somewhat less hydrated and therefore shows similar head group areas as the reference surfactant $C_{12}EO_{14.0}-OH$.

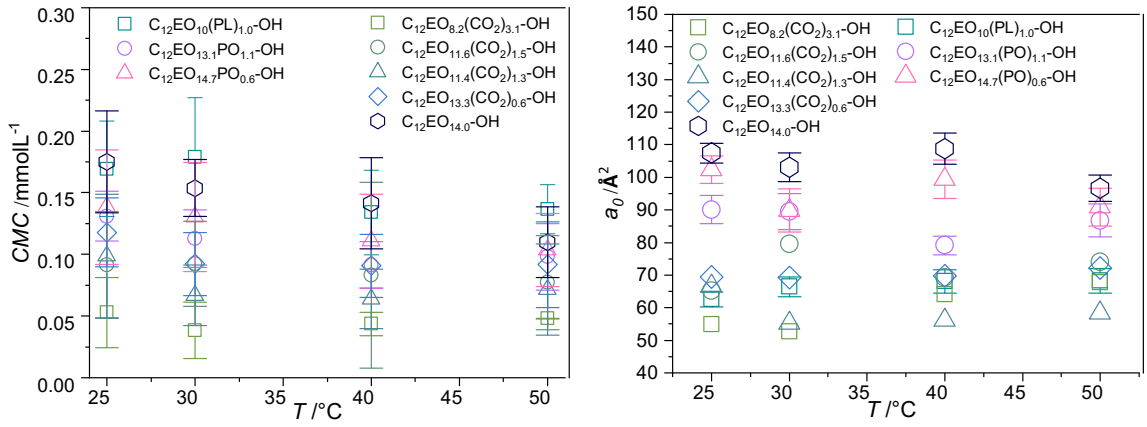

Figure 4.5: Temperature dependen cmc values (a) and head group areas (b) of all surfactants at 25, 30, 40 and 50 °C. Figure is reproduced from ref. [71].

Temperature Dependent Surface Tension Measurement

Ethylene oxide surfactants are known for their temperature dependent aggregation behavior.[97] Thus, it is important to investigate the surface activity depending on the temperature. The surface tension was measured at 25, 30, 40, and 50 °C. All the data of the temperature dependent surface tension measurements are summarized in the Appendix Chapter 4 and the corresponding cmc and head group area values are represented in Fig. 4.5. For nonionic surfactants, the cmc usually decreases with increasing temperature, which is caused by the reduction of hydrogen bonds between the water molecules and the surfactant hydrophilic group, rendering them more hydrophobic. This behavior is fairly typical for nonionic surfactants.[46] The cmcs of both the CO_2-containing surfactants and the reference sample exhibit similar trends. They initially decrease to a minimum at 30-40 °C and then increase at higher temperatures (Fig. 4.5a). This tendency can also be found among the surfactants with incorporated PO units.

The head group area a_0 for the PO and pure EO surfactants decrease somewhat with increasing temperature, which can be attributed to decreasing hydration of the head group and the increased probability of the more unpolar a-a-a-conformation, as described in chapter 1.3. A similar trend has been observed for other nonionic surfactants like MEGA-10.[104] In comparison, the CO_2 surfactants show rather constant values and the one with the highest CO_2 content ($C_{12}EO_{8.2}(CO_2)_{3.1}-OH$) even a prominent increase for higher temperatures (Fig. 4.5b). This one might be explained by the fact that hydration is already low and at higher temperaturess the larger thermal agitation and configurational change of the head group moieties can explain an increase of a_0.[97] Moreover, the configuration of the EO units is disrupted by the presence of the incorporated unit such as CO_2.

4.3.2. Thermodynamics of Micellization - the van't Hoff Isotherm

From the temperature dependent surface tension measurements, the thermodynamic parameters were calculated using the van't Hoff relation (Eq. 4.4, 4.5). The Gibbs energy ΔG_{mic} is determined by the cmc (Eq. 4.3) and generally decreases with increasing temperature (Fig. 4.6a). Even though the trend is the same for all nonionic surfactants, the CO_2 surfactants show lower values in comparison to the reference surfactant ($C_{12}EO_{14.0}-OH$). Thereby, the PO surfactants show

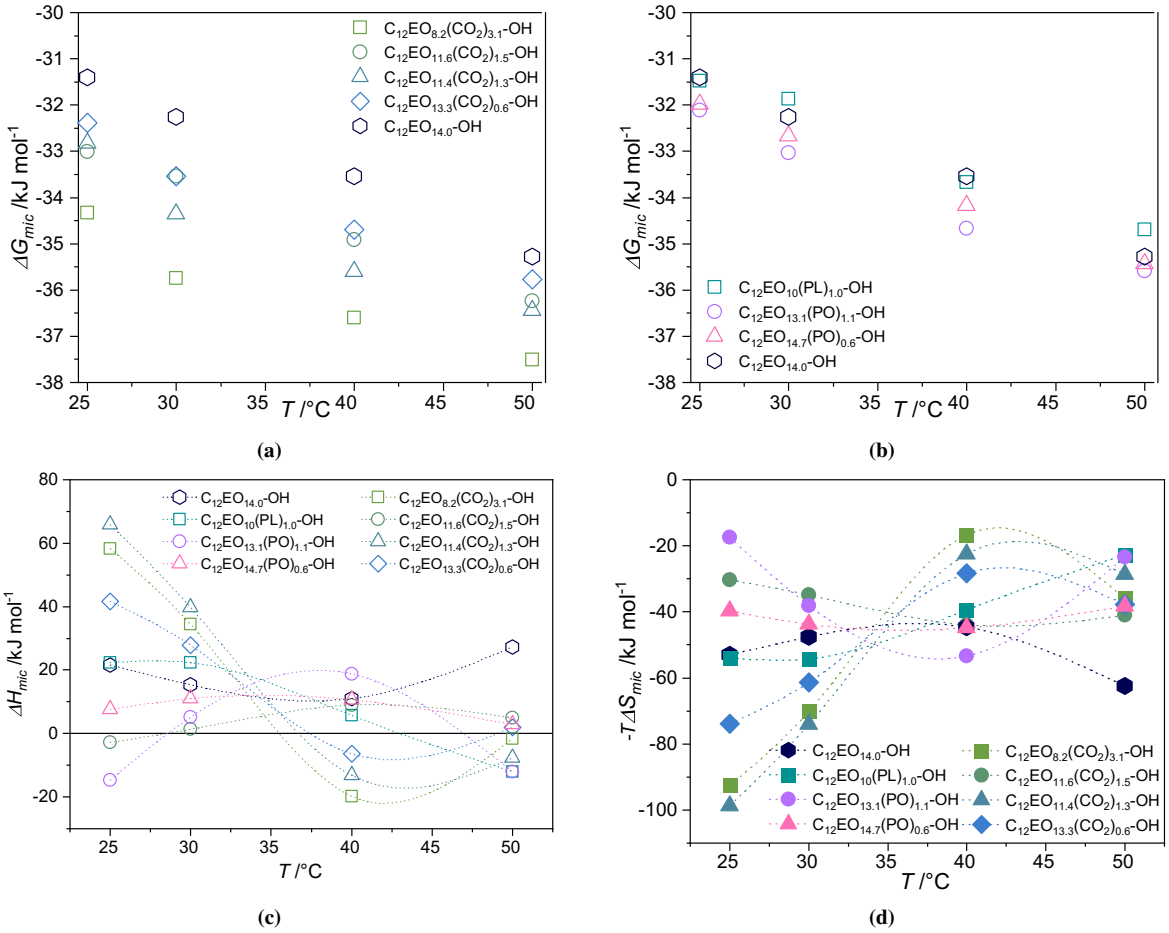

Figure 4.6: Top: Gibbs energy ΔG_{mic} depending on the temperature for all CO_2 surfactants (a) and the PO and propiolactone surfactants (b) obtained from surface tension measurements. Bottom: enthalpy of micellization ΔH_{mic} (c) and entropy of micellization $-T\Delta S_{mic}$ (d) values for all surfactants obtained from the van't Hoff relation. Lines are guides to the eye. Figure is reproduced from ref. [71].

comparable values like the pure EO surfactant, in contrast to the PL surfactant, which generally behaves more to the CO_2 surfactants (Fig. 4.6b).

Besides ΔG_{mic}, also enthalpy ΔH_{mic} and entropy ΔS_{mic} of micellization can be determined from the change of the cmc as a function of temperature (as described in the experimental section 4.2.1; see Fig. 4.1) and are given in Fig. 4.6c and 4.6d. From the van't Hoff evaluation, one can observe that the micellization process at 25 °C for all surfactants is an endothermic process with values for ΔH_{mic} ranging between 65 – 42 kJ/mol for the CO_2 surfactants and ranging from -14.7 kJ/mol for the PO surfactant with the highest PO content ($C_{12}EO_{13.2}(PO)_{1.1}-OH$) up to 22.3 kJ/mol for the surfactant with the PL unit ($C_{12}EO_{10.3}(PL)_{1.0}-OH$). The reference sample without any incorporated units $C_{12}EO_{14.0}-OH$ is 21.7 kJ/mol.

At lower temperatures, the entropy of micellization ΔS_{mic} is substantially higher for the CO_2 surfactants, which may be explained by the fact that they have fewer water molecules confined in their head group volume. With increasing temperature the micellization process becomes more exothermic, therefore an increase of ΔS_{mic} with increasing temperature can be observed. Only for the highest temperature of 50 °C it is increasing again. Somewhat similar behavior is seen for the PL surfactant, while for the other surfactants (PO and pure EO) ΔS_{mic} changes only slightly. The van't Hoff relation shows results with some tendencies for the thermodynamic interpretation of the CO_2 incorporation in terms of temperature dependency. One needs to consider high discrepancies

from the van't Hoff evaluation occurring from the derivation of the cmc values. However, a fundamental tendency of the micellization process of the modified surfactants can already be observed.

4.3.3. Thermodynamics of Micellization - Isothermal Titration Calorimetry (ITC)

To obtain deeper insights into the thermodynamic impact of the incorporation of the different hydrophobic units in the hydrophilic head group, ITC measurements were used. This method also provides a direct measure of the micellization enthalpy in comparison to the van't Hoff analysis. First information about the micellization process can be determined from the enthalpogram. The titration curves of the nonionic surfactants show significant differences depending on the incorporated unit. The data were normalized to provide a better comparison. The normalized data are shown in Fig. 4.7 (in the Appendix Chapter 4 in the section ITC Measurements the complete series of measurements is shown and the obtained values are summarized in Table 10.7). The CO_2 surfactants and the one with PL show a much broader and less sigmoidal curve than the pure EO surfactant. The shape of the curve varies systematically with the CO_2 content and, as expected, approaches the sigmoidal curve of the pure EO surfactant with decreasing CO_2 content. The PO surfactants behave comparable to the reference sample and show a sigmoidal shape (Fig. 4.7b). The similarity of the micellization behavior of the PO surfactants and the reference surfactant was already observed from surface tension measurements and can be validated by the ITC measurements.

It is known that, the shape and profile of the curves depend on different factors like the aggregation number, size distribution, solvation-desolvation, temperature, and micellar shape.[61, 105] Example curves of a normalized enthalpogram as a function of a normalized dimensionless concentration with different aggregation numbers is shown in Fig. 4.7b inset. These curves were determined by the following equation:[70]

$$\frac{\Delta H}{-\Delta H_{mic}} = \frac{1}{1+\bar{S}_{tot}^{n-1}} \tag{4.10}$$

The aggregation number influences the shape of the enthalpogram. With increasing aggregation number the shape becomes more sigmoidal, whereas, with decreasing aggregation number, the ITC curve becomes very broad and no transition can be observed anymore. Comparing to the experimental data, this description seems to be reasonable for the pure EO surfactant, but for the CO_2 surfactants one would end up with unrealistically small aggregation numbers. Lah *et al.*[106] investigated the structural correlation between the aggregation number and the ITC curves, which were in good agreement in the case of ethoxylate surfactants. In contrast, for bile salts (deoxycholate) it is known to have a significant broad region at the cmc.[68] Another reason for the change in the shape of the ITC curve could be impurities as shown for a series of Triton-X[105]. In this case, the micellization range can be very large and does not represent the aggregation number. Apparently, in the case of the CO_2 and PL surfactants, the broad ITC curves could also not be attributed to low aggregation numbers, since we know from scattering studies that they are in the range of 29 to 80 for the CO_2 surfactants (will be discussed in chapter 5).[79] Moreover, impurities can also not be the reason for the broad transition because all surfactants were prepared in the same fashion. An explanation for this rather continuous transition could be that the additional striking

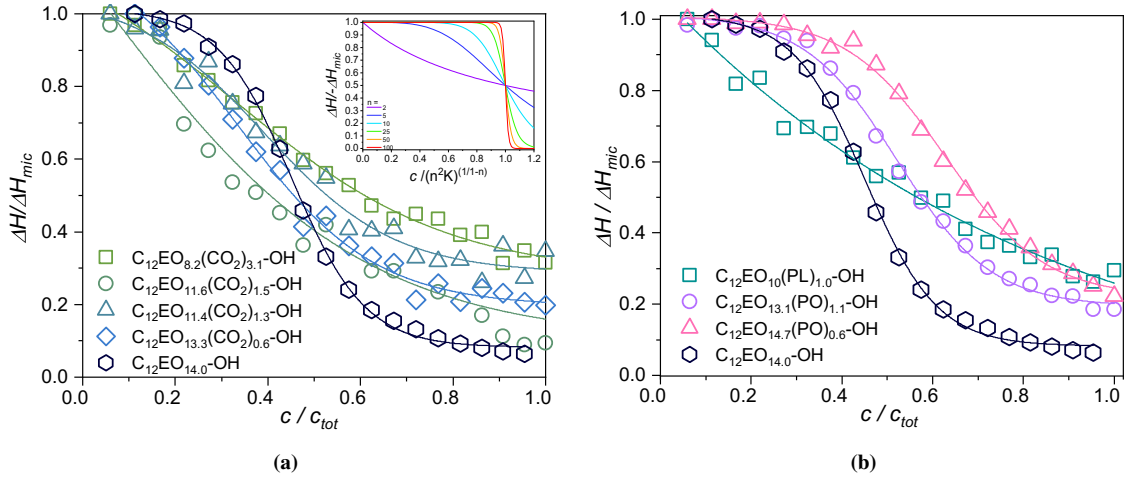

Figure 4.7: Normalized enthalpogram of 25°C ITC measurements of the CO_2 surfactants (a) and the PO and PL surfactants and the reference surfactant (b). Plotted is the normalized enthalpy $\Delta H/\Delta H_{min}$ against the concentration c divided by the total concentration at the end of the transition c_{tot} to compare the shape of the curve depending on the surfactant. Lines represent the Boltzmann fit. Inset: Comparison to normalized enthalpograms for n=2, 5, 10, 25, 50, 100 as a function of the non-dimensional free surfactant concentration $\bar{S}_{tot}$ for the mass action model as given by Eq. 4.10. Figure is reproduced from ref. [71].

hydrophobicity introduced by the CO_2 and PL units leads to additional attractive interactions between the surfactant molecules. This could result in a much broader range of premicellar aggregation that is seen in the ITC curves.

From obtained enthalpograms, the micellization enthalpy ΔH_{mic} and the cmc was obtained as described in the experimental section. The cmc values and thereby also ΔG_{mic} (Eq. 4.3) are in good agreement with the data obtained from the surface tension measurements (Fig. 4.10) and show the same dependency on the incorporated units. The only difference in cmc shows the PL surfactant.

The micellization process at 25 °C for all surfactants is endothermic with values for ΔH_{mic} ranging from ~ 13.7 kJ/mol for the reference surfactant and for the PO-containing surfactants ~ 15 kJ/mol determined by ITC. ΔH_{mic} is in very good agreement with published data by Anderson and Rosen who determined values for ΔH_{mic} with 16.3 kJ/mol for $C_{12}E_8$.[97, 107] It is also in good agreement with results found for long-chain carboxylates with values of ΔH_{mic} 9.1 kJ/mol for sodium dodecanoate (NaC12).[108] They also found, that for PEO surfactants both ΔH_{mic} and ΔS_{mic} seems to increase with an increasing number of EO units in the hydrophilic head group. For sugar-based nonionic surfactants like octylglucoside (OG) or decylmaltoside (DeM) values for ΔH_{mic} have been found to be -16.9 kJ/mol for OG or -12.68 kJ/mol for DeM determined by ITC at 27 °C and are exothermic in comparison to PEO nonionic surfactants.[109] The micellization process for the CO_2 containing surfactants and the PL containing surfactant is much less endothermic and reduced by about ΔH_{mic} ~ 6 – 8 kJ/mol (See Fig. 4.8a; Values are shown in Table 4.2). At the same time, ΔS_{mic} is reduced by ~ 20 J/Kmol and both effects may be explained by a lower number of H-bonds that are formed with the head groups and a correspondingly reduced hydration.[110] The change in hydration affinity introduced by the CO_2 unit may be attributed to a break in the symmetry of the EO chain, thereby rendering its polar a-g-a conformation less likely and the whole attractive interaction to water molecules becomes reduced (thereby leading to a reduction of ΔH_{mic}). This behavior may also be compared to the fact that polycarbonates are known to be highly hydrophobic.[111] Furthermore, CO_2 is known to by very hydrophobic from its use as supercritical fluid in the formation of microemulsion as reported by Eastoe *et al.*[112]

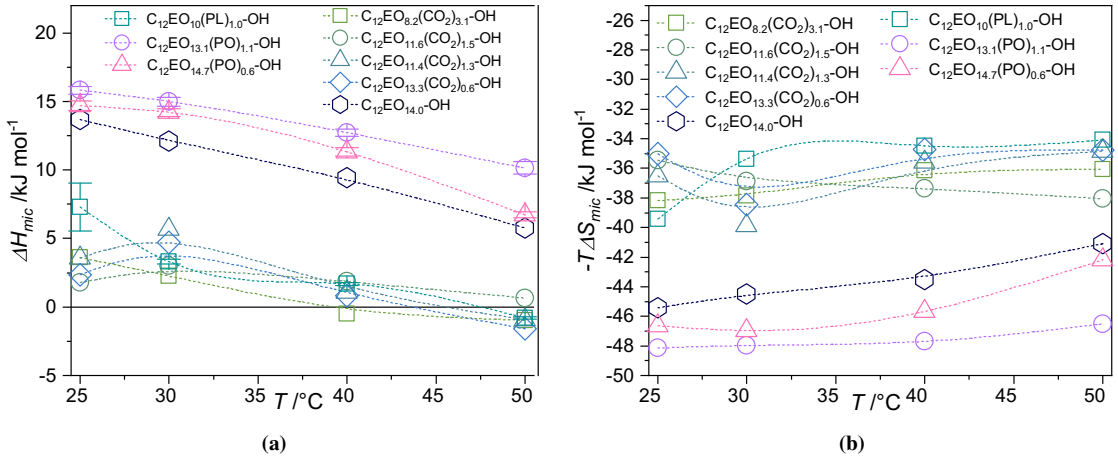

Figure 4.8: ΔH_{mic} (a) and $-T\Delta S_{mic}$(b) obtained from ITC measurements as a function of temperature is shown for all CO_2, PO and PL surfactants and the pure EO surfactant. Figure is reproduced from ref. [71].

The impact of the length of the hydrophilic head group on the micellization process was also investigated by Dai *et al.*[113] analyzing a homologous series of Triton-X with a variation of the PEG length. In that study, it was shown that ΔH_{mic} increases with an increasing number of PEG segments due to the larger number of H-bonds formed. Also, the MEGA-n surfactants show lower ΔH_{mic} values.[93] Interestingly, the PO surfactants show similar behavior as the pure EO surfactant, although a hydrophobic unit is incorporated in the head group. This indicates that the interaction between EO or PO and water in the head groups is rather comparable. Even though the incorporated PO unit is introducing a hydrophobic character, thereby lowering the cmc a bit, the general interaction to the water molecules and the driving force for the micellization process remains the same.

Since the micellization process for all investigated surfactants is endothermic, the contribution to the negative Gibbs energy is mainly derived from the entropy term, $-T\Delta S_{mic}$. It is negative for all surfactants ranging from ~ -35 kJ/mol for the CO_2 containing surfactants up to ~ -45 kJ/mol for the pure EO surfactant and the PO containing surfactants at 25 °C (Fig. 4.8b; Table 4.2). The PL containing surfactant has comparable values to the CO_2 surfactants. A shift of the entropy ΔS_{mic} to smaller values by incorporating CO_2 in the head group can mainly be explained by a lower degree of bound water.[113] Quantifying the hydrophobic effect by computer simulations and predicting the thermodynamic model of nonionic surfactants has been done by Stephenson *et al.*[114] For $C_{10}E_8$ it was shown that the interaction of the head group mainly consists of hydrogen bonds with water molecules and head group - head group interactions are largely suppressed, thereby the EO head group is strongly hydrated. Furthermore, studies from Bešter-Rogač *et al.* show that the results of the thermodynamic of micellization are strongly affected by the nature of the functional group of functionalized decyl dimethyl ammonium chlorides.[115] They also show that the hydration number is highly influenced by free monomers, where increasing polarity lowers the effective hydration number. From a comparison of the entropy and enthalpy term of micellization, one can conclude that the major driving force of the micellization of all nonionic surfactants shown in this study is the hydrophobic interactions because $T\Delta S_{mic} > \Delta H_{mic}$.

The contribution of the incorporated unit is the change in the hydration affinity of the head group, which leads to a decrease of ΔH_{mic} and an increase of $T\Delta S_{mic}$. In conclusion, one can state that the hydrophobic interactions are decreasing due to lower hydration with increasing incorporation of

Table 4.2: Summary of the thermodynamic parameters ΔH_{mic} and ΔS_{mic} derived from ITC measurements of all surfactants.

Surfactants	ΔH_{mic} /kJ/mol				ΔS_{mic} /J/K mol			
	25 °C	**30 °C**	**40 °C**	**50 °C**	**25 °C**	**30 °C**	**40 °C**	**50 °C**
$C_{12}EO_{8.2}(CO_2)_{3.1}-OH$	3.6	2.3	-0.5	-1.0	128	124.9	115.4	111.6
$C_{12}EO_{11.6}(CO_2)_{1.5}-OH$	1.8	3.0	1.9	0.6	118.9	121.6	119.3	117.7
$C_{12}EO_{11.4}(CO_2)_{1.3}-OH$	3.6	5.7	1.1	-0.9	122.5	131.5	113.6	107.9
$C_{12}EO_{13.3}(CO_2)_{0.6}-OH$	2.4	4.7	0.8	-1.6	117.4	126.8	110.9	107.5
$C_{12}EO_{10.3}(PL)_{1.0}-OH$	7.3	3.3	1.7	-0.8	132.3	116.7	110.1	105.4
$C_{12}EO_{13.2}(PO)_{1.1}-OH$	15.8	15.0	12.7	10.2	161.4	158.3	152.3	144
$C_{12}EO_{14.7}(PO)_{0.6}-OH$	14.7	14.2	11.3	6.7	156.4	154.9	145.8	130.6
$C_{12}EO_{14.0}-OH$	13.7	12.1	9.4	5.7	152.3	146.8	138.9	127.1

hydrophobic CO_2 (or PL) units, whereas the PO unit has similar or even higher hydration resulting in similar behavior as the reference sample.

Moreover, the micellization process was also observed at different temperatures. Upon increasing the temperature, both ΔH_{mic} and ΔS_{mic} appear to become less positive. ΔH_{mic} is decreasing linearly for all surfactants (Fig. 4.8a). Interestingly, for the CO_2 surfactant, ΔH_{mic} goes through zero around 40-45 °C and micellization is exothermic at higher temperatures. This phenomenon is quite known for surfactants (alkylglycosides[116], bile salts, and SDS[68], MEGA-n[93]) where the cmc undergoes a minimum at increasing temperatures resulting in a change of sign for ΔH_{mic}. In contrast, ΔH_{mic} remains positive at higher temperatures for the pure EO surfactant and the PO containing surfactant (Fig. 4.8a). The entropy of micellization ΔS_{mic} is decreasing significantly with temperature due to a lower contribution of the hydrophobic effect at higher temperatures caused by an increase of the hydrophobicity of water molecules with rising temperatures. This causes the reduction of the entropic term, whereas the enthalpic contribution is gaining more contribution at higher temperature caused by the reduced significance of the hydrogen bonds.[110] These findings are in good agreement with findings already obtained for other nonionic surfactants.[113, 116, 117]

4.3.4. Comparison between ITC and van't Hoff Isotherm

Comparing the cmc and the thermodynamic parameters of the two methods, one can observe major discrepancies for the thermodynamic parameters. The cmc determined from surface tension measurements and ITC are in good agreement for both methods, with a deviation of 15 %. In Fig. 4.9, one can observe the agreement of both methods for the cmc. Small deviations can be observed for cmcs at higher temperatures. The main reason could be heat exchange between the environment and sample for the surface tension measurements, whereas the ITC measurements were performed in a closed system, the temperature control was much more efficient and heat exchange with the environment was prevented.

The enthalpy and entropy values determined by ITC or surface tension measurements via the van't Hoff equation show quite remarkable differences as shown in Table 4.3. The trends for the dependence on temperature and number of incorporated units are comparable, but the absolute

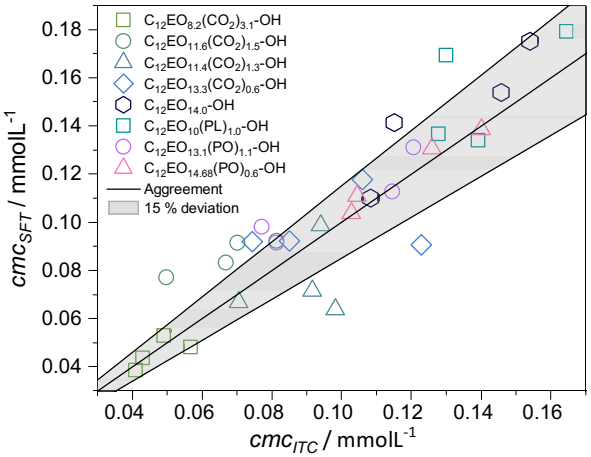

Figure 4.9: Comparison of the cmc values determined by surfcae tension measurements (SFT) vs. the cmc values determined by ITC. The line represents perfect agreement of both methods with a deviation of 15 % (grey area). Figure is reproduced from ref. [71].

numbers deviate strongly in some cases, especially for the enthalpy of micellization ΔH_{mic}. While for the pure EO and the PO modified surfactants comparable values are observed, ΔH_{mic} obtained from van't Hoff equation is higher by a factor of ~10 for the CO_2 surfactants, becoming larger with increasing CO_2 content. For higher temperatures, the deviations become less systematic. The entropy values show similar differences, but the discrepancy is not as high as for the enthalpy values. The error estimation for the van't Hoff data occurs from the error of $\ln x_{cmc}$, which is in the range of 5% for all surfactants and temperatures. The main deviation though occurs from the first derivative of the interpolated $\ln x_{cmc}$ vs. T data, which were used to obtain ΔH_{mic}. The error is substantially enhanced by the deviation of the interpolated data and is in the range of > 50 %. The direct measurements of the calorimetric heat by ITC and the obtained ΔH_{mic} have substantially lower errors < 1 %.

This difference of thermodynamic values depending on the used method has been reported for various surfactants. Moulik *et al.* have studied the agreement between the calorimetric method and the indirect van't Hoff method in thorough detail for different surfactants.[118, 119] These two methods have several basic differences, whose consideration is essential for the evaluation of the change in the enthalpy parameter. The van't Hoff method is a differential process, whereas calorimetry is an integral process, therefore error values for the van't Hoff analysis are expected to

Table 4.3: Summary of the factor of the thermodynamic parameters $f(\Delta H_{mic})$ and $f(\Delta S_{mic})$ derived from dividing the ITC data by the van't Hoff data.

Surfactants	$\|f(\Delta H_{mic})\|_{ITC/vH}$				$\|f(\Delta S_{mic})\|_{ITC/vH}$			
	25 °C	**30 °C**	**40 °C**	**50 °C**	**25 °C**	**30 °C**	**40 °C**	**50 °C**
$C_{12}EO_{8.2}(CO_2)_{3.1}-OH$	0.1	0.1	0	0.6	0.4	0.5	2.2	1
$C_{12}EO_{11.6}(CO_2)_{1.5}-OH$	-0.6	2.3	0.2	0.1	1.2	1.1	0.9	1.1
$C_{12}EO_{11.4}(CO_2)_{1.3}-OH$	0.1	0.1	0.1	0.1	0.4	0.5	1.6	0.8
$C_{12}EO_{13.3}(CO_2)_{0.6}-OH$	0.1	0.2	0.1	0.8	0.5	0.6	1.2	1.1
$C_{12}EO_{10.3}(PL)_{1.0}-OH$	0.3	0.1	0.3	0.1	0.7	0.7	0.9	0.3
$C_{12}EO_{13.2}(PO)_{1.1}-OH$	1.1	2.9	0.7	0.8	2.8	1.3	0.9	1.1
$C_{12}EO_{14.7}(PO)_{0.6}-OH$	1.9	1.3	1.1	2.3	1.2	1.1	1.0	1.9
$C_{12}EO_{14.0}-OH$	0.6	0.8	0.9	0.2	0.9	0.9	1.0	0.6

be much higher. Thus, general agreement between the two methods is not expected.[118] It was also shown by Moulik *et al.* that the discrepancies are most pronounced for ionic surfactants, where the analysis is based on hydrophobic and electrostatic contributions, whereas the deviations for nonionic surfactants are not as pronounced as for ionic surfactant. But it has to be said here that non-consideration of monomer non-ideality, micellar hydration, water structure modification, etc. is expected to have a major impact on the differences between the two methods also for nonionic surfactants.[118] Additionally, Holtzer *et al.*[120] postulated that the general thermodynamic analysis by the van't Hoff relation fails if the micelle aggregation number is temperature dependent, which in general is the case for nonionic surfactants.

In addition, a polydisperse surfactant system is considered, therefore, there are either zero, one, two, three, etc. discrete units of the CO_2 moieties present in the head group. This means a substantial spread in the hydrophilicity of the head group and the surfactant and its temperature dependence. However, this affects the surface tension measurements in a complex fashion and accordingly will have a substantial impact on the correctness of the van't Hoff analysis. As a somewhat related case, one may consider Polaxamers (Pluronics) that also possess a rather broad range of hydrophilicity in their mix of amphiphilic molecules. This leads to a rather broad micellization range and prominent changes of the micellar composition as a function of temperature[121] and this affects directly the observations in surface tension measurements.

As already discussed above, the major impact on the difference in micellization behavior of the CO_2 surfactants is the reduced hydration affinity of the head group. This can also be the major reason for the huge discrepancy between the two methods. As a result, the thermodynamic values derived from the ITC measurements should be considered more reliable due to being a direct method that gives more consistent results. Additionally, from the method, the cmc and the enthalpy can be determined from the same measurement. Moreover, the ITC method is more sensitive, accurate, and easy handling is possible, hence minimum errors arise from the method and data treatment.

4.3.5. Effect of head group modification on the transfer energy

The cmc values derived from ITC and surface tension are generally in good agreement (as described in the previous section) and can be used to determine ΔG_{mic} for the various surfactants in a reliable fashion. Taking the average value from both methods, ΔG_{mic} is plotted in Fig 4.10 as a function of the number of incorporated units CO_2, PO, or PL in the EO head group (Fig 4.10a at 25 °C, Fig 4.10b at 50 °C. For both methods, one observes a linear dependence of the free Gibbs energy ΔG_{mic} on the number of substituted moieties contained in the hydrophilic head group. For instance, at 25 °C, a linear regression fit of the change of ΔG_{mic} as a function of the incorporated moiety reveals a transfer energy of -0.36 $\pm$ 0.04 kT per CO_2 unit. This value becomes somewhat smaller with increasing temperature with a transfer energy of -0.23 $\pm$ 0.05 kT at 50 °C(Fig 4.10b). It is substantially smaller than the transfer energy of a CH_2 group in a hydrophobic chain (~1.2 kT), but nonetheless large enough to significantly influence the micellization process.

Incorporating PO into the hydrophilic chain results in a smaller transfer energy of -0.24 $\pm$ 0.02 kT/PO unit at 25 °C and the effect of PL is much smaller with only -0.10 kT/PL unit. The effect of adding PO and CO_2 units is therefore similar. In both cases facilitating the formation of micelles. For comparison, the transfer energy per EO unit is +0.16 kT[43] and thus the EO unit is causing a small contribution disfavoring micellization due to its hydrophilic character, i.e., it is a

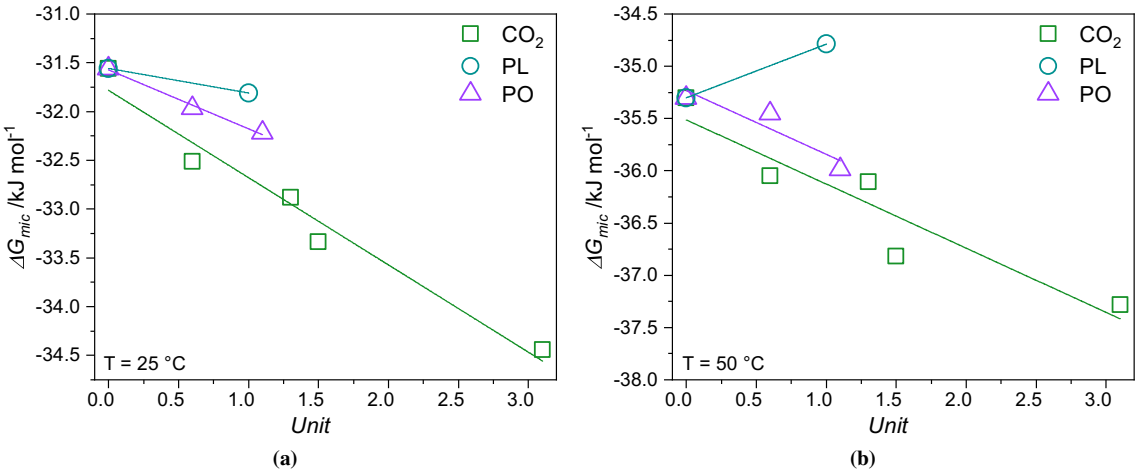

Figure 4.10: Dependency of the number of incorporated units on the Gibbs energy of micellization ΔG_{mic}, measured at 25°C (a) and at 50 °C (b). For ΔG_{mic} the average of the values from ITC and surface tension measurements was taken. Figure is reproduced from ref. [71].

hydrophilic component. With increasing temperature the transfer energy of PO remains almost constant with -0.23 ± 0.09 kT/PO unit at 50 °C. Interestingly, with increasing temperature, the transfer energy of PO and CO_2 is almost the same, due to the fact that the hydration effects are suppressed at higher temperatures (Fig. 4.11).

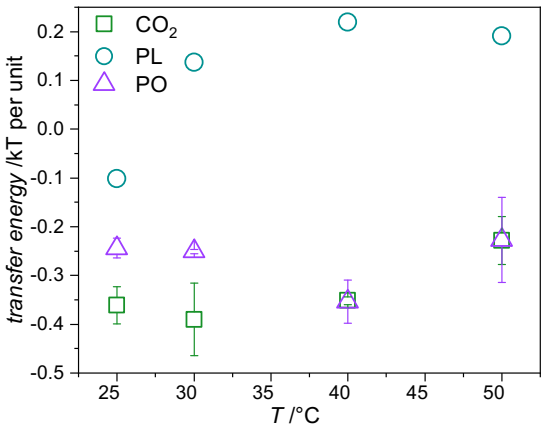

Figure 4.11: Dependency of the the temperature on transfer energy per incorporated unit. Transfer energy determined by the average ΔG_{mic} value from ITC and surface tension measurements. Figure is reproduced from ref. [71].

4.3.6. Enthalpy-Entropy Compensation

The thermodynamic values of micellization have been discussed in detail in the previous section. The phenomenon of an almost temperature independent free Gibbs energy, while enthalpy and entropy are changing as a function of temperature, is called enthalpy-entropy compensation, which is known for nonionic surfactants for quite a long time.[117, 122, 123] The linearity of the plot shown in Fig. 4.12 indicates a compensation of the enthalpy change by the changes in the entropy for the systems studied here. The compensation can be described in the form of:

$$\Delta H_{mic} = \Delta H^* + T_c \cdot \Delta S_{mic} \tag{4.11}$$

The intercept ΔH^* of this compensation plot is characteristic for the "chemical" part of the micellization process and represents the solute-solute interactions. Taking a closer look at

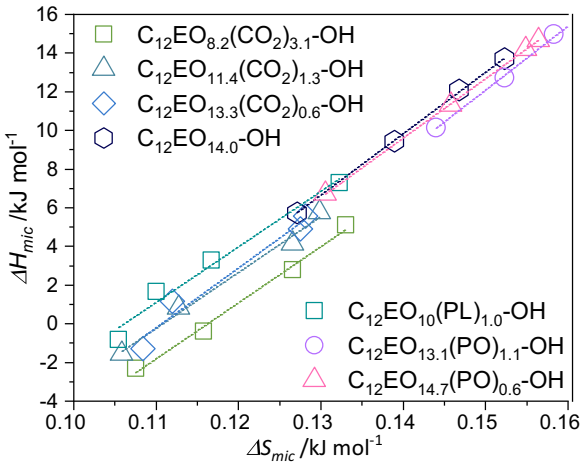

Figure 4.12: Shown is the enthalpy-entropy compensation plot for all surfactants. Values are obtained from ITC measurements. Figure is reproduced from ref. [71].

Fig. 4.12, one observes a shift of the CO_2 surfactants and the PL surfactant to smaller entropy and enthalpy values compared to the pure EO and the PO surfactants. This indicates a smaller impact on the reduction of the hydrogen bonds for the CO_2 unit and the PL unit as compared to the EO or PO unit. The slopes seen in Fig. 4.12 correspond to the compensation temperature T_c ($= d\Delta H_{mic}/d\Delta S_{mic}$) and characterize solvent-solute interactions, which is a measure of the "desolvation" part of the micellization process.[122] The T_c values are found to be in the range between ~ 318 K for the reference surfactant down to 280 K for the CO_2 containing surfactants (values are summarized in Table 4.4).

Moreover, the intercept ΔH^* is also shifted to less negative values from -34.7 kJ/mol for the pure EO surfactants up to -32.8 kJ/mol for the CO_2 surfactant. This result is similar as found by Chen *et al.*[117], who studied the effect of the alkyl chain length of C_iE_j surfactants, the enthalpy-entropy compensation plots are parallel to another and shifted downwards by increasing alkyl chain length. In other words, with increasing hydrophobicity, smaller entropy, and enthalpy values are obtained. The T_c values are in the range of 270-300 K[117] for the variation of the alkyl chain length, and thereby in a similar range as observed for Pluronic F127 with T_c ~ 298.08 K[67] and Pluronics F88 and 68 (294.9 K)[124], as well as for other nonionic surfactants like $C_{12}E_1$ and $C_{14}E_1$ (304 and 296 K).[110]

In general, it can be stated that the incorporation of CO_2 (or PL) moieties decreases the compensation temperature and the intercept ΔH^*. The decrease of the intercept value ΔH^* can be explained by the increasing stability of the micellar structure of the CO_2 surfactants in comparison to the reference and the PO surfactants. The addition of one methylene group to the alkyl chain length of nonionic surfactants leads to a decrease of the intercept ΔH^* of ~ 2.9 kJ/mol and by the reduction of the head group by one EO unit ΔH^* is reduced by ~ 0.24 kJ/mol.[117] In comparison, the incorporation of CO_2 in the hydrophilic head group with an increase of ΔH^* of ~ 1 kJ/mol indicates an increase in hydrophobicity. In comparison the addition of a PO units leads to an decrease of ΔH^* of ~ 2.8 kJ/mol. Due to the increasing number of hydrophobic units in the hydrophilic head group, less hydration water is present and as a result the total hydrophobicity of the surfactant changes in a similar fashion as extending its alkyl chain by CH_2 units.

The shift in T_c occurs if the structured water around the micelle is different from the water in the bulk. The shift in T_c confirms that the desolvation part of the head group during the micellization

Table 4.4: Values of the compensation temperature T_c for each surfactant.

Surfactants	ΔH^* / $^{kJ}/_{mol}$	T_c /K (ITC)
$C_{12}EO_{8.2}(CO_2)_{3.1}-OH$	-32.8	290.2
$C_{12}EO_{11.4}(CO_2)_{1.3}-OH$	-30.4	289.0
$C_{12}EO_{13.3}(CO_2)_{0.6}-OH$	-33.4	309.0
$C_{12}EO_{10.3}(PL)_{1.0}-OH$	-30.5	287.1
$C_{12}EO_{13.2}(PO)_{1.1}-OH$	-37.5	330.6
$C_{12}EO_{14.7}(PO)_{0.6}-OH$	-33.5	307.6
$C_{12}EO_{14.0}-OH$	-34.7	317.8

process depends on the incorporated units. This indicates that the incorporation of CO_2 (or PL) has a dramatic impact on the micellization behavior of the surfactant. However, the PO unit has a similar effect on reducing the cmc, but its way of enhancing hydrophobicity is different; thereby not varying the hydration of the hydrophilic head group in comparison to the EO unit.

4.4. Summary & Conclusion

In this chapter, the micellization and surface active behavior of the CO_2 surfactants was characterized and discussed in thorough detail. The focus of this chapter was the analysis of the influence of the CO_2 unit on the thermodynamics of the micellization process, thereby, comparing the CO_2 moiety to other hydrophobic units such as PO and PL. The incorporated hydrophobic units are substituting the EO units in the hydrophilic head group. The characterization and analysis were done by measurements of surface tension and isothermal titration calorimetry (ITC). The presence of CO_2 in the head group has the largest impact on the micellization process and reduces the critical micellar concentration (cmc) and the surface tension above the cmc, i.e. the surfactants become more efficient and effective, especially in comparison to a commercial reference surfactant such as Marlipal 24/90. The transfer energy for micellization is changed by -0.36 kT per CO_2 unit, whereas the PO unit only changes the energy of micellization by a factor of -0.24 kT and PL only by -0.10 kT per PL unit at 25 °C. Incorporating PO in the head group reduces the cmc, but to a lesser extent.

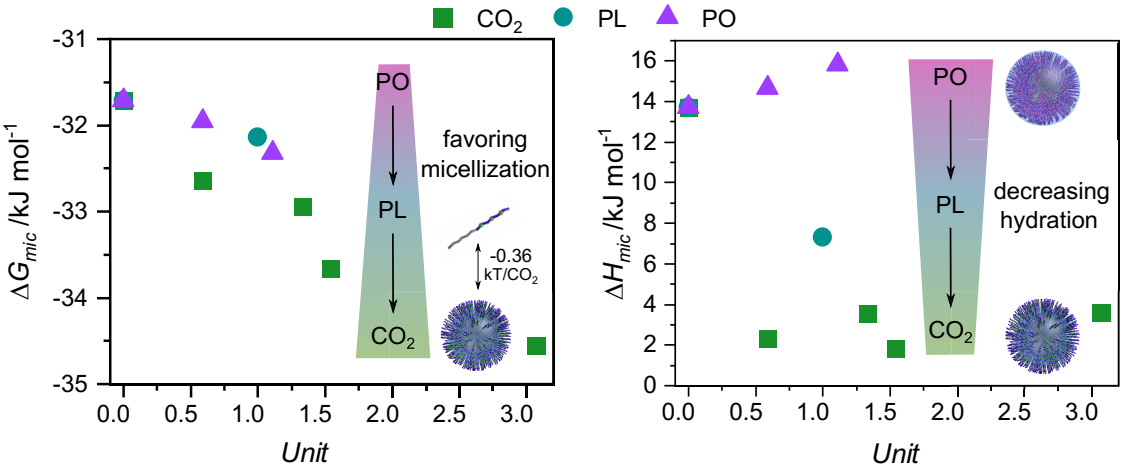

Figure 4.13: Graphical summary of the impact of an incorporated moiety on the thermodynamics of the micellization process.

Most interestingly, this chapter shows that the incorporation of CO_2 leads to a systematic reduction of the hydration of the head group, as indicated by a reduced enthalpy ΔH_{mic} and entropy ΔS_{mic} of micellization. In conclusion, one can state that the hydrophobic interactions are decreasing due to lower head group hydration with increasing incorporation of hydrophobic CO_2 units, whereas the PO unit has similar or even higher hydration resulting in similar behavior as the reference EO sample. Especially for the CO_2 surfactants, we could find drastic differences between the results from ITC and from the van't Hoff relation, which are mainly caused by the difference of hydration of the surfactant, which cannot be considered by the surface tension measurements. In such situations of changing hydration, the ITC method appears to be the more reliable method to obtain the thermodynamic parameters of the micellization process. These findings are supported by the enthalpy-entropy compensation plot. The CO_2 containing surfactants with their lower entropy and enthalpy values have a reduced compensation temperature T_c. The shift in T_c confirms that the desolvation part of the micellization process is depending on the structure of the head group, which changes upon addition of hydrophobic units.

In summary, incorporating a hydrophobic unit into the surfactant results in a systematic change of the hydration affinity of the head group and thereby to a controllable change of the micellization process. This can be used as an additional tuning parameter to achieve desired aggregation properties. These advantages, combined with the use of CO_2 as renewable resource (replacing the petrol-based EO units by up to 16% with CO_2), demonstrate that CO_2-containing surface-active compounds are a viable, "greener" alternative to conventional nonionic surfactants.

Chapter 5

Phase Behavior of CO_2 Containing Nonionic Surfactants

In the previous chapter, the surface activity and micellization behavior of the CO_2 surfactants were discussed and the impact of the CO_2 unit was compared to other incorporated moieties such as PL and PO. To obtain a thorough understanding of the properties and the phase behavior of the new sustainable surfactants, the structural properties of the micelles need to be analyzed. Therefore, in this chapter, the concentration and temperature phase dependent behavior will be discussed. Nonionic EO-based surfactants are widely used in commercial applications and normally form gel-like liquid crystalline phases at higher concentrations, rendering their handling under such conditions difficult. Therefore, the understanding of the phase behavior of the high concentration regime is a crucial aspect in terms of applications. The phase behavior was characterized by rheology and studied concerning its structural origin using light and small-angle neutron scattering (SANS). These experiments were done to obtain a deeper understanding of the structural impact of the incorporated unit. In addition, the temperature dependent phase behavior was investigated and the structural changes were studied by light and neutron scattering. In this chapter the phase behavior is studied in thorough detail, therefore aiming for a comprehensive analysis of the properties of the CO_2 surfactants with a comparison to commercial products. Understanding the influence of the CO_2 unit on the phase behavior opens up an enormous potential of these new surfactants in terms of applications.

Main parts of this chapter are based on the following publications:

◊ V. J. Spiering, A. Ciapetti, M. Tupinamba Lima, D. W. Hayward, L. Noirez, M.-S. Appavou, R. Schomäcker, M. Gradzielski: "Changes in Phase Behavior from the Substitution of Ethylene Oxide with Carbon Dioxide in the Head Group of Nonionic Surfactants", *ChemSusChem*, **2020**, *13*, 601-607, DOI https://doi.org/10.1002/cssc.201902855.

◊ V. J. Spiering, A. Prause, L. Noirez, M.-S. Appavou, M. Gradzielski: "Structural Characterization of Nonionic Surfactant Micelles with CO_2/EO Head Groups and their Temperature Dependence", *Langmuir*, **2021**, DOI https://doi.org/10.1021/acs.langmuir.1c01737.

5.1. Introduction

Alkyl ethoxylates are large scale commodity products, where the hydrophilic head group is based on classical oil chemistry. Due to their high importance, the properties of nonionic surfactants have been studied in thorough detail. Key features are in general their self-assembly behavior in aqueous solution which shows a prominent temperature dependence and at higher concentrations, they form liquid crystalline (LC) phases.[46, 83] The type and location of these LC phases in the phase diagram depends systematically on the molecular architecture of the nonionic EO surfactants.[83, 125] Typically, hexagonal and cubic phases are formed at higher concentrations, which exhibit prominent gel-like properties (with a shear modulus G_0 typically in the range of 104–106 Pa).[126, 127] This behavior is often problematic as for many formulations the formation of highly viscous phases during the preparation process is a major nuisance and therefore has to be avoided or circumvented. This often means one has to work in application/formulation with diluted surfactants from the very beginning, which leads to substantially higher logistic costs and volumes, thereby having a negative ecological impact.

In order to improve and tune the properties of the surfactants, usual approaches are the variation of the hydrophilic or hydrophobic chain length. Moreover, other units such as PO can be included in the EO chain.[84, 85] Extended surfactants are a class of surfactants, which contain moderate polar groups, such as EO and PO units, between the hydrophobic alkyl chain and the hydrophilic head group. This unit is called a linker. The properties of the concentrated regime can be systematically influenced by the presence of a linker.[128] In the context of more sustainable chemistry, it is interesting to mention the use of a sugar-based head group such as in MEGA-n surfactants. They suppress completely the phase separation at higher temperatures. They do not show a cloud point (CP) even for higher temperatures up to the boiling temperature. This unique property is due to the difference in the molecular structure of MEGA-n compared to the polyoxyethylene ether type surfactants.[93, 104] The substitution of at least one part of the hydrophilic head group with ones derived from a petrol-based resource can not only acquire new options for sustainable products but can also influence the phase behavior of the surfactants. It can lead to further optimization and tuning of the properties, which are desired for applications.

The surface activity and the thermodynamics of the CO_2 surfactants were studied in thorough detail in the previous chapter.[71] The influence of the CO_2 unit was compared systematically to other incorporated units such as PO or PL in the hydrophilic head group. From this study one can state, that the CO_2 units render the surfactants somewhat more hydrophobic, thereby lowering their cmcs. In this chapter, the concentration and temperature dependent phase behavior in an aqueous solution of four different CO_2-based nonionic surfactants was investigated. In addition, we investigated surfactants containing other hydrophobic units, such as propylene oxide (PO) or propiolactone (PL): $C_{12}EO_{14.7}(PO)_{0.6}-OH$, $C_{12}EO_{13.2}(PO)_{1.1}-OH$, $C_{12}EO_{10.3}(PL)_{1.0}-OH$. To have a direct comparison of the impact of the CO_2 unit with the other incorporated moieties. Moreover, a reference sample, $C_{12}EO_{14.0}-OH$, was used, which was synthesized under the same conditions as the CO_2 surfactants, in order to see directly the influence of the incorporated units on the surfactant properties. To compare the CO_2-surfactants with a commercial reference also a Marlipal 24/90 surfactant ($C_{12/14}EO_9-OH$) from Sasol was studied. These modified surfactants

will also be compared with their conventional analogous and the influence of a varied alkyl chain length on the phase behavior will be discussed as a short digression.

The self-assembled structures were characterized by static and dynamic light scattering (SLS, DLS), which give information about the size of the aggregates, and by small-angle neutron scattering (SANS), which provides more detailed structural information. The hydration properties were analyzed by a non-model approach and discussed in detail in terms of the incorporated unit. Moreover, the structural properties will be discussed by two ellipsoidal models, a core-shell model[129] and a micellar model with an ellipsoidal core with Gaussian chains attached.[130–133] In this way, we were able to obtain a comprehensive overview of the concentration- and temperature-dependent behavior of this novel type of eco-friendly surfactant and compare it to the other incorporated units PO and PL and to the corresponding, classical, nonionic alkyl ethoxylate surfactants.

5.2. Experimental Section

5.2.1. Polarization Microscopy

All samples were inspected visually and between crossed polarizers over a period of several weeks. In addition, the flow behavior was checked by the tube inversion method. Polarization microscopy was measured with a Jenapol light microscope by Carl Zeiss in a temperature chamber using crossed polarization filters. The samples were heated up to 60 °C and then cooled down to room temperature again.

5.2.2. Rheology measurements

Rheology measurements were performed with a Bohlin Gemini 200 HR nano rheometer (Malvern Instruments), using a cone-plate geometry (radius: 40 mm, gap size 150 µm, stainless steel geometry). The applied shear rates varied from 0.00014 to 50 1/s. To analyze the viscoelastic behavior of these samples, oscillatory measurements were performed with the same instrument and fixtures. A strain amplitude sweep was performed at a constant angular frequency of 6.3 1/s varying the amplitude of the shear stress from 0.01 – 15 Pa to identify the linear viscoelastic regime. Based on these measurements a frequency sweep at a shear stress of 0.5 Pa and angular frequencies varies from 0.6 – 314.2 1/s was performed to determine the storage modulus G’ and the loss modulus G". The reference surfactant was analyzed with a MCR301 rheometer (Anton Paar) under the same measurement conditions.

5.2.3. Light Scattering

Light scattering measurements (DLS and SLS) were conducted simultaneously on an ALV/CGS-3 instrument. All measurements were done at 25, 40, 50 and 60 °C. From the intensity fluctuations, the autocorrelation function was obtained by the ALV500/E multiple-τ correlator for measurements at angles from 30° to 120° in 5° steps. The diffusion coefficient was calculated from the slope of

the decay rate, Γ, plotted against q^2 (see explanation in chapter 2.4.2). The diffusion coefficient, D, was converted into the hydrodynamic radius, R_H, via the Stokes Einstein equation:

$$R_H = \frac{k \cdot T}{6\pi \cdot \eta_0 \cdot D} \tag{5.1}$$

with k being the Boltzmann constant and η_0 the viscosity. The real hydrodynamic radius R_H can only be directly obtained from the collective diffusion coefficient if the sample is highly diluted otherwise concentration effects need to be considered. With increasing concentration the particle interactions are increasing and therefore an increase of the collective diffusion coefficient D_{col} (decrease of R_H) is expected. To avoid this, the measurement needs do be corrected which can be done by assuming hard-sphere interactions to obtain the free particle diffusion coefficient D_0.[134]

$$D_{col} = D_0 \cdot (1 + 1.454 \cdot \phi_{HS}) \tag{5.2}$$

where the hydration of the micelles are considered within the hard sphere volume fraction ϕ_{HS}. ϕ_{HS} is calculated for each surfactant separately due to a variation of water content. The hydration of the micelles are obtained from SANS studies and will be given in the next section.

For SLS data, the scattering intensity at a given q-vector was calculated from the count rates of the sample, the solvent and a toluene standard. I(q) was plotted versus q^2 and the forward scattering, I(0), and the radius of gyration R_g were obtained using the Guinier approximation[135]. From the forward scattering I(0) the molecular weight was calculated via:

$$M_W = \frac{I(0)}{K_L \cdot c_g} \tag{5.3}$$

with mass concentration, c_g, and $K = [2\pi(dn/dc_g)n_{solvent}]^2 / (\lambda^4 \cdot N_A)$ as optical constant, including the refractive index increment dn/dc for the solute and N_A, the Avogadro constant. dn/dc was calculated from refractive index measurements at different surfactant concentrations and have values of 0.12 – 0.13 [mL/g] for the employed surfactants.

Refractive Index Increment

The change in the refractive index with changing concentration needs to be considered to address the contrast variation with changing concentration for light scattering measurements. This variation is described by the refractive index increment (dn/dc). The (dn/dc) measurement was performed with a dndc Orange 19" from Orange Analytics. The measurements were performed for 5 concentrations of each surfactant and the slope of refractive index as a function of the concentration corresponds to dn/dc. The obtained values are summarized in Table 10.9.

Table 5.1: Refractive index increment for all used CO_2 surfactants and the reference samples.

Surfactants	dn/dc /cm³/g	K_L /cm²mol/g²
$C_{12}EO_{8.2}(CO_2)_{3.1}-OH$	0.1325	$1.27 \cdot 10^{-7}$
$C_{12}EO_{11.6}(CO_2)_{1.5}-OH$	0.1248	$1.13 \cdot 10^{-7}$
$C_{12}EO_{11.4}(CO_2)_{1.3}-OH$	0.1297	$1.22 \cdot 10^{-7}$
$C_{12}EO_{13.3}(CO_2)_{0.6}-OH$	0.1302	$1.23 \cdot 10^{-7}$
$C_{12}EO_{10.3}(PL)_{1.0}-OH$	0.1297	$1.22 \cdot 10^{-7}$
$C_{12}EO_{13.2}(PO)_{1.1}-OH$	0.1327	$1.28 \cdot 10^{-7}$
$C_{12}EO_{14.7}(PO)_{0.6}-OH$	0.1327	$1.28 \cdot 10^{-7}$
$C_{12}EO_{14.0}-OH$	0.1280	$1.19 \cdot 10^{-7}$
$C_{12/14}EO_9-OH$	0.1378	$1.38 \cdot 10^{-7}$

5.2.4. Small-angle neutron scattering (SANS)

Small-angle neutron scattering was measured at the Heinz Maier-Leibnitz Zentrum (MLZ) in Munich, Germany, on the Instrument KWS-1[136] and at the Laboratoire Léon Brillouin (LLB) in Saclay, France, on the instrument PAXY. KWS-1 was operated at a wavelength of 5 Å and sample to detector distances (SDD) of 1.5 m to 20 m, to cover a q-range of 0.015 – 4 nm^{-1}. Sample transmissions were measured at a SDD of 8 m. For all scattering data, the intensities were divided by the corresponding transmission and sample thickness (1 mm), corrected for the empty cell and normalized with respect to the scattering of a 1 mm sample of light water, according to standard procedures.[137] The incoherent background was determined by a Porod plot. The SANS measurements performed at PAXY were carried out at a wavelength of 4 Å for SDDs of 1.2 m and 5 m, and a wavelength of 12 Å for an SDD of 6 m, thereby covering a q-range of 0.02 – 6 nm^{-1}.

The small-angle scattering intensity is given by:

$$I(q) = \phi \cdot \Delta SLD^2 \cdot V \cdot P(q) \cdot S(q) \tag{5.4}$$

With ϕ being the volume fraction of the surfactant, P(q) being the form factor and S(q) being the structure factor. The SANS data were firstly analyzed by a model free analysis using the forward scattering intensity I(0), which is generally described in chapter 2.4. The forward scattering intensity contains information about the molecular weight of the micelles and the corresponding aggregation number N_{agg}($N_{agg} = M_{w,agg}/M_{surf}$).

$$I(0) = \phi \cdot \Delta SLD^2 \cdot V \cdot S(0) \tag{5.5}$$

$$M_{w,agg} = \frac{I(0) \cdot N_{Av} \cdot \rho^2}{c_g \cdot (\Delta SLD)^2} \tag{5.6}$$

In order to obtain the molecular weight from the static intensity it needs to be corrected by the static structure factor S(0) which can be calculated by the Carnahan-Starling structure factor:[138]

$$S(0)^{-1} = \frac{(1+2\phi_{hs})^2 - 4\phi_{hs}^3 + \phi_{hs}^4}{(1-\phi_{hs})^4} \tag{5.7}$$

The effective hard sphere volume fraction ϕ_{hs} is the solvated volume fraction, which depends on the hydration of the micelles B and the interaction parameter A, which describes the interpenetration of the micelles.[139]

$$\phi_{hs} = B \cdot \phi_{dry} \cdot (1 - A\phi_{dry}) \tag{5.8}$$

From this approach the hydration number H (molecules water per molecules surfactant) of the surfactants can be obtained.

Furthermore, the obtained SANS data were analyzed by two different models and compared in terms of the scattering profile: a core-shell model with ellipsoidal core[129] and a constant scattering length density of the shell (P(q)cs), and a core-corona model with an ellipsoidal core and Gaussian chains attached by Pedersen et al. (P(q)cc).[130–133] The core-shell model is described by following total intensity $I(q)_{core-shell}$:

$$I(q)_{cs} = {}^{1}N \cdot P(q)_{cs} \cdot S(q)_{\beta} \tag{5.9}$$

The micellar model with an ellipsoidal core and Gaussian chains attached is described by the following equation:

$$I(q)_{cc} = {}^{1}N \cdot P(q)_{cc} \cdot S(q)_{\beta} \tag{5.10}$$

The core-shell form factor $P(q)_{cs}$ and the core-corona form factor $P(q)_{cc}$ are described in detail in the Appendix Chapter 5. Eventually, the SANS data were fitted by a model, which considered the absolute intensity and employed a weighted sum (factor $0<f<1$) of the form factors of both models (core-shell model and core-corona model):

$$I(q)_{tot} = f \cdot (I(q)_{cs}) + (1 - f) \cdot (I(q)_{cc}) + I_{bkg} \tag{5.11}$$

With this model, we account for the fact that the head group shell can be more or less diffuse, with f becoming smaller with having a more diffuse shell. The intensity of the incoherent background I_{bkg} was determined by a Porod estimation as described in the Appendix Chapter 5, from which the fractal exponent of the Porod regime n_{frac} is obtained. For the structure factor describing globular micelles which is described in terms of a decoupling approach[140], we employed the modified hard-sphere model due to Baxter[141–143], which added an additional repulsive contribution described by Y being fixed to -2kT. The temperature dependent data were fitted with a cylindrical model with spherical end-caps.[144–146] The development of the different models and the writing of the script for the SANS data treatment was done by Albert Prause.

A detailed description of the models and the structure factor is shown in the Appendix Chapter 5.

5.3. Results & Discussion

After the analysis of the surface activity and the micellization behavior of the CO_2 surfactant, the focus of this chapter is the structural analysis of the formed aggregates as a function of concentration and temperature and how it is affected by the presence of CO_2 units, or other incorporated moieties, such as PL and PO. This was elucidated by using static and dynamic light scattering and small-angle neutron scattering (SANS). Furthermore, the surfactants were studied in the high concentration regime by means of rheology and SANS. Whereby, the CO_2 surfactants are compared in a systematic fashion to the reference surfactants $C_{12}EO_{14.0}-OH$, and the commercial reference Marlipal 24/90 ($C_{12/14}EO_9-OH$).

5.3.1. Phase Behavior of the Low Concentration Regime

To investigate the structure of the formed aggregates in solution dynamic light scattering was performed to obtain information about the hydrodynamic radii from dynamic light scattering (DLS) and the molecular weight from static light scattering (SLD). Furthermore, detailed information on the structure of the micelles could be obtained by a model description of the SANS data. The main results of this study are discussed in an article which published in the Journal *Langmuir*.[147]

Static and Dynamic Light Scattering (SLS, DLS)

The hydrodynamic radii R_H (determined by DLS) for the different surfactants are shown in Fig. 5.1a as a function of the surfactant concentration. At low concentrations, R_H is in the range of 3.8 – 5.0 nm for all investigated surfactants and a slight increase of the hydrodynamic radii with increasing CO_2 content is observed (the corresponding autocorrelation functions are given in the Appendix Chapter 5 Fig. 10.6). A slight increase of the hydrodynamic radius with increasing CO_2 content is observed. One can also observe, that the PO surfactants have similar radii of 3.7 nm as the reference surfactant ($C_{12}EO_{14.0}-OH$), i.e, slightly smaller than the CO_2 surfactants. In comparison, the commercial reference $C_{12/14}EO_9-OH$ has a significantly higher R_H of 5.5 nm. The slight increase of the radius with increasing CO_2 content may be explained by a decrease of the head group area (as observed in the surface tension measurements described in the previous chapter), which leads to the formation of larger aggregates, in order to retain the surface/volume ratio. The obtained R_H is in the size range for spherical micelles, which is in good agreement with the theoretical packing parameter (all values are summarized in Table 5.2). The packing parameter gives the geometrical ratio between the volume and length of the alkyl chain and the head group area a_0 (Eq. 1.10). The obtained values are in the range of 0.32 up to 0.49 for the CO_2 surfactants, which is increasing with increasing CO_2 content. This already indicates a slight elongation of the micellar structure with increasing CO_2 content. The reference surfactant $C_{12}EO_{14.0}-OH$ and the PO and PL surfactants show values in the range up to 0.33, which the ideal value of spherical aggregates. However, the commercial reference $C_{12/14}EO_9-OH$ has a packing parameter of 0.5, which indicates an already elongated structure. This elongated structure would also explain the rather high values for R_H and M_w. However, the detailed structure information can not be obtained from DLS measurements and will be deepened in the next section.

With increasing concentration, the particle interaction is expected to lead to an increase of the apparent collective diffusion coefficient, D_{coll}, and consequently, to lower the observed hydrodynamic radii. A correction was therefore undertaken by calculating the hydrodynamic radius using the effective diffusion coefficient D_0, which is given by Eq. 5.2 for hard-sphere interactions. Within this correction, the volume fraction ϕ_{HS} is taken into account. It is considering the bound hydration water, which was determined from SANS measurement, which will be explained in the next section.

Table 5.2: Calculated molecular weight for the aggregates of all surfactants at 1 wt% from the intensity I(0) derived from SLS measurements. I(0) was corrected by the Carnahan Starling structure factor S(0)[138], as: $I(0)_{corr} = I(0)/S(0)$, where M_w is obtained from $I(0)_{corr}$. The hydrodynamic radii R_h from DLS measurements were corrected by the volume fraction ϕ_{HS} and P the packing parameter are shown.

Surfactants	**I(0)$_{corr}$ /cm^{-1}**	**ϕ_{HS}**	**M$_w$ /kg/mol**	**N$_{agg}$**	**R$_H$ / nm**	**P**
$C_{12}EO_{8.2}(CO_2)_{3.1}-OH$	$8.2\cdot10^{-5}$	0.015	65	95	4.38	0.49
$C_{12}EO_{11.6}(CO_2)_{1.5}-OH$	$6.6\cdot10^{-5}$	0.016	58	77	4.16	0.36
$C_{12}EO_{11.4}(CO_2)_{1.3}-OH$	$7.8\cdot10^{-5}$	0.017	61	82	4.07	0.37
$C_{12}EO_{13.3}(CO_2)_{0.6}-OH$	$8.5\cdot10^{-5}$	0.018	62	78	4.29	0.32
$C_{12}EO_{10.3}(PL)_{1.0}-OH$	$8.7\cdot10^{-5}$	0.015	72	104	4.32	0.31
$C_{12}EO_{13.2}(PO)_{1.1}-OH$	$1.1\cdot10^{-4}$	0.018	86	104	3.82	0.22
$C_{12}EO_{14.7}(PO)_{0.6}-OH$	$8.8\cdot10^{-5}$	0.017	69	80	4.06	0.22
$C_{12/14}EO_9-OH$	$1.8\cdot10^{-4}$	0.016	143	210	5.49	0.54
$C_{12}EO_{14.0}-OH$	$6.5\cdot10^{-5}$	0.017	55	69	3.73	0.20

From the static light scattering (SLS) intensity I(0), one can obtain the weight average molecular weight, M_w, and the aggregation number, N_{agg}. To obtain accurate values, the structure factor S(0) has to be considered. The results of the light scattering studies are summarized in Table 5.2 for all surfactants at 1 wt%. The results for the molecular weight and the aggregation number from SLS show that there is a some increase from 69 kg/ml for $C_{12}EO_{14.0}-OH$ to 95 kg/mol for $C_{12}EO_{8.2}(CO_2)_{3.1}-OH$. The PL and PO surfactants show values slightly higher with 104 kg/mol. The results for the molecular weight (and aggregation number) from static light scattering generally show little concentration effects in the observed concentration range up to 5 wt% (Fig. 5.1). Interestingly, only for the pure EO surfactant and the one with the highest CO_2 content an increase with increasing concentration is observed, indicating micellar growth (the aggregation number as a function of the concentration is shown in the Appendix Chapter 5 Fig. 10.8a).

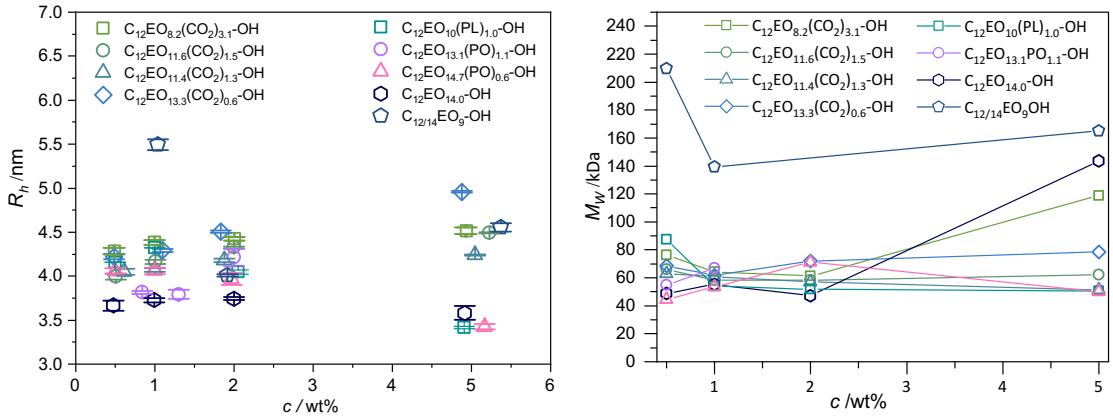

(a) **(b)**

Figure 5.1: (a) Hydrodynamic radius R_H as a function of the concentration of all surfactants determined by DLS usig D_0 obtained via Eq. 5.2. (b) Molecular weight determined by SLS as a function of the concentration of all surfactants measured at 25 °C. Lines are guide to the eye. Reprinted with permission from ref. [147]. Copyright 2021 American Chemical Society.

Small-Angle Neutron Scattering

More detailed structural information can be obtained by employing SANS, which were carried out for all surfactants in the low concentration range of 0.25 – 20 wt% at a constant temperature (25 °C). SANS measurements at a lower concentration of 1 wt% display similar scattering curves for all surfactants which are typical for globular aggregates (Fig. 5.2). When the SANS data are plotted as a Guinier plot (see Fig. 10.17 in Appendix Chapter 5) a linear behavior was found at low q for all surfactants, the slope of which was used to determine the radius of gyration, R_g. The radius of gyration R_g (evaluated in the q-range of 0.1 – 0.2 nm^{-1}), was determined to be in the range of 2.9 – 4.3 nm, consistent with the size seen in the light scattering measurements and expected from the form factor minima (summarized in Table. 5.4).

The SANS curves were analyzed, as described before, by a model based on coupling two analytical model (Eq. 5.11), the core-shell ellipsoid with a constant SLD for the shell and a core-corona model with Gaussian chains attached to the micellar surface, to obtain information about size and shape of the formed aggregates. The data were modeled with the following free parameters: the aggregation number N_{agg}, ellipticity ε (axes ratio), shell thickness T_{shell}, hard-sphere radius R_{HS}, the effective radius R_{eff} (representing the volume equivalent sphere radius of the ellipsoid) and the factor f, which weights the contribution of the two different models. N_{agg} is determined by the ratio of the core volume V_{core} and the volume of the alkyl chain in the core V_{alk} ($N_{agg} = V_{core}/V_{alk}$), where V_{core} is derived from the axial, R_{ax} and the equatorial radius, R_{eq}. R_{ax} and R_{eq} are determined by the form factor of each model. A detailed description is given in the Appendix Chapter 5, explaining further the individual fit parameters.

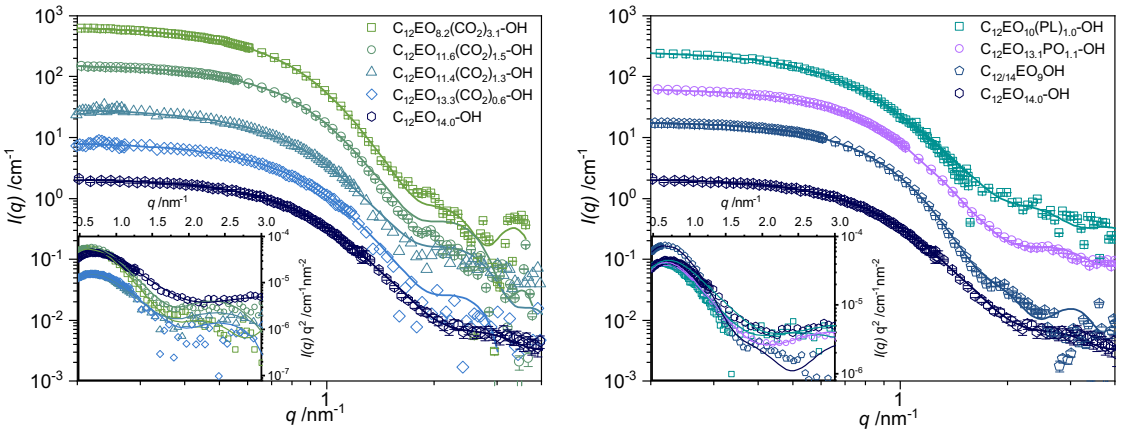

Figure 5.2: SANS curves of the CO_2 containing surfactants at low concentration (1 wt%) with the corresponding fits: (a) $C_{12}EO_{8.2}(CO_2)_{3.1}-OH$ (KWS-1), $C_{12}EO_{11.6}(CO_2)_{1.5}-OH$ (KWS-1), $C_{12}EO_{11.4}(CO_2)_{1.3}-OH$ (PAXY), $C_{12}EO_{13.3}(CO_2)_{0.6}-OH$ (PAXY), (b) the PO and PL surfactants $C_{12}EO_{13.2}(PO)_{1.1}-OH$ (KWS-1) and $C_{12}EO_{10.3}(PL)_{1.0}-OH$ (PAXY), the reference sample $C_{12}EO_{14.0}-OH$ (Paxy) and the commercial reference $C_{12/14}EO_9-OH$ (KWS-1) at 25 °C. All intensities are scaled at the y-axis. Reprinted with permission from ref. [147]. Copyright 2021 American Chemical Society.

The aim of using this combined two model approach was to account for the fact that the shell region of the micelles will depend on the extent of hydration of the head groups. For little hydrated head groups one can expect a compact shell with a rather constant ΔSLD (core-shell model), while for strongly hydrated head groups the core-corona model with a continuously decaying ΔSLD and scattering from individual head group chains (Gaussian coils) should be more suitable (see Fig. 10.14 in the Appendix Chapter 5). Accordingly, the relative contribution of the two models

(described by f) is the parameter sensitive to this important detail of the structure of the micellar corona that depends on the molecular properties of the head groups (values for f are shown in Table 5.3 and Fig.5.3). The difference in the scattering patterns is mainly seen in the high q regime and a comparison of the two models is shown in Fig. 10.13. Compared to the experimental data the core-corona model shows too high intensities and the core-shell model too low intensities. The mixed model approach then allows for a reliable description of the data that gives a good insight into structural details of the hydrophilic micellar corona. It might be noted that a different scattering behavior is directly seen in Fig. 5.2, where the form factor minimum of the CO_2 surfactants is clearly visible around 1.8 nm^{-1}, indicating a marked shell contrast, while the scattering pattern for the pure EO surfactant is smoothly decaying in that region.

The resulting fits are shown in Fig. 5.2a for the CO_2 surfactants and in Fig. 5.2b for the PO and PL surfactants and the commercial reference surfactant $C_{12/14}EO_9-OH$ and the obtained parameters are summarized in Table 5.3. All fits and obtained parameters of the concentration range from 0.25 up to 20 wt% are summarized in the Appendix Chapter 5 Fig. 10.16. A main difference is seen between the CO_2 surfactants and the pure EO and the PO surfactant, for the CO_2 surfactants the factor f is higher and approaching ~ 1 (Fig. 5.3). This higher value of f indicates a more compact corona structure for the CO_2 surfactants, while for pure EO and PO surfactants (f ~ 0.7) the chains are more hydrated, resulting in a more extended and continuously decreasing density profile of the corona. Interestingly, the commercial reference surfactant $C_{12/14}EO_9-OH$ has a low value for f, indicating a more diffusion corona structure, which is the opposite of the reference $C_{12}EO_{14.0}-OH$. However, it is not surprising because of the polydispers alkyl chain with C_{12} and C_{14} chains which reduces the compact packing of surfactant molecules.

Carefully looking at the data at high q one also still sees some discrepancies between the fit curves and the experimental data, which arise from the fact that at very high q the main scattering contribution comes from the EO chains, that are not accounted for here at a molecular level. However, this is also not relevant to our analysis and therefore has basically no impact on the interpretation. This difference in the structure of the corona of the CO_2 surfactants in comparison to the reference and PO surfactants is also seen in the Porod regime (q = 1.5 – 3 nm^{-1}), where the fractal exponent in the Porod regime n_{frac} ($I(q) \approx q^{-nfrac}$) gives information about the roughness (fractal dimension) of the micellar interface (see Table 5.3 and Fig. 5.3). The surfactants with

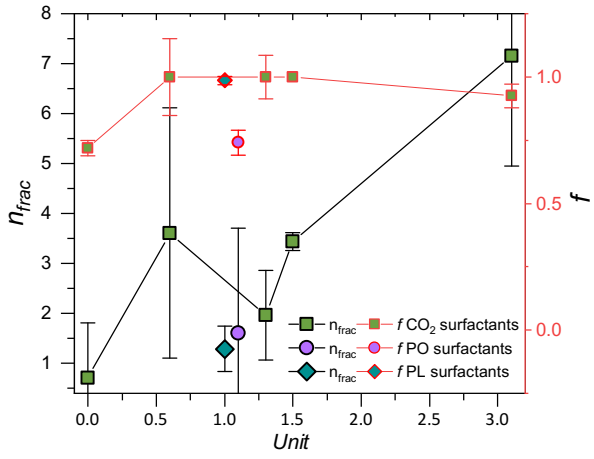

Figure 5.3: Factor f and the fractal exponent of the Porod regime n_{frac} as a function of the substituted EO units. Reprinted with permission from ref. [147]. Copyright 2021 American Chemical Society.

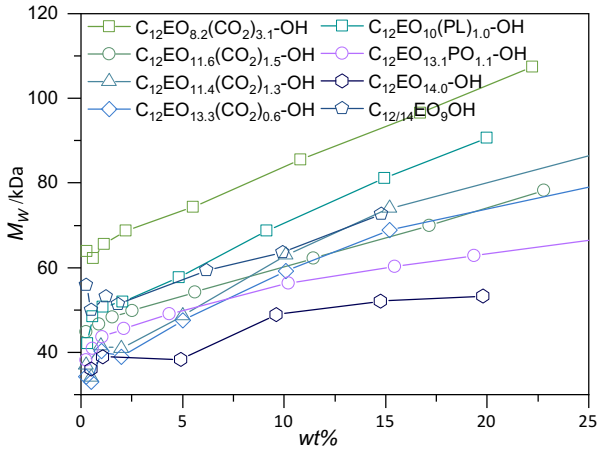

Figure 5.4: Obtained molecular weight of the aggregates derived from the model analysis of the SANS curves for the CO_2 containing surfactants at the low concentration regime: (a) all CO_2 containing surfactants, (b) the PO and PL surfactants and the reference samples $C_{12}EO_{14.0}-OH$ and $C_{12/14}EO_9-OH$ at 25 °C. Lines are guide to the eye. Reprinted with permission from ref. [147]. Copyright 2021 American Chemical Society.

higher CO_2 content show values larger than 3 for n_{frac}, indicating a relatively sharp interface, i.e., a collapsed state of polymer chains. The pure EO and the PO surfactant show values between 0.7 and 1.3, which indicate swollen coils with Gaussian statistics.[132] Moreover, the fit of the scattering curves for the 1 wt% samples (here one has good scattering intensity and at the same time still not so pronounced particle interactions that make the analysis more complicated) yields detailed insights into the structure of the formed aggregates and the obtained parameters, such as size and ellipticity of the micellar aggregates, which are summarized in Table 5.3. The structural model for the micelles are prolate ellipsoids with an equatorial core radius R_{eq} of 1.2 to 1.8 nm for all surfactants and the ellipticity ε is 1.1 to 2.5, i.e., the micelles are only slightly elongated. R_{eq} is in good agreement with what is expected for a C_{12} alkyl chain (1.67 nm) according to Tanfords rule[53] for the maximum length of an alkyl chain with n_c carbon atoms ($l_{max} = 0.15 + 0.1265 \cdot n_c$). The shell thickness is 1.5 to 2.0 nm for all surfactants, thereby substantially less than the value of 5.6 nm for a fully stretched EO_{14} chain. With increasing CO_2 content an overall increase of size is observed, where the PL surfactants show similar behavior and sizes as the CO_2 surfactants, whereas the PO surfactant is comparable to the pure EO surfactant.

From the micellar core volume, M_w values were determined and are given in Fig. 5.4 as a function of concentration. As already observed by light scattering (Fig. 5.1) one observes a trend for increasing M_w with increasing concentration, but always in agreement with rather low aggregation numbers of globular micelles, which in general can be attributed to the relatively large head groups. The M_w values generally increase with increasing CO_2 content (Table 5.3), as already observed from the light scattering data. This means one observes micellar growth with increasing concentration, as typically observed in micellar systems. It might be noted that N_{agg} values derived from light scattering are always somewhat higher than the ones from SANS, which could be due to the different way of analyzing, where in light scattering one automatically sees the whole aggregate and in SANS N_{agg} was derived from the core size. Comparing the result to literature one finds typical aggregation numbers for $C_{12}EO_{12}$ to be 81[148] and for $C_{12}EO_{18}$ to be 51[148] at 25 °C, i.e., in reasonable agreement with our finding for $C_{12}EO_{14}$.

In order to quantify the effective interaction between the micelles as a function of the content of the incorporated moieties of the different surfactants, we further analyzed the scattering data

Table 5.3: Obtained values form the model analysis of the SANS Scattering curves of all surfactants at 1 wt%: n_{frac} is the fractal exponent of the Porod regime, f is the model fraction, ε is the ellipticity of the aggregates with the equatorial radius R_{eq} and the axial radius R_{ax}, the shell thickness T_{shell}, the effective radius R_{eff}, the molecular weight M_w, the aggregation number $N_{agg}$and the hydration factor H.

Surfactants	n_{frac}	f	ε	R_{eq} /nm	R_{ax} /nm	T_{shell} /nm	R_{eff} /nm	M_w /kDa	N_{agg}	H
$C_{12}EO_{8.2}(CO_2)_{3.1}-OH$	7.16	0.93	1.8	1.6	2.9	1.9	3.9	66	96	76
$C_{12}EO_{11.6}(CO_2)_{1.5}-OH$	3.44	1.00	2.0	1.4	2.7	2	3.7	48	63	102
$C_{12}EO_{11.4}(CO_2)_{1.3}-OH$	1.96	1.00	1.9	1.2	2.4	2	3.6	34	46	125
$C_{12}EO_{13.3}(CO_2)_{0.6}-OH$	3.61	1.00	2.0	1.2	2.3	1.9	3.4	34	43	125
$C_{12}EO_{10.3}(PL)_{1.0}-OH$	1.60	0.99	2.5	1.3	3.3	1.8	3.7	51	74	82
$C_{12}EO_{13.2}(PO)_{1.1}-OH$	1.29	0.74	2.2	1.2	2.7	1.6	3.7	44	53	83
$C_{12}EO_{14.0}-OH$	0.71	0.72	2.4	1.2	2.8	1.5	3.6	39	49	82
$C_{12/14}EO_9-OH$	7.65	0.00	1.1	1.8	2.0	1.8	3.7	53	86	73

in the thermodynamic limit, i. e. $q \to 0$. The static intensity I(0) is shown for all surfactants as a function of the volume fraction ϕ (here considering the "dry" volume fraction ϕ resulting from the surfactant only) are given in Fig. 5.5. With increasing volume fraction the intensity I(0) shows an expected maximum at a given ϕ. The intensity first increases linearly with the number of dispersed particles but with increasing concentration, they become increasingly ordered. This effect is quantitatively described by the structure factor S(0), that leads to a reduction in forward scattering intensity. Moreover, one also observes a striking increase in intensity with increasing CO_2 content, and at the same time, the relative reduction of intensity beyond the maximum becomes much less pronounced.

To describe the experimentally observed scattering behavior, we employed the hard-sphere model according to Carnahan-Starling[138] as described in the experimental section 5.2.4 in equation 5.7. In the Carnahan-Starling analysis, one considers the hard-sphere volume fraction ϕ_{HS} which is the effective solvated volume fraction responsible for the hard-sphere interaction ($\phi_{HS} = B \cdot \phi(1 - A\phi)$). Thereby describes B the extend of hydration (the amount of water, which is strongly bound to the head group). The water content has to be considered when the aggregates are described as hard-spheres. The parameter A is a factor for the effective "softness" of the aggregates, which defines a certain interaction parameter and the extent of interpenetration. With increasing concentration, the aggregates can interpenetrate and thereby reducing the effective volume fraction. Based on this analysis the experimental static intensity I(0) was fitted according to the following equation:

$$I(0) = \phi \cdot \Delta SLD^2 \cdot V \cdot S(0) \tag{5.12}$$

Describing these data with this equation, as shown in Fig. 5.5, one observes that with increasing CO_2 content one has less hydration of the head groups (smaller B) and therefore a lower effective volume fraction (data summarized in Table 5.4). More importantly, the aggregates become much softer, as evidenced by the substantial increase of A, which means that at higher concentrations the effective volume fraction of the aggregates is less increasing. This means that the CO_2-containing micelles are much more interpenetrating and thereby much less repulsive.

These results are in good agreement with the studies of the thermodynamic micellization behavior described in chapter 4. With increasing CO_2 content the hydration is drastically reduced. The PO surfactant shows again similar behavior as the reference surfactant $C_{12}EO_{14.0}-OH$. The

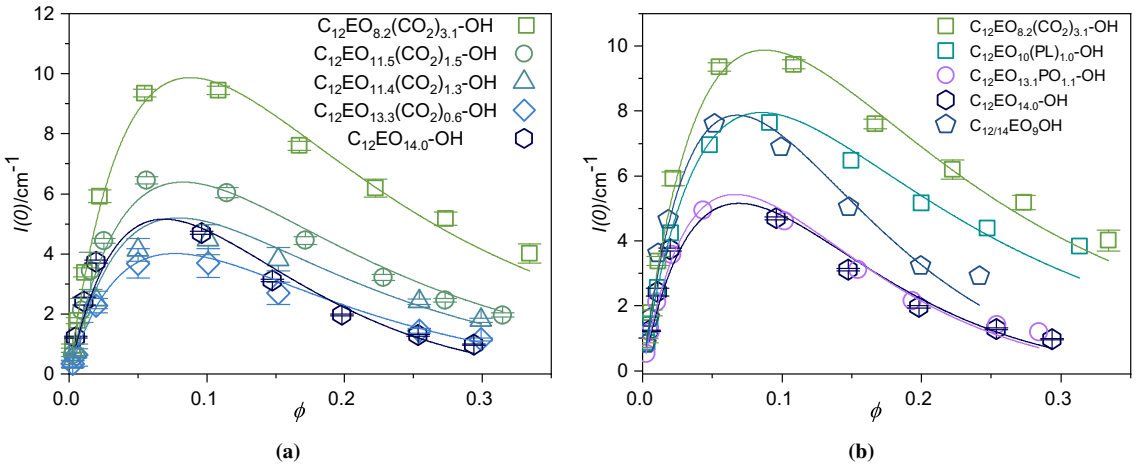

Figure 5.5: $I(0)_{exp}$ for all CO_2 surfactants (a) and PO and PL surfactants and the commercial reference $C_{12/14}EO_9-OH$ (b) from SANS data depending on the volume fraction ϕ_{dry}. Lines are $I(0)_{theoretical}$ considering the static structure factor $S(0)_{CS}$ which was calculated from the volume fraction ϕ_{HS} of the swollen aggregates with a certain amount of water B and an interaction parameter A. Figure (a) is reproduced from ref. [79] and figure (b) is reproduced from ref. [147].

commercial surfactant $C_{12/14}EO_9-OH$ has still lower values than the CO_2 surfactants, even though the comparison is not exact as it also has a different alkyl chain. Interestingly, the water content in the aggregate head group region, parameter B, and the resulting hydration factor, H defined as water molecules per surfactant molecules (H_2O)/n(surfactant), decrease prominently with increasing CO_2 content, however, the PO surfactants show similar H values as the reference surfactant $C_{12}EO_{14.0}-OH$. The hydration number H implies that for each EO group one has about 2 water molecules, while one can assign nominally 0 water molecules per CO_2 group. H decreases markedly with incorporated CO_2 or PL, while being similar for the PO and pure EO surfactants. For each EO or PO unit one has a contribution to H of about ~ 2, while CO_2 or PL units seem not to contribute to it. Accordingly, similar micelles are present but the incorporation of CO_2 and PL moieties is largely reducing the hydration affinity, while PEO is known to be strongly hydrated.[149, 150] The suppressed hydration of CO_2 surfactants can explain the smaller head group area. In addition, it appears that CO_2 of neighboring micellar head group coronas are less repulsively interacting with each other. In summary, the interaction potential between the nonionic micelles becomes much less repulsive.

The reduced hydration of the CO_2 surfactants can also be derived from the SANS modelling of the I(q) data (as discussed in the Appendix Chapter 5, see Fig. 10.12). The amount of bound water in the corona/shell is displayed in Fig. 10.12 and one sees a slight reduction of H with increasing CO_2 content. The absolute values of H are higher here than from the analysis of the I(0) data. This can be ascribed to the fact, that the data in Fig. 10.12 derive from the analysis of a dilute sample (1 wt%) where the hydrophilic shell is extended and in general contains more water than at high concentration where the micelles are densely packed (which is the situation relevant for the I(0) analysis).

Accordingly, similar micelles are present, but the incorporation of the CO_2 moieties into the hydrophilic head groups lead to a substantial alteration of the interaction potential and rendering them much softer. This arises first from the lower extent of hydration of the head groups and secondly from less repulsive interactions due to the presence of CO_2 units, that allow for interpenetration of the hydrophilic corona of the surfactants. PEO is known to be strongly

Table 5.4: Parameters from the fits shown in Fig. 5.5b for $I(0)_{exp}$ from SANS data for volume fractions up to 0.35: A, B, the hydration number H (molecules of water per surfactant molecule), the molecular weight Mw, the aggregation number N_{agg} and the head group area a_0.

Surfactants	A	B	H	Mw / kg/mol	N_{agg}	a_0 /nm^2	R_g /nm
$C_{12}EO_{8.2}(CO_2)_{3.1}-OH$	0.55	1.52	17.2	56	82	0.58	2.63
$C_{12}EO_{11.6}(CO_2)_{1.5}-OH$	0.52	1.58	19.7	35	46	0.65	2.33
$C_{12}EO_{11.4}(CO_2)_{1.3}-OH$	0.50	1.63	23.2	30	40	0.70	2.36
$C_{12}EO_{13.3}(CO_2)_{0.6}-OH$	0.37	1.64	25.2	23	29	0.46	2.26
$C_{12}EO_{10.3}(PL)_{1.0}-OH$	0.53	1.55	18.4	42	62	0.63	2.65
$C_{12}EO_{13.2}(PO)_{1.1}-OH$	0.01	1.79	32.8	34	41	0.72	2.36
$C_{12}EO_{14.0}-OH$	0.01	1.72	28.8	31	39	0.74	2.00
$C_{12/14}EO_9-OH$	0.01	1.75	23.1	46	75	0.59	2.15

hydrated[149, 150] but this tendency is reduced by the presence of CO_2 units. Such a reduction of the hydration goes with a reduced head group size a_0, which explains the formation of larger aggregates based on simple geometry. The head group area was already determined from surface tension measurements as described in thorough detail in the previous chapter 4. This value can also be derived from SANS measurements as the radius of a spherical micelle should be given as $R = 3v_h/a_0$, with v_h being the molecular volume of the hydrophobic part of the surfactant. For spherical micelles, this corresponds to a reduction of the head group area a_0 from 0.72 nm^2 for the pure EO surfactant ($C_{12}EO_{14.0}-OH$) to 0.58 nm^2 for $C_{12}EO_{8.2}(CO_2)_{3.1}-OH$ surfactant (Table 5.4). Showing a reduced head group area for the CO_2 and PL surfactant, whereas the PO surfactant shows similar values as the reference surfactant. The resulting values are in good agreement with the ones described previously. A rational explanation of this observation would be that with increasing CO_2 content the head group area a_0 is reduced due to a lower extent of hydration. The resulting parameters from the fit of the static intensity are summarized in Table 5.4. The resulting molecular weight, which is fitted based on the assumption of a constant aggregate size, is in good agreement with the data obtained from the model analysis, as described in the previous section.

This analysis combined with the information obtained from the model analysis, a precise picture of the micellar aggregates can be drawn. Thereby plays the hydration of the micellar head groups an important role. The suppressed hydration of the CO_2 surfactant in comparison to the reference surfactants and the PO surfactants varies the phase behavior systematically. The interaction and the extent of ordering at high concentration change largely upon the incorporation of CO_2 into the head groups. This makes it highly interesting to investigate the influence of the CO_2 moiety on the phase behavior at higher concentrations.

5.3.2. Phase Behavior of the High Concentration Regime

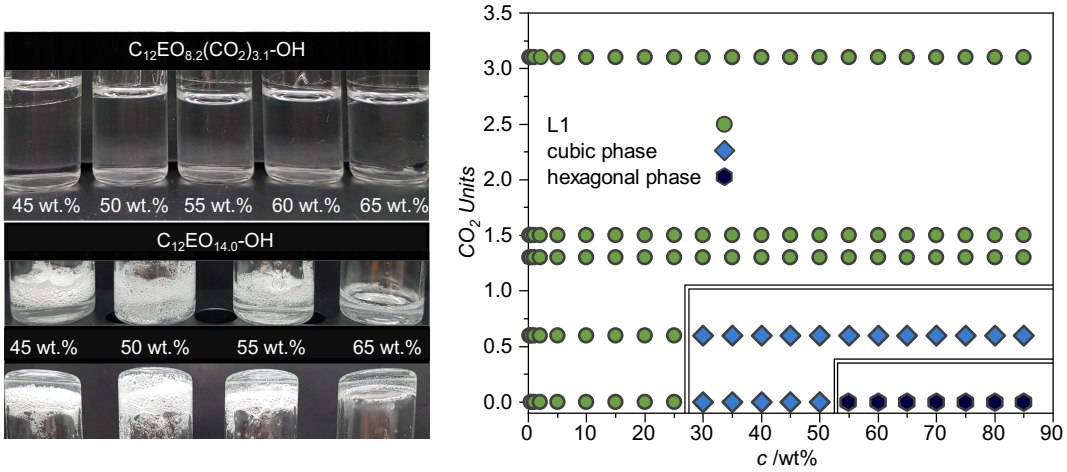

Figure 5.6: Left: Photos of different concentrations of the CO_2 surfactant with the highest CO_2 content and the reference surfactant $C_{12}EO_{14.0}-OH$ without CO_2 units. Right: Phase diagram at 25 °C as a function of the surfactant concentration and the number of CO_2 units contained in the hydrophilic head group (with isotropic L_1-phase, cubic phase and hexagonal phase). The reference (x = 0) is $C_{12}EO_{14.0}-OH$. Figure right is reprinted from ref. [79].

After investigating the phase behavior of the low concentration regime, one obtained detailed insights into the structure of the formed aggregates. Furthermore, the phase behavior of the high concentration regime (> 20 wt%) of the four different CO_2-containing surfactants, the PO and PL surfactants, and the two reference surfactants $C_{12}EO_{14.0}-OH$ and $C_{12/14}EO_9-OH$ was studied. The results of the CO_2 surfactants are mainly discussed in the article published in the journal *ChemSusChem*.[79] For this purpose, the samples were maintained at a given temperature and their texture observed visually and with polarized light microscopy (see Fig. 5.7). All of the CO_2 containing surfactants as well as the reference sample, dissolved homogeneously in water. The PO surfactants and both reference surfactants with only EO units form isotropic gels in a hexagonal or lamellar phase in the concentration range from 45 – 65 wt%, as shown in the phase diagram depicted in Fig. 5.6.

The formation of the so-called liquid crystalline phase is quite common for nonionic EO-based surfactants[83, 151, 152] and it is quite remarkable that for the surfactants with more than one CO_2 unit no liquid crystalline phases are shown over the entire concentration range. $C_{12}EO_{13.3}(CO_2)_{0.6}-OH$ showed an intermediate behavior with a somewhat smaller gel range (see photographs in Appendix Chapter 5 Fig. 10.5). This means that with little or no CO_2 in the head group gels are formed at higher concentrations, while the surfactant with more CO_2 in the head groups are viscous fluids at higher concentrations.

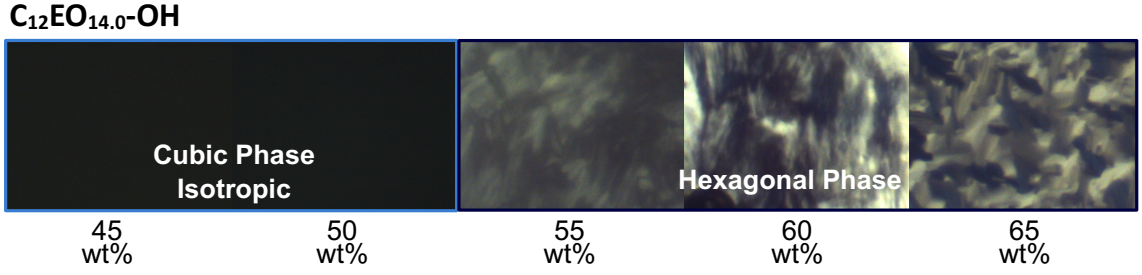

Figure 5.7: Photos from polarization microscopy: Images of the reference sample $C_{12}EO_{14.0}-OH$ at 45 and 65 wt% between crossed polarization filters. Figure is reproduced from ref. [79].

Moreover, one also observes a phase transition from cubic phases to hexagonal phases for the $C_{12}EO_{14.0}-OH$ surfactants. The assignment of the different liquid crystalline phases was done based on polarization microscopy (cubic phase is isotropic, while the hexagonal phase shows typical fan-like birefringence textures, as shown in Fig. 5.7. To investigate the visual differences at the high concentration regime in more detail and to obtain more information about the difference of the flow behavior of the surfactants rheology measurements were performed.

Rheological Behavior

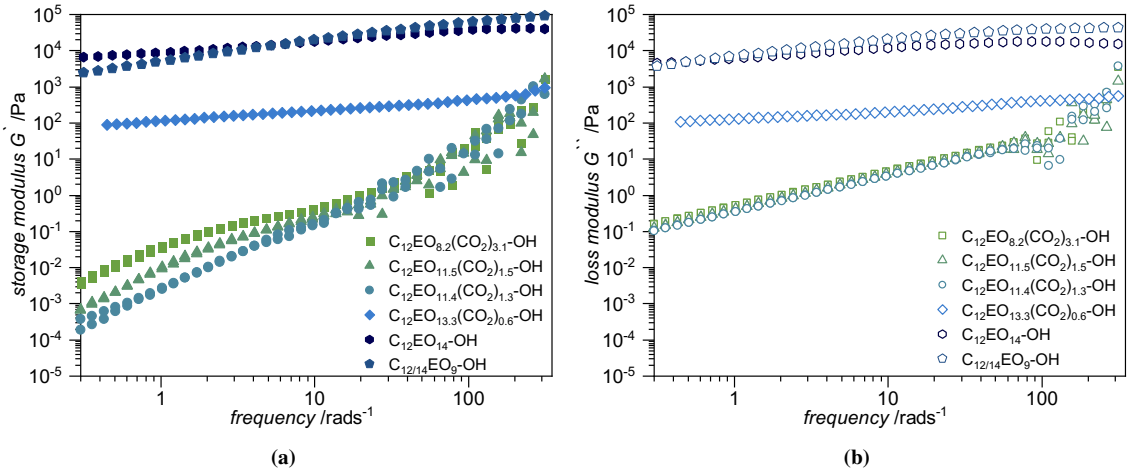

(a) (b)

Figure 5.8: : Oscillation measurements at a shear stress of 0.5 Pa of all CO_2-containing surfactants (65 wt%) and the reference samples at 25 °C. (a) is the storage modulus G‘ and (b) is the loss modulus G“. (cone-plate stainless steel geometry radius: 40 mm, gap size 150 µm. Figure is reproduced from ref. [79].

Rheological measurements were carried out of the different surfactant samples to characterize their viscoelastic properties. The behavior at high concentrations, as for conventional nonionic surfactants of this type, e.g. for $C_{12}EO_8$[83] or $C_{12}EO_{12}$[152], one observes with an increasing concentration above ~ 25 – 30 wt% first a cubic phase and at higher concentration a hexagonal phase is formed, both appear as highly viscous gels. This is observed for both reference surfactants without CO_2 and the CO_2 surfactant with the lowest CO_2 content ($C_{12}EO_{13.3}(CO_2)_{0.6}-OH$), which showed gel-like behavior in the concentration range of 45 – 65 wt%.[126, 153–155]

The storage modulus G’ as a function of frequency was obtained from oscillatory rheological measurements for the different surfactants at a given concentration of 65 *wt%* (Fig. 5.8a). It shows for $C_{12}EO_{14.0}-OH$ constant values of 2·104 Pa (rather stiff gel, these values depend somewhat on the concentration), which quantifies the gel-like properties of these samples. Already for the surfactant with the lowest CO_2 content, the value is reduced by two orders of magnitude. It is still rather constant, thereby confirming the gel properties, but being a much softer gel. In contrast, for the surfactants containing more than one CO_2 moiety, the values are smaller by four to six orders of magnitude (values are given in Fig. 5.8a for the samples with x < 1 are not really meaningful as for them the viscous properties (G”) clearly dominate the elastic properties (G’), a feature characteristic of viscous-like behavior liquids, as shown in Fig. 5.8b). This implies, that for CO_2 surfactants with more than one CO_2 unit per molecule in their hydrophilic head group, no longer liquid crystalline phases are formed. In comparison, the incorporation of a PO unit in the hydrophilic head group is not suppressing the formation of LC phases. The absence of the liquid crystalline phases for higher

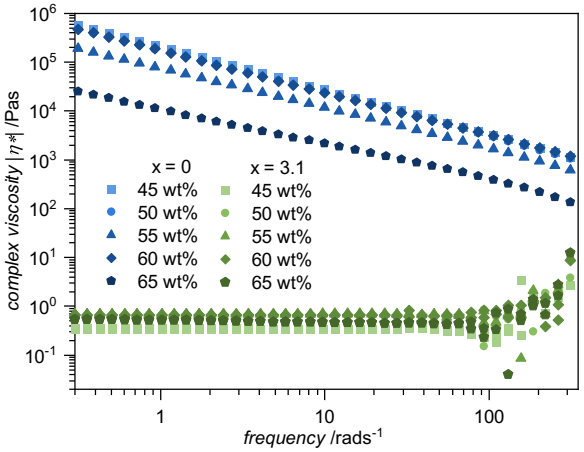

Figure 5.9: Magnitude of the complex viscosity η^* for the CO_2-richest surfactant (x=3.1) and the reference sample without CO_2 (x=0) different surfactant samples in the high-concentration regime of 45–65 wt% obtained at 25 °C from oscillation measurements at a shear stress of 0.5 Pa. Figure is reproduced from ref. [79].

CO_2 content is not only interesting for fundamental soft matter science but is also largely altering the flow behavior of such systems, and thereby the way they can be handled in terms of application.

The CO_2 containing surfactants with more than one CO_2 unit per molecule are always rather low viscous Newtonian fluids ($\eta < 1$ Pas), while conventional nonionic surfactants form highly viscous gels with yield stress. The effect of a largely changed flow behavior is quantified by the viscosity curves shown in Fig. 5.9 that directly compare the surfactant without CO_2 and the one containing 3.1 CO_2 units ($C_{12}EO_{8.2}(CO_2)_{3.1}-OH$) at different concentrations. In the concentration range from 45 to 65 wt% the CO_2 surfactants remain always as a Newtonian liquid with a viscosity of 0.4 – 0.8 Pas. The equivalent reference surfactant and the conventional reference without CO_2 have 4 – 6 orders of magnitude higher viscosities (and no finite zero-shear viscosity; corresponding to a yield stress) and a reduction with increasing frequency (corresponding to shear thinning) is observed. This is also observed for the CO_2 surfactant with the lowest CO_2 content ($C_{12}EO_{13.3}(CO_2)_{0.6}-OH$), the concentration dependent viscoelastic behavior of this sample shows gel-like behavior similar to the CO_2-free surfactant. Here, the CO_2 content in the surfactant is too low to significantly influence the flow as well as the phase behavior. The surfactant with the lowest CO_2 content represents the transition between the viscous-like behavior of the CO_2 surfactants and the gel-like highly viscous CO_2-free reference samples.

Small-Angle Neutron Scattering

Apparently, the flow and phase behavior of the concentrated nonionic surfactant solutions are largely changed by the incorporation of the CO_2 moieties into their head groups. To elucidate this interesting phenomenon, we studied the structure of the formed aggregates at the higher concentration regime to obtain information about their structural ordering. This investigation was done by SANS experiments. They confirm that at higher concentrations no liquid-crystalline ordering is formed for the CO_2 containing surfactants. Especially no cubic phases are observed, which typically show pronounced gel-behavior[151]. Liquid crystalline phases are usually manifested in the scattering patterns by pronounced peaks (“textures”) on the isotropic correlation peak[151, 153, 156–158] occurring from the highly ordered pattern, as seen for $C_{12}EO_{14.0}-OH$, $C_{12/14}EO_9-OH$ and $C_{12}EO_{13.3}(CO_2)_{0.6}-OH$ (shown in Fig. 5.10a for samples with 50 wt%, for

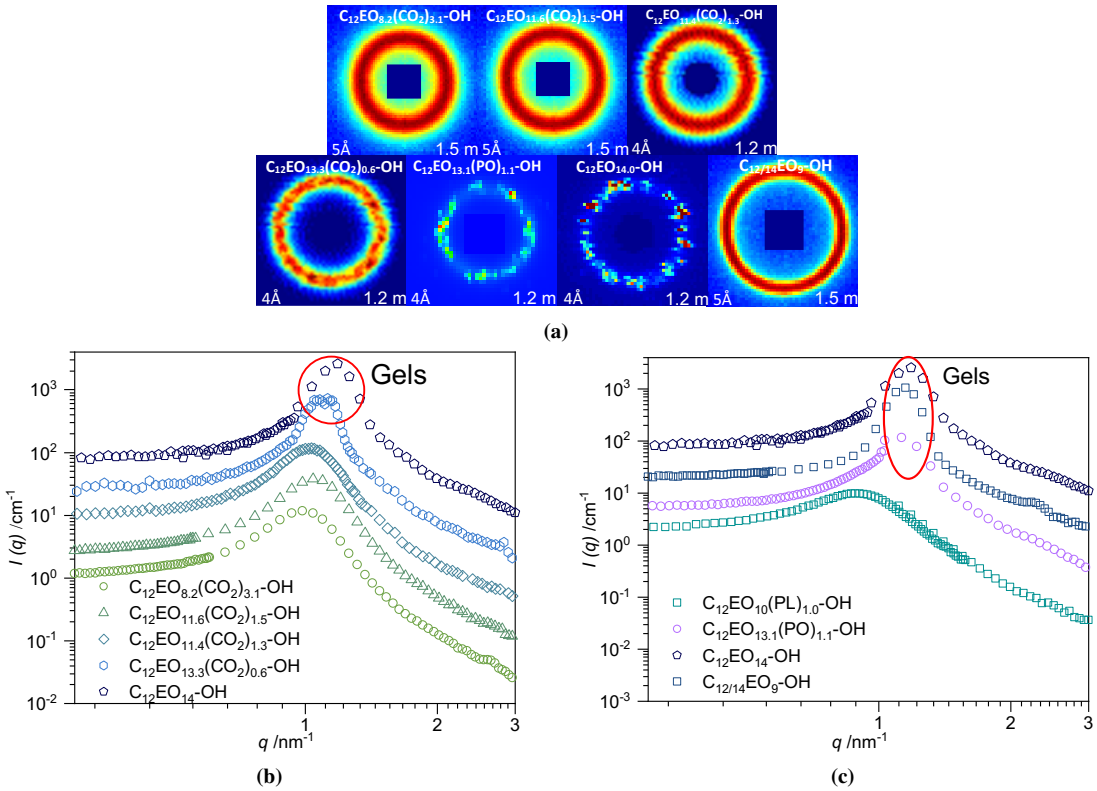

Figure 5.10: (a) Comparison of 2-D scattering patterns of the nonionic surfactants with different CO_2 content in their head groups for a constant concentration of 50 wt%. (b) Radially averaged intensity curves for the CO_2 surfactants and the reference surfactants at 50 wt% (indicating the prominently sharper peaks of the gels). The curves are scaled on the y-axis by the following multiplicators: $(CO_2)_{3.1} \cdot 1$; $(CO_2)_{1.5} \cdot 4$; $(CO_2)_{1.3} \cdot 412$; $(CO_2)_{0.6} \cdot 464$; $(CO_2)_0 \cdot 424$. (c) same plot for the PL and PO surfactants and the commercial reference $C_{12/14}EO_9-OH$. The curves are scaled on the y-axis by the following multiplicators: $(PL)_{1.0} \cdot 1$; $(PO)_{1.1} \cdot 65$; $(CO_2)_0 \cdot 260$; Marlipal24/90 $\cdot$ 2000. Figure is reproduced from ref. [79].

the scattering patterns at other concentrations see Fig.10.18). In contrast, the samples with higher CO_2 content show isotropic rings in the scattering pattern. The samples with the lowest CO_2 content, $C_{12}EO_{13.3}(CO_2)_{0.6}-OH$, exhibit pronounced peaks as typically observed for cubic phases. These peaks occur when the domains become so large that within the scattering volume only a rather small number of scatterers are present. For the reference sample without CO_2, $C_{12}EO_{14.0}-OH$ and $C_{12/14}EO_9-OH$, and the PO surfactant, characteristic peaks can be observed, depending on the concentration. By that, the surfactant with the lowest CO_2 content represents the transition between the liquid crystalline phase of the reference samples and the disordered phased behavior of the CO_2 containing surfactants.

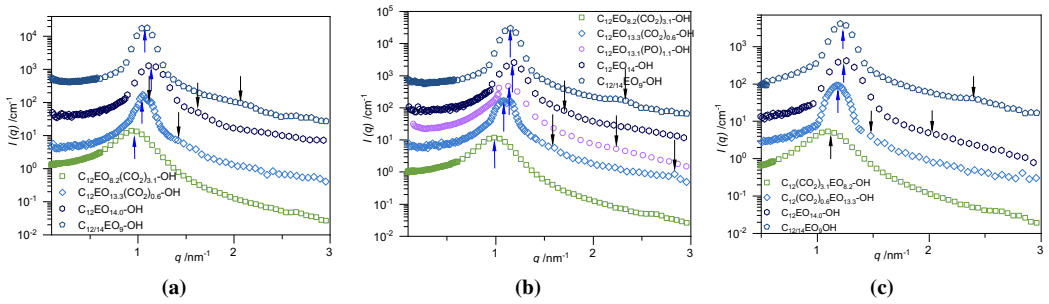

Figure 5.11: SANS scattering curves for the CO_2 surfactants with the highest (x = 3.1) and the lowest (x = 0.6) CO_2 content, PO surfactant and the reference samples $C_{12}EO_{14.0}-OH$ and $C_{12/14}EO_9-OH$ at 25 °C. The correlation peak positions as used to determine the liquid crystalline phase (a) for 45 wt%, (b) for 50 wt% and (c) for 65 wt%.The peak position of peak one is represented by the blue arrow and the peak position of the second peak is shown by the black arrow. Figure is reproduced from ref. [79, 147].

Table 5.5: Resulting values for the peak position from the samples shown in Fig. 5.11.

Surfactants	q_2/q_1	phase	q_2/q_1	phase	q_2/q_1	phase
	45 /wt%		**50 /wt%**		**65 /wt%**	
$C_{12}EO_{8.2}(CO_2)_{3.1}-OH$		L1		L1		L1
$C_{12}EO_{13.3}(CO_2)_{0.6}-OH$	1.35	cubic	1.45	cubic	1.25	cubic
$C_{12}EO_{13.2}(PO)_{1.1}-OH$			1.99	lamellar		
$C_{12}EO_{14.0}-OH$	1.43	cubic	1.44	cubic	1.72	hexagonal
$C_{12/14}EO_9-OH$	1.99	Lamellar	2	lamellar	1.97	lamellar

When looking more closely at the radially averaged correlation peak at a given concentration of 50 wt% (Fig. 5.10b and Fig. 5.10c), one notices that the peaks become increasingly wider and less sharp with increasing CO_2 content (for instance if one compares $C_{12}EO_{8.2}(CO_2)_{3.1}-OH$ with the reference samples $C_{12}EO_{14.0}-OH$ and $C_{12/14}EO_9-OH$). This indicates a much lower degree of order (correlative a lower effective volume fraction), which generally could be attributed to softer interactions with a higher degree of interpenetration between micelles. At the same time, the peak position moves somewhat towards smaller q values, which indicates a micellar growth with increasing CO_2 content in the head group.

The structure of the liquid crystalline phase was determined by the relative position of the higher-order SANS peaks (for details see Fig.5.11).[159, 160] The ratio between the first and second peak is characteristic for the formed phase. For lamellar phases, a ratio of 2 is expected. For hexagonal phases a ratio of $\sqrt{3}$ and for primitive cubic phases a factor of $\sqrt{2}$. The resulting phases for the CO_2 surfactants with the highest and the lowest CO_2 content, the PO surfactant, and the two reference samples at 45, 50, and 65 wt% are summarized in Table 5.5. The information was used for the phase diagram in Fig. 5.6. The peak position indicated a cubic phase (hexagonal at 65 wt%) for the reference sample without CO_2 ($C_{12}EO_{14.0}-OH$) and a lamellar phase for the commercial reference sample, $C_{12/14}EO_9-OH$, (Fig. 5.11). Interestingly, the CO_2 surfactant with the lowest CO_2 content, $C_{12}EO_{13.3}(CO_2)_{0.6}-OH$, shows characteristic textures but the spacing of the peaks

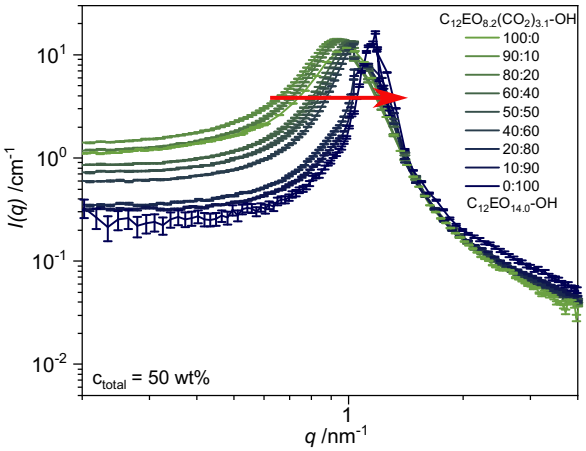

Figure 5.12: SANS measurements of mixtures of the CO_2 surfactant $C_{12}EO_{8.2}(CO_2)_{3.1}-OH$ and the reference surfactant $C_{12}EO_{14.0}-OH$ at ratios between 90:10 and 10:90 with a total concentration of 50 wt%. the pure surfactants at 50 wt% are also shown. All measurements were performed at MLZ KWS-1 except for $C_{12}EO_{14.0}-OH$ which was measured at LLB PAXY.

indicates a disordered cubic phase, which would explain the lower viscosity as usually expected for cubic phases.

The differences in phases behavior between the CO_2 surfactants and the reference surfactant allow for a systematic variation of the viscosity by mixing the two surfactants ($C_{12}EO_{8.2}(CO_2)_{3.1}-OH$ and $C_{12}EO_{14.0}-OH$) with different ratios (see Fig. 5.12). One can observe a smooth transition from the highly ordered, viscous system of the reference sample to a fluid, Newtonian like system (L1) such as the CO_2 surfactant. This phenomenon allows for a systematic variation of the viscosity as desired for applications.

The SANS measurements confirm that the incorporation of CO_2 moieties into the hydrophilic head groups leads to a substantial alteration of the interaction potential and suppresses the formation of liquid crystalline phases with gel-like properties (as already seen in the phase and rheology studies). As described previously, if the CO_2 content in the head group is sufficiently high, the micelles have a lower extend of hydration (decreasing B) and the interaction becomes less repulsive (decreasing A) and gel-like cubic phases are no longer formed. That allow for interpenetration of the hydrophilic corona of the surfactants (see schematic description Fig. 5.13). This is very important from a practical point of view, as such systems are much easier to handle at high concentrations in terms of processability. Moreover, this effect can be tuned by mixing the CO_2 surfactants with reference surfactants to systematically vary the hydration affinity of the aggregates and therefore vary the phase behavior.

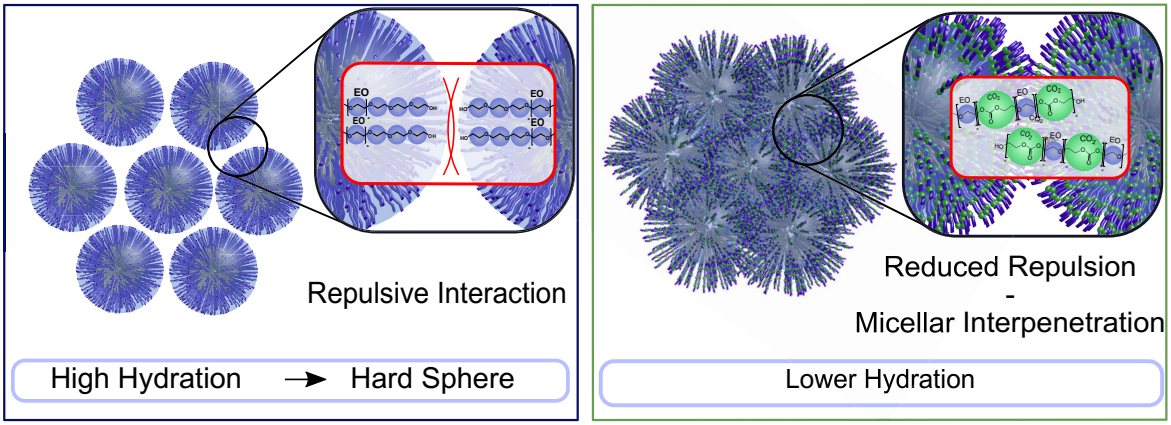

Figure 5.13: Scheme for the packing conditions prevailing in the case of nonionic surfactants without and with incorporated CO_2 units in the head group. A higher CO_2 content reduces hydration, and lowers the repulsive interactions and thereby allows for interpenetration of the hydrophilic micelles shells. Figure is reproduced from ref. [79].

5.3.3. Temperature Dependent Phase Behavior of CO_2 Containing Nonionic Surfactants

Nonionic surfactants of the C_iE_j type typically show a pronounced temperature dependence of their aggregation behavior, forming increasingly larger, elongated aggregates upon approaching the cloud point.[83, 161] For instance, this is also important for their performance in important applications, such as detergency.[162] We also investigated the temperature response of the novel CO_2 containing surfactants by measuring light scattering (Fig. 5.14) and SANS (Fig. 5.15) at 25, 40, 50 and 60 °C. These measurements generally show an increase of micelle size with increasing temperature. This temperature dependence is an effect that is most pronounced for the surfactant

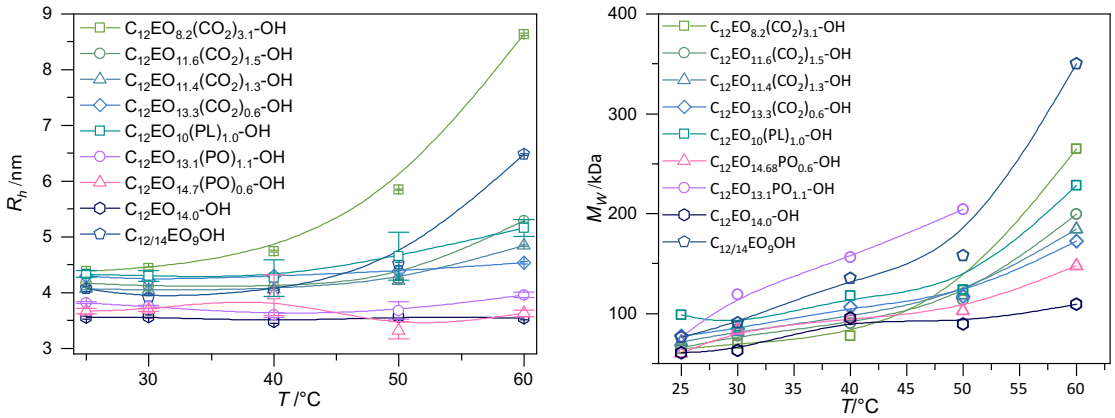

(a) **(b)**

Figure 5.14: (a) Hydrodynamic radii from DLS Measurements for all CO_2, PO and Pl surfactants and both reference samples. (b) Temperature dependent molecular weight of all CO_2, PO and PL surfactants and both reference samples from SLS measurements. Lines are guide to the eye. Figure is reproduced from ref. [147].

with the highest CO_2 content, $C_{12}EO_{8.2}(CO_2)_{3.1}-OH$. In contrast, the surfactants with lower CO_2 content, $C_{12}EO_{13.3}(CO_2)_{0.6}-OH$ and $C_{12}EO_{11.4}(CO_2)_{1.3}-OH$ as well as the reference surfactant without CO_2, $C_{12}EO_{14.0}-OH$, exhibit almost no change. Interestingly, the PL surfactant, $C_{12}EO_{10.3}(PL)_{1.0}-OH$, shows a temperature response not as high as the one with the highest CO_2 concentration. Moreover, the commercial surfactant, $C_{12/14}EO_9-OH$, shows a temperature response comparable to the one with the highest CO_2 concentration, while the reference sample $C_{12}EO_{14.0}-OH$ shows the least temperature response. The PO surfactant shows again a comparable response like the reference surfactant. This indicates that the temperature dependence of the aggregation behavior can be controlled by the CO_2 content in the head group but is also affected by the precise composition of the hydrophilic chain.

The increase in size can be observed in an increase of the hydrodynamic radii obtained from DLS measurements (Fig. 5.14a) and an increase of the molecular weight obtained from SLS measurements (Fig. 5.14b). The increase of size can be interpreted in terms of a structural transition from spherical micelles up to cylindrical micelles. This structural transition can hardly be described by DLS measurements therefore SANS measurements were performed to obtain the detailed picture of the formed aggregates at higher temperatures.

Looking in more detail at the SANS data (Fig. 5.15b) one observes an elongation of the micellar structures (sphere-rod transition) at higher temperature as typically seen for C_iE_j surfactants.[163–165] This is manifested in an increase in forward scattering intensity, I(0), and a change of the slope to q^{-1} indicating the presence of locally rod-like structures. Temperature dependent SANS curves for the other surfactants are given in the Appendix Chapter 5. However, at lower q a leveling off indicates the finite length of these cylinders. This structural transition was described by a core-shell cylinder model with spherical end-caps. This model describes the shape of the formed aggregates the best and considers the core-shell structure. From this model the molecular weight M_w, the aggregation number N_{agg} and the length of the formed cylinder can be derived. The length of the cylinder can be determined by $2 \cdot R_{ax}$ and the radius of the end caps ($2 \cdot R_{eq}$) and the addition of the shell thickness ($L_{cylinder} = L_{core} + 2 \cdot R_{eq} + 2 \cdot T_{shell}$).

The obtained parameters from the model are depicted in Fig. 5.15a which represent the molecular weight M_w and length of the cylinder as a function of temperature. One can observe a

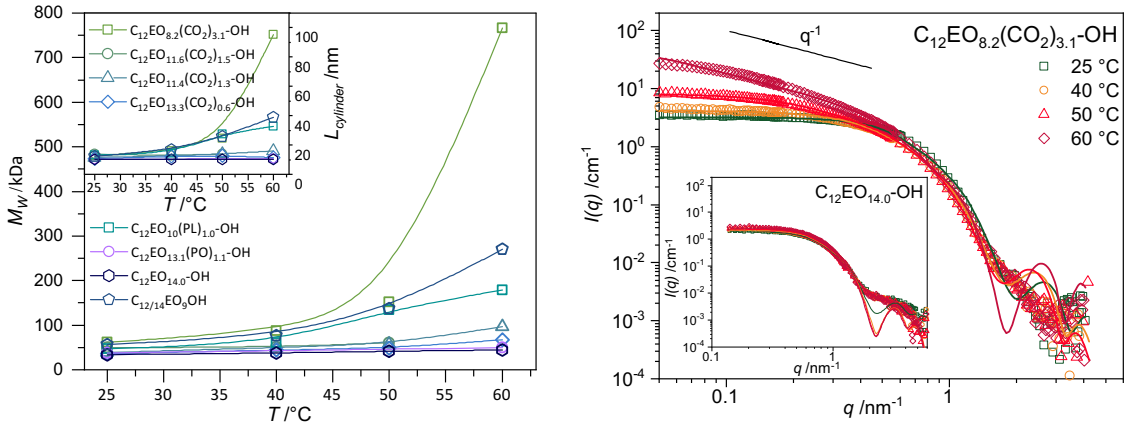

Figure 5.15: (a) Molecular weight M_W as a function of the temperature for the different surfactants (1 wt%) from SANS and (b) SANS intensity curves for concentrations of 1 wt% of $C_{12}EO_{8.2}(CO_2)_{3.1}-OH$ recorded at 25, 40, 50 and 60 °C (KWS-1 data at MLZ). The q^{-1} slope at high temperature indicates a transition to a rod-like surfactant shape. Figure is reproduced from ref. [147].

pronounced increase in size for the CO_2 surfactant, $C_{12}EO_{8.2}(CO_2)_{3.1}-OH$. Followed by the PL surfactants, $C_{12}EO_{10.3}(PL)_{1.0}-OH$, which also shows a prominent response, as well as the commercial reference surfactant $C_{12/14}EO_9-OH$. The CO_2 surfactant, $C_{12}EO_{8.2}(CO_2)_{3.1}-OH$, shows cylinder length of ~ 90 nm and the PL surfactant and $C_{12/14}EO_9-OH$ shows length of ~ 40 nm (at 60 °C). In contrast, and as stated before $C_{12}EO_{13.2}(PO)_{1.1}-OH$ and $C_{12}EO_{14.0}-OH$ (L ~ 10 nm) show almost no temperature response. It is quite interesting that the CO_2 surfactant have the most pronounced response to the temperature change because the cmc values show only little effect on the temperature.

The structural transition occurs from a change of conformation of the EO unit as depicted in Fig. 5.16. As described by Lindman *et al.*[166], the preferred conformation of the EO unit is a polar conformation (a-g-a), which indicates a large dipole moment, low statistical weight, and interact favorably with water. With increasing temperature, the amount of the less polar conformation (a-a-a) increases making the interaction with water less favorable. When EO-containing molecules are brought into contact with water at such temperature these less polar conformations are less soluble due to a lower polarity of the EO chain in the solution. Once the temperature reaches a certain value (depending on the EO chain length) the cloud point (CP) is reached and the system is phase separating. Before this point is reached, due to the conformational changes of the head group, a structural transition from spherical up to cylindrical aggregates is observed. This sphere-rod-transition depends on the length of the head group and the alkyl chain. For short head groups, very long micelles can be formed, whereas for larger head groups the growth is limited and even an association of spherical micelles is indicated.[166]

Considering these effects as an explanation for the enhanced temperature response of the CO_2 surfactants, one observes an interesting correlation with the CP. The CP is drastically reduced for the CO_2 surfactant, $C_{12}EO_{8.2}(CO_2)_{3.1}-OH$, with values of 69 °C in comparisons to >100 °C for the reference surfactant $C_{12}EO_{14.0}-OH$. Consequently, at a temperature of 60 °C it is only 9 °C below the cloud point of the $C_{12}EO_{8.2}(CO_2)_{3.1}-OH$ surfactant, whereas it is still 40 °C below the cloud point of the reference surfactant. Therefore, a lower response to temperature would be expected. The reason for a reduced cloud point could be a break in the symmetry of the EO chain by the incorporated CO_2 units, which could enhance the formation of the less polar a-a-a

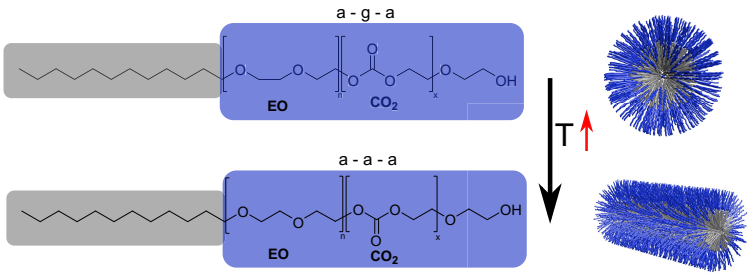

Figure 5.16: Schematic description of the conformation change from "anti – gauche – anti" a-g-a conformation at low temperature, to "anti – anti - anti" a-a-a conformation at higher temperatures. This conformation change leads to a transition from spherical micelles up to cylindrical micelles. Figure is reproduced from ref. [147].

conformation. But this explanation is only speculative and would require a theoretical analysis of the molecules in terms of temperature response. The PL unit has again a quite similar phase behavior than the CO_2 surfactants, one could assume, that the PL unit also introducing similar effects. However, the PO surfactant response similar than the reference surfactant $C_{12}EO_{14.0}-OH$, which can also be explained by a high CP (>100 °C). It should also be mentioned, that the reference surfactant and the PO surfactant have somewhat longer head group length (x + n > 14), which could also be an explanation for a reduced temperature response. Especially in comparison to the commercial reference surfactant $C_{12/14}EO_9-OH$, which shows a structural transition and a reduced CP with a shorter EO chain length of 9 units.

In summary, the temperature dependence of the CO_2-containing surfactants can be tuned with respect to the sizes and structures that they form by modifying the content of CO_2 in the head group. Moreover, a reduced CP and consequently a higher temperature response is a favored property in terms of application potential as a detergent; a reduced CP indicating a higher washing efficiency even at lower temperatures.[167]

5.3.4. Phase Behavior of C_{16} based CO_2 Containing Nonionic Surfactants

The phase behavior and typical properties of nonionic surfactants can also be varied by the length of the alkyl chain. Therefore, the phase behavior of CO_2 surfactants with a C_{16} alkyl chain has also been studied. The main feature of the C_{16} surfactants is that they are not soluble at room temperature. Therefore, the Krafft temperature T_K of the C_{16} surfactants was determined by transmittance measurements, as shown in Fig. 5.17a. T_K is in the range of ~ 40 °C for the C_{16} CO_2 surfactants, whereas the reference surfactant, $C_{16}EO_{14.6}-OH$, shows no Krafft temperature or cloud point in the temperature range between 25 and 60 °C, which indicates a lower T_K and a higher CP. The commercial reference surfactant Lutensol AT13, $C_{16/18}EO_{13}-OH$, shows a Krafft temperature at ~ 49 °C.

Accordingly, the hydrodynamic radius obtained from DLS measurements show high values below the Krafft temperature for the CO_2 containing C_{16} surfactants (see Fig. 5.17b). The radii are in the size range between 20 nm up to 100 nm. This indicates that the C_{16} surfactants are not water-soluble below T_K and show a two-phase region. Indicating that the surfactant is present as dispersion droplets and not as micellar aggregates. At temperatures, around 40 °C the measured sizes are decreasing and are in the range of ~ 10 up to 20 nm and with increasing temperatures an increase in size indicates a structural change. Only the reference surfactant, $C_{16}EO_{14.6}-OH$, shows

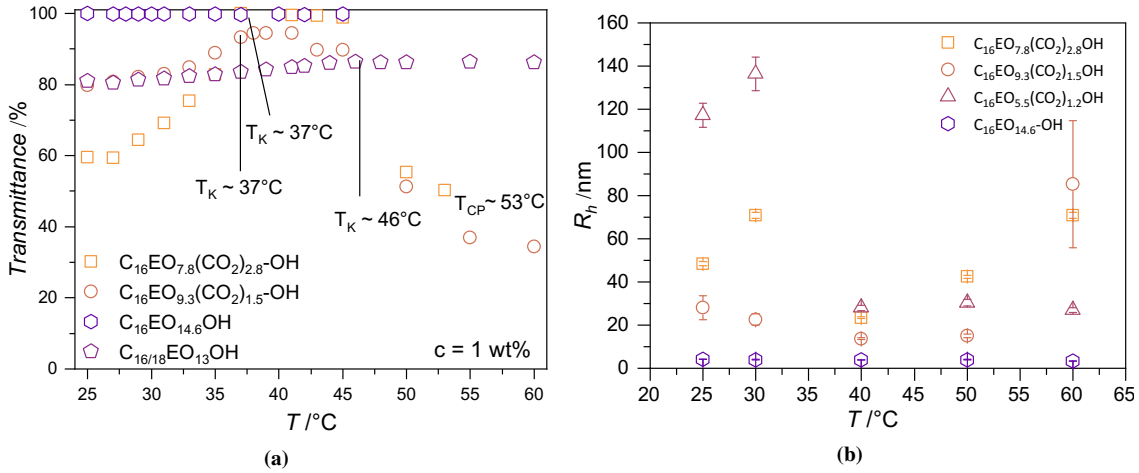

Figure 5.17: (a) Transmittance measurements at λ = 750 nm of the C16 CO_2 surfactants at 1 wt% in the temperature regime from 15 up to 60 °C. T_K is the Krafft temperature and T_{CP} is the temperature at which the cloud point occurs. (b) Hydrodynamic radius as a function of the temperature obtained from DLS measurements for all C16 CO_2 surfactants.

small aggregates in the range of ~ 4 nm in the temperature range from 25 up to 60 °C. It is in good agreement with the transmittance measurements, assuming a T_K below 25 °C and a CP value higher than 60 °C.

The characteristic structures for the C_{16} surfactants were also investigated with SANS measurements, as shown in Fig. 5.18. From the SANS scattering curves one can obtain a characteristic form factor minimum for all C_{16} surfactants at ~1.5 nm^{-1}, which corresponds to a radius of ~ 3 nm at 25 °C (Fig. 5.18a).

However, for C_{16} CO_2 surfactants and $C_{16/18}EO_{13}-OH$ a significant increase of the scattering intensity at low q values can be observed, which indicates larger sizes. The increase in intensity occurs from the dispersion droplets of insoluble surfactant at 25 °C. Only the reference surfactant, $C_{16}EO_{14.6}-OH$, shows no increase, which is in good agreement with the results from DLS measurements. With increasing temperature, the commercial reference surfactant, $C_{16/18}EO_{13}-OH$, shows a decrease of intensity and a plateau regime at low q at 40 °C. This indicates, that with increasing temperature the insoluble dispersion droplets disappear and the surfactant forms spherical aggregates in the size range of ~ 3 nm. Whereas, the surfactant with

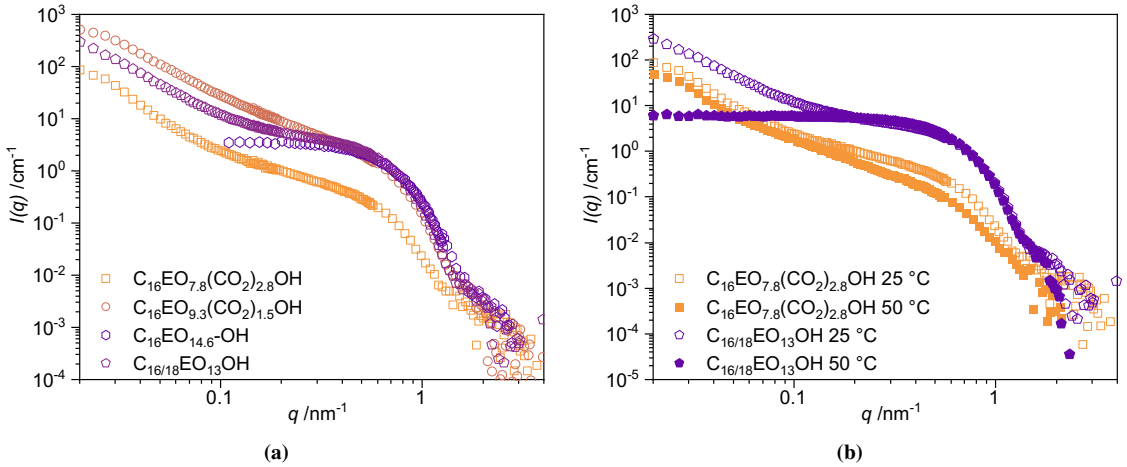

Figure 5.18: (a) SANS intensity curves for the different C16 surfactants (1 wt%) (a) and the SANS intensity curves for the surfactants $C_{16}EO_{7.8}(CO_2)_{2.8}-OH$ and $C_{16/18}EO_{13}-OH$ at 25°C and 50 °C. All surfactants were measured at the instrument KWS-1 at MLZ, except the surfactant $C_{16}EO_{14.6}-OH$, which was measured at LLB at the instrument PAXY.

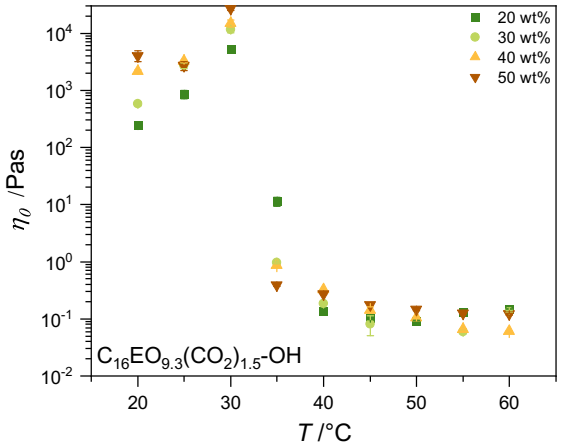

Figure 5.19: Viscosity measurements as a function of temperature in the range from 25 up to 60 °C in 5 °C steps, of the surfactant $C_{16}EO_{9.3}(CO_2)_{1.5}-OH$ at 20, 30, 40 and 50 wt%.

CO_2 moieties, $C_{16}EO_{7.8}(CO_2)_{2.8}-OH$, still shows an increase in intensity, which indicates remaining dispersion droplets of insoluble surfactant.

Furthermore, the phase behavior at the higher concentration regime (20 - 50 wt%) of the C_{16} surfactants show a rather high viscosities which are increasing from ~ 500 up to ~ 15000 Pas at temperature from 20 °C up to 30 °C (as shown in Fig. 5.19). Whereas with increasing temperature, the viscosity is reduced by a factor of 5. At temperatures higher than 40 °C, viscosity below 1 Pas can be observed. This behavior indicates, that below the Krafft temperature the viscosities remain rather high in comparison to the C_{12} CO_2 surfactants. It indicates, that the solid C_{16} surfactants form insoluble dispersion droplets, and with rising temperatures the structures dissolve and form liquid-like structures.

5.4. Summary & Conclusion

In this chapter, we studied the effect of incorporated CO_2 moieties on the structural and phase behavior in terms of concentration and temperature variation. Structural information obtained from light and neutron scattering measurements showed that prolate ellipsoidal micelles are formed with a core radius in the size range of 2 nm and a shell thickness of approximately 2 nm and an overall increase of size with increasing CO_2 content. Thereby remains the size almost constant in the low concentration regime. The PL surfactants show similar behavior and sizes than the CO_2 surfactants, whereas the PO surfactant is comparable to the reference surfactant, $C_{12}EO_{14.0}-OH$. Moreover, one obtains the information from the fractal exponent of the Porod regime, that the polymers in the shell are collapsed for the CO_2 surfactants and fully swollen up to Gaussian chains for the reference surfactant and the PO surfactant.

This phenomenon can be explained in terms of hydration. e.g. bound water molecules in the hydrophilic head group. This information can be obtained from scattering experiments, which implies that the CO_2 surfactants show substantial dehydration of the head groups and a much reduced repulsive interaction and interpenetration of the aggregates. The PO surfactants show similar hydration affinities as the reference surfactants. These results also explain the difference in the fractal exponent of the Porod regime, resulting in a collapsed or swollen state of the polymer in the hydrophilic head group. Moreover, of high interest are the regime at high concentrations, where

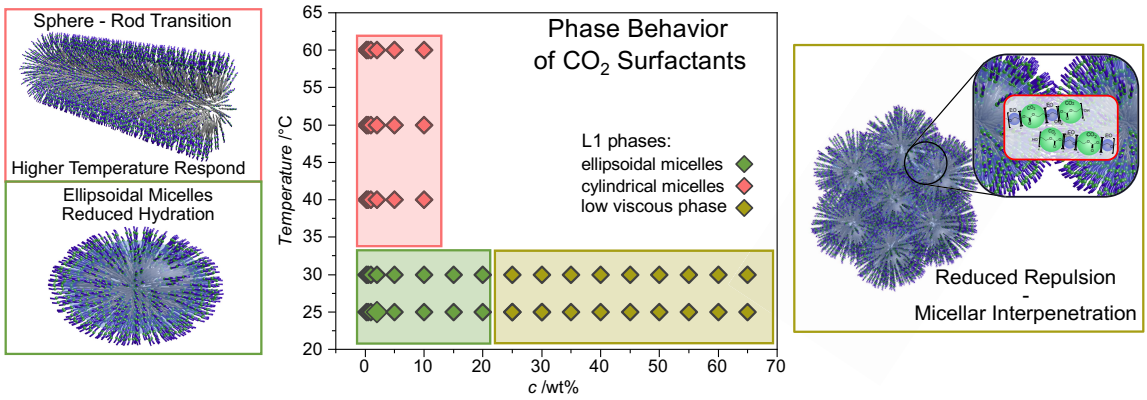

Figure 5.20: Schematic summary of the phase behavior in dependency of the concentration and temperature of the CO_2 containing surfactants.

phase studies up to 65 wt% show that the CO_2 surfactants (CO_2 content > 1 unit) do not form liquid crystalline (LC) cubic and hexagonal phases as usually observed for C_iE_j surfactants. This can be attributed to lower repulsive interactions and therefore a lower effective degree of ordering, i.e. a lower effective volume fraction, due to the presence of the CO_2 units in the head group. This absence of LC phases means that no gelation is observed which has the effect of a drastically reduced viscosity. The PO surfactant, the reference sample, and the commercial reference, $C_{12/14}EO_9-OH$, exhibit a yield stress and shear thinning behavior, whereas the CO_2-containing surfactants (CO_2 content > 1) displayed viscosities below 1 Pas and Newtonian like flow behavior. This is not only fundamentally a very interesting observation but also one of high practical importance. These properties facilitates enormously the handling of these surfactants at higher concentrations, as it is typically required in almost all applications at some stage. It should also be noted that this behavior is unique for CO_2 and PL incorporation. The suppressed hydration affinity by the incorporation of CO_2 or PL moieties leads to a lower degree of ordering, whereby the reduced repulsiveness of the interactions allow an interpenetration of the micelles and therefore no liquid crystalline phases are formed.

The temperature dependent phase behavior shows a rather complex response. The reference surfactant, $C_{12}EO_{14.0}-OH$, and the PO surfactants show almost no response to temperature increase. The CO_2 surfactants with rather high CO_2 content (> 1.3) and the PL surfactant show an increase in size with increasing temperature. This phenomenon is known as a sphere-rod transition, which is normally observed for C_iE_j surfactants. The high response of the CO_2 and PL surfactants to the temperature rise can be explained by a break in symmetry which enhance the formation of the less polar a-a-a configuration. These phenomenon reduces the cloud point of the CO_2 surfactants with higher CO_2 content (> 1.3) and thereby leads to a higher response. From these findings, the temperature response can be tuned by modifying the content of CO_2 incorporation in the head group, thereby rendering the surfactants much more effective as detergents even at lower temperatures.

This is an interesting example where a fundamental investigation of the structural and phase behavior of a surfactant system allows for a systematic understanding based on molecular architecture. All the findings demonstrate the versatile properties of these new CO_2-containing surfactants, which can be tuned in detail by the CO_2 content. Being able to work at any concentration allows for a better processability, thereby reducing substantially the ecological impact of the logistics for this large-scale commodity product. This information can be applied directly in surfactant science for formulation at high concentrations. In addition, these

CO_2 containing surfactants contribute to the aim of a more sustainable chemistry as the petrol-based EO units are replaced by CO_2 (up to 20%). This renders these greener surfactants as a very promising alternative to conventional nonionic surfactants, simultaneously reducing the consumption of oil-based resources with increased efficiency and tunable phase behavior.

Chapter 6

Solubilization Potential of Hydrophobic Drugs by CO_2 Containing Nonionic Surfactants

In the previous chapters, a thorough understanding of the micellization and phase behavior of the CO_2 containing surfactants could be obtained. This knowledge is essential to understand the fundamental properties of the CO_2 surfactants and use this knowledge to improve and tune their application potential. One potential application of these types of surfactants would be the solubilization of hydrophobic compounds to enhance the bioavailability and to substitute conventional, fossil-based nonionic surfactants. Therefore, the solubilization behavior of the CO_2 modified surfactants was investigated in thorough detail. Three hydrophobic compounds namely carbamazepine, fenofibrate, and isoproturon, with significant different water solubilities and polarities, were used to evaluate the solubilization behavior systematically. The solubility was determined using UV-Vis measurements and compared systematically to literature and commercially available surfactants. In this process, the influence of the CO_2 unit as an interaction parameter on the solubilization mechanism was investigated. This was determined using Nuclear Overhauser Effect Spectroscopy (NOESY)-NMR measurements. Small-angle neutron scattering (SANS) measurements were performed to obtain the size and shape of the formed aggregates. Furthermore, the solubilization behavior of triblock polyether carbonate polyols with different degrees of CO_2 functionalization in either their hydrophilic head group (ethylene oxide; EO) and/or their hydrophobic part (propylene oxide; PO) was compared to a commercial Pluronic® (F38; Poloxamer).

Main parts of this chapter are based on the following publication:

◊ V. J. Spiering, B. Hanf, M. Tupinamba Lima, L. Noirez, M.-S. Appavou, R. Schomäcker, M. Gradzielski: "Solubilization Potential of Hydrophobic Compounds by CO_2 Containing Surfactants", *Journal to come*, **in Preparation**.

6.1. Introduction

Most pharmaceutical hydrophobic compounds or active ingredients are organic molecules that are highly hydrophobic and are in general poorly water-soluble.[168, 169] The insufficient ability to become dispersed in aqueous solution limits their bioavailability and is a major issue in drug development. One approach to improve the bioavailability is the use of colloidal particles[170], or surfactant/polymer micelles.[171–175] An important property of amphiphiles is the formation of micellar aggregates above the critical micellization concentration (cmc), which have a particular significance in pharmacy as only above the cmc one observes a larger increase of the solubility of hydrophobic compounds in water.

In this context, solubilization can be defined as the spontaneous dissolution of a substance by the micelles of a surfactant in water to form a thermodynamically stable isotropic solution with a reduced thermodynamic activity of the solubilized material.[176] Apart from normal, low molecular weight surfactants, commonly used system for solubilization of hydrophobic compounds like pharmaceutical drugs or oils are nonionic poloxamers like Pluronics®. This linear triblock copolymer with a hydrophobic propylene oxide block (PO) and hydrophilic ethylene oxide blocks (EO) can be varied systematically with respect to their molecular structure, thereby also controlling their mesoscopic structure and aggregation behavior, as well as their solubilization properties. In that way they can become adapted to a given solubilizate. Extensive studies on Pluronic® structures were carried out at different temperatures, concentrations, and pH values showing a large influence of the molecular architecture on the solubilization behavior.[177, 178] Therefore, the major approach is that they show already promising results for formulations in the fields of pharmacy or agriculture.

In many approaches, polymeric micelles are already used for oral drug delivery systems. They have the advantage that they are moderately hydrophobic and water-soluble.[172] For example, the application of Pluronics® in anticancer therapeutics was shown by Raval *et al.*[179] The in vitro cytotoxicity of the drug-loaded micelles were investigated on MCF-7 breast cancer cells which showed higher anticancer activity as compared to free drugs. To achieve enhanced solubilization it is of major interest to understand the interaction of the hydrophobic compound and the polymers depending on the structure and the interaction. Nguyen-Kim *et al.*[180] analyzed the influence of the molecular architecture of Pluronics® with different PO and EO length on the solubilization behavior of carbamazepine and fenofibrate. Resulting in improved solubilization of fenofibrate in the micelles depending systematically on the polymer concentration and the PO chain length.

In this chapter, three different hydrophobic compounds namely fenofibrate, carbamazepine, and isoproturon with different chemical structures and polarities were investigated. Fenofibrate is less water-soluble (0.77 μmol/L) in comparison to isoproturon (0.33 mmol/l) and carbamazepine (0.40 mmol/L) at 25 °C. The solubilization of these hydrophobic compounds has already been studied in thorough detail. Several solubilization techniques have been established to improve the solubilization by changing the structure of the solubilizate, also the effect of alkyl chain length, and temperature have been studied.[175, 180–185] Fenofibrate showed good incorporation into formulations[186] with distinct dependence on the hydrophobic chain composition.[175] Bahloul *et al.* investigated the approach to the use of HLB values to optimize the solubilization of self-emulsifying drug delivery systems.[181] Considering different types of surfactants all with a

C_{12} alkyl chain, the best solubilization of fenofibrate was achieved with a sulfate head group. Vinarov *et al.*[175] observed that the solubilization capacity of fenofibrate decreases with increasing EO chain length between the alkyl chain and the sulfate group, while the EO chain length of nonionic ethoxylate surfactant shows no significant influence on the solubility capacity.

The solubilization of carbamazepine increases with the rise in temperature and concentration of Pluronics®, whereas the addition of salt shows no significant influence on the solubilization potential.[187] For the case of nonionic surfactants, it was recently found that carbamazepine is typically better solubilized with a C_{12} hydrophobic chain in comparison to a C_{16} chain length. However, it is predominantly solubilized in the micellar core, it prefers the interaction with the EO groups.[184] Similar findings have been shown by Jain *et al.*[188]. The carbamazepine solubilization is remarkably enhanced by D-α-Tocopheryl polyethylene glycol succinate (TPGS) micelles where the position of the hydrophobic compound is in the core. In contrast, Nguyen-Kim *et al.*[180] reported that the solubilization of carbamazepine is mainly enhanced by the lowering of the chemical potential of the solvent by the addition of triblock copolymer independent of the structure of Pluronics®.

The focus of this chapter will be the direct impact of the modification of the hydrophilic head group of nonionic surfactants and triblock polyether carbonate polyols by CO_2 and systematically characterize the solubilization potential. The incorporated CO_2 unit in the hydrophilic head group (ethylene oxide; EO) can maintain an additional interaction position with the hydrophobic compound, which can enhance solubilization. Furthermore, we investigated the effect of the alkyl chain length of the surfactants and the temperature on the solubilization behavior and compared the results to reference samples without CO_2 and to commercial reference samples, that were already used in industry. For the triblock polyether carbonate polyols, the EO head group, as well as the PO hydrophobic group, was modified with CO_2 units to analyze the direct impact of the CO_2 unit on the solubilization potential and investigate the solubilization mechanism depending on the additional interaction with the CO_2 unit. The solubility performance was experimentally determined by UV-Vis measurements at 25 °C and 40 °C. For a further structural understanding, we performed a structural characterization of these systems employing small-angle neutron scattering (SANS) to determine the size and structure of the micelles. Furthermore, nuclear Overhauser effect (NOESY)-NMR was applied to determine the interaction and correlation to the CO_2 unit. The use of CO_2 should not only gives insights into the interaction mechanism of the solubilizer and hydrophobic compounds, it should also enhance the understanding of the solubilization process. But moreover, the use of CO_2 as a feedstock for chemical synthesis has the potential to reduce the overall environmental impact of production processes, saving valuable fossil resources and paving the way towards a circular economy.[11]

6.2. Experimental Section

6.2.1. Materials

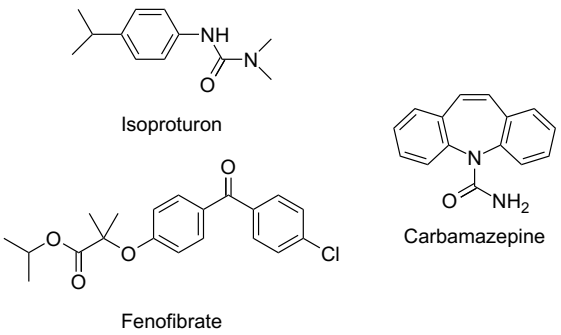

Figure 6.1: Structural formula of the pharmaceutical drug isoproturon, carbamazepine and fenofibrate.

The three hydrophobic compounds isoproturon, carbamazepine, and fenofibrate were purchased from Sigma-Aldrich, all with analytical purity (>99%). Their water solubility at 25 and 40 °C was also determined by us via UV/Vis spectroscopy and is listed in Table 6.1. The structure of the hydrophobic compounds is given in Fig. 6.1. All hydrophobic compounds show a pronounced peak in the UV-Vis spectra (see Appendix Chapter 6). The absorption peaks are listed in Table 6.1.

Table 6.1: Summary of classification, CAS number, maximum absorption λ_{max}, molecular weight M_w, and water solubility S_w at 25 and 40 °C of all three pharmaceutical compounds.

Compounds	Classification	CAS	λ_{Max} /nm	M_w / g/mol	$S_{w,\,25\,°C}$ /mmol/L	$S_{w,\,40\,°C}$ /mmol/L
Isoproturon	Herbicide	34123-59-6	242.0	206.29	0.33	0.34
Carbamazepine	Antiepileptics	298-46-4	285.0	206.29	0.40	0.34
Fenofibrate	Fibrates	49562-28-9	275.0	360.83	0.00077	0.0047

6.2.2. Measurements of Solubilization Capacity

Measurements of the solubilization capacity was done by UV-Vis measurements at the Cary 50 by Varian. The hydrophobic compound was equilibrated in the aqueous surfactant solution (1.0 wt.%) at 25 °C under continuous stirring for 24 h. The solubilization was also determined at 40 °C. The samples were constantly stirred for 24 h in a temperature-controlled water bath. The undissolved hydrophobic compound was then removed with Millipore PVDF filters (0.45 µm pore size).

The filtered sample was measured using UV-Vis spectroscopy measuring from 200-800 nm. Calibration curves of the hydrophobic compounds were measured by measuring different concentrations of the hydrophobic compound in ethanol. The calibration curve and the spectra of all hydrophobic compounds are summarized in the Appendix Chapter 6 (Fig. 10.21). The solvent and polymer signal was subtracted as a baseline to consider only the absorbance of the hydrophobic compound. The concentration was determined at 285.0 nm for carbamazepine, 275.0 nm for fenofibrate, and 242.0 nm for isoproturon. From the evaluation of the UV-Vis data we obtained the total drug solubility S_{tot} (Summarized data shown in the Appendix Chapter 6 Table 10.14). The solubilization of a compound by a surfactant can be described by the

solubilization capacity χ and the micelle-water partition coefficient P. [43] The χ value is defined as the number of moles of the solute that can be solubilized by one mol of micellar surfactant:

$$\chi = \frac{S_{tot} - S_w}{c_{surf} - cmc} \tag{6.1}$$

where S_{tot} is the total drug solubility, S_W is the water solubility of the hydrophobic compound, C_{surf} is the molar concentration of surfactant in solution, and cmc is the critical micelle concentration. The solubilization capacity characterizes the ability of the surfactant to solubilize the hydrophobic compound and is used to compare the efficiency of the solubilization between the different surfactants. The micelle-water partition coefficient is the factor of solubility enhancement and gives the ratio of drug concentration in the micelle to the drug concentration in water, as follows:

$$P = \frac{c_{surf} - cmc}{S_W} \tag{6.2}$$

From the thermodynamic point of view, the solubilization can be considered as a normal partitioning of the drug between two phases, micelle and aqueous, and the standard free energy of solubilization (ΔG_S) can be represented by the following expression:

$$\Delta G_s = -RT\,ln(P) \tag{6.3}$$

where R is the ideal gas constant, T is the absolute temperature, and P is the partition coefficient between the micelle and the aqueous phase.[176]

6.2.3. Small-angle neutron scattering (SANS)

Small-angle neutron scattering has been carried out at the MLZ in Munich on the instrument KWS-1 and at LLB in Saclay at the instrument PAXY to analyze the size and shape of the micelles. Samples were prepared in D_2O, as described in section 6.2.2, and the scattering intensity was measured in quartz cuvettes of 1 mm pathway. The instrument KWS-1 was operated at a wavelength of 5 Å and sample to detector distances (SDD) of 1.5 m, 8 m to 20 m , to cover a q-range of 0.015-4 nm^{-1}. Sample transmissions were measured at a SDD of 8 m. In all scattering data, the intensities were divided by the corresponding transmission and sample thickness (1 mm), corrected for the empty cell and normalized with respect to the scattering of a 1 mm sample of light water, according to the standard procedure.[137] The incoherent background was determined by a Porod analysis. The SANS measurements performed at PAXY were carried out at a wavelength of 4 Å for SDDs of 1.2 m and 5 m, and a wavelength of 12 Å for an SDD of 6 m.

6.2.4. NOESY Measurements

NMR measurements have been carried out using a Bruker Avance III 500 spectrometer at 700 MHz equipped with a TXI 5 mm broadband inverse detection probe with Z-Gradient (1H/19F, 13C, 15N, Z-Gradient, ATM). All samples were prepared in D_2O and all measurements were taken at 25 °C. The Nuclear Overhauser Effect (NOESY)-NMR measurements were performed simultaneously. The spectra were recorded at up to 50 scans per increment with altogether 256 increments. The software TopSpin 3.5 was used for analyzing these experiments. Individual rows of the quasi-2-D diffusion databases were phased and baseline corrected. The NOESY spectrum was processed without additional processing parameter modifications.

6.3. Results & Discussion

In our experiments, we investigated the influence of the incorporated moiety CO_2 in the hydrophilic head groups of conventional EO-based nonionic surfactants and triblock Pluronic type copolymers on their solubilization properties for isoproturon, fenofibrate, and carbamazepine.

6.3.1. Solubilization Behavior – Effect of Hydrophobic Chain Length and Head Group Modification

Here, the newly synthesized alkyl CO_2 surfactants were compared to commercial references (Marlipal 24/90 and LutensolAT13) and the temperature dependence of the solubilization was investigated by measuring at 25 and 40 °C. The solubilization capacity of the three hydrophobic compounds was determined for the various surfactants and is summarized in Fig. 6.2. For the C_{12} surfactants (Fig. 6.2a) a reduction of the solubilization capacity is observed, for isoproturon and carbamazepine by incorporating CO_2 units in the hydrophilic head group compared to the reference and the commercial surfactant. This phenomenon is similarly observed for the C_{16} surfactants (Fig. 6.2b). Interestingly, for the most hydrophobic component fenofibrate, the C_{12} CO_2 surfactant ($C_{12}EO_{8.2}(CO_2)_{3.1}-OH$) has a slightly higher solubilization capacity in comparison to the reference samples. For fenofibrate it could also be found, that the solubilization capacity is higher for the commercial surfactant with its polydisperse alkyl chains ($C_{12/14}EO_9-OH$; $C_{16/18}EO_{13}-OH$) in comparison to the reference surfactant with only a pure C_{12} or C_{16} alkyl chain ($C_{12}EO_{14.0}-OH$; $C_{16}EO_{14.6}-OH$).

This already indicates that the locus of fenofibrate is in the dehydrated micellar core. Comparing the impact of the alkyl chain length for the three different hydrophobic compounds, a drastic increase of solubility is not observed, even though it would in general be expected from the increasing alkyl chain length. An increase of solubilization is caused by the increased volume of the hydrophobic micellar core, which has already been reported by Vinarov *et al.*[175] In contrast, for carbamazepine better solubilization was reported for a surfactant with a C_{12} than with a C_{16} chain.[184] Plotting the solubilization capacity as a function of the aggregation number one observes even a decrease of

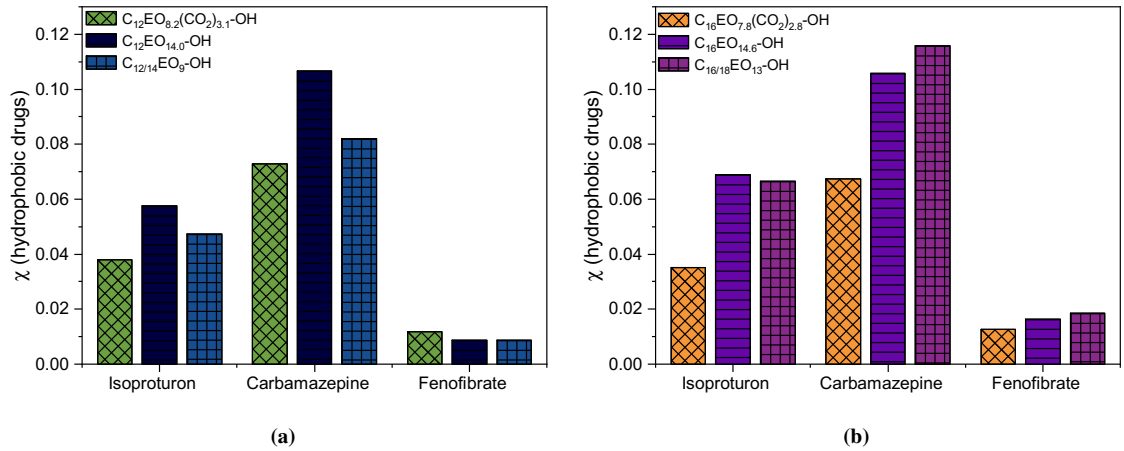

Figure 6.2: Solubilization capacity of the $C_{12}EO/CO_2$ (left) and the $C_{16}EO/CO_2$ (right) surfactants and their reference samples at a surfactant concentration of 1 wt% for all three hydrophobic drugs isoproturon, carbamazepine and fenofibrate (T = 25.0 °C).

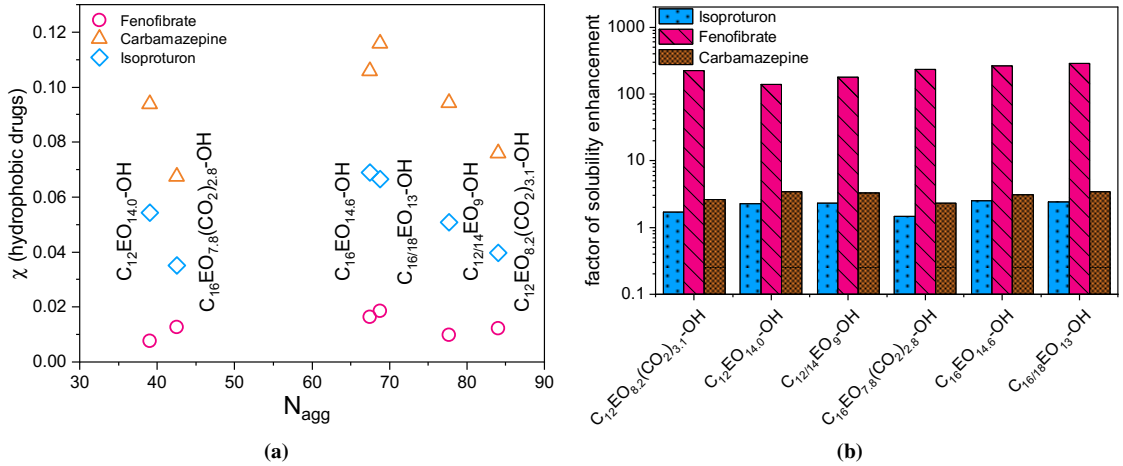

(a) (b)

Figure 6.3: (a) The solubilization capacity as a function of the aggregation number N_{agg} and (b) the solubility enhancement P compared to the water solubility of the hydrophobic compounds for all C_{12} EO/CO_2 and C_{16} EO/CO_2 surfactants and their reference samples (with a surfactant concentration of 1 wt%) at 25 °C.

solubility at higher aggregation numbers for isoproturon and carbamazepine, as similarly reported by Maswal *et al.*[184] (Fig. 6.3a). This indicates a locus of the hydrophobic compound in the palisade layer (EO head group) of the surfactant. This is also in good agreement with previous studies[184] and with the reduced solubility with incorporated CO_2 units.

Investigating the factor of solubility enhancement P (Fig. 6.3b, Eq. 6.2) one can observe a pronounced increase in solubilization, especially for fenofibrate. The solubility of this highly unpolar and water-insoluble active ingredient is enhanced by a factor > 100 for all surfactants. In contrast, the solubilization enhancement is somewhat smaller with P ~ 2-3 for the more polar compounds isoproturon and carbamazepine. In general, one can state that for the CO_2 containing nonionic surfactants the solubilization of isoproturon and carbamazepine is somewhat reduced by the incorporation of CO_2 into the hydrophilic head group in comparison to the reference sample. This is shown for the C_{12} as well as the C_{16} surfactants. As mentioned above this could be caused by the locus of the hydrophobic compounds in the palisade layer of the micelles.

6.3.2. Small Angle Neutron Scattering (SANS)

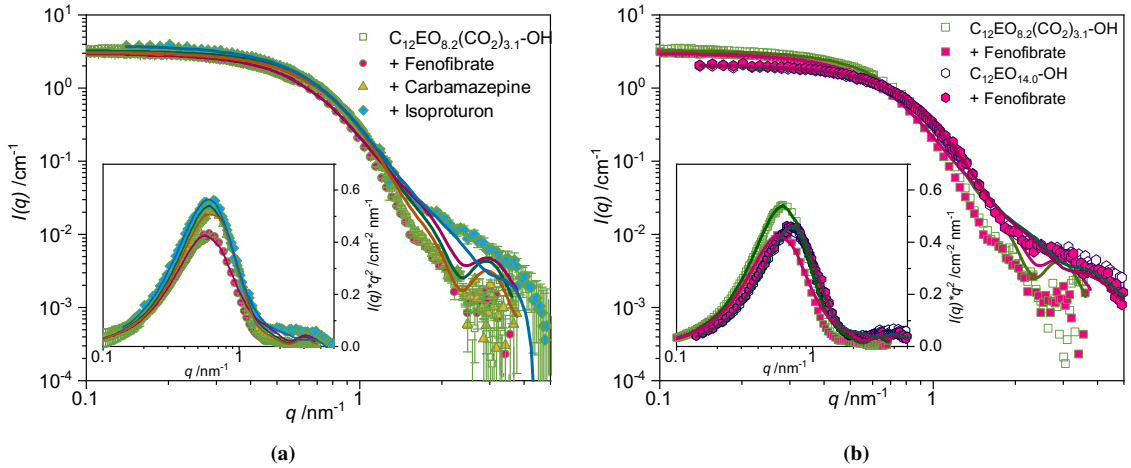

Figure 6.4: SANS spectra of the $C_{12}EO/CO_2$ surfactant with all three hydrophobic compounds (a). Comparison of the aggregates of the $C_{12}EO/CO_2$ surfactant with and without the hydrophobic compound fenofibrate and as a comparison the reference surfactant with and without the hydrophobic compound fenofibrate (b). Inset shows the SANS curves plotted as $I \cdot q^2$ vs. q. The lines represent the fit performed on the SANS data. Fit model is described in the previous chapter and in the Appendix Chapter 5.

To characterize the micellar structures, SANS measurements were performed, were the focus was on the C_{12} surfactants $C_{12}EO_{8.2}(CO_2)_{3.1}-OH$ and $C_{12}EO_{14.0}-OH$ (see Fig. 6.4; all other SANS measurements are summarized in Appendix Chapter 6). The C_{12} EO/CO_2 surfactants form ellipsoidal core-shell micelles and the size and shape have already been studied in thorough detail in the previous chapter.[79, 147] Already known is that the CO_2 surfactants form slightly bigger aggregates in comparison to the reference surfactant. This can also be seen in Fig. 6.4. The addition of the different drug molecules has hardly any effect on the scattering curves. The scattering curves were analyzed by a core-shell micellar model. This model was already used in the previous chapter and describes the ellipsoidal micelles in terms of their ellipticity ε, aggregation number N_{agg}, the molecular weight and the effective radius R_{eff}, representing the volume equivalent sphere radius of the ellipsoid. The fit is depicted in Fig. 6.4. One can observe that even though the aggregates of the CO_2 surfactants are slightly larger than the aggregates of the reference surfactant, there is no increase in size observed by the solubilization of hydrophobic compounds. The obtained parameters from the fit are summarized in Table 6.2 and shows also no increase in aggregation number or size of the aggregates. This is not surprising because the size of the micellar size by solubilization can be estimated with the following equation:

$$R_s = R_{eff} \cdot \left(1 + \frac{N_o \cdot v_o}{N_s \cdot v_s}\right) \tag{6.4}$$

With R_{eff} being the effective radius of the ellipsoid, N_o the number and v_o the volume of drug molecules and Ns is the number and v_s the volume of the surfactant molecules (thereby only considering the volume of the alkyl chain). By this calculation, one would not expect any increase in size by the amount of the solubilized compound. Even though the solubilization of fenofibrate is higher for the CO_2 surfactant in comparison to the reference surfactant. In previous SANS experiment analyzing the solubilization of hydrophobic compounds, one could determine an increase in size by solubilization.[177, 178, 180] This effect cannot be observed for these aggregates considering the small solubilization with 0.012 mol fenofibrate per mol surfactant for

Table 6.2: Obtained values form the model analysis of the SANS Scattering curves of the CO_2 surfactant $C_{12}EO_{8.2}(CO_2)_{3.1}-OH$ and the reference sample $C_{12}EO_{14.0}-OH$ with and without the hydrophobic compound fenofibrate: ε is the ellipticity of the aggregates, the effective radius R_{eff}, the molecular weight M_w and the aggregation number N_{agg} and the theoretical solubilization radius R_s.

Surfactants	ε	R_{eff} /nm	M_w /kDa	N_{agg}	R_s /nm
$C_{12}EO_{8.2}(CO_2)_{3.1}-OH$	1.00	4.6	57	84	
$C_{12}EO_{8.2}(CO_2)_{3.1}-OH$ + fenofibrate	1.27	4.7	58	85	4.6
$C_{12}EO_{14.0}-OH$	1.28	3.7	31	39	
$C_{12}EO_{14.0}-OH$ + fenofibrate	1.38	3.7	32	40	3.7

the CO_2 surfactant and only 0.0087 mol per mol surfactant for the reference surfactant. This would mean that with the obtained aggregation number one fenofibrate molecule is solubilized per micelle, whereas only 1 fenofibrate molecule per four micelles is solubilized for the reference surfactant. By this small solubilization, one would not expect an increase in the size of the aggregates even though one can observe an increase of the aggregation number by 1. The increase of N_{agg} by 1 can also be observed for carbamazepine and isoproturon. It should be mentioned here that the value is within the error of the obtained fit results. For the CO_2 surfactant and the reference surfactant carbamazepine and isoproturon also do not show any effect on the size of the micellar aggregates.

6.3.3. Effect of temperature

The temperature dependency of the solubilization capacity of the different C_{12} and C_{16} surfactants was investigated by performing additional measurements at 40 °C. In Fig. 6.5a the solubility enhancement of the three different hydrophobic compounds is shown. In comparison to Fig. 6.3a one can see a prominent decrease in the factor of solubility enhancement for fenofibrate. This is derived mainly by the fact that the water solubility of fenofibrate is increased from 0.77 µmol/L at 25 °C up to 4.78 µmol/L at 40 °C. In contrast, the water solubility of carbamazepine and isoproturon is almost constant (see Table 6.1). In Fig. 6.5b one can observe the solubility capacity of carbamazepine at 25 °C and 40 °C (temperature dependent solubility capacity of fenofibrate and

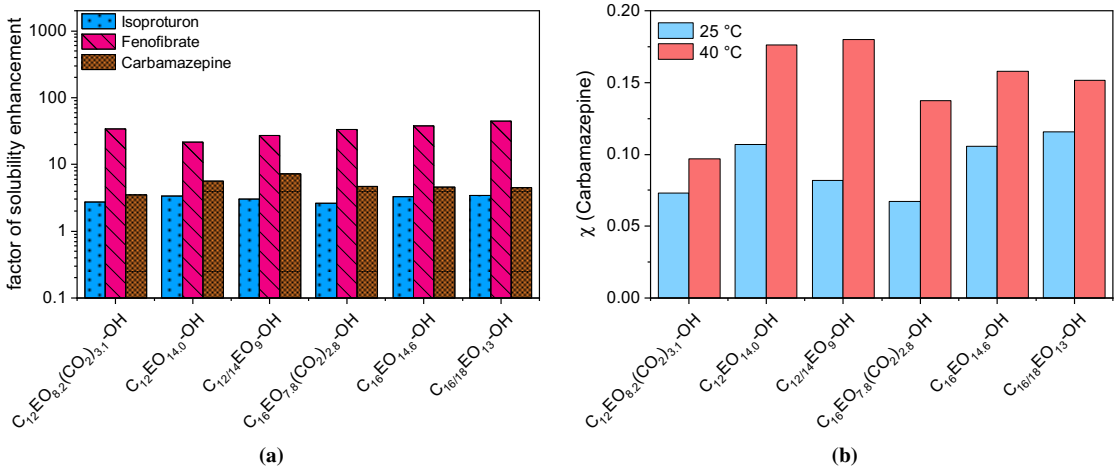

Figure 6.5: Solubility enhancement P (Eq. x) for the different hydrophobic compounds for all C_{12} and C_{16} surfactants at 40 °C (left). Comparison of the solubilization capacity of carbamazepine for all different surfactants 25 and 40 °C (right).

isoproturon can be found in Appendix Chapter 6). It is quite interesting that for fenofibrate the solubility decreases somewhat for all surfactants at higher temperatures, whereas for isoproturon and carbamazepine one can observe an increase. This points to different solubilization sites for the two different types of drug molecules. The increase of temperature leads to a change in polarity of the formed aggregates, thereby also reducing the hydration, which leads to an increased solubilization potential as shown by Singla *et al.*[178] As we know from the previous chapter, the aggregates of the C_{12} CO_2 surfactants are increasing in size and aggregation number by a sphere-rod transition.[147] This structural transition is resulting in an increased solubilization potential.

For the C_{16} surfactants, the enhanced solubilization may occur from a different phase behavior. They have a Krafft temperature at ~ 40 °C which means that the surfactant is much more water-soluble above this temperature indicating the formation of micelles. Consequently, one would expect an increase of solubilization with the formation of micelles. Even though one can observe an increase of solubilization with increasing temperature, the enhancement for the C_{16} surfactant is not as high as one would expect. From the solubility capacity, the standard free energy of solubilization ΔG_s can be determined as described in the experimental section. All obtained parameters for 25 and 40 °C are summarized in Table 6.3. Here it is obvious that the solubilization of all hydrophobic compounds is an exergonic process with values for ΔG_s ranging from ~ -1 up to -3 kJ/mol at 25 °C and ~ -2 up to ~ -5 at 40 °C for isoproturon and carbamazepine. Fenofibrate shows for 25 °C ΔG_s ranging from ~ -12 up to -14 kJ/mol at 25 °C and -8 up to -9 kJ/mol at 40 °C. Accordingly, the solubilization process is more favored at 25 °C for fenofibrate and almost temperature independent for carbamazepine and isoproturon. Moreover, one can observe that ΔG_s for each hydrophobic compound is the most negative for the C_{16} reference surfactants $C_{16}EO_{14.6}-OH$ and $C_{16/18}EO_{13}-OH$, indicating a correlation with the length of the alkyl chain. In general, ΔG_s indicates that the solubilization is less favored for the CO_2 surfactants in comparison to their reference samples except for fenofibrate, were $C_{12}EO_{8.2}(CO_2)_{3.1}-OH$ has the highest energy of solubilization. However, the results indicate that the CO_2 moiety disfavors the solubilization of hydrophobic compounds and not contributing positively here.

Table 6.3: Comparison of the standard free energy of solubilization ΔG_s for all surfactants with C_{12} and C_{16} chain length and their reference samples as well as the commercial reference sample for all three hydrophobic compounds at 25 °C and 40 °C.

ΔG_s						
	Isoproturon		**Carbamazepine**		**Fenofibrate**	
Surfactants	**25 /°C**	**40 /°C**	**25 /°C**	**40 /°C**	**25 /°C**	**40 /°C**
$\mathbf{C_{12}EO_{8.2}(CO_2)_{3.1}-OH}$	-1.29	-2.59	-2.38	-4.03	-13.41	-9.16
$\mathbf{C_{12}EO_{14.0}-OH}$	-2.03	-3.15	-3.05	-3.99	-12.22	-8.01
$\mathbf{C_{12/14}EO_{9}-OH}$	-2.10	-2.87	-2.94	-3.91	-12.85	-8.61
$\mathbf{C_{16}EO_{7.8}(CO_2)_{2.8}-OH}$	-0.98	-2.53	-2.07	-3.24	-13.53	-9.12
$\mathbf{C_{16}EO_{14.6}-OH}$	-2.27	-3.10	-2.81	-4.50	-13.81	-9.48
$\mathbf{C_{16/18}EO_{13}-OH}$	-2.20	-3.20	-3.06	-5.13	-14.02	-9.89

6.3.4. Solubilization by Triblock Copolymers of Different Degree of CO_2 Functionalization

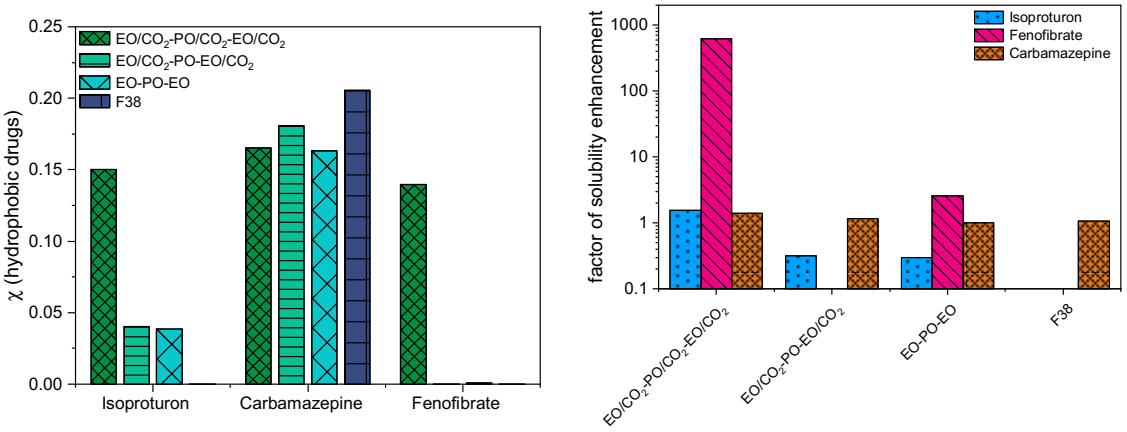

Figure 6.6: Solubilization capacity of all four triblock polyether carbonate polyols at a concentration of 1 wt% for all three hydrophobic drugs isoproturon, carbamazepine and fenofibrate (a). Factor of solubility enhancement (b) in comparison to the water solubility of the hydrophobic compounds for all four triblock polyether carbonate polyols at 25 °C.

In the next step, we studied the influence of the CO_2 moiety on the solubilization potential of triblock polyether polyols (CO_2 triblock copolymers). Their commercial analogous are poloxamers also called Pluronics®, which are of high interest for solubilization enhancement of hydrophobic compounds. We intensively studied the effect of the functionalization of the EO head group with CO_2, whereby the hydrophobic propylene oxide (PO) part remains unfunctionalized (EO/CO_2-PO-EO/CO_2) and we studied the effect on solubilization, whereby the hydrophilic head group EO, as well as the hydrophobic part PO, is functionalized with CO_2 (EO/CO_2-PO/CO_2-EO/CO_2) all structures are summarized in Fig. 3.2. As a comparison, we also studied an unfunctionalized triblock polymer, which was synthesized by the same process (EO-PO-EO) and a commercial product a Pluronic® F38, all with comparable molecular weights and PO chain length.

Triblock copolymers with PO chain length around 1000 g/mol are not forming micellar aggregates at room temperature and are only present as single molecules. This has been reported for the F38 Pluronic®[189] and is also the case for all other polymers except for the one with the highest degree of CO_2 functionalization (EO/CO_2-PO/CO_2-EO/CO_2). This was shown by SANS measurements (Fig. 6.4). All other polymers are present as Gaussian coils as shown in Fig. 6.7b for EO-PO-EO (all other SANS curves are shown in Fig. 10.24 in the Appendix Chapter 6). The copolymers show the radius of gyration in the range from 1.2 and 1.3 nm for EO/CO_2-PO-EO/CO_2 and EO-PO-EO and are increasing in size for F38 with a radius of gyration of 2.2 nm. The polymer EO/CO_2-PO/CO_2-EO/CO_2 is showing different scattering curves with a shift to lower q values and a much-increased intensity. The length of the PO chain is much longer, therefor indicating micelle formation. Approximate micelle sizes of 9 nm are shown in Fig. 6.6a (blue line), which is in good agreement with the length of the triblock copolymer. With the addition of hydrophobic compounds, a slight shift to smaller q values can be observed for the copolymer EO/CO_2-PO/CO_2-EO/CO_2, which mainly indicates an increase in size. However, the hydrophilic head group of the polymer is quite short with only 11 units. Therefore only some of the polymer

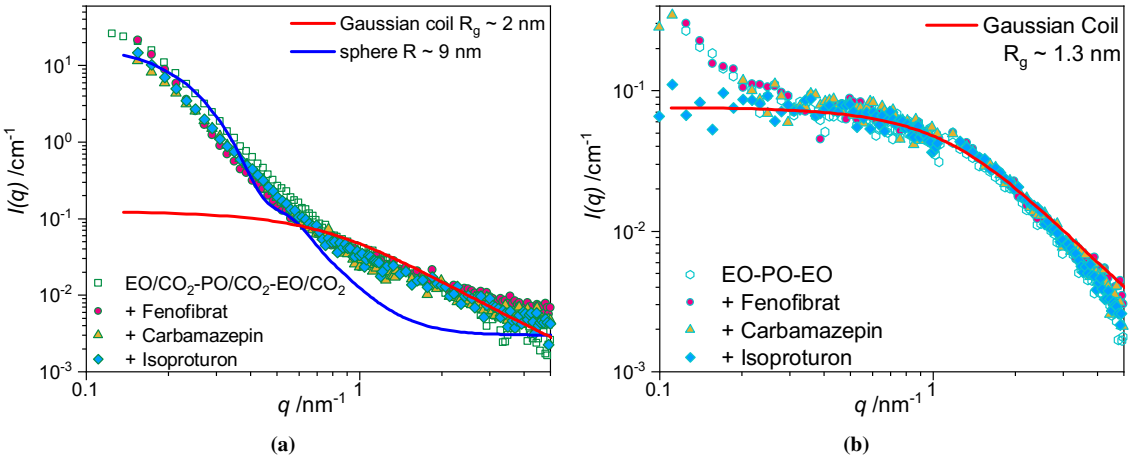

Figure 6.7: SANS spectra of EO/CO_2-PO/CO_2-EO/CO_2 and EO-PO-EO with all three hydrophobic compounds. The red line represents the polymer as a Gaussian chain fit. The fit was performed for the pure polymer without addition of hydrophobic compound.

chains are forming micelles. Other polymer chains with a lower degree of polymerization are water insoluble and not forming any aggregates. As a result, in solution some polymer chains are forming micelles and other are similarly behaving to PO chains and are dispersed in the aqueous solution. This can indicate a contribution of Gaussian polymer coils with a R_g of ~ 2 nm. Therefore, the highly hydrophobic polymer chains have a high solubilization potential, as well as the formed aggregates, which results in high factor of solubility enhancement of fenofibrate. The SANS spectra of the other polymers with the addition of hydrophobic compounds are shown in Appendix Chapter 6.

As shown in Fig. 6.6 we studied the solubilization capacity of four different triblock copolymer. From the solubilization experiments, we can observe, that the solubilization capacity for carbamazepine is enhanced equally by every polymer, independent from the degree of CO_2 functionalization. This indicates already that the solubilization of carbamazepine is enhanced by the change of the chemical potential of the solvent by the addition of the polymer. This has also been reported by Nguyen-Kim *et al.*[180] with different types of Pluronics and carbamazepine, were the solubilization is almost structure independent. These findings are also indicating, that carbamazepine is not mainly solubilized by the interaction with EO in the head group, as suggested by Maswal *et al.*[184]

However, the solubilization of carbamazepine is enhanced by all triblock copolymer, most interesting is that the polymer EO/CO_2-PO/CO_2-EO/CO_2 shows remarkable solubilization capacities for every hydrophobic compound, as depicted in Fig. 6.6a. For isoproturon, the solubilization capacity is also increased for the polymer with the CO_2 functionalized EO head group EO/CO_2-PO-EO/CO_2 and the reference without CO_2 EO-PO-EO. But most pronounced is the solubilization of fenofibrate by EO/CO_2-PO/CO_2-EO/CO_2 because the polymer with the highest degree of CO_2 functionalization has the highest factor of solubilization enhancement P for fenofibrate which shows almost no solubility enhancement for all other polymers (as shown by Fig. 6.6b). Indicating a striking increase in solubility by the CO_2 functionalization of EO and PO, even when no aggregates are formed.

These findings are quite remarkable because this could indicate that the incorporation of CO_2 adds an interaction parameter and increases the solubility even without micelle formation. It

Table 6.4: Standard free energy of solubilization ΔG_s for all four triblock polyether carbonate polyols their reference samples as well as the commercial reference sample for all three hydrophobic compounds at 25 °C.

ΔG_s			
Surfactants	**Isoproturon**	**Carbamazepine**	**Fenofibrate**
EO/CO_2-PO/CO_2-EO/CO_2	-1.1	-0.82	-15.93
EO/CO_2-PO-EO/CO_2	2.98	-0.39	
EO-PO-EO	3.18	-0.02	-2.46
F38		-0.16	

is already known that even without micelles the solubilization can be enhanced, which has been shown by Singla *et al.*[178] Onother reason could be, that the enhanced solubilization of EO/CO_2-PO/CO_2-EO/CO_2 can be described by the formation of micelles of at least parts of the copolymer and also some excess starter PO/CO_2 which is water insoluble but can be a favored solubilization enhancer and stabilized as a dispersion. CO_2 as an additional interaction parameter would also explain why the reference polymers show almost no solubilization capacity for all three surfactants. These findings indicate that the solubilization potential is suppressed without aggregate formation.

Having a closer look at the thermodynamic aspect of the solubilization as seen in Table 6.4 one can say that for fenofibrate the solubilization is exergonic for the two polymers with CO_2 incorporation. The solubilization of fenofibrate is highly favored for EO/CO_2-PO/CO_2-EO/CO_2 and EO-PO-EO. For isoproturon, the solubilization is even endergonic and even disfavored for the Polymers EO/CO_2-PO-EO/CO_2 and EO-PO-EO. The solubilization of carbamazepine is exergonic for all polymers.

Homonuclear H,H-NOESY NMR

Further information on the interaction between the copolymers and the hydrophobic compound can be obtained using NOESY-NMR experiments. This method reveals specific local interaction of the hydrophobic compound with specific units of the polymer. In our case, the polymer in general consists of PO units for the hydrophobic part of the polymer and EO units for the hydrophilic part of the polymer. And additionally, CO_2 can be functionalized either in the EO unit or in the PO unit at the hydrophobic part. The ^{1}H NMR spectra of the different polymers with and without the hydrophobic compounds are summarized in the Appendix Chapter 6. In Fig. 6.8 the specific NOESY spectra of an aqueous solution of EO/CO_2-PO/CO_2-EO/CO_2 with either fenofibrate (a), isoproturon (b), and carbamazepine (c) is shown. From this spectra, one can obtain that the characteristic resonance signal of the fenofibrate is interacting with the resonance signal of the protons of the PO methyl group (~ 1.25 ppm) and with the protons of the PO unit at (~ 3.75 ppm). The same can also be observed for isoproturon, which is only slightly interacting with the methyl unit of the PO moiety at ~ 1.25 ppm. Whereas carbamazepine is also interacting with the protons next to the CO_2 unit (~ 4.30 ppm). This indicates an interaction of carbamazepine, not only to the PO and EO units but also with the CO_2 moiety. This indicates that the fenofibrate and isoproturon molecules are coupling exclusively to the PO units, whereas carbamazepine is also coupling to the EO units and CO_2 moieties. A systematic coupling to the CO_2 unit could not be revealed for

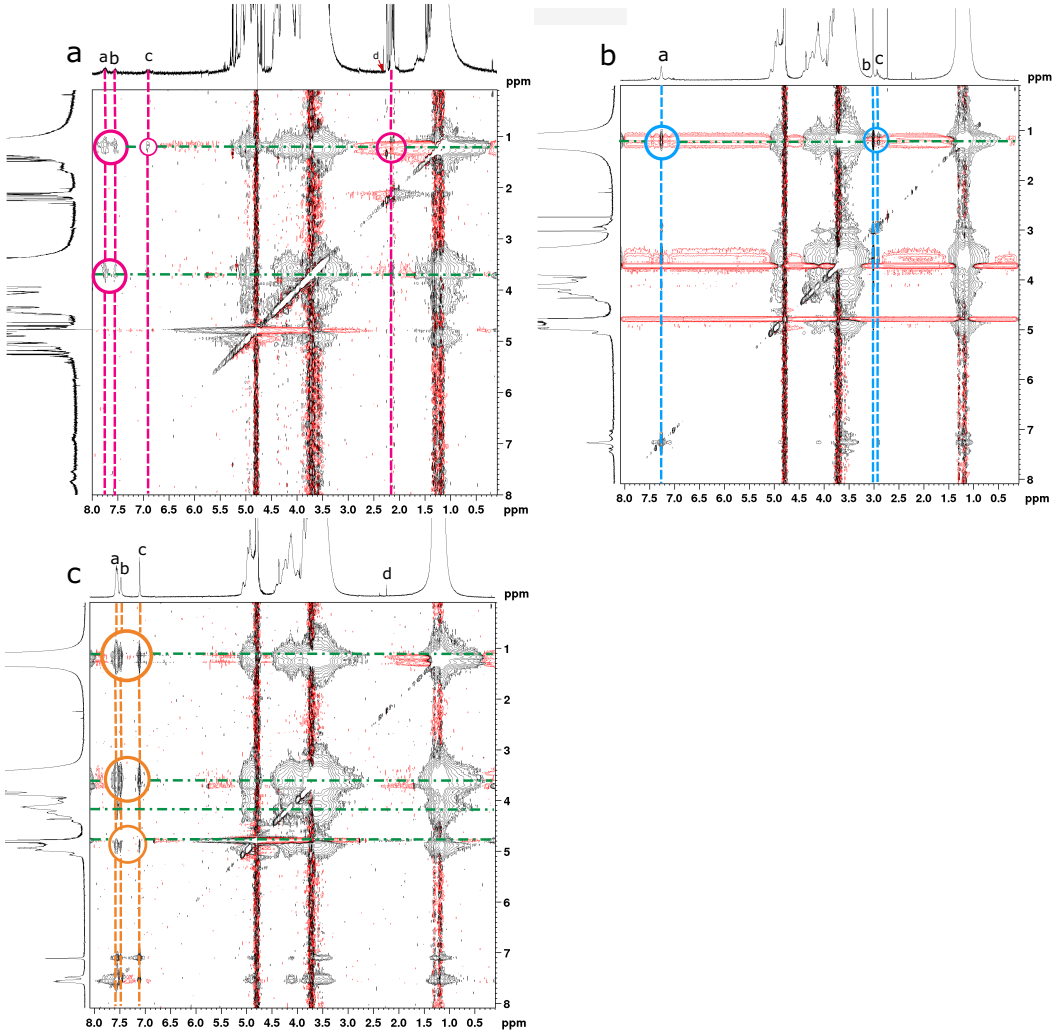

Figure 6.8: NOESY spectra of the polymer EO/CO_2-PO/CO_2-EO/CO_2 with fenofibrate (a), isoproturon (b) and carbamazepine (c).

fenofibrate and isoproturon. The reason for this could also be the overlapping of the resonance signal so no specific signal of the neighboring protons of the CO_2 units could be determined.

In general, it can be stated that the polymer EO/CO_2-PO/CO_2-EO/CO_2 is interacting with each hydrophobic compound. However, for fenofibrate the solubility is strikingly enhanced, but no correlation to the CO_2 functionalization could be observed. Furthermore, for the other polymers only an interaction of the resonance spectra of the polymer EO-PO-EO and isoproturon and carbamazepine and from the polymer F38 and carbamazepine can be found. These results show, that the polymer EO/CO_2-PO/CO_2-EO/CO_2 has specific interactions with each hydrophobic compound, resulting in enhanced solubilization. Moreover, one obtains the information, that carbamazepine is interacting with each polymer, whereby the specific units are not important to enhance the solubilization. In the case of EO/CO_2-PO-EO/CO_2 and EO-PO-EO the solubilization can be enhanced even without a formation of aggregates. These findings indicate that a small amount of copolymer would be sufficient to enhance the solubilization of hydrophobic compounds. Moreover, the polymers with CO_2 functionalization are not only more effective, but they also have a higher biodegradability and are thereby more eco-friendly than their petroleum-based analogs.

6.4. Summary & Conclusion

In this chapter, we studied the solubilization potential of the CO_2 surfactants and the CO_2 triblock copolymers of three different hydrophobic compounds, namely carbamazepine, fenofibrate, and isoproturon. Enhancing the solubility of hydrophobic compounds is a major application of nonionic surfactants. The motivation of this study was to determine if the incorporated CO_2 moieties represent a further interaction position for hydrophobic organic molecules.

Investigating the solubilization capacity of the CO_2 containing surfactants with different alkyl chain length one observes, that fenofibrate is best solubilized by the C_{12} CO_2 surfactant in comparison to the reference surfactants, whereby the factor of solubility enhancement P shows a pronounced enhancement. The solubility of this highly unpolar and water-insoluble active ingredient is enhanced by a factor > 100 for all surfactants indicating solubilization in the hydrophobic core. Carbamazepine and isoproturon are solubilized in the palisade layer and interacting with the EO units. This also explains the reduced solubilization by incorporating CO_2 moieties. Moreover, carbamazepine is better solubilized by C_{12} alkyl chains in comparison to C_{16} chains, as already reported in the literature. However, the solubility is enhanced for all hydrophobic compounds the amount is so small, that no structural changes could be observed from SANS measurements. With increasing temperature, the solubility decreases for fenofibrate for all surfactants, whereas for isoproturon and carbamazepine one can observe an increase. The increase of temperature leads to a change in polarity of the formed aggregates and a sphere-rod transition, thereby also reducing the hydration, which leads to an increased solubilization potential.

In this chapter, it could be shown that the solubility of the three hydrophobic compounds could be enhanced by CO_2 containing surfactants. The factor of solubility enhancement is quite comparable for all surfactants, whereby the CO_2 incorporation leads to a slight decrease in solubilization. However, it can be stated that the CO_2 surfactants show comparable results. These findings combined with a better biodegradability and higher efficiency allows the use at lower concentrations. Therefore, the CO_2 surfactants are a suitable alternative to conventional nonionic surfactants for hydrophobic compound solubilization.

The solubilization by CO_2 containing triblock copolymers shows quite different results. The CO_2 triblock copolymers EO/CO_2-PO-EO/CO_2, EO-PO-EO and the referent polymer Pluronic® F38 are not forming micellar aggregates at 25 °C, which could be shown by SANS measurements. The polymers are present as Gaussian chains, whereby the polymer EO/CO_2-PO/CO_2-EO/CO_2 shows large aggregates or dispersed insoluble copolymer chains. Nevertheless, they are enhancing the solubilization of hydrophobic compounds. Thereby it is quite remarkable that the solubilization of carbamazepine is enhanced by all four observed polymers. But most interestingly is the prominent enhancement of the solubility of fenofibrate by EO/CO_2-PO/CO_2-EO/CO_2, which is the polymer with the highest degree of CO_2 functionalization. By NOESY measurements one can observe that fenofibrate is interacting with the EO and PO units but no pronounced interaction with the protons next to the CO_2 moiety could be observed. In comparison, carbamazepine is interacting with the protons next to the CO_2 unit, indicating a further interaction position by the CO_2 unit.

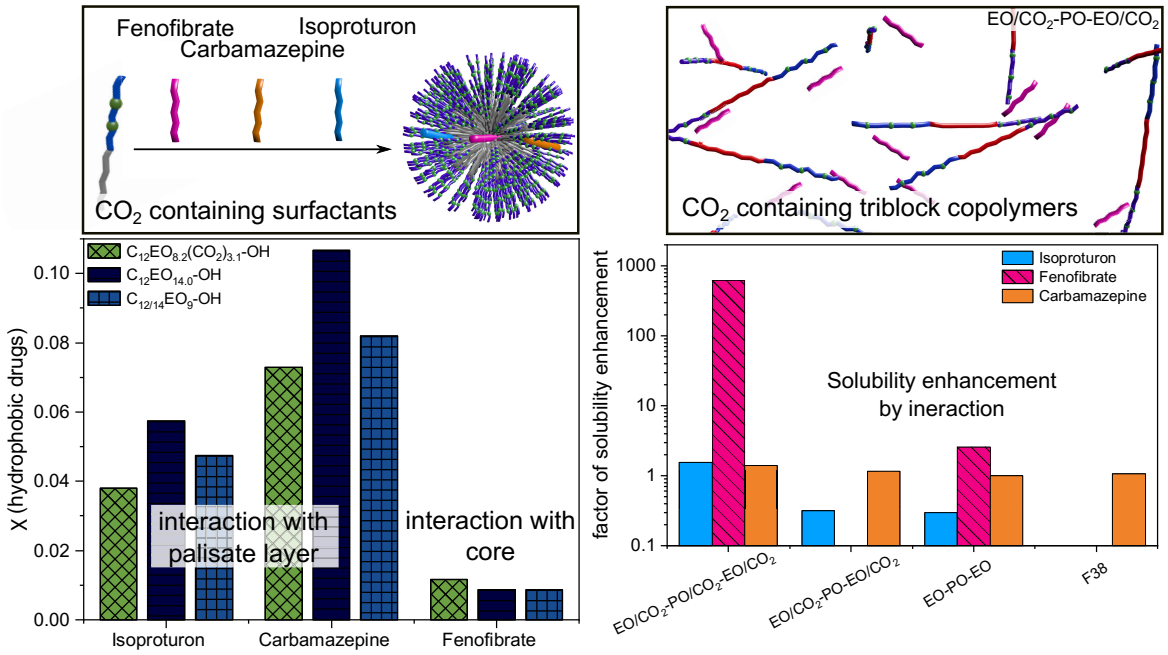

Figure 6.9: Schematic summary of the solubilization potential of CO_2 containing surfactants and triblock copolymer.

Even though no pronounced interaction with the CO_2 moiety could be found, except for carbamazepine, the results are still quite remarkable to enhance the solubility of fenofibrate by < 1000.

This study shows, that the functionalization of either nonionic surfactants or triblock copolymers with CO_2 moieties are showing promising results for application as solubilizers for hydrophobic compounds. This knowledge can direly be applied to further studies of the solubility of other hydrophobic compounds, such as other hydrophobic pharmaceuticals or even oils. It would also be interesting to study the solubilization of CO_2 functionalization triblock copolymers, that are forming micellar aggregates to obtain a comprehensive picture of the solubilization mechanism and the interaction with the CO_2 moiety. Especially the enhanced biodegradability of the CO_2 surfactants renders them of high interest for the use as pharmaceutical carriers or in the formulation in agricultural products.

Chapter 7

Adsorption Behavior at the Oil/Water Interface of CO_2 Containing Nonionic Surfactants

In the previous chapters, detailed information on the surface activity at the water/air interface, the micellization behavior, and the phase behavior in terms of concentration and temperature dependency of the CO_2 surfactants could be given. The impact of the CO_2 moiety was investigated in thorough detail. Moreover, the solubilization potential of hydrophobic compounds such as pharmaceutical drugs was also characterized. In this chapter, the adsorption properties at the water/oil interface will be discussed with respect to the CO_2 incorporation. Understanding the impact of the CO_2 moiety on the interfacial activity gives detailed insights into the basic principles of interfacial adsorption which is crucial for further investigations such as microemulsion formation. These aspects are important for several applications, e.g. cosmetics, enhanced oil recovery, emulsion stability, and personal care. The adsorption properties at the oil/water interface are measured in terms of interfacial tension measurements with the pendant drop method in the temperature range from 20 up to 55 °C against decane and hexadecane. For the change of interfacial tension with the temperature, a thermodynamic analysis gives information about the impact of the CO_2 moiety and the adsorption at the oil/water interface.

Main parts of this chapter are based on the following publication:

◊ V. J. Spiering, R. Marschall, H. Matsubara, M. Gradzielski: "Temperature Dependent Adsorption Behavior of Nonionic CO_2/EO Surfactants at the Oil/Water Interface", *Journal To Come*, **in Preparation**.

7.1. Introduction

The adsorption behavior of surfactants at the oil/water interface plays a major role in many applications. For instance cleaning, detergency, personal care, cosmetics, emulsification, and enhanced oil recovery. The surfactants are decreasing the interfacial tension which enables the formation of emulsions or microemulsions. The effectiveness of surfactants to decrease the surface

or interfacial tension is mainly derived by their chemical composition and in the case of interfacial tension, it depends on the solubility of the surfactant in both phases.

Understanding the relationship of the structure and the properties lead to a better understanding of further applications like oil solubilization for enhanced oil recovery and microemulsion formation.[97] Using surfactants is an important method for enhanced oil recovery because the residual oil is mobilized through decreasing oil/water interfacial tension (IFT) to overcome the capillary force.[190–194] High efficiencies are achieved by developing new types of surfactants, that possess several hydrophobic and hydrophilic moieties in the same molecule which have extraordinary surface activity.[195] Further applications of nonionic surfactants are the formation of microemulsions which are thermodynamically stable systems of water, oil, and an amphiphile. Microemulsions play an important role for many applications, for example in cosmetics and catalysis caused by their excellent solubilization properties for active ingredients.[196, 197] The system is single phased and usually show microemulsion droplets in the size range of a few nm, which renders the sample isotropic.[56, 198, 199]

But not only microemulsions are of high interest for many applications. Also, the formation of kinetically stable emulsions, are of great interest. The formation of stable emulsions by surface freezing was shown by Matsubara *et al.*[200–202] The effect of surface freezing of hexadecyltrimethylammonium chloride (CTAC) at the tetradecane/water interface stabilizes oil-in-water (OW) emulsion. Moreover, the impact of chain length of the oil in the presence of cetyltrimethylammonium bromide (CTAB) was also investigated.

The use of surfactants in large scale industrial processes requires not only high efficiencies but also a good bioavailability and biodegradability. Therefore, it is of high interest to investigate the interfacial properties of the new CO_2 surfactants to employ the impact of the CO_2 unit on the adsorption behavior at the water/oil interface. In this chapter, we investigated the adsorption properties at the water/oil interface of the four different CO_2-based nonionic surfactants with a C_{12} alkyl chain. We compared the temperature dependent adsorption properties to the reference sample, $C_{12}EO_{14.0}-OH$, and the effect of the CO_2 moiety to the incorporation of PO and PL units. The adsorption properties were investigated in terms of interfacial tension (IFT) measurement with the pendant drop method. This is a suitable technique to investigate interfacial tension data also in the sense of temperature control.[203] These IFT data were interpreted with respect to their thermodynamic interpretation and compared to the reference surfactant and literature values. This analysis of the data gives detailed insights in the understanding of adsorption properties of the surfactants at the interface and the impact of the incorporated moieties. Moreover, the influence of the alkyl chain length by studying the adsorption behavior of the C_{16}/CO_2 surfactants and the type of oil was also investigated.

Obtaining knowledge about the temperature dependent adsorption properties of these types of nonionic surfactants improves the understanding of further properties such as emulsion and microemulsion formation, which opens up opportunities for several applications. This information on the adsorption at the oil/water interface is important since the solubilization of hydrophobic components in water is the main application of surfactants.

7.2. Experimental Section

7.2.1. Interfacial Tension Measurements

Interfacial tension measurements were performed with a pendant drop instrument (OCA 15) with the hanging drop method. The instrument software is SCA20. The temperature was set by a water chamber tempering the oil in a glass container and the surfactant solution (0.1 mM) in the syringe. The following oils were used decane (min 98%, Fluka) and hexadecane (Aldrich). The surfactant solution is forming a droplet whereas the contour line was used to calculate the interfacial tension via the Young-Laplace equation and the equation for the Laplace-pressure ΔP.

$$\Delta P = P_{int} - P_{ext} = \gamma \left(\frac{1}{R_1} + \frac{1}{R_2} \right) \tag{7.1}$$

$$\Delta P(z) = \Delta P_0 \pm \Delta \rho g z \tag{7.2}$$

With R_i being the main curvature radii, γ the interfacial tension, P the Laplace pressure, ρ the density, g the gravitational acceleration and z the height of the droplet. The density differences between the two immiscible fluid water and oil at a given temperature was taken from literature[204] and set for each temperature measurement to obtain the interfacial tension. The surfactant/oil solutions were equilibrated for 12 h before measuring. At each temperature, the sample was equilibrated before measurement for at least 30 minutes. The interfacial tension was measured time-dependent until a constant value is achieved.

7.2.2. Evaluation of Interfacial Tension Measurements

From interfacial tension measurements standard parameters of adsorption can be calculated, such as the free Gibbs energy of adsorption ΔG_{ads}, ΔS_{ads} and ΔH_{ads}. Standard free energies of adsorption ΔG_{ads}, at the water/oil interface can be calculated from interfacial tension data, by the use of following equation:[205]

$$\Delta G_{ads} = RT \ln x_{c\Pi} - \Pi a_0 \tag{7.3}$$

with $x_{c\Pi}$ is the mole fraction of the surfactant at a given surface pressure Π. For the measurements the surface pressure is given at a certain temperature and a fixed surfactant concentration of 0.1 mM ($\Pi(T) = \gamma_{oil}(T) - \gamma(T)$). The temperature dependent interfacial tension data of the two different oils were taken from literature (decane[206] and hexadecane[207]). The temperature dependent head group area a_0 was estimated from temperature dependent surface tension measurements as shown in chapter 4.3.1. This was done because the temperature dependent interfacial tension measurements were only measured at 0.1 mM, thus no temperature dependent head group area a_0 could be obtained from those measurements. The entropy of adsorption was determined from the first derivative from ΔG_{ads}, which is shown in this relation:

$$\frac{d\Delta G_{ads}}{dT} = -\Delta S_{ads} \tag{7.4}$$

the first derivative of the ΔG_{ads} data was performed with the program OriginPro with an smoothing of the data of second order. From this approach the enthalpy of adsorption can be obtained from the Gibbs-Helmholtz equation:

$$\Delta G_{ads} = \Delta H_{ads} - T \cdot \Delta S_{ads} \tag{7.5}$$

7.3. Results & Discussion

7.3.1. Concentration Dependent Interfacial Tension Measurements

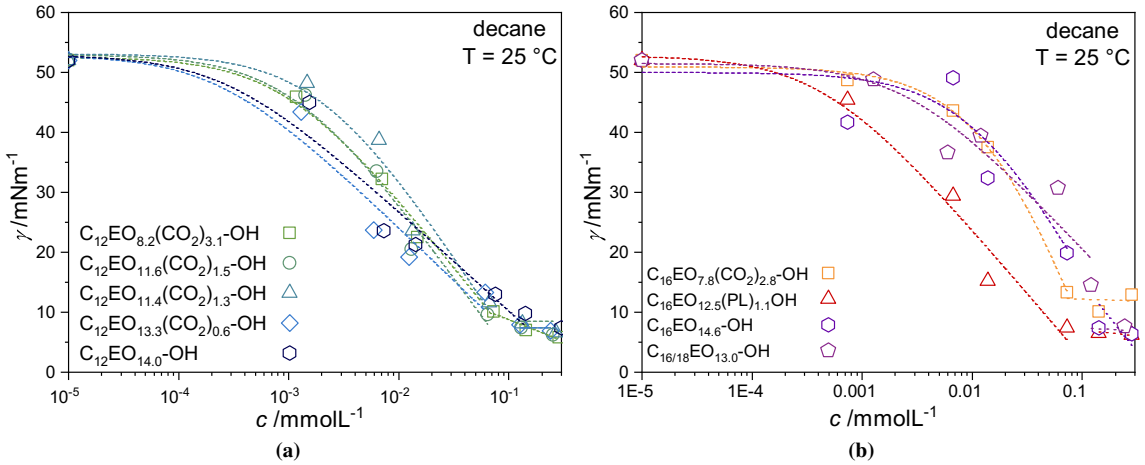

Figure 7.1: Interfacial tension measurements as a function of the surfactant concentration at 25 °C for the C_{12} (a) and the C_{16} surfactants. All data were fitted with the Szyszkowski equation Eq. 4.1.

We firstly studied the interfacial tension (IFT) at the water/decane interface in dependency of the concentration at 25 °C of the CO_2 containing C_{12} and C_{16} surfactants as shown in Fig. 7.1. The resulting IFT tension behavior is not surprising and quite similar to the adsorption behavior at the air/water interface. With increasing concentration the interfacial tension γ is decreasing until a certain plateau is reached at the cmc, which is generally similar to the surface tension measurements of the C_{12} surfactants as shown in chapter 4 Fig. 4.2.

The IFT values for the surfactants at the water/decane interface reaches for all CO_2 surfactants values below 10.0 mN/m. With increasing CO_2 content the IFT values are reduced to 7.0 mN/m for the surfactant with the highest CO_2 content at a concentration of 0.1 mmol/L. The C_{12} surfactants show a quite similar trend as seen from surface tension measurements. With increasing CO_2 content a faster decrease of the IFT can be observed and also smaller IFT values are reached. The C_{16} surfactants show a decrease in IFT down to 6 mN/m, with a stronger effect of the incorporated

Table 7.1: Summary of the interfacial measurements and comparison to the surface tension (ST) measurements: critical micelle concentration cmc_{ST}, surface tension σ_{cmc} at the cmc, head group area a_0(ST), interfacial tension γ, and head group area a_0(IFT).

Surfactants 25 ° C	**cmc_{ST} /mmol/L**	**σ_{cmc} /mN/m**	**a_0(ST) /nm^2**	**γ_{cmc} /mN/m**	**a_0(IFT) /nm^2**
$C_{12}EO_{8.2}(CO_2)_{3.1}-OH$	0.053	34.4	0.55	7.0	0.37
$C_{12}EO_{11.6}(CO_2)_{1.5}-OH$	0.091	35.9	0.65	7.4	0.37
$C_{12}EO_{11.4}(CO_2)_{1.3}-OH$	0.099	35.5	0.67	8.1	0.32
$C_{12}EO_{13.3}(CO_2)_{0.6}-OH$	0.118	35.9	0.69	7.9	0.53
$C_{12}EO_{14.0}-OH$	0.175	40.1	1.07	9.8	0.51
$C_{16}EO_{7.8}(CO_2)_{2.8}-OH$	0.034	36.5	0.49	10.1	0.18
$C_{16}EO_{12.5}(PL)_{1.1}-OH$	0.001	38.6	0.36	6.6	0.44
$C_{16}EO_{14.6}-OH$	0.005	38.8	0.35	6.4	0.28
$C_{16/18}EO_{13}-OH$	0.012	44.4	0.27	14.5	0.48

units in the head group area. The C_{16} reference surfactants without CO_2 and the C_{16} PL surfactant reduced the interfacial tension significantly more than the CO_2 containing C_{16} surfactant. However, the results of the C_{16} surfactant needs do be considered carefully, because as shown in chapter 5 they are not water-soluble at 25 °C.

The measurements of the CO_2 surfactants are also giving values for the head group area from the Langmuir-Szyszkowski isotherm (Eq. 4.1), which vary significantly compared to the values from surface tension (ST) measurements (summarized in table 7.1). These discrepancies can occur from a different packing of the CO_2 surfactants at the oil/water interface in comparison to the water/air interface. For surfactants in aqueous solution, the efficiency increases with an increase in the hydrophobic character of the surfactant.

7.3.2. Temperature Dependent Interfacial Tension Measurements

Investigating the temperature dependent adsorption in terms of interfacial tension gives insights about the effectiveness of these types of surfactants. It is quite known for nonionic EO type surfactants, that the solubilization capacity is enhanced with increasing temperature, due to increased dehydration of the EO chains, hence an increase of lipophilic character. This phenomenon is shown in a decrease in interfacial tension.

To observe these dependencies we investigated the temperature dependent adsorption behavior at the hexadecane/water interface for all four C_{12} CO_2 surfactants and compared them in a systematic fashion to the pure EO surfactant and the ones modified with PO or PL. The temperature dependent IFT measurements for all observed surfactants are shown in Fig. 7.2. For the reference surfactant (Fig. 7.2b) one observes first a decrease of the interfacial tension until a minimum is reached and then the IFT is increasing again. Such a behavior has been observed before for nonionic surfactants.[43] This change is taking place in a continuous fashion. The effect of the PO and PL units is to shift the overall value of the IFT upwards and to move the minimum to higher temperatures. Furthermore, for the PL surfactant almost no temperature dependence is seen.

In contrast, the temperature dependent IFT data of the CO_2 surfactants are showing a completely different behavior. At low temperatures, the IFT is almost constant up to a certain

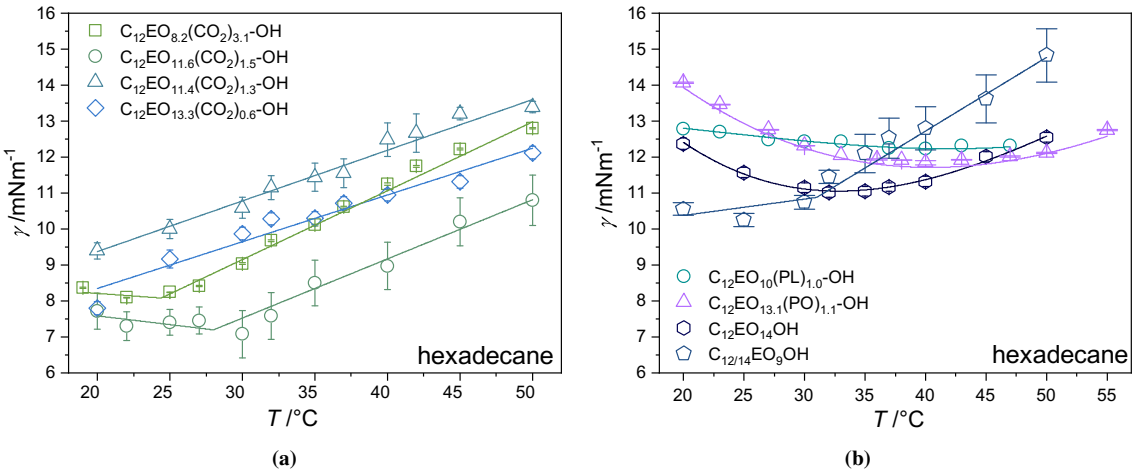

Figure 7.2: Temperature dependent interfacial tension measurements at the water/hexadecane interface at the temperature regime from 18 up to 50 °C for the CO_2 containing surfactants (a) and for the pure EO surfactant and the ones with PO or PL modification (b).

transition temperature, at which a sudden increase of the IFT is seen. With increasing temperatures the IFT is increasing for the CO_2 surfactant with the highest CO_2 content ($C_{12}EO_{8.2}(CO_2)_{3.1}-OH$) to IFT values up to 12.8 mN/m. These results are already quite surprising because usually a decrease of IFT would be expected. It should be noted here that in general, the CO_2 surfactants have a much smaller IFT below the transition temperature with 7 – 8 mN/m for 0.1 mM in comparison to the PO and PL surfactants with 12 – 13 mN/m and the pure EO surfactant with 11 mN/m around their minimum. The transition temperature is shown in Table 7.2 and is shifted to lower temperatures with increasing CO_2 content. For $C_{12}EO_{13.3}(CO_2)_{0.6}-OH$ and $C_{12}EO_{11.4}(CO_2)_{1.3}-OH$ no flat plateau is seen, but the measurements could not be extended to lower temperature because of the freezing temperature of hexadecane at 18 °C.

The reason for the difference in adsorption behavior of the CO_2 surfactants can be explained by thermodynamic analysis of the adsorption behavior.

Thermodynamic Analysis of the Adsorption at the Water/Hexadecane Interface

The thermodynamic analysis was done as explained in the experimental section. The Gibbs energy of adsorption ΔG_{ads} is given by Eq. 7.5 and is negative for all surfactants indicating that adsorption of these compounds at the water/hexadecane interface is spontaneous (see Fig. 7.3). It is thereby quite interesting that ΔG_{ads} is more negative for the reference surfactant $C_{12}EO_{14.0}-OH$. ΔG_{ads} is increasing with increasing CO_2 content, indicating less favored adsorption at the water/hexadecane interface in comparison to the reference surfactant. The CO_2 surfactant $C_{12}EO_{8.2}(CO_2)_{3.1}-OH$ has a ΔG_{ads} of -46.7 kJ/mol in comparison to $C_{12}EO_{14.0}-OH$ with -59.3 kJ/mol. The PO surfactant thereby behaves similarly to the reference surfactant with values of ΔG_{ads} of -54.1 kJ/mol and the PL surfactant similarly to the CO_2 surfactant with values of -48.1 kJ/mol. The difference of the ΔG_{ads} of the CO_2 surfactants in comparison to the reference surfactant ($\Delta\Delta G_{ads}$) is shown in Fig. 7.3a in the inset. The difference $\Delta\Delta G_{ads}$ for the CO_2 surfactant $C_{12}EO_{8.2}(CO_2)_{3.1}-OH$ is at 25 °C 14 kJ/mol, whereas the surfactant with the lowest CO_2 content has only a difference of 8 kJ/mol. This visualizes, that with increasing CO_2 content ΔG_{ads} is reduced and therefore the adsorption is less favored.

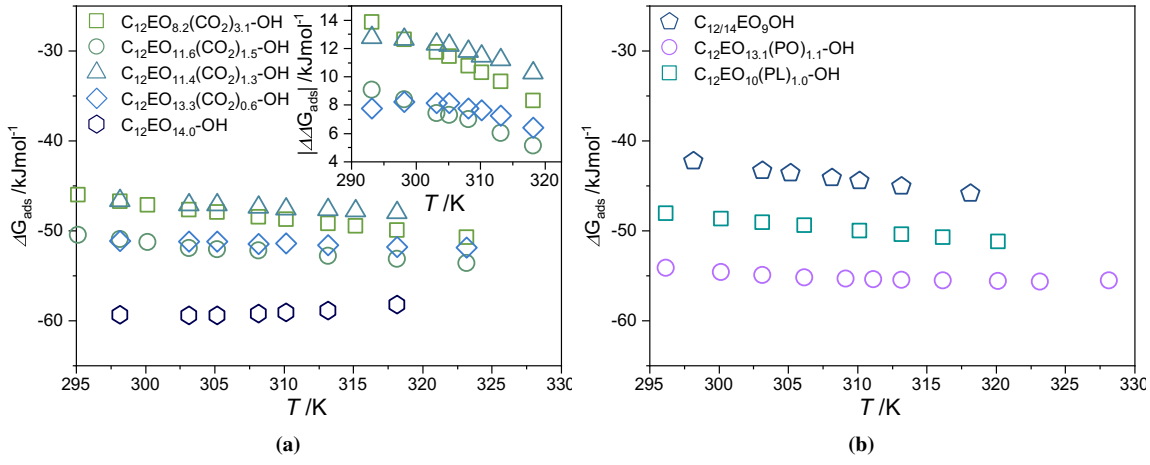

Figure 7.3: Gibbs energy of adsorption ΔG_{ads} depending on the temperature for all CO_2 surfactants (a) and the PO, PL surfactants and the commercial reference surfactant (b) obtained from interfacial tension measurements and from Eq. 7.5. Inset in (a) shows the difference in ΔG_{ads} ($\Delta\Delta G_{ads}$) between the reference surfactant $C_{12}EO_{14.0}-OH$, and the CO_2 surfactant.

Generally, the negative values of ΔG_{ads} are in good agreement with the literature. As reported by Rosen *et al.*, ΔG_{ads} values for a $C_{12}EO_8$ surfactant at the water/hexadecane interface was found to be -51.1 kJ/mol at 25 °C.[208] The commercial reference $C_{12/14}EO_9-OH$, however, shows much smaller negative ΔG_{ads} values, which may occur from the polydisperse alkyl chain which also indicates a reduced head group area which may be the reason for the larger ΔG_{ads} values.

From the Gibbs energy of adsorption ΔG_{ads} (Fig. 7.3), the entropy of adsorption ΔS_{ads} was evaluated from Eq. 7.4 and the Gibbs Helmholtz relation gives the enthalpy of adsorption ΔH_{ads}. All resulting values in dependency of the temperature are shown in Fig. 7.5 for the temperature dependent measurements at the water/hexadecane interface. As already observed from ΔG_{ads}, with increasing CO_2 content the adsorption at the interface is less favored. This can also be observed for the enthalpy values ΔH_{ads}, with even positive values for the CO_2 surfactants of 8.3 kJ/mol for $C_{12}EO_{8.2}(CO_2)_{3.1}-OH$ at 25 °C and negative values for the reference surfactant with -51.6 kJ/mol for $C_{12}EO_{14.0}-OH$. The CO_2 surfactants show also with decreasing CO_2 content a decrease of ΔH_{ads} with values quite similar to the reference surfactant for the $C_{12}EO_{13.3}(CO_2)_{0.6}-OH$ with -50.9 kJ/mol. The PO surfactant show also negative values for ΔH_{ads} with -15.5 kJ/mol, whereas the PL surfactant show very small negative values with -1.3 kJ/mol.

These abrupt changes of the thermodynamic parameters of adsorption with increasing CO_2 content are shown in Fig. 7.4 and can also be observed for the entropy of adsorption ΔS_{ads}. ΔS_{ads} is positive at 25 °C for all CO_2 surfactants and the reference surfactant, whereby the reference surfactant shows values for ΔS_{ads} with 25 J/K mol. With increasing CO_2 content the entropy of adsorption is also increasing up to values of 184 J/K mol for $C_{12}EO_{8.2}(CO_2)_{3.1}-OH$. This indicates a higher contribution of the entropy for the adsorption at the water/hexadecane interface for the CO_2 surfactants at 25 °C. But nevertheless, as already indicated by the negative ΔG_{ads} value, the main driving force of the adsorption process is the hydrophobic interactions because $T\Delta S_{ads} > \Delta H_{ads}$and is reduced for the CO_2 surfactants.

This observation is quite interesting because it is the opposite of what is observed for the micellization process and the adsorption at the water/air interface as described in chapter 4. The incorporation of CO_2 units usually renders the CO_2 surfactants somewhat more hydrophobic, thereby favoring the formation of micelles and the adsorption at the water/air surface. Once the adsorption occurs at a water/oil (in this case hexadecane) interface the adsorption is less favored.

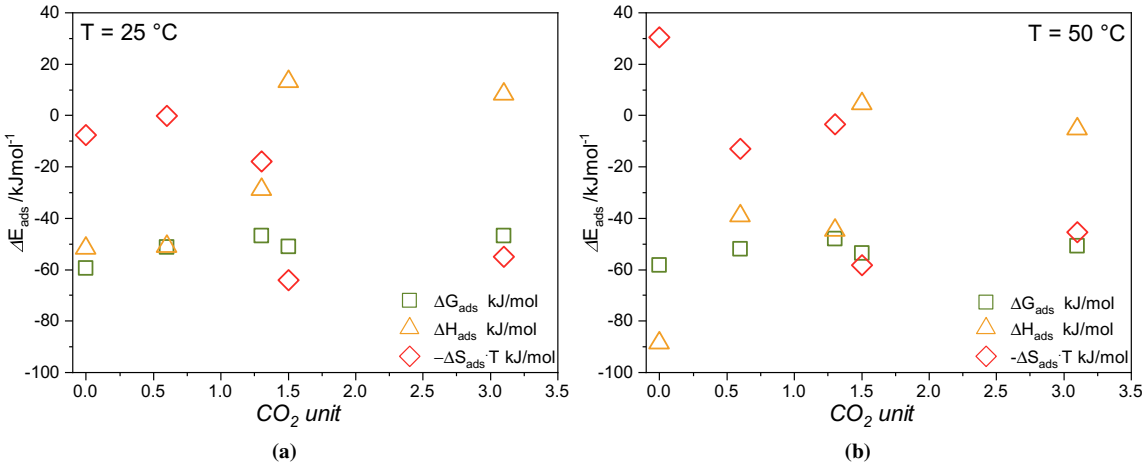

Figure 7.4: Dependency of the thermodynamic parameters of adsorption at the water/hexadecane interface ΔG_{ads}, ΔH_{ads} and $T*\Delta S_{ads}$ on the number of incorporated CO_2 units measured at 25°C (a) and at 50 °C (b).

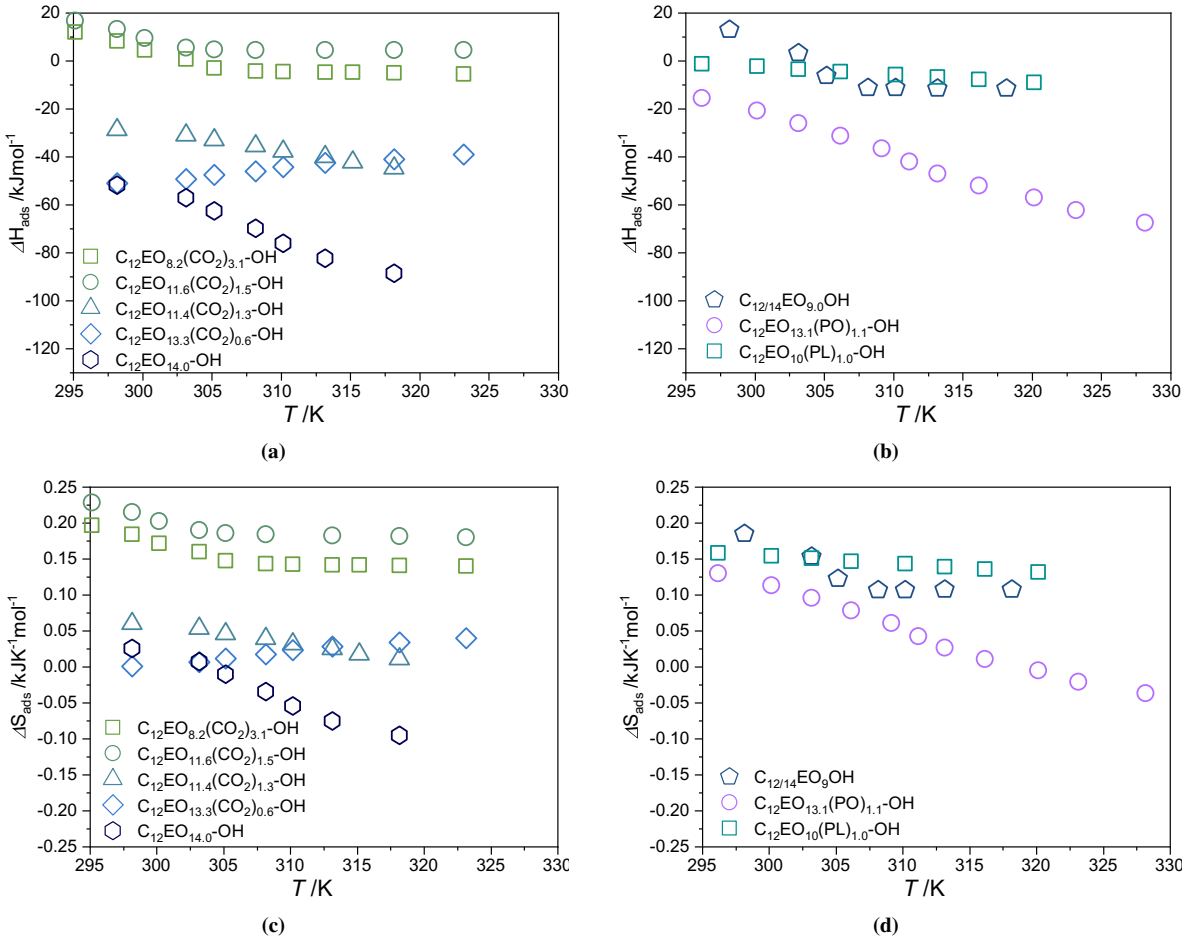

Figure 7.5: Enthalpy ΔH_{ads} and entropy ΔS_{ads} of adsorption depending on the temperature for all CO_2 surfactants ΔH_{ads} (a), ΔS_{ads} (c) and the PO, PL surfactants and the commercial reference surfactant (b) and (d) obtained from interfacial tension measurements.

This phenomenon may be induced by the hydrophobic character of the incorporated CO_2 moiety. Therefore, the CO_2 unit in the hydrophilic head group is less water affine and therefore avoids water contact. Favored adsorption at the interface, as seen from ΔH_{ads} and ΔS_{ads}, only occurs for the reference surfactant, the PO, and PL surfactants and CO_2 surfactant with CO_2 content below 1.3 (Fig. 7.4a). This indicates, that with decreasing hydration affinity of the surfactants head group, the driving force of the adsorption process is reduced (decreasing disruption of hydrogen bonds). Moreover, the higher hydrophobicity of the CO_2 surfactants could also lead to a higher degree of desorption into the oil phase which could be the reason for the lower affinity to remain at the interface.

Besides the measurements at 25 °C we also investigated the interfacial tension temperature dependence and therefore we also obtained thermodynamic information about the temperature dependent adsorption of the CO_2 surfactants (as seen in Fig. 7.5). It can be observed for all surfactants, that with increasing temperature ΔH_{ads} and ΔS_{ads} are decreasing, whereas ΔG_{ads} remains almost temperature independent (only small changes can be observed) for all surfactants. The temperature response of the CO_2 surfactants varies from the behavior of the reference and PO surfactants. For the reference surfactant and PO surfactant ΔH_{ads} and ΔS_{ads} is decreasing linearly, which appears to indicate dehydration of the surfactant molecules with increasing temperature and due to the thermal agility the adsorption at the interface is more favored. The dehydration leads to a disruption of hydrogen bonds and a release of water molecules

which results in negative values for ΔH_{ads} and ΔS_{ads} which is the driving force of the adsorption process. At higher temperatures, the surfactant is less hydrated, requires less dehydration to adsorb, and adsorbs more readily.[43, 97]. ΔH_{ads} of the reference surfactant increases to higher negative values to -88.6 kJ/mol at 50 °C and the PO surfactant to values of -62.3 kJ/mol for ΔH_{ads}. ΔS_{ads} is also reduced to values of -95.3 J/K mol for $C_{12}EO_{14.0}-OH$ and -20.5 J/K mol for the PO surfactant at 50 °C.

The difference for the CO_2 surfactant is the lower hydration affinity, as already mentioned above. Therefore, the CO_2 surfactants are only showing a small reduction of ΔH_{ads} and ΔS_{ads} with increasing temperature, only upon a certain temperature at which the parameters remain constant at values for $C_{12}EO_{8.2}(CO_2)_{3.1}-OH$ of -5.4 kJ/mol for ΔH_{ads} and 140 J/K mol for ΔS_{ads} at 50 °C. This phenomenon implies, that the adsorption of the CO_2 surfactants at the water/hexadecane interface is more favored with increasing temperature up to a certain temperature at which they show an independence in terms of interfacial adsorption. Interestingly, the commercial reference $C_{12/14}EO_9-OH$, is showing a similar behavior as shown in Fig. 7.5. The commercial reference has a $C_{12/14}$ alkyl chain. Moreover it has a shorter head group in comparison to the reference $C_{12}EO_{14.0}-OH$. This indicates, that the adsorption behavior of the CO_2 surfactants resembles the behavior of a conventional nonionic surfactant with a shorter EO chain. The reason for this could be the increasing ability to resolve in the oil phase once the interface is saturated. So the desorption is not only into the water phase but also into the oil phase.

This would also explain the very long equilibration times of the CO_2 surfactants which usually take several hours. The adsorption-desorption equilibrium of the CO_2 surfactants is influenced by the low hydration and the incorporation of the CO_2 units. This implies that the CO_2 moieties are somehow changing the equilibrium. Moreover, the surfactants are polydisperse products with a distribution of the CO_2 content. This meant that some surfactants have higher CO_2 content than others and some have non. Therefore, the several species could also change the adsorption behavior and would require longer equilibration times.

7.3.3. Variation of Oil

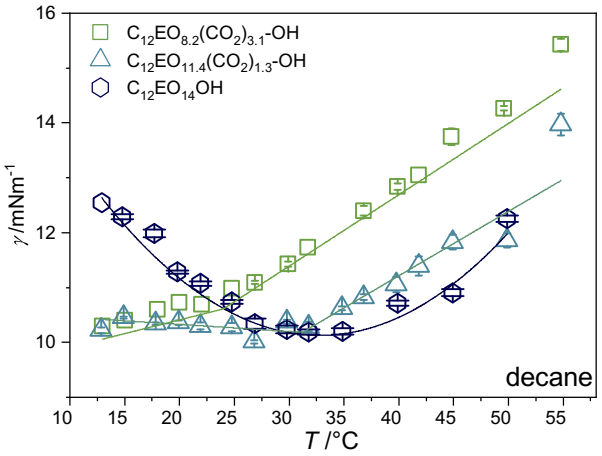

Figure 7.6: Temperature dependent interfacial tension measurements at the water/decane interface at the temperature regime from 13 up to 55 °C for the CO_2 containing surfactants $C_{12}EO_{8.2}(CO_2)_{3.1}-OH$ and $C_{12}EO_{11.4}(CO_2)_{1.3}-OH$ and the reference surfactant $C_{12}EO_{14.0}-OH$.

The temperature depended IFT at the water/hexadecane interface of the reference surfactant shows a decrease of IFT upon a certain temperature and an increase of IFT with further temperature rise (Fig. 7.2b). Investigating the adsorption at lower temperatures would give insights, if the IFT dependency of the CO_2 surfactants is shifted to lower temperatures. For this purpose the IFT was measured at the water/decane interface to generalize our findings of these type of IFT measurement and to be able to extent the measurement range to lower temperatures. The obtained data (Fig. 7.8) show the same behavior as observed for the water/hexadecane interface. While for the pure EO surfactant a continuous change as a function of temperature with a prominent minimum is seen. For the CO_2 surfactants two relatively linear regions are seen, which are separated by a transition temperature.

The IFT values are reduced to somewhat smaller IFT values for the reference surfactant, $C_{12}EO_{14.0}-OH$, which is in good agreement with literature.[208, 209] The reduction of the chain length of the oil phase leads to a reduction of the IFT values as shown for a range of oils from pentane to dodecane measured at the water/oil interface with sorbitane surfactants.[209]

Table 7.2: Values of the interfacial tension at 0.1 mM surfactant concentration at 25 °C and the transition temperature $T_{I \rightarrow II}$ for each surfactant at the water/hexadecane and water/decane interface.

Surfactants	$\gamma_{hexadecane}$ /mN/m	γ_{decane} /mN/m	$T_{I \rightarrow II}$ (hexadecane) /°C	$T_{I \rightarrow II}$ (decane) /°C
$C_{12}EO_{8.2}(CO_2)_{3.1}-OH$	8.2	11.0	24.4	24.0
$C_{12}EO_{11.6}(CO_2)_{1.5}-OH$	7.4	-	28.0	-
$C_{12}EO_{11.4}(CO_2)_{1.3}-OH$	10.0	10.3	< 20	31.2
$C_{12}EO_{13.3}(CO_2)_{0.6}-OH$	9.2	-	< 20	-
$C_{12}EO_{10.3}(PL)_{1.0}-OH$	12.5	-	37.3	-
$C_{12}EO_{13.2}(PO)_{1.1}-OH$	12.8	-	37.4	-
$C_{12}EO_{14.0}-OH$	11.6	10.7	33.3	32.6
$C_{12/14}EO_9-OH$	10.3	-	31.0	-

Interestingly, this is not the case for the analyzed CO_2 surfactant, whereby the IFT at the water/decane interface slightly increases for $C_{12}EO_{11.4}(CO_2)_{1.3}-OH$ and even prominently increases for $C_{12}EO_{8.2}(CO_2)_{3.1}-OH$. The transition temperature remains almost constant for both interface, but the $C_{12}EO_{11.4}(CO_2)_{1.3}-OH$ surfactants shows an increase of the transition temperature.

Thermodynamic Analysis of the Adsorption at the Water/Decane Interface

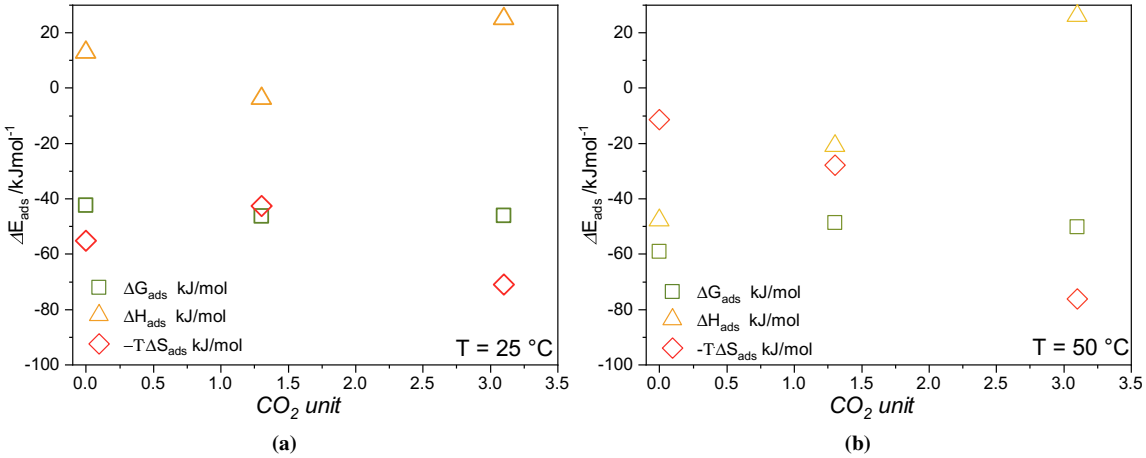

Figure 7.7: Dependency of the thermodynamic parameters of adsorption at the water/decane interface ΔG_{ads}, ΔH_{ads} and $T*\Delta S_{ads}$ on the number of incorporated CO_2 units measured at 25°C (a) and at 50 °C (b).

Form a thermodynamic analysis of the IFT data at the water/decane interface, one can observe quite comparable results. With the incorporation of CO_2 moieties, adsorption at the water/decane interface becomes less favored as shown by smaller negative values of ΔG_{ads} as shown in Fig. 7.7. However, the adsorption is again mainly entropy-driven as seen by $T\Delta S_{ads} > \Delta H_{ads}$. However, the adsorption at the interface is a favored process, the CO_2 surfactants are less favoring the adsorbion in comparison to the reference surfactant. This phenomenon is independent of the observed oil phase. The ΔH_{ads} and ΔS_{ads} values at 25 °C are 24 kJ/mol and -238 J/K mol, for the CO_2 surfactant $C_{12}EO_{8.2}(CO_2)_{3.1}-OH$. Whereas the reference surfactant shows at 25 °C exotherm enthalpy values of -47.9 kJ/mol and entropy values of 38 J/K mol.

For the temperature dependent, IFT measurements of the water/decane interface one can observe again a linear decrease of ΔH_{ads} and ΔS_{ads} for the reference surfactant with values up to -146 kJ/mol for ΔH_{ads} and -280 J/K mol for ΔS_{ads} at 50 °C. In contrast, the CO_2 surfactant with the highest CO_2 content shows almost no temperature response for ΔH_{ads} and ΔS_{ads} and $C_{12}EO_{11.4}(CO_2)_{1.3}-OH$ shows only a small decrease.

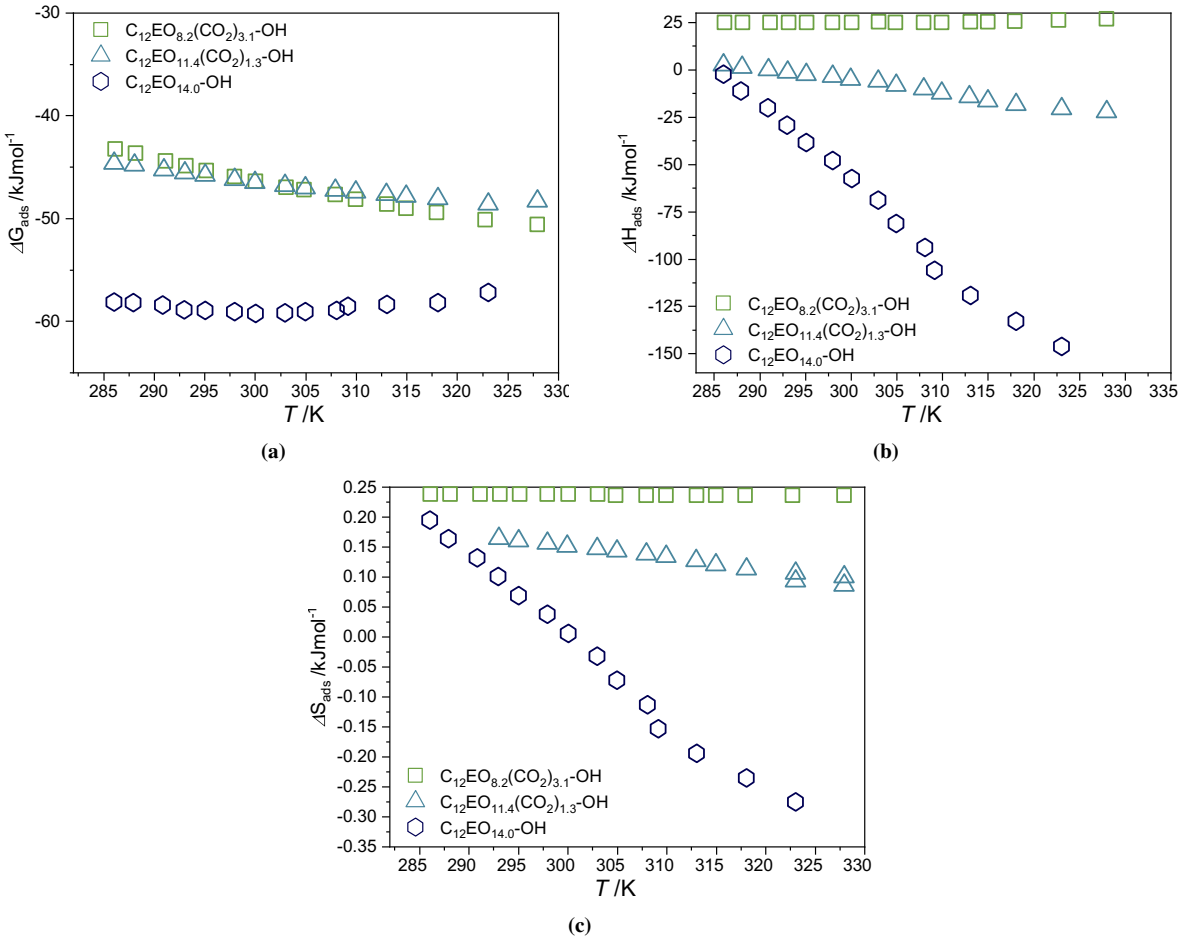

Figure 7.8: Energy of adsorption ΔG_{ads} (a) enthalpy ΔH_{ads} (b) and entropy ΔS_{ads} (c) of adsorption depending on the temperature for the CO_2 surfactants $C_{12}EO_{8.2}(CO_2)_{3.1}-OH$ and $C_{12}EO_{11.4}(CO_2)_{1.3}-OH$ and the reference surfactant $C_{12}EO_{14.0}-OH$ from interfacial tension measurements.

7.3.4. Variation of Alkyl Chain length

The IFT measurements at water/hexadecane interface have also been performed for the C_{16} CO_2 surfactants to investigate the influence of the alkyl chain length on the adsorption behavior. In Fig. 7.9 the temperature dependent IFT measurements are shown for the C_{16} CO_2 surfactants in comparison to the C_{16} PL surfactant and the reference surfactants $C_{16}EO_{14.6}-OH$. One can already see that the C_{16} CO_2 and PL surfactants show a transition at higher temperatures in comparison to the C_{12} surfactants and an increasing IFT in the low-temperature regime. As a comparison, the reference surfactants $C_{16}EO_{14.6}-OH$ and $C_{16/18}EO_{13}-OH$ show a decreasing IFT at the low-temperature regime (below the transition temperature). The transition temperature of the C_{16} CO_2 surfactant was determined to be 45.5 °C and for the PL surfactant the transition temperature is 41.1 °C.

As a comparison, the reference surfactant without CO_2 and only ethylene oxide was also measured with IFT temperature dependent. Additionally, LutensolAT13 is a commercial reference sample from the company BASF with a mixed alkyl chain with C_{16} and C_{18} units. Interestingly, both reference surfactants are showing a transition temperature but with decreasing interfacial tension with increasing temperature; directly opposite to the dependency of the C_{16} CO_2 and PL surfactants. The transition temperature reference sample is 38.4 °C and for LutensolAT13 it is

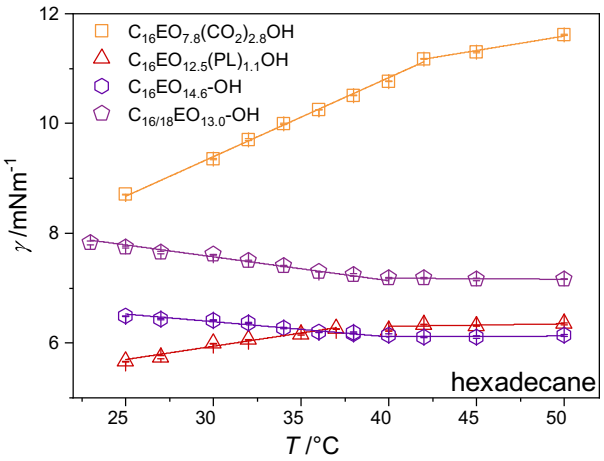

Figure 7.9: Temperature dependent interfacial tension measurements at the water/hexadacne interface of the C_{16} CO_2 surfactants at the temperature regime from 18 up to 50 °C.

39.3 °C. So, the reference surfactants are showing the transition at the same temperature, whereas the CO_2 surfactant has a much higher transition temperature.

The dependency of the IFT values for the C_{16} surfactants have a different origin. As described in chapter 5.3.4, the C_{16} surfactants have a Krafft temperature at ~ 40 °C. Measuring the IFT at the temperature regime from 18 up to 50 °C one can observe the melting process of the surfactants and the influence on the IFT. Nevertheless, it is quite surprising that the CO_2 surfactants shows lower IFT values below the Krafft temperature with values of 8.7 mN/m at 25 °C. The C_{16} PL surfactants has even lower values at 25 °C with 5.7 mN/m. These values are increasing up to 11.6 mN/m for $C_{16}EO_{7.8}(CO_2)_{2.8}-OH$ and 6.4 mN/m for PL surfactant at 50 °C.

The adsorption at the water/hexadecane interface of the C_{16} surfactants is favored in the observed temperature regime. The thermodynamic parameters are shown in the Appendix Chapter 7.

7.4. Summary & Outlook

In this chapter, we studied the adsorption at the water/oil interface of the CO_2 containing surfactants. Understanding the adsorption properties in terms of temperature dependence opens up several opportunities to new properties, such as emulsion and microemulsion formation.

The IFT values for the surfactants at the water/decane interface reaches for all CO_2 surfactants values below 10 mN/m. With increasing CO_2 content the IFT values are reduced with 7.0 mN/m for the surfactant with the highest CO_2 content at a concentration of 0.1 mmol/L. The measurements of the interfacial tension as a function of the concentration give values for the head group area, which varies significantly comparing the values from surface tension measurements. These discrepancies can occur from a different packing of the CO_2 surfactants at the oil/water interface in comparison to the water/air interface.

The adsorption process is for all surfactants an energetically spontaneous process indicated by a negative ΔG_{ads}. Interestingly, ΔG_{ads} is increasing with increasing CO_2 content, indicating less favored adsorption at the water/oil interface in comparison to the reference surfactant. This phenomenon may be induced by the hydrophobic character of the incorporated CO_2 moiety. Favored adsorption at the interface, as seen from ΔH_{ads} and ΔS_{ads}, only occurs for the reference surfactant, the PO, and PL surfactants and CO_2 surfactant with CO_2 content below 1.3. This

indicates, that with decreasing hydration affinity (increasing CO_2 content) of the surfactants head group, the driving force of the adsorption process is reduced (decreasing disruption of hydrogen bonds). Moreover, the higher hydrophobicity of the CO_2 surfactants could also lead to a higher degree of desorption into the oil phase which could be the reason for the lower affinity to remain at the interface.

For all surfactants, a temperature dependent adsorption at the water/oil interface could be observed. With increasing temperature ΔH_{ads} and ΔS_{ads} are decreasing, whereas ΔG_{ads} remains almost temperature independent (only small changes can be observed) for all surfactants. Dehydration with rising temperatures results in a linear decrease of ΔH_{ads} and ΔS_{ads} for the reference surfactant and the PO and PL surfactants, thereby the adsorption at the interface is more favored with rising temperature. The CO_2 surfactants show a different temperature dependency. With rising temperatures, ΔH_{ads} and ΔS_{ads} remain almost constant upon a certain temperature. This phenomenon implies, that the adsorption of the CO_2 surfactants at the water/hexadecane interface is more favored with increasing temperature. The reason for this could be the reduced hydration affinity which indicates that no further hydrogen bond disruption occurs from the temperature rise. Moreover, an increasing ability to resolve in the oil phase once the interface is saturated could also be indicated. So the desorption is not only into the water phase but also into the oil phase. All the findings are independent of the oils phase, as measurements of the water/hexadecane and water/decane interface leads to comparable results.

The investigation of the adsorption phenomenon at the water/oil interface was followed by the study of the formation of microemulsions by the CO_2 surfactants. These studies were performed within the master thesis of Rahel Marschall. In this framework, the solubilization of decane by the CO_2 surfactants was studied in thorough detail. Interestingly, the CO_2 surfactants show a remarkable enhancement of the oil solubilization, which implies the impact of the CO_2 moiety. Investigating, the phase behavior of the CO_2 surfactants in terms of oil solubilization and microemulsion formation shows very promising results and further studies will be performed.

Chapter 8

General Conclusion and Outlook

In this work, the micellization and phase behavior of CO_2 containing nonionic surfactants was studied in thorough detail. Furthermore, the application as solubilizers of hydrophobic compounds and the adsorption at the water/oil interface was characterized. The use of CO_2 containing surfactants in commercial applications is of great interest because the abundant greenhouse gas CO_2 could be incorporated in the EO head group, which allows the utilization of CO_2 as a resource. Thereby the use of CO_2 in surfactants is very interesting in terms of exchanging at least parts of the fossil-based materials, moreover, they are also much more biodegradable, which renders the CO_2 surfactants as an excellent alternative to conventional nonionic surfactants. This work gives a comprehensive picture of the phase behavior of CO_2 surfactants and the specific influence of the CO_2 moiety on the physico-chemical properties, which renders the incorporation of a CO_2 moiety in the hydrophilic head group as an additional tuning parameter.

At first, the micellization and the surface-active behavior of the CO_2 surfactants were characterized and discussed in thorough detail. The focus of this chapter was the analysis of the influence of the CO_2 unit on the thermodynamics of the micellization process. The analysis of surface tension and ITC measurements shows, that the incorporation of CO_2 moieties has the largest impact on the micellization process in comparison to the incorporation of PO and PL, and reduces the cmc and the surface tension above the cmc. The CO_2 incorporation renders the surfactants somewhat more efficient and effective especially in comparison to a commercial reference surfactant such as Marlipal 24/90 and also in comparison to the incorporation of other hydrophobic units such as PO. The transfer energy for micellization is changed by -0.36 kT per CO_2 unit, whereas the PO unit only changes the energy of micellization by a factor of -0.24 kT and PL only by -0.10 kT per PL unit at 25 °C, which indicates an enhanced energetically favored micellization process by incorporating CO_2 moieties. The incorporation of the CO_2 moiety thereby introduces a hydrophobic impact, even though the CO_2 moiety contributes to the hydrophilic head group of the surfactant.

Most interestingly, this chapter shows that the incorporation of CO_2 leads to a systematic reduction of the hydration affinity of the head group, as indicated by a reduced enthalpy ΔH_{mic} and entropy ΔS_{mic} of micellization. This can also be confirmed by a reduced head group area, which allows a denser packing at the surface. In summary, incorporating a hydrophobic unit in the head group results in a systematic reduction of the hydration of the head group and thereby to a

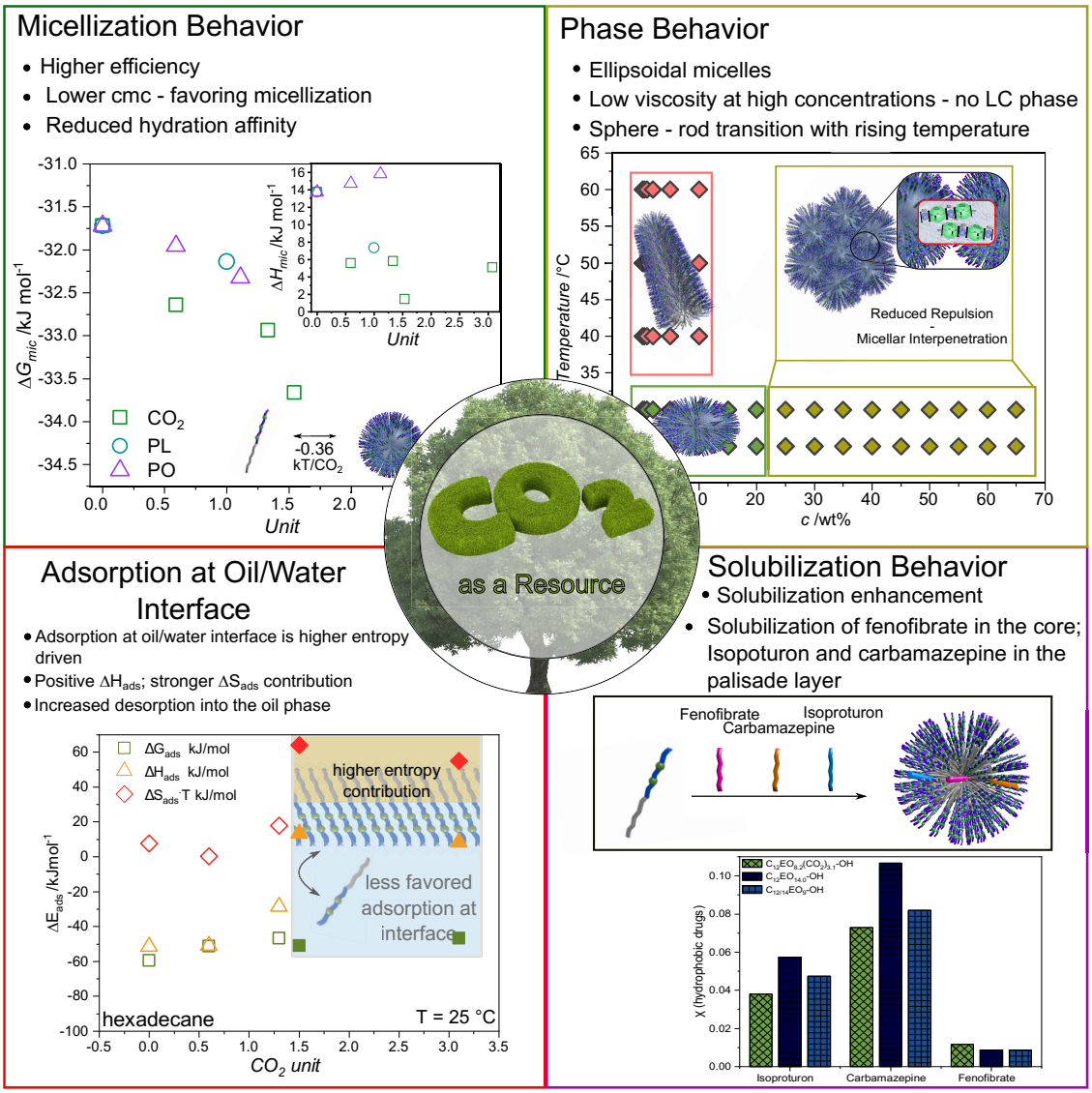

Figure 8.1: Schematic summary of the characterization of the CO_2 containing nonionic C_{12} surfactants.

controllable change of the micellization process. This can be used as an additional tuning parameter to achieve desired aggregation properties.

Further characterization of the phase behavior in terms of concentration and temperature variation showed, that the incorporation of the CO_2 moiety has a prominent impact of the structural ordering of the CO_2 surfactants. Structural information obtained from light and neutron scattering measurements showed that prolate ellipsoidal micelles are formed with an overall effective radius between 3.7 and 4.9 and an increase of size with increasing CO_2 content. Moreover, one obtains the information from the fractal exponent in the Porod regime, that the polymers in the shell are collapsed for the CO_2 surfactants and fully swollen up to Gaussian chains for the reference surfactant and the PO surfactant.

However, the most interesting phenomenon is the reduced hydration (e.g., bound water molecules in the hydrophilic head group) of the CO_2 surfactants, which also explains the collapsed shell as indicated by the fractal exponent of the Porod regime. The information on the hydration was obtained from scattering experiments, which implies that the CO_2 surfactants show substantial

dehydration of the head groups and a much reduced repulsive interaction between the head groups. The reduced hydration shows also pronounced effects at the high concentration regime, whereby the CO_2 surfactants do not form liquid crystalline phases as usually observed for C_iE_j surfactants. These findings have an origin in a reduced repulsive interaction of the CO_2 aggregates and therefore a lower effective degree of ordering due to the presence of the CO_2 units in the head group. The introduction of CO_2 moieties reduces the repulsive interactions and thereby allows an overlapping of the micellar aggregates, which results in a low viscous Newtonian flow behavior. The absence of LC phases means that no gelation is observed and has the effect of a drastically reduced viscosity. This is not only fundamentally a very interesting observation but also one of high practical importance, which facilitates enormously the handling of these surfactants at higher concentrations, as it is typically required in almost all applications at some stage. It should also be noted that this behavior is unique for CO_2 incorporation.

The temperature dependent phase behavior shows a rather complex response. The CO_2 surfactants show a sphere-rod transition with rising temperatures. The conformation of the EO units in the head group thereby changes to a more unpolar configuration with increasing temperature, which enhances the formation of elongated, rod-like structures. The incorporation of CO_2 moieties could thereby enhance the formation of the unpolar a-a-a configuration, which could be the reason for the striking temperature response. This results also in a lowered cloud point of the CO_2 surfactants with higher CO_2 content. By incorporating CO_2 moieties the temperature response can be tuned depending on the desired application, thereby rendering the surfactants much more effective as detergents even at lower temperatures.

The studies on the phase behavior were followed by a thorough study of the solubilization potential of the CO_2 surfactants and the CO_2 triblock copolymers for three different hydrophobic compounds. From these studies, it could be shown that the solubility of the three hydrophobic compounds could be enhanced by CO_2 containing surfactants. The factor of solubility enhancement is quite comparable for all surfactants, whereas the CO_2 incorporation leads to a slight decrease in solubilization. However, it can be stated that the CO_2 surfactants show comparable results and combined with better biodegradability and higher efficiency which allows the use at lower concentrations, the CO_2 surfactants are a suitable alternative to conventional nonionic surfactants for hydrophobic compound solubilization.

The solubilization by CO_2 containing triblock copolymers shows quite different results. The triblock copolymers EO/CO_2-PO-EO/CO_2, EO-PO-EO and the referent copolymer Pluronic® F38 are not forming micellar aggregates at 25 °C, but they are enhancing the solubilization of hydrophobic compounds. Thereby it is quite remarkable that the solubilization of carbamazepine is enhanced by all four observed polymers. But most interestingly is the prominent enhancement of the solubility of fenofibrate by the polymer with the highest degree of CO_2 functionalization. It could be shown, that the functionalization of either nonionic surfactants or triblock copolymers with CO_2 moieties are promising alternatives for application as solubilizers for hydrophobic compounds. This knowledge can direly be applied to study further hydrophobic compounds such as other hydrophobic pharmaceuticals or even oils. It would also be interesting to study the solubilization of CO_2 functionalization triblock copolymers which are forming micellar aggregates to obtain a comprehensive picture of the solubilization mechanism and the interaction with the

CO_2 moiety. Especially the enhanced biodegradability of the CO_2 surfactants renders them of high interest for the use in as pharmaceutical carriers or in the formulation of agricultural products.

Further investigation of the adsorption at the water/oil interface shows a quite unique adsorption behavior of the CO_2 surfactants. The enhanced hydrophobicity and reduced hydration of the CO_2 surfactants results in less favored adsorption at the water/oil interface. Moreover, the higher hydrophobicity of the CO_2 surfactant favors desorption into the oil phase. The adsorption at the water/oil interface is temperature dependent. The CO_2 surfactants show a prominent increase with increasing temperature, whereas the reference surfactants show a reduction followed by an increase of interfacial tension with rising temperatures. The investigation of the adsorption behavior at the water/oil interface is substantially interesting for certain applications such as detergency. Moreover, these measurements give already the fundamental information to investigate furthermore the emulsification and microemulsion behavior of the CO_2 surfactants.

The characterization of microemulsion formation and oil solubilization behavior of these new type of surfactants will be addressed in further studies. The understanding of the microemulsion formation and structural transition by addition of cosurfactants gives important information for further potential applications such as cosmetics, or carrier systems for insoluble compounds. Moreover, the characterization of other CO_2 containing polymers with a higher degree of CO_2 functionalization, such as end-capped ethylene oxide polymers, which are promising new products, will be of high interest. These further investigations will be carried out within the subsequent BMBF project called “Dream Resource Conti”. Further goals of the project will be the scaled-up synthesis of these CO_2 surfactants performed by the company Covestro Deutschland AG, which will allow the commercial production of the CO_2 surfactants.

The characterization of the physico-chemical properties of the new and sustainable CO_2 surfactants showed that they are promising alternative to conventional nonionic surfactants. Fundamental investigation of the surface-active and micellization of the CO_2 surfactants proves that the incorporation of CO_2 moieties renders the surfactants more efficient and effective. All these findings demonstrate the versatile properties of these new CO_2-containing surfactants, which can be tuned in detail by the CO_2 content. Being able to work at any concentration allows a better processability, thereby reducing substantially the ecological impact of the logistics for this large-scale commodity product. In addition, these CO_2 containing surfactants contribute to the aim of a more sustainable chemistry as the fossil-based EO units are replaced by CO_2 (by up to 20%). This renders these greener surfactants a very promising alternative to conventional nonionic surfactants, simultaneously reducing the consumption of fossil-based resources with an increased efficiency and tunable phase behavior.

Chapter 9

References

[1] P. Markewitz, W. Kuckshinrichs, W. Leitner, J. Linssen, P. Zapp, R. Bongartz, A. Schreiber, T. E. Müller, "Worldwide innovations in the development of carbon capture technologies and the utilization of CO_2", *Energy and Environmental Science* **2012**, *5*, 7281, DOI 10.1039/c2ee03403d.

[2] M. N. Anwar, A. Fayyaz, N. F. Sohail, M. F. Khokhar, M. Baqar, A. Yasar, K. Rasool, A. Nazir, M. U. Raja, M. Rehan, M. Aghbashlo, M. Tabatabaei, A. S. Nizami, "CO_2 utilization: Turning greenhouse gas into fuels and valuable products", *Journal of Environmental Management* **2020**, *260*, 110059, DOI 10.1016/j.jenvman.2019.110059.

[3] M. Peters, B. Köhler, W. Kuckshinrichs, W. Leitner, P. Markewitz, T. E. Müller, "Chemical technologies for exploiting and recycling carbon dioxide into the value chain", *ChemSusChem* **2011**, *4*, 1216, DOI 10.1002/cssc.201000447.

[4] M. Mikkelsen, M. Jørgensen, F. C. Krebs, "The teraton challenge. A review of fixation and transformation of carbon dioxide", *Energy and Environmental Science* **2010**, *3*, 43, DOI 10.1039/b912904a.

[5] F. Dadgar, R. Myrstad, P. Pfeifer, A. Holmen, H. J. Venvik, "Direct dimethyl ether synthesis from synthesis gas: The influence of methanol dehydration on methanol synthesis reaction", *Catalysis Today* **2016**, *270*, 76, DOI 10.1016/j.cattod.2015.09.024.

[6] M. Takimoto, M. Kawamura, M. Mori, "Nickel(0)-mediated sequential addition of carbon dioxide and aryl aldehydes into terminal allenes", *Organic Letters* **2003**, *5*, 2599, DOI 10.1021/ol0344801.

[7] J. Langanke, L. Greiner, W. Leitner, "Substrate dependent synergetic and antagonistic interaction of ammonium halide and polyoxometalate catalysts in the synthesis of cyclic carbonates from oleochemical epoxides and CO_2", *Green Chemistry* **2013**, *15*, 1173, DOI 10.1039/c3gc36710j.

[8] Y. Wang, D. J. Darensbourg, "Carbon dioxide-based functional polycarbonates: Metal catalyzed copolymerization of CO_2 and epoxides", *Coordination Chemistry Reviews* **2018**, *372*, 85, DOI 10.1016/j.ccr.2018.06.004.

[9] J. Langanke, A. Wolf, J. Hofmann, K. Böhm, M. A. Subhani, T. E. Müller, W. Leitner, C. Gürtler, "Carbon dioxide (CO_2) as sustainable feedstock for polyurethane production", *Green Chem.* **2014**, *16*, 1865, DOI 10.1039/C3GC41788C.

[10] E. Alper, O. Yuksel Orhan, "CO_2 utilization: Developments in conversion processes", *Petroleum* **2017**, *3*, 109, DOI 10.1016/j.petlm.2016.11.003.

[11] I. Omae, "Aspects of carbon dioxide utilization", *Catalysis Today* **2006**, *115*, 33, DOI 10.1016/j.cattod.2006.02.024.

[12] G. Centi, S. Perathoner, "Opportunities and prospects in the chemical recycling of carbon dioxide to fuels", *Catalysis Today* **2009**, *148*, 191, DOI 10.1016/j.cattod.2009.07.075.

[13] M. Aresta, A. Dibenedetto, A. Angelini, "Catalysis for the Valorization of Exhaust Carbon: from CO_2 to Chemicals, Materials, and Fuels. Technological Use of CO_2", *Chemical Reviews* **2014**, *114*, 1709, DOI 10.1021/cr4002758.

[14] N. von der Assen, A. Bardow, "Life cycle assessment of polyols for polyurethane production using CO_2 as feedstock: insights from an industrial case study", *Green Chem.* **2014**, *16*, 3272, DOI 10.1039/C4GC00513A.

[15] N. von der Assen, P. Voll, M. Peters, A. Bardow, "Life cycle assessment of CO_2 capture and utilization: a tutorial review", *Chem. Soc. Rev.* **2014**, *43*, 7982, DOI 10.1039/C3CS60373C.

[16] N. von der Assen, A. Sternberg, A. Kätelhön, A. Bardow, "Environmental potential of carbon dioxide utilization in the polyurethane supply chain", *Faraday Discuss.* **2015**, *183*, 291, DOI 10.1039/C5FD00067J.

[17] Y. Xu, L. Lin, M. Xiao, S. Wang, A. T. Smith, L. Sun, Y. Meng, "Synthesis and properties of CO_2-based plastics: Environmentally-friendly, energy-saving and biomedical polymeric materials", *Progress in Polymer Science* **2018**, *80*, 163, DOI 10.1016/j.progpolymsci.2018.01.006.

[18] S. Inoue, H. Koinuma, T. Tsuruta, "Copolymerization of carbon dioxide and epoxide", *Journal of Polymer Science Part B: Polymer Letters* **1969**, *7*, 287, DOI 10.1002/pol.1969.110070408.

[19] X.-B. Lu, W.-M. Ren, G.-P. Wu, "CO_2 Copolymers from Epoxides: Catalyst Activity, Product Selectivity, and Stereochemistry Control", *Accounts of Chemical Research* **2012**, *45*, 1721, DOI 10.1021/ar300035z.

[20] D. K. Chattopadhyay, K. V. Raju, "Structural engineering of polyurethane coatings for high performance applications", *Progress in Polymer Science (Oxford)* **2007**, *32*, 352, DOI 10.1016/j.progpolymsci.2006.05.003.

[21] D. J. Darensbourg, "Making plastics from carbon dioxide: Salen metal complexes as catalysts for the production of polycarbonates from epoxides and CO_2", *Chemical Reviews* **2007**, *107*, 2388, DOI 10.1021/cr068363q.

[22] S. Klaus, M. W. Lehenmeier, C. E. Anderson, B. Rieger, "Recent advances in CO_2/epoxide copolymerization—New strategies and cooperative mechanisms", *Coordination Chemistry Reviews* **2011**, *255*, 1460, DOI 10.1016/j.ccr.2010.12.002.

[23] M. R. Kember, A. Buchard, C. K. Williams, "Catalysts for CO_2/epoxide copolymerisation", *Chemical Communications* **2011**, *47*, 141, DOI 10.1039/c0cc02207a.

[24] D. J. Darensbourg, R. M. Mackiewicz, A. L. Phelps, D. R. Billodeaux, "Copolymerization of CO_2 and epoxides catalyzed by metal salen complexes", *Accounts of Chemical Research* **2004**, *37*, 836, DOI 10.1021/ar030240u.

[25] D. J. Darensbourg, S. J. Wilson, "What's new with CO_2? Recent advances in its copolymerization with oxiranes", *Green Chemistry* **2012**, *14*, 2665, DOI 10.1039/c2gc35928f.

[26] S. J. Poland, D. J. Darensbourg, "A quest for polycarbonates provided via sustainable epoxide/CO_2 copolymerization processes", *Green Chem.* **2017**, *19*, 4990, DOI 10.1039/C7GC02560B.

[27] I. Kim, M. J. Yi, K. J. Lee, D.-w. Park, B. U. Kim, C.-s. Ha, "Aliphatic polycarbonate synthesis by copolymerization of carbon dioxide with epoxides over double metal cyanide catalysts prepared by using ZnX_2 (X = F , Cl , Br , I)", **2006**, *111*, 292, DOI 10.1016/j.cattod.2005.10.039.

[28] G. Fiorani, W. Guo, A. W. Kleij, "Sustainable conversion of carbon dioxide: the advent of organocatalysis", *Green Chemistry* **2015**, *17*, 1375, DOI 10.1039/C4GC01959H.

[29] M. Tamura, K. Ito, M. Honda, Y. Nakagawa, H. Sugimoto, K. Tomishige, "Direct Copolymerization of CO_2 and Diols", *Scientific Reports* **2016**, *6*, 1, DOI 10.1038/srep24038.

[30] J. Wang, H. Zhang, Y. Miao, L. Qiao, X. Wang, F. Wang, "Waterborne polyurethanes from CO_2 based polyols with comprehensive hydrolysis/oxidation resistance", *Green Chemistry* **2016**, DOI 10.1039/c5gc01373a.

[31] Y. Wang, J. Fan, D. J. Darensbourg, "Construction of Versatile and Functional Nanostructures Derived from CO_2-based Polycarbonates", *Angewandte Chemie* **2015**, *127*, 10344, DOI 10.1002/ange.201505076.

[32] J. Geschwind, H. Frey, "Poly(1,2-glycerol carbonate): A fundamental polymer structure synthesized from CO_2 and glycidyl ethers", *Macromolecules* **2013**, *46*, 3280, DOI 10.1021/ma400090m.

[33] M. Scharfenberg, J. Hilf, H. Frey, "Functional Polycarbonates from Carbon Dioxide and Tailored Epoxide Monomers: Degradable Materials and Their Application Potential", *Advanced Functional Materials* **2018**, *28*, 1, DOI 10.1002/adfm.201704302.

[34] F. Suriano, R. Pratt, J. P. K. Tan, N. Wiradharma, A. Nelson, Y.-y. Yang, P. Dubois, J. L. Hedrick, "Biomaterials Synthesis of a family of amphiphilic glycopolymers via controlled ring-opening polymerization of functionalized cyclic carbonates and their application in drug delivery", *Biomaterials* **2010**, *31*, 2637, DOI 10.1016/j.biomaterials.2009.12.022.

[35] M. Scharfenberg, J. Seiwert, M. Scherger, J. Preis, M. Susewind, H. Frey, "Multiarm Polycarbonate Star Polymers with a Hyperbranched Polyether Core from CO_2 and Common Epoxides", *Macromolecules* **2017**, *50*, 6577, DOI 10.1021/acs.macromol.7b01131.

[36] L. Kunze, S. Y. Tseng, R. Schweins, T. Sottmann, H. Frey, "Nonionic Aliphatic Polycarbonate Diblock Copolymers Based on CO_2 , 1,2-Butylene Oxide, and mPEG: Synthesis, Micellization, and Solubilization", *Langmuir* **2019**, *35*, 5221, DOI 10.1021/acs.langmuir.8b04265.

[37] CO2Plus- BMBF Projekt-Kohlendioxid als Ressource Neue Wege zu einer nach haltigen Rohstoffversorgung, **2016**.

[38] Pressemitteilung, CO2Plus- BMBF Projekt-Kohlendioxid als Ressource Neue Wege zu einer nach haltigen Rohstoffversorgung, **2016**.

[39] Abschlussbericht, CO_2 Plus – Stoffliche Nutzung von CO_2 zur Verbreiterung der Rohstoffbasis, tech. rep., DECHEMA Gesellschaft für Chemische Technik und Biotechnologie e.V., **2019**.

[40] L. Mennicken, A. Janz, S. Roth, "The German R&D Program for CO_2 Utilization—Innovations for a Green Economy", *Environmental Science and Pollution Research* **2016**, *23*, 11386, DOI 10.1007/s11356-016-6641-1.

[41] B. Kronberg, K. Holmberg, B. Lindman in *Surface Chemistry of Surfactants and Polymers*, John Wiley & Sons, Ltd, **2014**, Chapter Types of Surfactants, their Synthesis, and Applications, pp. 1–47, DOI 10.1002/9781118695968.ch1.

[42] J. Eastoe, *1 . Surfactant chemistry and general phase behaviour*, **2003**, pp. 2–11.

[43] M. J. Rosen, *Surfactants and Interfacial Phenomena*, 3., Wiley-Interscience, New York, **2004**, p. 427.

[44] J. Sajbidor, B. Kronberg, K. Holmberg, B. Lindman in, Chapter 9, **2014**, Chapter Surface and interfacial tension, pp. 231–249, DOI 10.1002/9781118695968.ch8.

[45] B. von Szyszkowski, "Experimentelle Studien über kapillare Eigenschaften der wässerigen Lösungen von Fettsäuren", *Zeitschrift für Physikalische Chemie* **1908**, *64U*, 385, DOI 10.1515/zpch-1908-6425.

[46] M. Schick, *Nonionic Surfactants*, Marcel Dekker, Inc, New Zork and Basel, **1987**, p. 1135.

[47] B. Kronberg, K. Holmberg, B. Lindman in *Surface Chemistry of Surfactants and Polymers*, John Wiley & Sons, Ltd, **2014**, Chapter Surfactant Self-Assembly, 75, DOI 10.1002/9781118695968.ch4.

[48] K. Holmberg, B. Jönsson, B. Kronberg, B. Lindman, *Surfactant Micellization*, John Wiley & Sons, Ltd, Chichester, UK, **2004**, pp. 39–66, DOI 10.1002/0470856424.ch2.

[49] H.-J. Butt, K. Graf, M. Kappl, *Surfactants, Micelles, Emulsions, and Foams*, Wiley-VCH Verlag GmbH & Co. KGaA, Weinheim, FRG, **2004**, pp. 246–279, DOI 10.1002/3527602313.ch12.

[50] J. N. Israelachvili, *Intermolecular and Surface Forces*, 3rd ed., Academic Press, **2010**, p. 710.

[51] B. Kronberg, K. Holmberg, B. Lindman in *Surface Chemistry of Surfactants and Polymers*, John Wiley & Sons, Ltd, Chichester, UK, **2014**, 113, DOI 10.1002/9781118695968.ch6.

[52] J. N. Israelachvili, D. J. Mitchell, B. W. Ninham, "Theory of self-assembly of hydrocarbon amphiphiles into micelles and bilayers", *Journal of the Chemical Society Faraday Transactions 2: Molecular and Chemical Physics* **1976**, *72*, 1525, DOI 10.1039/F29767201525.

[53] C. Tanford, "Micelle shape and size", *Journal of Physical Chemistry* **1972**, *76*, 3020, DOI 10.1021/j100665a018.

[54] B. Kronberg, K. Holmberg, B. Lindman, B. Jönsson in *Surfactants and Polymers in Aqueous Solution*, John Wiley & Sons, Ltd, Chichester, UK, **2002**, Chapter Microemulsions, pp. 139–155, DOI 10.1002/0470856424.ch6.

[55] T. P. Hoar, J. H. Schulman, "Transparent Water-in-Oil Dispersions: the Oleopathic Hydro-Micelle", *Nature* **1943**, *152*, 102, DOI 10.1038/152102a0.

[56] M. Kahlweit, R. Strey, "Phase Behavior of Ternary Systems of the Type H_2O/Oil/Nonionic Amphiphile (Microemulsions)", *Angewandte Chemie International Edition in English* **1985**, *24*, 654, DOI 10.1002/anie.198506541.

[57] R. Strey, "I. Experimental Facts: Water-Nonionic Surfactant Systems, and the Effect of Additives", *Berichte der Bunsengesellschaft für physikalische Chemie* **1996**, *100*, 182, DOI 10.1002/bbpc.19961000303.

[58] B. Jakobs, T. Sottmann, R. Strey, J. Allgaier, L. Willner, D. Richter, "Amphiphilic block copolymers as efficiency boosters for microemulsions", *Langmuir* **1999**, *15*, 6707, DOI 10.1021/la9900876.

[59] T. Sottmann, "Solubilization efficiency boosting by amphiphilic block co-polymers in microemulsions", **2002**, 57, DOI 10.1016/s1359-0294(02)00003-1.

[60] J. Lyklema, *Fundamentals of Interface and Colloid Science: Liquid-Fluid Interfaces*, Academic Press, **2000**.

[61] W. Loh, C. Brinatti, K. C. Tam, "Use of isothermal titration calorimetry to study surfactant aggregation in colloidal systems", *Biochimica et Biophysica Acta (BBA) - General Subjects* **2016**, *1860*, 999, DOI 10.1016/j.bbagen.2015.10.003.

[62] K. Bouchemal, F. Agnely, A. Koffi, M. Djabourov, G. Ponchel, "What can isothermal titration microcalorimetry experiments tell us about the self-organization of surfactants into micelles?", *Journal of Molecular Recognition* **2010**, *23*, 335, DOI 10.1002/jmr.998.

[63] H. A. Barnes, *Handbook Of Rheology*, The University of Wales Institute of Non-Newtonian Fluid, **2000**.

[64] B. J. Berne, R. Pecora, *Dynamic Light Scattering*, Wiley, New York, **1976**.

[65] T. Brückel, D. Richter, G. Roth, A. Wischnewski, R. Zorn, *NEUTRON SCATTERING*, *Vol. 106*, (Eds.: F. J. In, at the Heinz Maier-Leibnitz Zentrum Garching), **2015**.

[66] L. Cipelletti, V. Trappe, D. J. Pine in *Fluids, Colloids and Soft Materials: An Introduction to Soft Matter Physics*, John Wiley & Sons, Inc, Hoboken, NJ, USA, **2016**, Chapter Scattering Techniques, pp. 131–148, DOI 10.1002/9781119220510.ch8.

[67] K. Bouchemal, F. Agnely, A. Koffi, G. Ponchel, "A concise analysis of the effect of temperature and propanediol-1, 2 on Pluronic F127 micellization using isothermal titration microcalorimetry", *Journal of Colloid and Interface Science* **2009**, *338*, 169, DOI 10.1016/j.jcis.2009.05.075.

[68] S. Paula, W. Sues, J. Tuchtenhagen, A. Blume, "Thermodynamics of Micelle Formation as a Function of Temperature: A High Sensitivity Titration Calorimetry Study", *The Journal of Physical Chemistry* **1995**, *99*, 11742, DOI 10.1021/j100030a019.

[69] N. E. Olesen, P. Westh, R. Holm, "Determination of thermodynamic potentials and the aggregation number for micelles with the mass-action model by isothermal titration calorimetry: A case study on bile salts", *Journal of Colloid and Interface Science* **2015**, *453*, 79, DOI 10.1016/j.jcis.2015.03.069.

[70] N. E. Olesen, R. Holm, P. Westh, "Determination of the aggregation number for micelles by isothermal titration calorimetry", *Thermochimica Acta* **2014**, *588*, 28, DOI 10.1016/j.tca.2014.04.028.

[71] V. J. Spiering, J. Lutzki, M. Gradzielski, "Thermodynamics of Micellization of Nonionic Surfactants – The Effect of Incorporating CO_2 Moieties into the Head Group", *Journal of Colloid and Interface Science* **2020**, *581*, 794, DOI 10.1016/j.jcis.2020.07.141.

[72] T. Mezger, *Applied Rheology*, **2017**.

[73] R. Moreno in *Encyclopedia of Materials: Science and Technology (Second Edition)*, i, **2003**, DOI https://doi.org/10.1016/B0-08-043152-6/01468-6.

[74] H. Tatlisu, F. Hameed, A. Hilger, N. Kardjilov, H. Rauch, "AP / AM-03 Non-destructive inspection of SiC f / SiC composites structure AP / AM-03", 1.

[75] B. Hammouda, "Probing Nanoscle Structure - SANS Toolbox: Small-Angle Neutron Scattering Polymers Complex Fluids Biology Materials Science", **2016**.

[76] T. Müller, C. Gürtler, A. Kermagoret, Y. Dienes, I. Busygin, B. Köhler, W. Leitner, "Verfahren zur Herstellung von Polycarbonatpolyolen durch immortale Polymerisation von cyclischen Carbonaten", *Patent WO2012/05955* **2012**.

[77] A. M. I. Stute, M. Meuresch, C. Gürtler, A. Wolf, R. Schomäcker, M. Gradzielski, M. Tupinamba Lima, V. J. Spiering, "Diblock Copolymers and their Use as Surfactants", *Patent WO2019076862* **2018**.

[78] M. Tupinamba Lima, V. J. Spiering, S. N. Kurt-Zerdeli, D. C. Brüggemann, M. Gradzielski, R. Schomäcker, "The hydrophilic-lipophilic balance of carboxylate and carbonate modified nonionic surfactants", *Colloids and Surfaces A: Physicochemical and Engineering Aspects* **2019**, *569*, 156, DOI 10.1016/j.colsurfa.2019.03.001.

[79] V. J. Spiering, A. Ciapetti, M. Tupinamba Lima, D. W. Hayward, L. Noirez, M.-S. Appavou, R. Schomäcker, M. Gradzielski, "Changes in Phase Behavior from the Substitution of Ethylene Oxide with Carbon Dioxide in the Head Group of Nonionic Surfactants", *ChemSusChem* **2020**, *13*, 601, DOI 10.1002/cssc.201902855.

[80] W. C. Griffin, "Classification of surface-active agents by HLB", *J. Soc. Cosmet. Chem.* **1949**, *1*, 311.

[81] M. Tupinamba Lima, S. N. Kurt-Zerdeli, D. Brüggemann, V. J. Spiering, M. Gradzielski, R. Schomäcker, "The dynamics of surface adsorption and foam formation of carbonate modified nonionic surfactants", *Colloids and Surfaces A: Physicochemical and Engineering Aspects* **2020**, *588*, 124386, DOI 10.1016/j.colsurfa.2019.124386.

[82] K. Kuotsu, K. Karim, A. Mandal, N. Biswas, A. Guha, S. Chatterjee, M. Behera, "Niosome: A future of targeted drug delivery systems", *Journal of Advanced Pharmaceutical Technology & Research* **2010**, *1*, 374, DOI 10.4103/0110-5558.76435.

[83] D. J. Mitchell, G. J. T. Tiddy, L. Waring, T. Bostock, M. P. McDonald, "Phase behaviour of polyoxyethylene surfactants with water. Mesophase structures and partial miscibility (cloud points)", *Journal of the Chemical Society Faraday Transactions 1: Physical Chemistry in Condensed Phases* **1983**, *79*, 975, DOI 10.1039/f19837900975.

[84] I. Hama, M. Sakaki, H. Sasamoto, "Properties of Polyoxyethylene/Polyoxypropylene-Type Nonionic Surfactant with Narrow Adduct Distribution.", *Journal of Japan Oil Chemists' Society* **1996**, *45*, 1247, DOI 10.5650/jos1996.45.1247.

[85] S. Yada, T. Suzuki, S. Hashimoto, T. Yoshimura, "Adsorption and Aggregation Properties of Homogeneous Polyoxypropylene–Polyoxyethylene Alkyl Ether Type Nonionic Surfactants", *Langmuir* **2017**, *33*, 3794, DOI 10.1021/acs.langmuir.7b00104.

[86] W. von Rybinski, K. Hill, "Alkyl Polyglycosides—Properties and Applications of a new Class of Surfactants", *Angewandte Chemie International Edition* **1998**, *37*, 1328, DOI 10.1002/(sici)1521-3773(19980605)37:10<1328::aid-anie1328>3.0.co;2-9.

[87] R. Lebeuf, C. Y. Liu, C. Pierlot, V. Nardello-Rataj, "Synthesis and Surfactant Properties of Nonionic Biosourced Alkylglucuronamides", *ACS Sustainable Chemistry and Engineering* **2018**, *6*, 2758, DOI 10.1021/acssuschemeng.7b04456.

[88] H. Wenk, J. Meyer, "Polyglycerol – A Versatile Building Block for Sustainable Cosmetic Raw Materials", *SOFW Journal* **2009**, *135*, 25.

[89] A. Thomas, S. S. Müller, H. Frey, "Beyond Poly(ethylene glycol): Linear Polyglycerol as a Multifunctional Polyether for Biomedical and Pharmaceutical Applications", *Biomacromolecules* **2014**, *15*, 1935, DOI 10.1021/bm5002608.

[90] W. von Rybinski, B. Guckenbiehl, H. Tesmann, "Influence of co-surfactants on microemulsions with alkyl polyglycosides", *Colloids and Surfaces A: Physicochemical and Engineering Aspects* **1998**, *142*, 333, DOI 10.1016/S0927-7757(98)00527-5.

[91] H. Wenk, R. Scheuermann, J. Meyer, "Combining convenience and sustainability: simple processing of PEG-free nanoemulsions and classical emulsions", *SOFW Journal* **2008**, *134*, 58.

[92] P. Heunemann, S. Prévost, I. Grillo, C. M. Marino, J. Meyer, M. Gradzielski, "Formation and structure of slightly anionically charged nanoemulsions obtained by the phase inversion concentration (PIC) method", *Soft Matter* **2011**, *7*, 5697, DOI 10.1039/c0sm01556c.

[93] M. Okawauchi, M. Hagio, Y. Ikawa, G. Sugihara, Y. Murata, M. Tanaka, "A Light-Scattering Study of Temperature Effect on Micelle Formation of N -Alkanoyl- N -methylglucamines in Aqueous Solution", *Bulletin of the Chemical Society of Japan* **1987**, *60*, 2719, DOI 10.1246/bcsj.60.2719.

[94] A. J. Kamphuis, F. Picchioni, P. P. Pescarmona, "CO_2-fixation into cyclic and polymeric carbonates: principles and applications", *Green Chemistry* **2019**, *21*, 406, DOI 10.1039/C8GC03086C.

[95] E. Matijević, B. A. Pethica, "The heats of micelle formation of sodium dodecyl sulphate", *Transactions of the Faraday Society* **1958**, *54*, 587, DOI 10.1039/tf9585400587.

[96] J. N. Phillips, "The energetics of micelle formation", *Transactions of the Faraday Society* **1955**, *51*, 561, DOI 10.1039/tf9555100561.

[97] M. J. Rosen, A. W. Cohen, M. Dahanayake, X. Y. Hua, "Relationship of structure to properties in surfactants. 10. Surface and thermodynamic properties of 2-dodecyloxypoly(ethenoxyethanol)s, $C_{12}H_{25}(OC_2H_4)_xOH$, in aqueous solution", *The Journal of Physical Chemistry* **1982**, *86*, 541, DOI 10.1021/j100393a025.

[98] K. Shinoda, T. Yamaguchi, R. Hori, "The Surface Tension and the Critical Micelle Concentration in Aqueous Solution of beta-D-Alkyl Glucosides and their Mixtures", *Bulletin of the Chemical Society of Japan* **1961**, *34*, 237, DOI 10.1246/bcsj.34.237.

[99] A. W. Cohen, M. J. Rosen, "Wetting properties of nonionic surfactants of homogeneous structure $C_{12}H_{25}(OC_2H_4)_xOH$", *Journal of the American Oil Chemists' Society* **1981**, *58*, 1062, DOI 10.1007/BF02679327.

[100] P. H. Elworthy, C. B. Macfarlane, "Surface Activity of a Series of Synthetic Non-Ionic Detergents", *Journal of Pharmacy and Pharmacology* **1962**, *14*, 100T, DOI 10.1111/j.2042-7158.1962.tb10540.x.

[101] J. M. Corkill, J. F. Goodman, R. H. Ottewill, "Micellization of homogeneous non-ionic detergents", *Transactions of the Faraday Society* **1961**, *57*, 1627, DOI 10.1039/tf9615701627.

[102] B. M. Folmer, K. Holmberg, "The cross-sectional headgroup area of nonionic surfactants – the influence of polydispersity", *Colloids and Surfaces A: Physicochemical and Engineering Aspects* **2001**, *180*, 187, DOI 10.1016/S0927-7757(00)00760-3.

[103] S. Yada, T. Suzuki, S. Hashimoto, T. Yoshimura, "Adsorption dynamics of homogeneous polyoxypropylene-polyoxyethylene alkyl ether nonionic surfactants at the air/water interface", *Journal of Molecular Liquids* **2018**, *255*, 208, DOI 10.1016/j.molliq.2018.01.150.

[104] S. B. Sulthana, P. V. Rao, S. G. Bhat, T. Y. Nakano, G. Sugihara, A. K. Rakshit, "Solution properties of nonionic surfactants and their mixtures: polyoxyethylene (10) alkyl ether [C_nE_{10}] and MEGA-10", *Langmuir* **2000**, *16*, 980, DOI 10.1021/la990730o.

[105] G. Olofsson, W. Loh, "On the use of titration calorimetry to study the association of surfactants in aqueous solutions", *Journal of the Brazilian Chemical Society* **2009**, *20*, 577, DOI 10.1590/S0103-50532009000400002.

[106] J. Lah, M. Bešter-Rogač, T. M. Perger, G. Vesnaver, "Energetics in correlation with structural features: The case of micellization", *Journal of Physical Chemistry B* **2006**, *110*, 23279, DOI 10.1021/jp062796f.

[107] B. Anderson, G. Olofsson, "Calorimetric Study of Non-ionic Surfactants", *Journal of chemical society Faraday Transactions* **1988**, *84*, 4087.

[108] Ž. Medoš, M. Bešter-Rogač, "Two-Step Micellization Model: The Case of Long-Chain Carboxylates in Water", *Langmuir* **2017**, *33*, 7722, DOI 10.1021/acs.langmuir.7b01700.

[109] P. R. Majhi, A. Blume, "Thermodynamic Characterization of Temperature-Induced Micellization and Demicellization of Detergents Studied by Differential Scanning Calorimetry", *Langmuir* **2001**, *17*, 3844, DOI 10.1021/la001660k.

[110] M. N. Islam, T. Kato, "Temperature Dependence of the Surface Phase Behavior and Micelle Formation of Some Nonionic Surfactants", *The Journal of Physical Chemistry B* **2003**, *107*, 965, DOI 10.1021/jp021212g.

[111] D. J. Darensbourg, F. T. Tsai, "Postpolymerization functionalization of copolymers produced from carbon dioxide and 2-vinyloxirane: Amphiphilic/water-soluble CO_2-Based polycarbonates", *Macromolecules* **2014**, *47*, 3806, DOI 10.1021/ma500834r.

[112] J. Eastoe, "Fluorinated surfactants in supercritical CO_2", *Current Opinion in Colloid & Interface Science* **2003**, *8*, 267, DOI 10.1016/S1359-0294(03)00053-0.

[113] S. Dai, K. C. Tam, "Isothermal titration calorimetric studies of alkyl phenol ethoxylate surfactants in aqueous solutions", *Colloids and Surfaces A: Physicochemical and Engineering Aspects* **2003**, *229*, 157, DOI 10.1016/j.colsurfa.2003.09.007.

[114] B. C. Stephenson, A. Goldsipe, K. J. Beers, D. Blankschtein, "Quantifying the Hydrophobic Effect. 2. A Computer Simulation-Molecular-Thermodynamic Model for the Micellization of Nonionic Surfactants in Aqueous Solution", *The Journal of Physical Chemistry B* **2007**, *111*, 1045, DOI 10.1021/jp065697a.

[115] Ž. Medoš, N. V. Plechkova, S. Friesen, R. Buchner, M. Bešter-Rogač, "Insight into the Hydration of Cationic Surfactants: A Thermodynamic and Dielectric Study of Functionalized Quaternary Ammonium Chlorides", *Langmuir* **2019**, *35*, 3759, DOI 10.1021/acs.langmuir.8b03993.

[116] R. G. Angarten, W. Loh, "Thermodynamics of micellization of homologous series of alkyl mono and di-glucosides in water and in heavy water", *The Journal of Chemical Thermodynamics* **2014**, *73*, 218, DOI 10.1016/j.jct.2014.01.001.

[117] L.-J. Chen, S.-Y. Lin, C.-C. Huang, "Effect of Hydrophobic Chain Length of Surfactants on Enthalpy-Entropy Compensation of Micellization", *The Journal of Physical Chemistry B* **1998**, *102*, 4350, DOI 10.1021/jp9804345.

[118] S. P. Moulik, D. Mitra, "Amphiphile self-aggregation: An attempt to reconcile the agreement–disagreement between the enthalpies of micellization determined by the van't Hoff and Calorimetry methods", *Journal of Colloid and Interface Science* **2009**, *337*, 569, DOI 10.1016/j.jcis.2009.05.064.

[119] S. P. Moulik, D. Mitra in *Recent Trends in Surface and Colloid Science*, **2012**, 51, DOI 10.1142/9789814299428_0005.

[120] A. Holtzer, M. F. Holtzer, "Use of the van't Hoff relation in determination of the enthalpy of micelle formation", *The Journal of Physical Chemistry* **1974**, *78*, 1442, DOI 10.1021/j100607a026.

[121] W. Batsberg, S. Ndoni, C. Trandum, S. Hvidt, "Effects of Poloxamer Inhomogeneities on Micellization in Water", *Macromolecules* **2004**, *37*, 2965, DOI 10.1021/ma030567a.

[122] C. Jolicoeur, P. R. Philip, "Enthalpy–Entropy Compensation for Micellization and Other Hydrophobic Interactions in Aqueous Solutions", *Canadian Journal of Chemistry* **1974**, *52*, 1834, DOI 10.1139/v74-262.

[123] A. Pan, T. Biswas, A. K. Rakshit, S. P. Moulik, "Enthalpy-Entropy Compensation (EEC) Effect: A Revisit", *Journal of Physical Chemistry B* **2015**, *119*, 15876, DOI 10.1021/acs.jpcb.5b09925.

[124] H. W. Tsui, Y. H. Hsu, J. H. Wang, L. J. Chen, "Novel behavior of heat of micellization of Pluronics F68 and F88 in aqueous solutions", *Langmuir* **2008**, *24*, 13858, DOI 10.1021/la803272y.

[125] T. Kato, N. Taguchi, T. Terao, T. Seimiya, "Structure of Networks Formed in Concentrated Solutions of Nonionic Surfactant Studied by the Pulsed-Gradient Spin-Echo Method", *Langmuir* **1995**, *11*, 4661, DOI 10.1021/la00012a014.

[126] S. Radiman, C. Toprakcioglu, T. McLeish, "Rheological study of ternary cubic phases", *Langmuir* **1994**, *10*, 61, DOI 10.1021/la00013a009.

[127] G. T. Dimitrova, T. F. Tadros, P. F. Luckham, "Investigations of the Phase Changes of Nonionic Surfactants Using Microscopy, Differential Scanning Calorimetry, and Rheology. 1. Synperonic A7, a C13/C15 Alcohol with 7 mol of Ethylene Oxide", *Langmuir* **1995**, *11*, 1101, DOI 10.1021/la00004a012.

[128] A. Klaus, G. J. Tiddy, D. Touraud, A. Schramm, G. Stühler, W. Kunz, "Phase behavior of an extended surfactant in water and a detailed characterization of the concentrated phases", *Langmuir* **2010**, *26*, 16871, DOI 10.1021/la103037q.

[129] J. A. Finnigan, D. J. Jacobs, "Light scattering by ellipsoidal particles in solution", *Journal of Physics D: Applied Physics* **1971**, *4*, 72, DOI 10.1088/0022-3727/4/1/310.

[130] J. S. Pedersen, M. C. Gerstenberg, "Communications to the Editor", *Macromolecules* **1996**, *29*, 1363, DOI 0024-929719612229-1363$12.00/00.

[131] J. S. Pedersen, "conference papers Form factors of block copolymer micelles with spherical , ellipsoidal and cylindrical", **2000**, 637, DOI 10.1107/S0021889899012248.

[132] J. S. Pedersen, C. Svaneborg, "Scattering from block copolymer micelles", *Current Opinion in Colloid & Interface Science* **2002**, *7*, 158, DOI 1359-0294?02.

[133] B. Hammouda, M. H. Kim, "The empirical core-chain model", *Journal of Molecular Liquids* **2017**, *247*, 434, DOI 10.1016/j.molliq.2017.09.114.

[134] B. Cichocki, B. U. Felderhof, "Diffusion of Brownian particles with hydrodynamic interaction and hard core repulsion", *The Journal of Chemical Physics* **1991**, *94*, 556, DOI 10.1063/1.460319.

[135] G. André, F. Gérard, *Small-angle scattering of X-rays*, (Ed.: M. Goeppert Mayer), John Wiley & Sons, New York, **1955**, pp. 1–276, DOI 10.1016/0146-3535(89)90023-3.

[136] A. V. Feoktystov, H. Frielinghaus, Z. Di, S. Jaksch, V. Pipich, M.-S. Appavou, E. Babcock, R. Hanslik, R. Engels, G. Kemmerling, H. Kleines, A. Ioffe, D. Richter, T. Brückel, "KWS-1 high-resolution small-angle neutron scattering instrument at JCNS: current state", *Journal of Applied Crystallography* **2015**, *48*, 61, DOI 10.1107/S1600576714025977.

[137] S.-H. Chen, T.-L. Lin in *Meth. Exp. Phys*, *Vol. 23B*, **1987**, 489, DOI 10.1016/S0076-695X(08)60576-1.

[138] N. F. Carnahan, K. E. Starling, "Equation of State for Nonattracting Rigid Spheres", *The Journal of Chemical Physics* **1969**, *51*, 635, DOI 10.1063/1.1672048.

[139] A. M. Cazabat, D. Langevin, "Diffusion of interacting particles: Light scattering study of microemulsions", *The Journal of Chemical Physics* **1981**, *74*, 3148, DOI 10.1063/1.441525.

[140] M. Kotlarchyk, S. H. Chen, "Analysis of small angle neutron scattering spectra from polydisperse interacting colloids", *The Journal of Chemical Physics* **1983**, *79*, 2461, DOI 10.1063/1.446055.

[141] R. J. Baxter, "Percus–Yevick Equation for Hard Spheres with Surface Adhesion", *The Journal of Chemical Physics* **1968**, *49*, 2770, DOI 10.1063/1.1670482.

[142] J. S. Pedersen, "Structure factors effects in small-angle scattering from block copolymer micelles and star polymers", *Journal of Chemical Physics* **2001**, *114*, 2839, DOI 10.1063/1.1339221.

[143] S. V. Menon, C. Manohar, K. Srinivasa Rao, "A new interpretation of the sticky hard sphere model", *The Journal of Chemical Physics* **1991**, *95*, 9186, DOI 10.1063/1.461199.

[144] H. Kaya, "Scattering from cylinders with globular end-caps", *Journal of Applied Crystallography* **2004**, *37*, 223, DOI 10.1107/S0021889804000020.

[145] H. Kaya, N. R. De Souza, "Erratum: Scattering from capped cylinders. Addendum (Journal of Applied Crystallography (2004) 37 (223-230))", *Journal of Applied Crystallography* **2004**, *37*, 508, DOI 10.1107/S0021889804005709.

[146] Sasview - Capped cylinder model.

[147] V. J. Spiering, A. Prause, L. Noirez, M.-S. Appavou, M. Gradzielski, "Structural Characterization of Nonionic Surfactant Micelles with CO_2/Ethylene Oxide Head Groups and their Temperature Dependence", *Langmuir* **2021**, DOI 10.1021/acs.langmuir.1c01737.

[148] P. Becher, "Nonionic surface-active compounds IV. Micelle formation by polyoxyethylene alkanols and alkyl phenols in aqueous solution", *Journal of Colloid Science* **1961**, *16*, 49, DOI https://doi.org/10.1016/0095-8522(61)90061-7.

[149] R. Kjellander, E. Florin, "Water structure and changes in thermal stability of the system poly(ethylene oxide)-water", *J.Chem. Soc* **1981**, *Faraday Tr*, 2053.

[150] P. G. Nilsson, H. Wennerström, B. Lindman, "Structure of micellar solutions of nonionic surfactants. Nuclear magnetic resonance self-diffusion and proton relaxation studies of poly(ethylene oxide) alkyl ethers", *Journal of Physical Chemistry* **1983**, *87*, 1377, DOI 10.1021/j100231a021.

[151] H. Hoffmann, W. Ulbricht, "Surfactant gels", *Current Opinion in Colloid & Interface Science* **1996**, *1*, 726, DOI 10.1016/s1359-0294(96)80074-4.

[152] P. Sakya, J. M. Seddon, R. H. Templer, R. J. Mirkin, G. J. T. Tiddy, "Micellar Cubic Phases and Their Structural Relationships: The Nonionic Surfactant System $C_{12}EO_{12}$ /Water", *Langmuir* **1997**, *13*, 3706, DOI 10.1021/la9701844.

[153] M. Gradzielski, H. Hoffmann, G. Oetter, "Ringing gels: Their structure and macroscopic properties", *Colloid & Polymer Science* **1990**, *268*, 167, DOI 10.1007/BF01513196.

[154] M. Gradzielski, H. Hoffmann, J.-C. Panitz, A. Wokaun, "Investigations on L2 Phase and Cubic Phase in the System AOT/1 -Octanol/Water", *Journal of Colloid and Interface Science* **1995**, *169*, 103, DOI 10.1006/jcis.1995.1011.

[155] C. Rodríguez-Abreu, M. García-Roman, H. Kunieda, "Rheology and Dynamics of Micellar Cubic Phases and Related Emulsions", *Langmuir* **2004**, *20*, 5235, DOI 10.1021/la0498962.

[156] K. Fontell, "Some aspects on the cubic phases in surfactant and surfactant-like lipid systems", *Advances in Colloid and Interface Science* **1992**, *41*, 127, DOI 10.1016/0001-8686(92)80010-U.

[157] K. Mortensen, Y. Talmon, "Cryo-TEM and SANS Microstructural Study of Pluronic Polymer Solutions", *Macromolecules* **1995**, *28*, 8829, DOI 10.1021/ma00130a016.

[158] K. L. Walther, M. Gradzielski, H. Hoffmann, A. Wokaun, G. Fleischer, "Mobilities in cubic liquid crystals ("ringing gels") determined by NMR self-diffusion measurements", *Journal of Colloid and Interface Science* **1992**, *153*, 272, DOI 10.1016/0021-9797(92)90318-G.

[159] K. Holmberg, S. T. Hyde in *Handbook of Applied Surface and Colloid Chemistry*, *Vol. 2*, John Wiley & Sons, Ltd, **2001**, Chapter 16.

[160] P. Alexandridis, U. Olsson, B. Lindman, "A Record Nine Different Phases (Four Cubic, Two Hexagonal, and One Lamellar Lyotropic Liquid Crystalline and Two Micellar Solutions) in a Ternary Isothermal System of an Amphiphilic Block Copolymer and Selective Solvents (Water and Oil)", *Langmuir* **2002**, *14*, 2627, DOI 10.1021/la971117c.

[161] R. Zana, C. Weill, "Effect of temperature on the aggregation behaviour of nonionic surfactants in aqueous solutions", *Journal de Physique Lettres* **1985**, *46*, 953, DOI 10.1051/jphyslet:019850046020095300.

[162] Y. YU, J. ZHAO, A. E. Bayly, "Development of Surfactants and Builders in Detergent Formulations", *Chinese Journal of Chemical Engineering* **2008**, *16*, 517, DOI 10.1016/S1004-9541(08)60115-9.

[163] A. Bernheim-Groswasser, E. Wachtel, Y. Talmon, "Micellar Growth, Network Formation, and Criticality in Aqueous Solutions of the Nonionic Surfactant $C_{12}E_5$", *Langmuir* **2000**, *16*, 4131, DOI 10.1021/la991231q.

[164] D. Danino, Y. Talmon, R. Zana, "Aggregation and microstructure in aqueous solutions of the nonionic surfactant $C_{12}E_8$", *Journal of Colloid and Interface Science* **1997**, *186*, 170, DOI 10.1006/jcis.1996.4599.

[165] B. Lindman, H. Wennerström, "Nonionic micelles grow with increasing temperature", *Journal of Physical Chemistry* **1991**, *95*, 6053, DOI 10.1021/j100168a063.

[166] B. Lindman, B. Medronho, G. Karlström, "Clouding of nonionic surfactants", *Current Opinion in Colloid and Interface Science* **2016**, *22*, 23, DOI 10.1016/j.cocis.2016.01.005.

[167] M. F. Cox, "Effect of Alkyl Carbon Chain Length and Ethylene Oxide Content on the Performance of Linear Alcohol Ethoxylates 1", *Journal of the American Oil Chemists Society* **1989**, *66*, 367.

[168] Y. Kawabata, K. Wada, M. Nakatani, S. Yamada, S. Onoue, "Formulation design for poorly water-soluble drugs based on biopharmaceutics classification system : Basic approaches and practical applications", *International Journal of Pharmaceutics* **2011**, *420*, 1, DOI 10.1016/j.ijpharm.2011.08.032.

[169] H. Chen, C. Khemtong, X. Yang, X. Chang, J. Gao, "Nanonization strategies for poorly water-soluble drugs", *Drug Discovery Today* **2011**, *16*, 354, DOI 10.1016/j.drudis.2010.02.009.

[170] M. N. Ravi Kumar, "Nano and microparticles as controlled drug delivery devices.", *Journal of pharmacy & pharmaceutical sciences : a publication of the Canadian Society for Pharmaceutical Sciences Société canadienne des sciences pharmaceutiques* **2000**, *3*, 234.

[171] G. Gaucher, M. H. Dufresne, V. P. Sant, N. Kang, D. Maysinger, J. C. Leroux, "Block copolymer micelles: Preparation, characterization and application in drug delivery", *Journal of Controlled Release* **2005**, *109*, 169, DOI 10.1016/j.jconrel.2005.09.034.

[172] G. Gaucher, P. Satturwar, M.-C. Jones, A. Furtos, J.-C. Leroux, "Polymeric micelles for oral drug delivery", *European Journal of Pharmaceutics and Biopharmaceutics* **2010**, *76*, 147, DOI 10.1016/j.ejpb.2010.06.007.

[173] G. S. Kwon, K. Kataoka, "Block copolymer micelles as long-circulating drug vehicles", *Advanced Drug Delivery Reviews* **1995**, *16*, 295, DOI 10.1016/0169-409X(95)00031-2.

[174] V. P. Torchilin, "Structure and design of polymeric surfactant-based drug delivery systems", *Journal of Controlled Release* **2001**, *73*, 137, DOI 10.1016/S0168-3659(01)00299-1.

[175] Z. Vinarov, V. Katev, D. Radeva, S. Tcholakova, N. D. Denkov, "Micellar solubilization of poorly water-soluble drugs: effect of surfactant and solubilizate molecular structure", *Drug Development and Industrial Pharmacy* **2018**, *44*, 677, DOI 10.1080/03639045.2017.1408642.

[176] C. d. O. Rangel-Yagui, A. Pessoa, L. C. Tavares, "Micellar solubilization of drugs", *Journal of Pharmacy and Pharmaceutical Sciences* **2005**, *8*, 147.

[177] P. Singla, S. Chabba, R. K. Mahajan, "A systematic physicochemical investigation on solubilization and in vitro release of poorly water soluble oxcarbazepine drug in pluronic micelles", *Colloids and Surfaces A: Physicochemical and Engineering Aspects* **2016**, *504*, 479, DOI 10.1016/j.colsurfa.2016.05.043.

[178] P. Singla, O. Singh, S. Sharma, K. Betlem, V. K. Aswal, M. Peeters, R. K. Mahajan, "Temperature-Dependent Solubilization of the Hydrophobic Antiepileptic Drug Lamotrigine in Different Pluronic Micelles - A Spectroscopic, Heat Transfer Method, Small-Angle Neutron Scattering, Dynamic Light Scattering, and in Vitro Release Study", *ACS Omega* **2019**, *4*, 11251, DOI 10.1021/acsomega.9b00939.

[179] A. Raval, S. A. Pillai, A. Bahadur, P. Bahadur, "Systematic characterization of Pluronic® micelles and their application for solubilization and in vitro release of some hydrophobic anticancer drugs", *Journal of Molecular Liquids* **2017**, *230*, 473, DOI 10.1016/j.molliq.2017.01.065.

[180] V. Nguyen-Kim, S. Prévost, K. Seidel, W. Maier, A. K. Marguerre, G. Oetter, T. Tadros, M. Gradzielski, "Solubilization of active ingredients of different polarity in Pluronic® micellar solutions - Correlations between solubilizate polarity and solubilization site", *Journal of Colloid and Interface Science* **2016**, *477*, 94, DOI 10.1016/j.jcis.2016.05.017.

[181] B. Bahloul, M. A. Lassoued, S. Sfar, "A novel approach for the development and optimization of self emulsifying drug delivery system using HLB and response surface methodology: Application to fenofibrate encapsulation", *International Journal of Pharmaceutics* **2014**, *466*, 341, DOI 10.1016/j.ijpharm.2014.03.040.

[182] G. G. Kim, B. K. Poudel, N. Marasini, D. W. Lee, T. T. Hiep, K. Y. Yang, J. O. Kim, C. S. Yong, H. G. Choi, "Enhancement of oral bioavailability of fenofibrate by solid self-microemulsifying drug delivery systems", *Drug Development and Industrial Pharmacy* **2013**, *39*, 1431, DOI 10.3109/03639045.2012.719903.

[183] H. Lee, S.-A. Park, H. Sah, "Surfactant effects upon dissolution patterns of carbamazepine immediate release tablet", *Archives of Pharmacal Research* **2005**, *28*, 120, DOI 10.1007/BF02975147.

[184] M. Maswal, A. H. Pandith, N. Islam, A. A. Dar, "Co-solubilization of the hydrophobic drugs carbamazepine and nifedipine in aqueous nonionic surfactant media", *Journal of Solution Chemistry* **2013**, *42*, 1374, DOI 10.1007/s10953-013-0036-4.

[185] B. Yang, L. Wu, J. Ke, L. Zhou, M. Chen, S. Li, X. Feng, "Effects of Polymer/Surfactant as Carriers on the Solubility and Dissolution of Fenofibrate Solid Dispersion", *AAPS PharmSciTech* **2019**, *20*, 1, DOI 10.1208/s12249-018-1273-z.

[186] R. Kumar, "Solubility and Bioavailability of Fenofibrate Nanoformulations", *ChemistrySelect* **2020**, *5*, 1478, DOI 10.1002/slct.201903647.

[187] Y. Kadam, U. Yerramilli, A. Bahadur, "Solubilization of poorly water-soluble drug carbamezapine in Pluronic® micelles: Effect of molecular characteristics, temperature and added salt on the solubilizing capacity", *Colloids and Surfaces B: Biointerfaces* **2009**, *72*, 141, DOI 10.1016/j.colsurfb.2009.03.027.

[188] S. Jain, S. Pandey, P. Sola, H. Pathan, R. Patil, D. Ray, V. K. Aswal, P. Bahadur, S. Tiwari, "Solubilization of Carbamazepine in TPGS Micelles: Effect of Temperature and Electrolyte Addition", *AAPS PharmSciTech* **2019**, *20*, 1, DOI 10.1208/s12249-019-1412-1.

[189] L. Fan, M. Degen, N. Grupido, S. Bendle, P. Pennartz, "Effects of molecular weight, temperature and salt on the self assembly of triblock copolymer solutions", *Materials Science and Engineering A* **2010**, *528*, 127, DOI 10.1016/j.msea.2010.08.060.

[190] P. Chen, K. K. Mohanty, "Surfactant-enhanced oil recovery from fractured oil-wet carbonates: Effects of low IFT and wettability alteration", *Proceedings - SPE International Symposium on Oilfield Chemistry* **2015**, *2*, 1225, DOI 10.2118/173797-ms.

[191] P. Jiang, N. Li, J. Ge, G. Zhang, Y. Wang, L. Chen, L. Zhang, "Efficiency of a sulfobetaine-type surfactant on lowering IFT at crude oil-formation water interface", *Colloids and Surfaces A: Physicochemical and Engineering Aspects* **2014**, *443*, 141, DOI 10.1016/j.colsurfa.2013.10.061.

[192] X. Liu, Y. Zhao, Q. Li, T. Jiao, J. Niu, "Surface and interfacial tension of nonylphenol polyethylene oxides sulfonate", *Journal of Molecular Liquids* **2016**, *216*, 185, DOI 10.1016/j.molliq.2016.01.009.

[193] Z. Liu, L. Zhang, X. Cao, X. Song, Z. Jin, L. Zhang, S. Zhao, "Effect of electrolytes on interfacial tensions of alkyl ether carboxylate solutions", *Energy and Fuels* **2013**, *27*, 3122, DOI 10.1021/ef400458q.

[194] M. J. Rosen, H. Wang, P. Shen, Y. Zhu, "Ultralow Interfacial Tension for Enhanced Oil Recovery at Very Low Surfactant Concentrations", *Langmuir* **2005**, *21*, 3749, DOI doi.org/10.1021/la0400959.

[195] C. C. Lai, K. M. Chen, "Preparation and surface activity of polyoxyethylene-carboxylated modified Gemini surfactants", *Colloids and Surfaces A: Physicochemical and Engineering Aspects* **2008**, *320*, 6, DOI 10.1016/j.colsurfa.2007.12.056.

[196] A. R. Rahate, J. M. Nagarkar, "Emulsification of vegetable oils using a blend of nonionic surfactants for cosmetic applications", *Journal of Dispersion Science and Technology* **2007**, *28*, 1077, DOI 10.1080/01932690701524802.

[197] M. Hakemi-Vala, H. Rafati, A. Aliahmadi, A. Ardalan, *Nanoemulsions: A Novel Antimicrobial Delivery System*, Elsevier Inc., **2017**, pp. 245–266, DOI 10.1016/B978-0-323-52727-9.00013-3.

[198] P. G. De Gennes, C. Taupin, "Microemulsions and the flexibility of oil/water interfaces", *The Journal of Physical Chemistry* **1982**, *86*, 2294, DOI 10.1021/j100210a011.

[199] M. Gradzielski, D. Langevin, B. Farago, "Experimental investigation of the structure of nonionic microemulsions and their relation to the bending elasticity of the amphiphilic film", *Physical Review E* **1996**, *53*, 3900, DOI 10.1103/PhysRevE.53.3900.

[200] H. Matsubara, M. Aratono, "Unique interfacial phenomena on macroscopic and colloidal scales induced by 2D phase transitions", *Langmuir* **2018**, DOI 10.1021/acs.langmuir.8b01203.

[201] Y. Tokiwa, H. Sakamoto, T. Takiue, M. Aratono, H. Matsubara, C. D. Bain, "Effect of Surface Freezing on Stability of Oil-in-Water Emulsions", *Langmuir* **2018**, *34*, 6205, DOI 10.1021/acs.langmuir.8b01088.

[202] Y. Tokiwa, H. Sakamoto, T. Takiue, M. Aratono, H. Matsubara, "Effect of alkane chain length and counterion on the freezing transition of cationic surfactant adsorbed film at alkane mixture - water interfaces", *Journal of Physical Chemistry B* **2015**, *119*, 6235, DOI 10.1021/acs.jpcb.5b02448.

[203] J. W. Jennings, N. R. Pallas, "An Efficient Method for the Determination of Interfacial Tensions from Drop Profiles", *Langmuir* **1988**, *4*, 959, DOI 10.1021/la00082a030.

[204] R. A. Orwoll, P. J. Flory, "Equation-of-State Parameters for Normal Alkanes. Correlation with Chain Length", *Journal of the American Chemical Society* **1967**, *89*, 6814, DOI 10.1021/ja01002a002.

[205] M. J. Rosen, S. Aronson, "Standard free energies of adsorption of surfactants at the aqueous solution/air interface from surface tension data in the vicinity of the critical micelle concentration", *Colloids and Surfaces* **1981**, *3*, 201, DOI 10.1016/0166-6622(81)80037-6.

[206] S. Zeppieri, J. Rodríguez, A. L. López De Ramos, "Interfacial tension of alkane + water systems", *Journal of Chemical and Engineering Data* **2001**, *46*, 1086, DOI 10.1021/je000245r.

[207] R. Aveyard, D. A. Haydon, "Thermodynamic properties of aliphatic hydrocarbon/water interfaces", *Transactions of the Faraday Society* **1965**, *61*, 2255, DOI 10.1039/tf9656102255.

[208] M. J. Rosen, "Effect of the Nonaqueous Phase on Interfacial Properties of Surfactants. 2. Individual and Mixed Nonionic Surfactants in Hydrocarbon/Water Systems", **1991**, 2630, DOI 10.1021/la00059a039.

[209] L. Peltonen, J. Hirvonen, J. Yliruusi, "The behavior of sorbitan surfactants at the water-oil interface: Straight-chained hydrocarbons from pentane to dodecane as an oil phase", *Journal of Colloid and Interface Science* **2001**, *240*, 272, DOI 10.1006/jcis.2001.7612.

Chapter 10

Appendix

A. List of Abbreviations

A.1. Chemicals

MeOH	:	methanol
EO	:	ethylene oxide
PO	:	propylene oxide
CO_2	:	carbon dioxide
PL	:	propiol lactone
H_2O	:	water
D_2O	:	deuterated water
DMC	:	Double metal cyanide
DEC	:	diethyl carbonate

A.2. Symbols

α	:	cone angle
A	:	interaction parameter
a_0	:	head group area
B	:	water content
c	:	concentration
c_g	:	mass concentration
cmc	:	critical micelle concentration
ρ	:	density
D_0	:	diffusion coefficient
D_{col}	:	collective diffusion coefficient

ET	:	end of transition
η	:	viscosity
ε_0	:	permittivity of vacuum
ε_r	:	relative permittivity
F	:	shear force
ΔG_{mic}	:	Gibbs energy of micellization
$\dot{\gamma}$	:	shear rate
Γ	:	decay time
γ	:	interfacial tension
Γ	:	surface excess concentration
G”	:	loss modulus (viscous modulus)
G	:	shear modulus
G’	:	storage modulus (elastic modulus)
G^*	:	complex shear modulus
$g^1(\tau)$	:	field-auto-correlation
$g^2(\tau)$	:	intensity-auto-correlation
ΔH	:	enthalpy
ΔH_{mic}	:	enthalpy of micellization
H	:	hydration number
h	:	Planck´s constant
I(0)	:	forward scattering intensity
$I(0)_{corr}$	:	corrected static intensity
I(q)	:	scattering intensity
k_B	:	Boltzmann constant
K_L	:	optical constant
λ	:	wavelength
l_c	:	length of alkyl chain
M_w	:	molecular weight
ν	:	velocity
^1N	:	particle number density
N_{agg}	:	aggregation number
(dn/dc)	:	refractive index increment
n	:	refractive index
N_{Av}	:	Avogadro constant
P(q)	:	form factor
P	:	packing parameter
PDI	:	polydispersity index

q	:	head flow
$\vec{q}$	:	scattering vector
ϕ	:	volume fraction
ϕ_{hs}	:	hard sphere volume fraction
R	:	ideal gas constant
R	:	radius
R_{hs}	:	hard sphere radius
R_g	:	radius of gyration
R_h	:	hydrodynamic radius
ΔS_{mic}	:	entropy of micellization
σ	:	surface tension
σ_0	:	surface tension of water
S_{tot}	:	solubilized molecules
S_W	:	water solubility
S(0)	:	static structure factor
S(q)	:	structure factor
SLD	:	scattering length density
ΔSLD	:	contrast of scattering length density
ST	:	start of transition
T	:	temperature
t	:	time
T_K	:	Krafft temperature
τ	:	shear stress
τ_K	:	decay time
Θ	:	scattering angle
χ	:	solubilization capacity
χ_{cmc}	:	mole fraction of the cmc
V	:	volume
V_p	:	particle volume
$w_{(ring)}$	:	weight of ring

A.3. other Abbreviations

bkg	:	background
BMBF	:	Federal Ministry of Education and Research
CP	:	Cloud Point
CS	:	Carnahan Starling

DLS	:	dynamic light scattering
HLB	:	hydrophilic-lipophilic-balance
IFT	:	interfacial tension
ITC	:	isothermal titration calorimetry
LC	:	liquid crystal
LLB	:	Laboratoire Léon Brillouin
MLZ	:	Heinz Maier-Leibnitz Zentrum
PIT	:	phase inversion temperature
SANS	:	small angle neutron scattering
SFT	:	surface tension
SLS	:	static light scattering

B. List of used Programs

Blender 3.1	:	visualization and illustration
ChemDraw 17	:	chemical structures
DLS SLS evaluator vers. 1.1.4 beta	:	light scattering analysis
Excel 365	:	data summary and analysis
Inkscape 0.92.4	:	Graphic illustration
NanoAnalyzer	:	ITC data analysis
Origin 2020	:	Data visualization; Data analysis
SASFit 0.94.11	:	SANS Data analysis
SASView 5.0.1	:	SANS Data analysis
TopSpin 3.5	:	NMR data analysis

C. Appendix Chapter 4

C.1. Surface tension data

The surface tension was measured over an extended period. After a sufficiently long waiting time (typically 15 mins), the surface tension reached an equilibrium state and remained constant thereafter. These data of the static regime (approximately > 10) were averaged to determine the static surface tension for the given concentration. The surface tension curves were fitted with the Szyszkowski isotherm (Eq. 4.1).

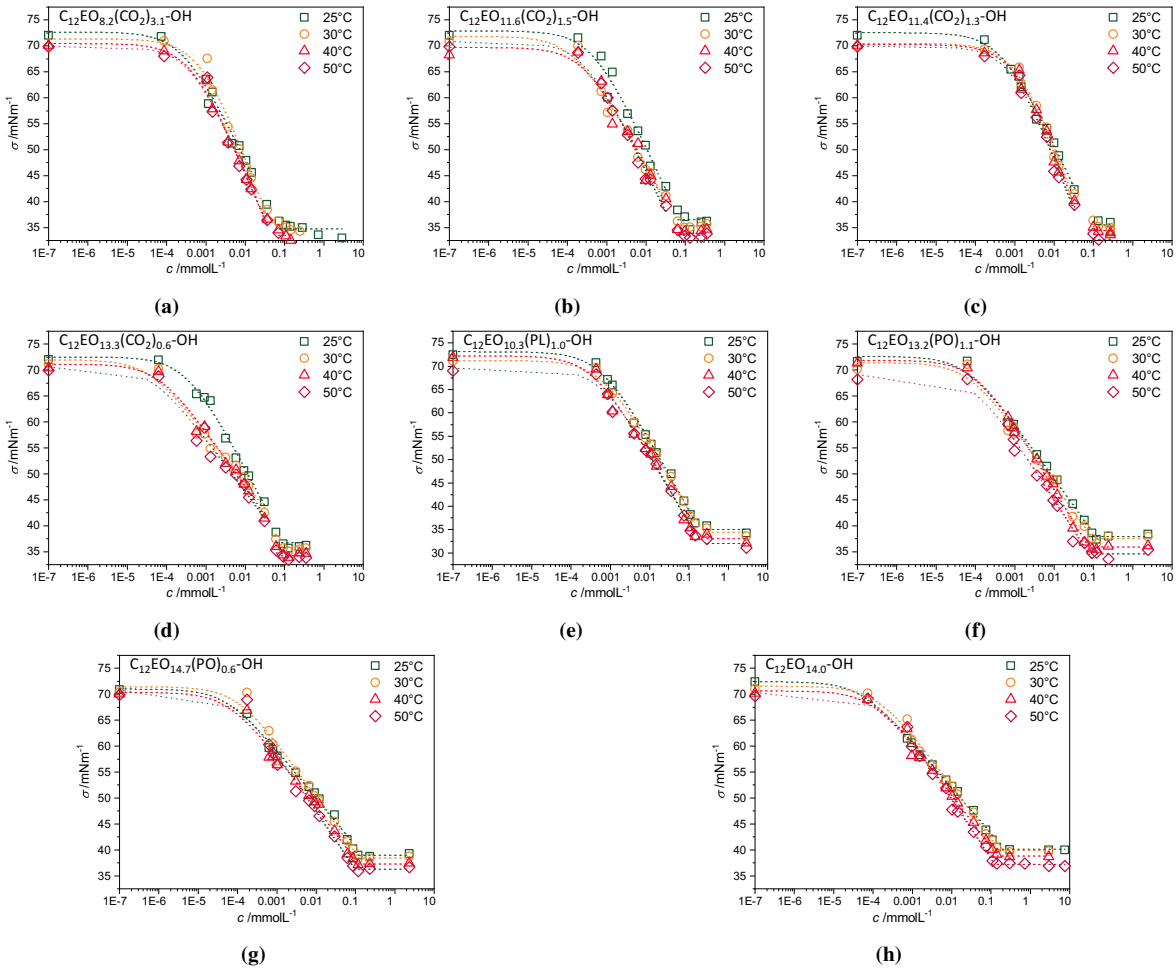

Figure 10.1: Temperature depending surface tension measurement of all surfactants at 25, 30, 40 and 50 °C. All data were fitted with the Szyszkowski equation.

Table 10.5: Summary of the surface tension measurements: critical micelle concentration cmc, surface tension σ_{cmc} at the cmc, head group area a_0, and Gibbs free energy of micellization ΔG_{mic} for all surfactants at 25, 30, 40 and 50 °C.

T /K	cmc /mg/L	cmc /mmol/L	σ_{cmc} /mN/m	Γ /mol/m^2	a_0 /Å^2	M_n /g/mol	ΔG_{mic} /kJ/mol
$C_{12}EO_{8.2}(CO_2)_{3.1}-OH$							
298.15	36.4	0.054	38.2	$3.88 \cdot 10^{-6}$	55	680	-34.3
303.15	26.2	0.039	36.9	$3.57 \cdot 10^{-6}$	53	680	-35.7
313.15	29.6	0.044	35.0	$3.01 \cdot 10^{-6}$	64	680	-36.6
323.15	32.6	0.048	34.3	$2.94 \cdot 10^{-6}$	68	680	-37.5

$C_{12}EO_{11.6}(CO_2)_{1.5}-OH$							
298.15	69.7	0.091	36.1	$2.90 \cdot 10^{-6}$	65	762	-33.0
303.15	70.3	0.092	34.9	$2.32 \cdot 10^{-6}$	80	762	-33.5
313.15	63.3	0.083	33.4	$2.45 \cdot 10^{-6}$	69	762	-34.9
323.15	58.8	0.077	33.2	$2.58 \cdot 10^{-6}$	74	762	-36.2
$C_{12}EO_{11.4}(CO_2)_{1.3}-OH$							
298.15	73.4	0.099	36.4	$2.83 \cdot 10^{-6}$	67	744	-32.8
303.15	49.7	0.067	35.4	$3.63 \cdot 10^{-6}$	55	744	-34.4
313.15	47.5	0.064	34.5	$3.55 \cdot 10^{-6}$	56	744	-35.6
323.15	53.2	0.071	32.7	$3.33 \cdot 10^{-6}$	58	744	-36.4
$C_{12}EO_{13.3}(CO_2)_{0.6}-OH$							
298.15	93.3	0.118	35.6	$2.55 \cdot 10^{-6}$	69	792	-32.4
303.15	73.1	0.092	35.4	$1.66 \cdot 10^{-6}$	69	792	-33.5
313.15	71.9	0.091	34.1	$1.63 \cdot 10^{-6}$	70	792	-34.7
323.15	72.7	0.092	33.4	$1.66 \cdot 10^{-6}$	72	792	-35.8
$C_{12}EO_{10.3}(PL)_{1.0}-OH$							
298.15	116.2	0.169	36.2	$2.44 \cdot 10^{-6}$	68	686	-31.5
303.15	122.8	0.179	35.9	$2.32 \cdot 10^{-6}$	71	686	-31.9
313.15	92.0	0.134	33.9	$2.65 \cdot 10^{-6}$	63	686	-33.7
323.15	93.7	0.137	33.8	$2.58 \cdot 10^{-6}$	64	686	-34.7
$C_{12}EO_{13.2}(PO)_{1.1}-OH$							
298.15	107.6	0.131	37.6	$1.76 \cdot 10^{-6}$	94	821	-32.1
303.15	92.6	0.113	37.1	$1.75 \cdot 10^{-6}$	95	821	-33.0
313.15	75.1	0.091	35.6	$1.97 \cdot 10^{-6}$	84	821	-34.7
323.15	80.6	0.098	34.1	$1.77 \cdot 10^{-6}$	94	821	-35.6
$C_{12}EO_{14.7}(PO)_{0.6}-OH$							
298.15	118.9	0.138	38.8	$1.77 \cdot 10^{-6}$	94	859	-32.0
303.15	112.1	0.131	38.3	$1.80 \cdot 10^{-6}$	92	859	-32.7
313.15	95.1	0.111	37.2	$1.81 \cdot 10^{-6}$	92	859	-34.2
323.15	89.1	0.104	36.0	$1.79 \cdot 10^{-6}$	93	859	-35.4
$C_{12}EO_{14.0}-OH$							
298.15	140.3	0.175	40.3	$1.55 \cdot 10^{-6}$	107	802	-31.4
303.15	123.3	0.154	40.1	$1.75 \cdot 10^{-6}$	103	802	-32.3
313.15	113.4	0.141	39.0	$1.67 \cdot 10^{-6}$	109	802	-33.5
323.15	88.2	0.110	37.5	$1.85 \cdot 10^{-6}$	97	802	-35.3

C.2. ITC Measurements

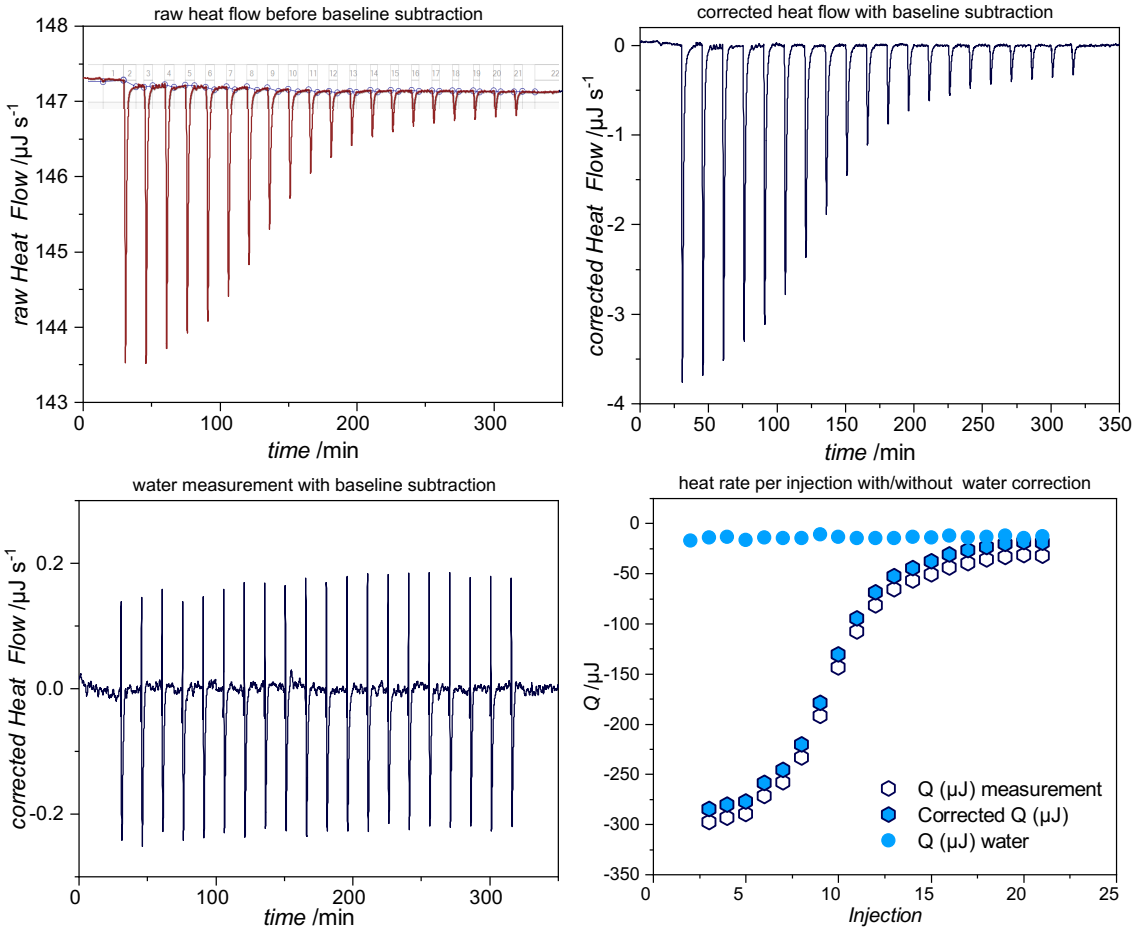

Figure 10.2: Overview of the evaluation of the ITC curves. Raw heat flow before (top left) and after (top right) baseline subtraction. Water-to-water measurement (bottom left) at the same temperature than the sample measurement. Comparison of the heat rate per injection of the sample measurement with and without water subtraction.

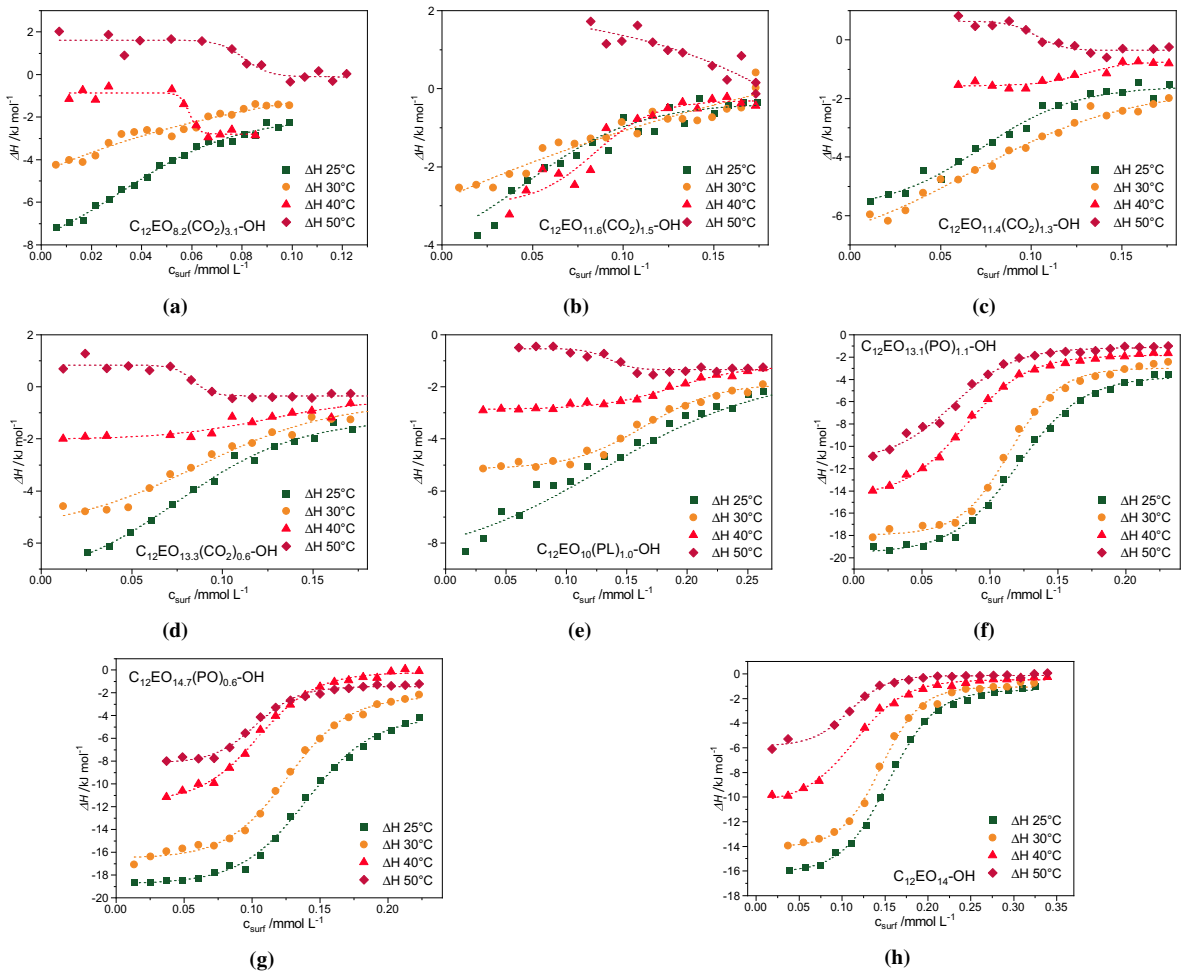

Figure 10.3: Temperature dependent ITC measurement of all surfactants at 25, 30, 40 and 50 °C.

Table 10.7: Summary of the ITC measurement data: critical micelle concentration cmc, ΔH_{mic}, ΔS_{mic}, and Gibbs free energy of micellization $\Delta G_{mic}$for all surfactants at 25, 30, 40 and 50 °C.

T /K	cmc / mmol/L	ΔH_{mic} / kJ/mol	χ_{cmc}	ΔG_{mic} / kJ/mol	$-T\Delta S_{mic}$ / kJ/mol	ΔS_{mic} / J/K mol
$C_{12}EO_{8.2}(CO_2)_{3.1}-OH$						
298.15	0.049	5.1	$8.83 \cdot 10^{-7}$	-34.6	-39.7	133.0
303.15	0.041	2.8	$7.39 \cdot 10^{-7}$	-35.6	-38.4	126.6
313.15	0.043	-0.4	$7.75 \cdot 10^{-7}$	-36.6	-36.2	115.7
323.15	0.057	-2.3	$1.02 \cdot 10^{-6}$	-37.1	-34.7	107.5
$C_{12}EO_{11.6}(CO_2)_{1.5}-OH$						
298.15	0.07	1.4	$1.27 \cdot 10^{-6}$	-33.7	-35.1	117.7
303.15	0.081	1.2	$1.46 \cdot 10^{-6}$	-33.9	-35.1	115.7
313.15	0.067	2.3	$1.21 \cdot 10^{-6}$	-35.5	-37.8	120.7
323.15	0.05	-3.2	$8.99 \cdot 10^{-7}$	-37.4	-34.2	105.8
$C_{12}EO_{11.4}(CO_2)_{1.3}-OH$						
298.15	0.094	5.8	$1.70 \cdot 10^{-6}$	-32.9	-38.7	129.9
303.15	0.071	4.1	$1.27 \cdot 10^{-6}$	-34.2	-38.4	126.5
313.15	0.098	0.8	$1.77 \cdot 10^{-6}$	-34.5	-35.3	112.7
323.15	0.092	-1.6	$1.65 \cdot 10^{-6}$	-35.8	-34.2	105.9

$C_{12}EO_{13.3}(CO_2)_{0.6}-OH$						
298.15	0.106	5.56	$1.91 \cdot 10^{-6}$	-32.6	-38.2	128.1
303.15	0.085	4.91	$1.53 \cdot 10^{-6}$	-33.7	-38.7	127.5
313.15	0.123	1.15	$2.21 \cdot 10^{-6}$	-33.9	-35.1	111.9
323.15	0.074	-1.29	$1.34 \cdot 10^{-6}$	-36.3	-35.0	108.4
$C_{12}EO_{10.3}(PL)_{1.0}-OH$						
298.15	0.13	7.3	$2.34 \cdot 10^{-6}$	-32.1	-39.4	132.3
303.15	0.165	3.3	$2.96 \cdot 10^{-6}$	-32.1	-35.4	116.7
313.15	0.139	1.7	$3.39 \cdot 10^{-6}$	-32.8	-34.5	110.1
323.15	0.128	-0.8	$2.30 \cdot 10^{-6}$	-34.9	-34.1	105.4
$C_{12}EO_{13.2}(PO)_{1.1}-OH$						
298.15	0.121	15.8	$2.17 \cdot 10^{-6}$	-32.3	-48.1	161.4
303.15	0.115	15.0	$2.06 \cdot 10^{-6}$	-33.0	-48.0	158.3
313.15	0.081	12.7	$1.47 \cdot 10^{-6}$	-35.0	-47.7	152.3
323.15	0.077	10.2	$1.39 \cdot 10^{-6}$	-36.2	-46.5	144.0
$C_{12}EO_{14.7}(PO)_{0.6}-OH$						
298.15	0.14	14.7	$2.52 \cdot 10^{-6}$	-32.0	-46.6	156.4
303.15	0.126	14.2	$2.27 \cdot 10^{-6}$	-32.8	-47.0	154.9
313.15	0.104	11.3	$1.88 \cdot 10^{-6}$	-34.3	-45.6	145.8
323.15	0.103	6.7	$1.85 \cdot 10^{-6}$	-35.5	-42.2	130.6
$C_{12}EO_{14.0}-OH$						
298.15	0.154	13.7	$2.77 \cdot 10^{-6}$	-31.7	-45.4	152.3
303.15	0.146	12.1	$2.63 \cdot 10^{-6}$	-32.4	-44.5	146.8
313.15	0.115	9.4	$2.07 \cdot 10^{-6}$	-34.1	-43.5	138.9
323.15	0.108	5.7	$1.95 \cdot 10^{-6}$	-35.3	-41.1	127.1

D. Appendix Chapter 5

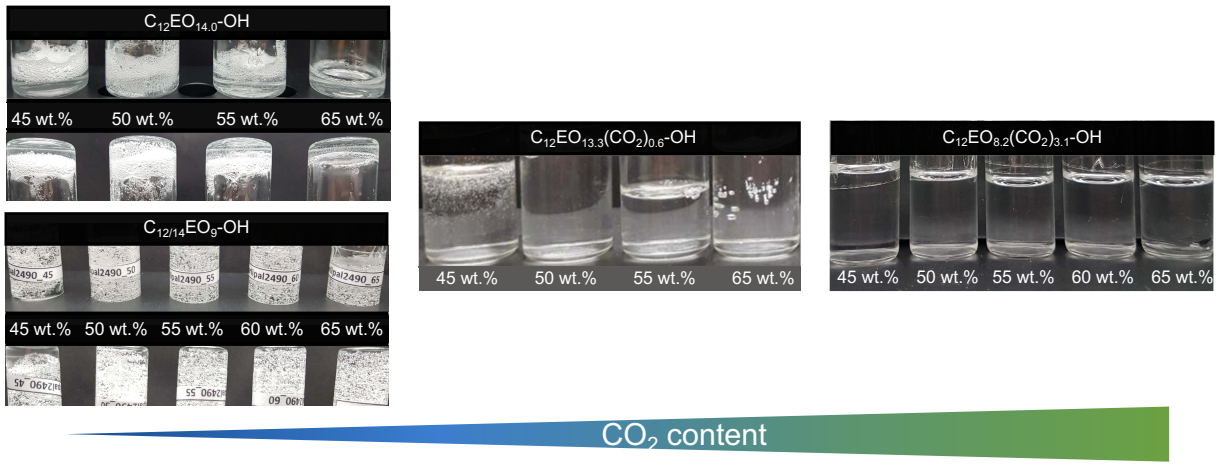

Figure 10.4: Photographs of surfactant samples of $C_{12}EO_{8.2}(CO_2)_{3.1}-OH$, $C_{12}EO_{13.3}(CO_2)_{0.6}-OH$ and the reference sample $C_{12}EO_{14.0}-OH$ and C12/14EO9-OH in the concentration range from 45 to 65 wt% at 25°C, 24 h after preparation.

D.1. Polarization Microscopy

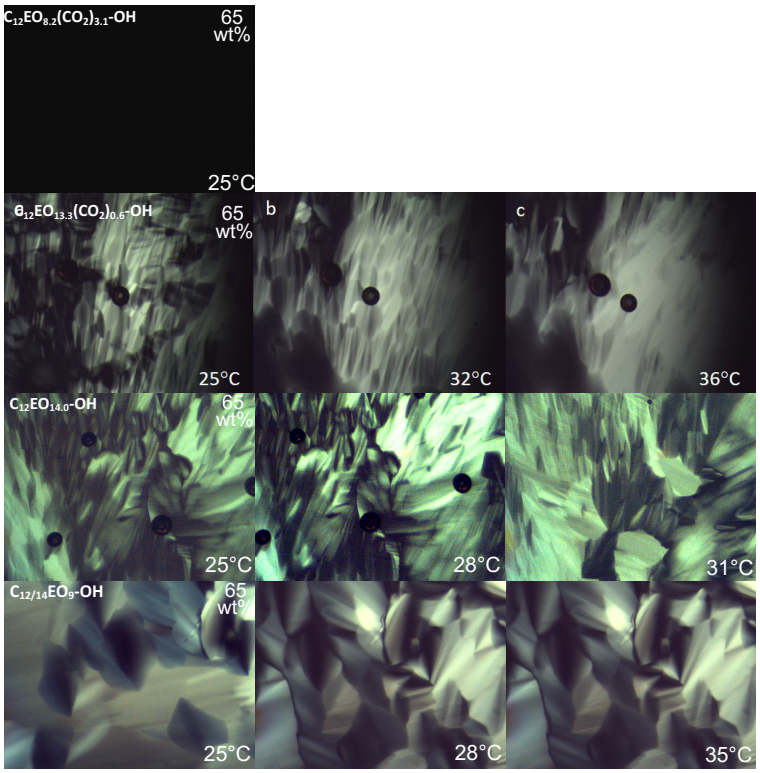

Figure 10.5: Photos from polarization microscopy: comparison of the CO_2 containing surfactant with the highest (3.1 units) and the lowest CO_2 content (0.6 units) in comparison of the reference surfactant $C_{12}EO_{14.0}-OH$ at 65 wt%.

D.2. Light Scattering

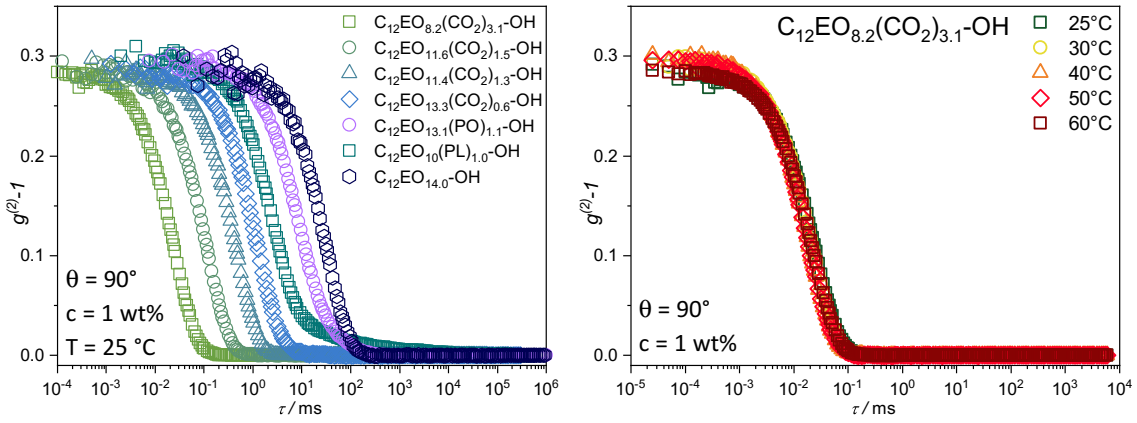

(a) **(b)**

Figure 10.6: Autocorrelation function of dynamic light scattering measurements. (a) shows all correlation functions from all surfactants at 1 wt% and the reference surfactants at 25 °C at an angle of 90°. (b) Shows the correlation function of the surfactants $C_{12}EO_{8.2}(CO_2)_{3.1}-OH$ at 1 wt% at an angle of 90° for different temperatures.

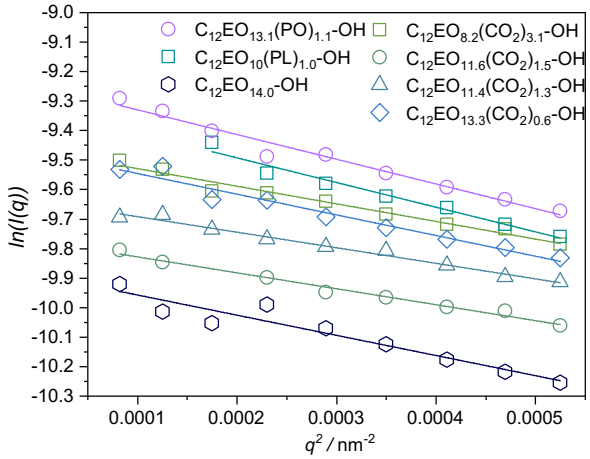

Figure 10.7: Guinier Plot of the light scattering data of all surfactants. The resulting intercept of the linear fit represent the static scattering I(0) which is corrected by the Carnahan Starling structure factor and summarized in the table.

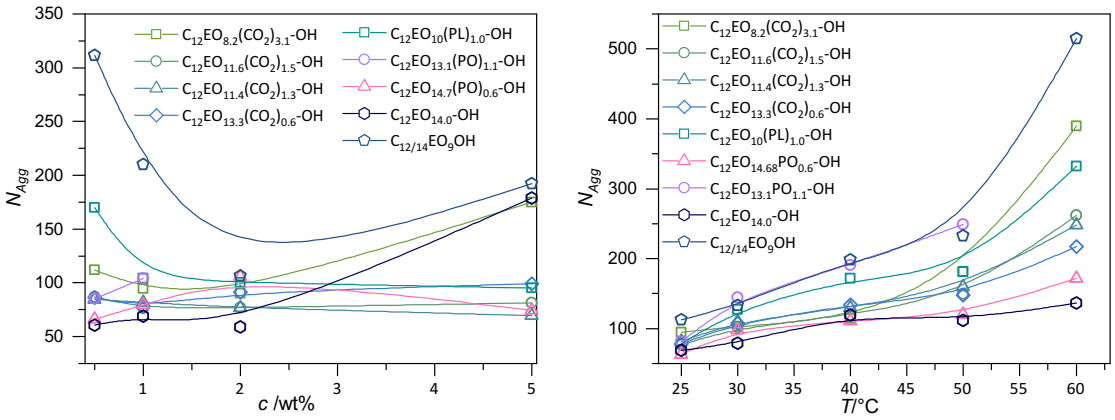

(a) (b)

Figure 10.8: Aggregation number of the aggregates out of SLS measurements at 25 °C for all surfactants in a concentration range from 0.5 up to 5 wt% (a) and for all surfactants at 1 wt% at different temperature. The intensity to calculate the molecular weight was corrected by the structure factor, which was calculated by the Carnahan-Starling equation.

D.3. Model Description

The model used to describe the SANS data of the CO_2 surfactants and the reference surfactants consist of two different form factor models: the ellipsoidal core-shell model and the micellar model, which are combined by a weighting factor f. Each model is by itself consistent concerning the overall scattering mass. The different models and the script to fit the SANS data was developed by Albert Prause. The two different models are described in the following sections separately. For all model approaches following SLD values for every surfactant were used:

Table 10.9: SLD values of the core, the shell and the solvent for all used CO_2 surfactants and the reference samples.

Surfactants	SLD_{core} /Å^{-2}	SLD_{shell} /Å^{-2}	SLD_{D2O} /Å^{-2}	ρ_{core} /g/cm^3	ρ_{shell} /g/cm^3
$C_{12}EO_{8.2}(CO_2)_{3.1}-OH$	$-3.66\cdot10^{-7}$	$9.47\cdot10^{-7}$	$6.38\cdot10^{-6}$	0.75	0.91
$C_{12}EO_{11.6}(CO_2)_{1.5}-OH$	$-3.66\cdot10^{-7}$	$6.71\cdot10^{-7}$	$6.38\cdot10^{-6}$	0.75	0.90
$C_{12}EO_{11.4}(CO_2)_{1.3}-OH$	$-3.66\cdot10^{-7}$	$6.41\cdot10^{-7}$	$6.38\cdot10^{-6}$	0.75	0.90
$C_{12}EO_{13.3}(CO_2)_{0.6}-OH$	$-3.66\cdot10^{-7}$	$5.49\cdot10^{-7}$	$6.38\cdot10^{-6}$	0.75	0.90
$C_{12}EO_{10.3}(PL)_{1.0}-OH$	$-3.66\cdot10^{-7}$	$6.83\cdot10^{-7}$	$6.38\cdot10^{-6}$	0.75	0.87
$C_{12}EO_{13.2}(PO)_{1.1}-OH$	$-3.66\cdot10^{-7}$	$5.48\cdot10^{-7}$	$6.38\cdot10^{-6}$	0.75	0.87
$C_{12}EO_{14.0}-OH$	$-3.66\cdot10^{-7}$	$4.75\cdot10^{-7}$	$6.38\cdot10^{-6}$	0.75	0.89
$C_{12/14}EO_9-OH$	$-3.66\cdot10^{-7}$	$5.09\cdot10^{-7}$	$6.38\cdot10^{-6}$	0.75	0.89

Background Estimation

The intensity of the incoherent background I_{bkg} was determined by a power-law fit of the Porod regime and from it, the Porod exponent was obtained. The analysis was performed by an analysis of the high q regime (q = 1.2 – 4 nm^{-1}). From this estimate the incoherent background I_{bkg} and the exponent in the Porod regime n_{porod} were obtained. This estimate was done for all models.

$$I(q)\cdot = A\cdot q^{-n_{porod}} + I_{bkg} \tag{10.1}$$

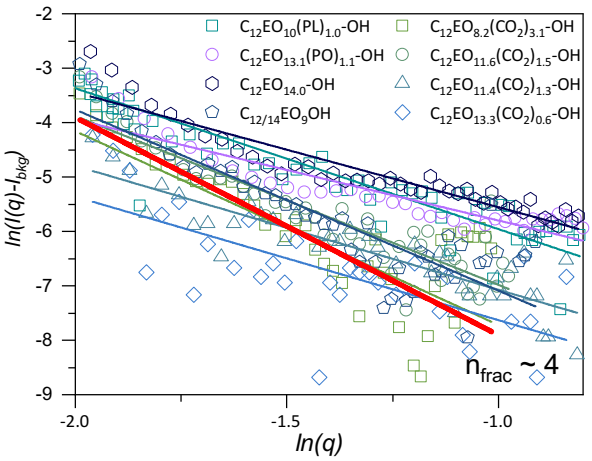

Figure 10.9: Estimation of the porod exponenet n_{porod} for all surfactants. The obtained values for nPorod are summarized in Table 5.3.

Core-Shell Ellipsoid Model

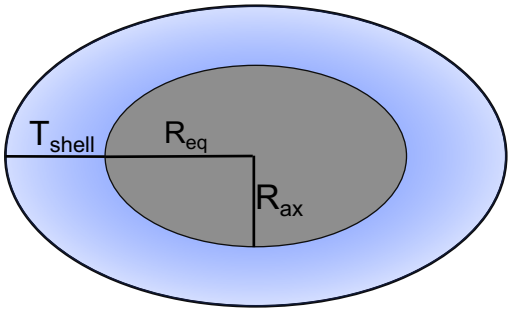

Figure 10.10: Schematic description of the core-shell ellipsoid model.

The SANS data of the surfactants can be described by an ellipsoidal core-shell model as described by Finnigan *et al.*[129] The core shell model is described by following total intensity $I(q)_{core-shell}$:

$$I(q)_{core-shell} = {}^{1}N \cdot P(q)_{core-shell} \cdot S(q)_{core-shell} \tag{10.2}$$

The particle density ${}^{1}N$ can be described by the volume fraction ϕ divided by the volume of the aggregate V_{agg}, which is described by the core volume V_{core} and the shell volume V_{shell}:

$$\begin{aligned} {}^{1}N &= \frac{\phi}{V_{agg}} \\ V_{agg} &= V_{core} + V_{shell} \\ V_{core} &= N_{\text{agg}} \cdot V_{n,core} \\ V_{shell} &= N_{\text{agg}} \cdot V_{n,shell} \end{aligned} \tag{10.3}$$

with $V_{n,core/n,shell}$ as the partial molecule volumes of the core and the head group respectively. The form factor $P(q)_{core-shell}$ is defined as follows:

$$P(q)_{core-shell} = \int_0^{\frac{\pi}{2}} A_{core-shell}(q,\alpha)^2 \cdot \sin(\alpha) d\alpha \tag{10.4}$$

$$\langle A_{core-shell}(q) \rangle = \int_0^{\frac{\pi}{2}} A_{core-shell}(q,\alpha) \cdot \sin(\alpha) d\alpha \tag{10.5}$$

The Amplitude of an ellipsoid can be described as follows:

$$A_{e,i}(q,R) = V_{ellipsoid} \cdot \frac{3\left[\sin(qR) - qR \cdot \cos(qR)\right]}{(qR)^3} \tag{10.6}$$

$$\text{with: } R(R_{eq}, R_{ax}, \alpha) = \sqrt{R_{eq}^2 \cdot \sin^2(\alpha) + R_{eq}^2 \cdot \cos^2(\alpha)}$$

$$V_{ellipsoid} = \frac{4}{3}\pi \cdot R_{eq}^2 R_{ax}$$

with an equatorial and an axial radius of the inner core, which defines the ellipsoidal volume and an angle α defined as the orientation angle.

The contrast variation of the shell is considered in terms of a core-shell variation:

$$A_{core-shell}(q,\alpha) = \rho_0 \cdot A_{e,0}\left(q, R(R_{eq}, R_{ax}, \alpha)\right) + \rho_{shell} \cdot \left[\begin{array}{c} A_{core-shell}\left(q, R(R_{eq}+T_{shell}, R_{ax}+T_{shell}, \alpha)\right) \\ -A_{core}\left(qR(R_{eq}, R_{ax}, \alpha)\right) \end{array}\right] \tag{10.7}$$

with:

$$\rho_{shell} = \phi_{shell} \cdot \Delta SLD_{shell} + (1 - \phi_{shell}) \cdot SLD_{solvent}$$

$$\phi_{shell} = \frac{V_{head}}{V_{shell}} \tag{10.8}$$

$$V_{head} = N_{\text{agg}} \cdot V_{n,head} = \frac{V_{n,core}}{V_core} \cdot V_{n,head} \tag{10.9}$$

$$V_{shell} = \frac{4}{3}\pi(R_{eq} + T_{shell})^2(R_{ax} + T_{shell}) - \frac{4}{3}\pi \cdot R_{eq}^2 R_{ax}$$

To obtain the total scattering intensity of the core-shell model some parameters were calculated and could be fixed:

$$R_{eq} = \sqrt[3]{\frac{N_{\text{agg}} \cdot V_{n,core}}{\varepsilon \cdot \frac{4}{3}\pi}} \tag{10.10}$$

$$R_{ax} = \varepsilon \cdot R_{eq} \tag{10.11}$$

$$R_{eff} = \sqrt[3]{(R_{eq} + T_{shell})^2(R_{ax} + T_{shell})} \tag{10.12}$$

With R_{eq} being the equatorial radius, with ε as the axis ratio of the ellipsoid. The effective radius R_{eff} is the volume equivalent sphere radius of the ellipsoid. From this approach the parameters N_{agg}, ε and T_{shell} could be determined. And moreover, these parameters could be calculated as a result:

$$\phi hs = {}^1N \cdot \frac{4}{3}\pi \cdot R_{hs}^3 \text{ hard sphere volume fraction, not penetrable} \tag{10.13}$$

$$\phi shs = {}^1N \cdot \frac{4}{3}\pi \cdot R_{eff}^3 \text{ soft sphere volume fraction, with penetrable shell} \tag{10.14}$$

Ellipsoidal core with Gaussian Chains Attached Model (Micellar Model)

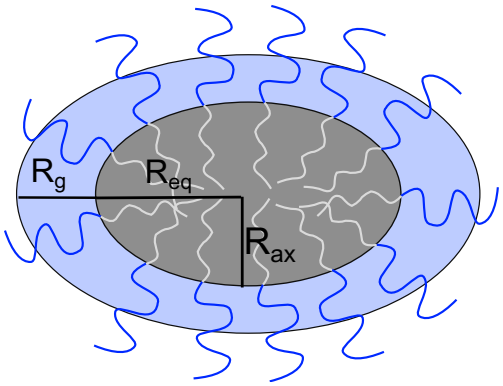

Figure 10.11: Schematic description of the ellipsoid with Gaussian chains attached model.

This model is based on several works by Pedersen *et al.*[130–133]. The core shell model is described by following total intensity I(q)$_{micelle}$:

$$I(q)_{micelle} = {}^{1}N \cdot P(q)_{micelle} \cdot S(q)_{micelle} \tag{10.15}$$

The overall form factor P(q)$_{micelle}$ consist of defined terms for the ellipsoidal core P(q)$_e$, the form factor of the chains in the corona P(q)$_{ch}$ and interference cross section terms between the core and the chains S(q)$_{e-ch}$ and the chains and the corona S(q)$_{ch-ch}$, which also needs to be considered:

$$P(q)_{micelle} = {N_{\text{agg}}}^2 \cdot V_e^2 \rho_e^2 \cdot P(q)_e + {N_{\text{agg}}}^2 \cdot V_{ch}^2 \rho_{ch}^2 \cdot P(q)_{ch} + 2 \cdot {N_{\text{agg}}}^2 \cdot V_e V_{ch} \rho_e \rho_{ch} cdot S(q)_{e-ch} + N_{\text{agg}}(N_{\text{agg}} - 1) \cdot V_{ch}^2 \rho_{ch}^2 \cdot S(q)_{ch-ch} \tag{10.16}$$

The form-factor of the ellipsoidal core P(q)$_e$ is again described by an ellipsoidal core as described in the previous section:

$$P(q)_e = \int_0^{\frac{\pi}{2}} A_e^2(q,R) \cdot \sin(\alpha) d\alpha \tag{10.17}$$

$$A_e(q,R) = V_{ellipsoid} \cdot \frac{3\left[\sin(qR) - qR \cdot \cos(qR)\right]}{(qR)^3}$$

$$\text{with: } R(R_{eq}, R_{ax}, \alpha) = \sqrt{R_{eq}^2 \cdot \sin^2(\alpha) + R_{eq}^2 \cdot \cos^2(\alpha)}$$

$$V_{ellipsoid} = \frac{4}{3}\pi \cdot R_{eq}^2 R_{ax}$$

The polymer scattering is modified to account for excluded volume effects after Hammouda *et al.*[133]

$$P(q)_{ch} = A_{ch}(q) - \frac{1}{\nu \cdot U^{\frac{1}{\nu}}} \tag{10.18}$$

$$A_{ch}(q,R_g) = \frac{1}{2\nu \cdot U^{\frac{1}{2\nu}}} \cdot \gamma\left(\frac{1}{2\nu}, U\right)$$

$$\text{with } U = \frac{q^2 R_g^2 (2\nu+1)(2\nu+2)}{6}$$

ν is the excluded volume parameter (1/2 for Gaussian chain, 3/5 for a fully swollen chain; valid range is between 1/3 and 3/5) and γ represents the incomplete Gamma function and is described as followed:

$$\gamma(x,a) = \int_0^{\alpha} \exp(-t)^{x-1} dt \tag{10.19}$$

The interference terms between ellipsoid and the chains $S(q)_{e-ch}$ and the chain–chain scattering $S(q)_{ch-ch}$, are described respectively:

$$S(q)_{e-ch} = A_{ch}(q,R_g) \cdot \int_0^{\frac{\pi}{2}} A_e(q,R) \cdot \frac{\sin(q \cdot (R+dR_g))}{q \cdot (R+dR_g)} \cdot \sin(\alpha) d\alpha \tag{10.20}$$

$$S(q)_{ch-ch} = \int_0^{\frac{\pi}{2}} \left(A_{ch}(q,R_g) \left[\frac{\sin(q \cdot (R+dR_g))}{q \cdot (R+dR_g)} \right] \right)^2 \cdot \sin(\alpha) d\alpha \tag{10.21}$$

From this model the same parameters N_{agg}, ε and T_{shell} ($T_{shell} = 2 \cdot R_g$) could be determined. And moreover, these parameters could be calculated as a result:

$$\phi hs = {}^1N \cdot \frac{4}{3}\pi \cdot R_{hs}^3 \text{ hard sphere volume fraction, not penetrable} \tag{10.22}$$

$$\phi shs = {}^1N \cdot \frac{4}{3}\pi \cdot R_{eff}^3 \text{ soft sphere volume fraction, with penetrable shell} \tag{10.23}$$

Water-Content from Model Description

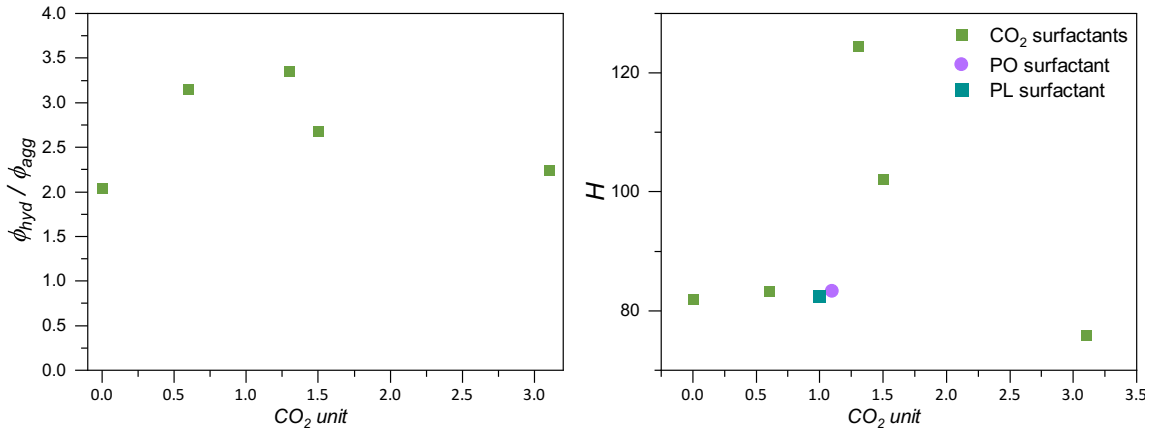

Figure 10.12: (a) Obtained water content of the micellar corona (ϕ_{hyd}/ϕ_{agg}) from the model description as a function of the CO_2 content. (b) Obtained hydration factor derived from the water content from the SANS model

The reduced hydration of the CO_2 surfactants was determined by the description of the SANS model. The hydration is described by the model in terms of bound water in the corona (ϕ_{hyd}/ϕ_{agg}).

$$\begin{aligned} \phi_{agg} &= \phi_{dry} \\ {}^{1}N_{agg} &= \frac{\phi_{agg}}{V_{agg}} \\ V_{agg} &= V_{core} + V_{shell} \\ \phi_{hyd} &= {}^{1}N_{agg} \cdot V_{hyd} \end{aligned} \tag{10.24}$$

The volume of the hydrated aggregate V_{hyd} was derived from the model by the SLD profile of the corona. One can observe a difference in the obtained water contents, whereby the CO_2surfacatnt, $C_{12}EO_{8.2}(CO_2)_{3.1}-OH$, has somewhat smaller water content in the corona than the reference surfactant. The form factor has a certain SLD profile, which considers the mass-balance. Therefore, the form factor considers not only the water which is strongly bound in the corona, and therefore overestimates the water content. This results in an overestimation of the water conten, and and only small difference can be observed between the CO_2 surfactants and the reference surfactant $C_{12}EO_{14.0}-OH$.

Model Comparison

In comparison between the single core-shell and micelle model and the total intensity of the combination of both models is shown in Fig. 10.13. One can already observe the high discrepancies in the high q regime. The core-shell model with a power-law decay of the shell contrast, shows an underestimation of the scattering intensity in the high q regime, as it completely neglects the scattering of the EO chains. In contrast, the micellar model with a Gaussian chain profile overestimates the scattering intensity. Even though both model are only slightly different by the change in scattering contrast, the change in the SLD profile already shows a marked influence at the high q regime. This supports the use of the combination of both models.

The ΔSLD profiles of both single models are shown in Fig. 10.14. The ΔSLD profile of the core-shell model is a stepwise profile with exponential decay. The profile for the micellar model results

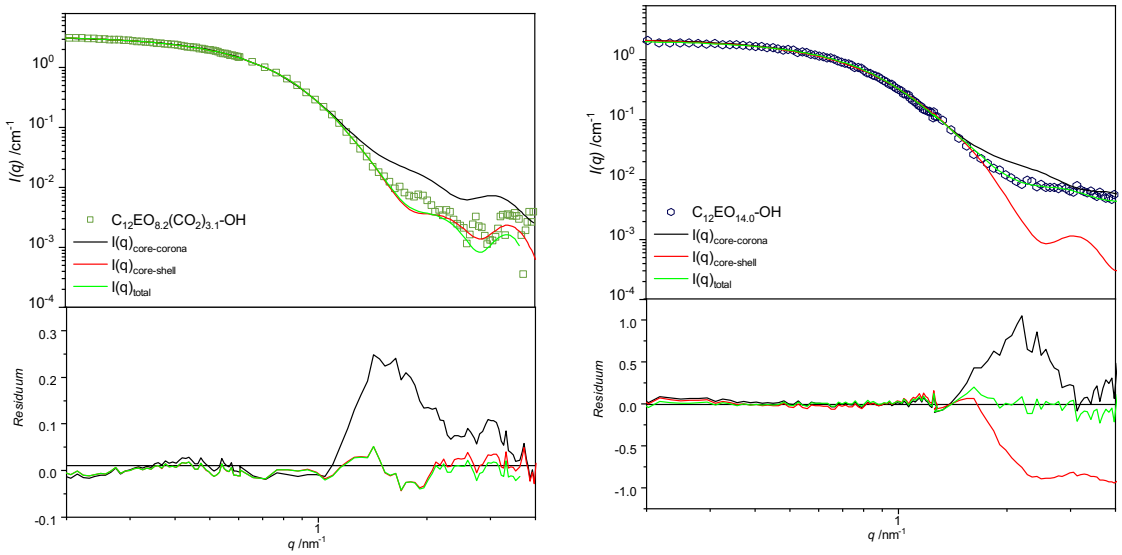

(a) **(b)**

Figure 10.13: Comparison of the single core-shell model and the micellar model and the total intensity $I(q)_{tot}$ from both fits correlated with the factor f, for the CO_2 surfactant ($C_{12}EO_{8.2}(CO_2)_{3.1}-OH$) (a) and for the reference surfactant ($C_{12}EO_{14.0}-OH$) (b). Fit residuum $\left(\frac{(I(q)-I_{bkg})-(I_{fit}(q)-I_{bkg})}{\sqrt{(dI(q))^2+(dI_{bkg})^2}}\right)$ is shown below the fit.

from an inverse Fourier transform of the corresponding averaged scattering amplitude following Pederson *et al.*[142]

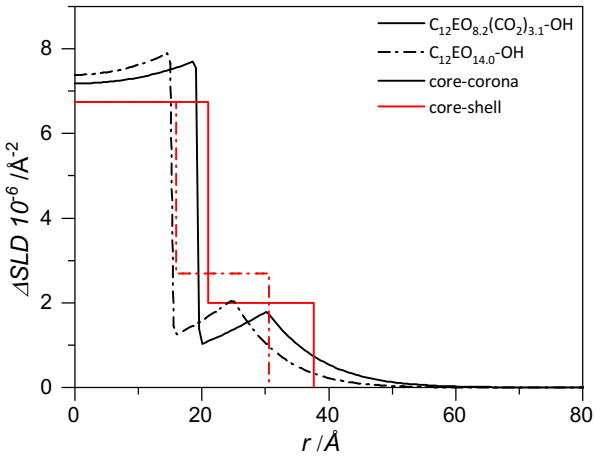

Figure 10.14: Comparison of the ΔSLD profile of the single core-shell model and the micellar model for the CO_2 surfactant ($C_{12}EO_{8.2}(CO_2)_{3.1}-OH$) and for the reference surfactant ($C_{12}EO_{14.0}-OH$).

Core-Shell Cylinder Model

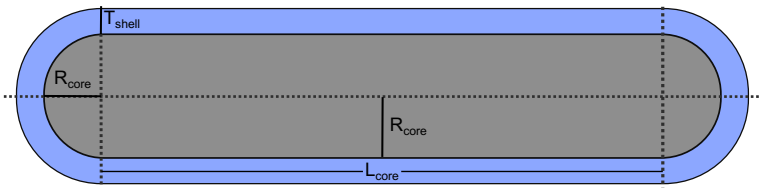

Figure 10.15: Schematic description of the core-shell cylinder model.

The temperature dependent data were fitted with a cylindrical model with spherical end-caps for the data obtained at higher temperature.[144–146]

$$I(q)_{cyl,core-shell} = {}^{1}N \cdot P(q)_{cyl,core-shell} \cdot S(q)_{core-shell} \tag{10.25}$$

The form factor P(q)$_{cyl,core-shell}$ is defined as follows:

$$P_{cyl,core-shell}(q,R_{core},L_{core},T_{shell}) = \int_0^{\frac{\pi}{2}} \left|A_{cyl,core-shell}(q,R_{core},L_{core},T_{shell},\alpha)\right|^2 \cdot \sin(\alpha) d\alpha \tag{10.26}$$

The amplitude of an cylinder A$_{cyl}$ can be described as follows:

$$\begin{aligned} A_{cyl}(q,R_{core},L_{core},T_{shell},\alpha) = {} & \pi R_{core}^2 L_{core} sinc\left(\frac{1}{2} q L_{core}\cos(\alpha)\right) \cdot 2 \cdot jinc\left(qR_{core}\sin(\alpha)\right) \\ & + 4\pi R_{cap}^3 \int_{\frac{-h}{R_{cap}}}^{1} \cos\left[q\cos(\alpha)\cdot\left(Rt + h + \frac{1}{2}L_{core}\right)\right] \cdot (1-t^2) \\ & \cdot jinc\left(qR_{cap}\sin\alpha \cdot \sqrt{(1-t^2)}\right) dt \end{aligned} \tag{10.27}$$

with the following equations defined and J_1 as a first-order Besser function:

$$sinc(x) = \frac{\sin(x)}{x} \text{and} jinc(x) = \frac{J_1(x)}{x}$$

$$R_{cap} = R_{core} \text{ and } h = -\sqrt{R_{cap}^2 - R_{core}^2} = 0$$

The contrast variation of the shell is considered in terms of a core-shell expression with a decaying shell SLD constructed of n shell-steps with a step size of dr=0.2 nm:

$$\begin{aligned} A_{cyl,core-shell}(q,\alpha) = {} & \rho_{core} \cdot A_{core}(q,R_{core},L_{core},T_{shell},\alpha) + \rho_{shell} \cdot \\ & \begin{bmatrix} A_{core-shell}(q,R_{core}+L_{core},T_{shell},\alpha) \\ -A_{core}(q,R_{core}+L_{core},\alpha) \end{bmatrix} \end{aligned} \tag{10.28}$$

with:

$$\rho_{shell} = \phi_{shell} \cdot \Delta SLD_{shell} + (1-\phi_{shell}) \cdot SLD_{solvent}$$

$$\phi_{shell} = \frac{V_{head}}{V_{shell}} \tag{10.29}$$

$$V_{head} = N_{\text{agg}} \cdot V_{n,head} = \frac{V_{n,core}}{V_{c}ore} \cdot V_{n,head} \tag{10.30}$$

$$V_{shell} = \left[\pi(R_{core}+T_{shell})^2 L_{core} + \frac{4}{3}\pi(R_{core}+T_{shell})^3\right] - \left[\pi R_{core}^2 L_{core} + \frac{4}{3}\pi R_{core}^3\right]$$

V_{shell} is given for a defined shell thickness T_{shell}. To obtain the total scattering intensity of the core-shell cylinder model some parameters were calculated and could be fixed:

$$R_{core} = \sqrt[3]{\frac{N_{\text{agg}} \cdot V_{n,core}}{2\pi\varepsilon + \frac{4}{3}\pi}} \tag{10.31}$$

$$L_{core} = 2\varepsilon \cdot R_{core} \longrightarrow \left(\varepsilon = \frac{L_{core}}{2R_{core}}\right) \tag{10.32}$$

$$R_{eff} = \sqrt[3]{\frac{6}{4}\pi\varepsilon(R_{core} + T_{shell})^3 + (R_{core} + T_{shell})^3} \tag{10.33}$$

volume equivalent sphere radius of the cylinder, rotational radius would be probably more accurate, but concentration is too low to see that difference. From this model the same parameters N_{agg}, ε and T_{shell} could be determined.

Sticky Hard-Sphere Structure Factor

In order to describe the interparticular interactions of the micellar system of the nonionic surfactants, a sticky hard sphere structure factor was used. The structure factor is applied for all different models in terms of a decoupling approach after Pederson.[140, 142]

$$S(q)_\beta = (1 + \beta(q) \cdot [S(q) - 1]) \tag{10.34}$$

$$\text{with: } \beta(q) = \frac{\langle A_{model}(q)\rangle^2}{P_{model}(q)}$$

The structure factor itself S(q) is related to the direct correlation function C(q):

$$S(q) = \frac{1}{1 - {}^1NC(q)} \tag{10.35}$$

Thereby can the direct correlation function C(q) written as the sum of the different, independent contributions of the interaction potential U_{eff}, if the random phase approximation is applied:

$${}^1NC(q) = {}^1NC_0(q) - \frac{1}{k_bT}{}^1N \cdot U_{eff}(q) \tag{10.36}$$

The underlying potential of the sticky hard-sphere structure factor is as follows:

$$U = \begin{cases} \infty \text{ for} & R \leq R_{hs} \leq R \\ -Y \text{ for} & 2R_{hs} < R \leq rR_{hs} + \delta \\ 0 \text{ for} & t_i > R + T_{shell} \end{cases} \tag{10.37}$$

Thereby is $2R_{hs}$ the hard-sphere diameter, δ is the width of the potential and Y is the depth of the potential in units of kT and the so-called stickiness parameter. $Y = -2kT$ for this model (arbitrarily chosen, important is only the repulsive potential step). The potential was solved with the Percus-Yervick approximation:[141, 143]

$$\begin{aligned} C_0(q) = {} & \frac{2\eta\lambda}{\kappa} - \frac{2\eta^2\lambda^2}{\kappa^2}(1 - \cos\kappa) \\ & - [\alpha\kappa^3(\sin\kappa - \kappa\cos(\kappa)) + \beta\kappa^2\left(2\kappa\sin(\kappa) - (\kappa^2 - 2)\cos(\kappa) - 2\right) \\ & + \frac{\eta\alpha}{2}\left((4\kappa^3 - 24\kappa)\sin(\kappa) - (\kappa^4 - 12\kappa^2 + 24)\cos(\kappa) + 24\right)] \end{aligned} \tag{10.38}$$

with: $\kappa = q \cdot 2R_{hs}$

$$\eta = \phi_{hs}\left(\frac{2R_{hs}+\delta}{2R_{hs}}\right)^3$$

$$\varepsilon = Y + \frac{\eta}{1-\eta}$$

$$\Delta = \phi_{hs}\frac{1+\eta/2}{3(1-\eta)^2}$$

$$\lambda = \frac{6}{\eta}\left(\varepsilon - \sqrt{\varepsilon^2-\Delta}\right)$$

$$\mu = \lambda\eta(1-\eta)$$

$$\beta = -\frac{3\eta(2+\eta)^2 - 2\mu(1+7\eta+\eta^2)+\mu^2(2+\eta)}{2(1-\eta)^4}$$

$$\alpha = \frac{(1+2\eta-\mu)^2}{(1-\eta)^4}$$

The hard-sphere volume fraction is defined by:

$$\phi_{hs} = \nu_{mic} \cdot \frac{4}{3}\pi \cdot R_{hs} \tag{10.39}$$

with R_{hs} being the hard-sphere radius, which can be obtained from the the model fit by R_{eff}:

$$R_{hs} = R_{eff} - \frac{T_{shell}}{2} \tag{10.40}$$

Carnahan-Starling Evaluation

Calculation of $I(0)_{theo}$ was done using Eq. 10.41, where the concentration is determined by the mass ratio and therefore from the directly weighed masses. It is assumed that both the water content and the molecular weight remain constant over the considered concentration range.

$$I(0)_{theo} = \frac{\phi_1^2 \cdot M_w}{c_g \cdot N_{Av}} \cdot (\Delta SLD)^2 \cdot S(0) \tag{10.41}$$

The structure factor was assumed to be given by the Carnahan-Starling approximation with the additional freely adjustable interaction parameter, A, which, to a first approximation, is calculated from the second virial coefficient of the osmotic pressure.

$$S(0)^{-1} = \frac{(1+2\phi_{hs})^2 - 4\phi_{hs}^3 + \phi_{hs}^4}{(1-\phi_{hs})^4} \tag{10.42}$$

The water content, B, of the micelles was then calculated from the dry volume fraction, ϕ_1, and thus gives the volume fraction of the swollen aggregates, $\phi_{1,s}$:

$$\phi_{1,s} = B \cdot \phi_1 \cdot (1 - A\phi_1) \tag{10.43}$$

The formula as implemented in the Origin software package is given by:

$$\phi_1 = w_1/\rho_1/(w_1/\rho_1 + (1-w1_)/\rho_2) \tag{10.44}$$

$$\phi_{1s} = \phi_1 \cdot B \cdot (1 - A \cdot phi_1)$$

$$\rho = \rho 1 \cdot \phi_1 + \rho_2 \cdot (1 - phi_1)$$

$$c_{g1} = w_1 \cdot \rho$$

$$S(0) = 1/(((1+2\cdot\phi_{1s})^2 - 4\cdot phi_{1s}^3 + phi_{1s}^4)/(1-\phi_{1s})^4)$$

$$I(0) = \phi_1^2 \cdot Mw/(c_{g1}\cdot N_{Av}) \cdot (\Delta SLD)^2 \cdot S(0)$$

At concentrations higher than 0.4 volume fraction, this approach would no longer be valid, but the maximum intensity around volume fractions of 0.05-0.10 is well-described for all surfactants. The interaction parameter, A, is clearly positive for all surfactants, which indicates repulsive interactions, and shows a slight increase with decreasing CO_2 content. This indicates that with higher CO_2 content, the repulsive interactions ("effective volume fraction") are smaller.

D.4. SANS Data

Concentration Dependent SANS Data

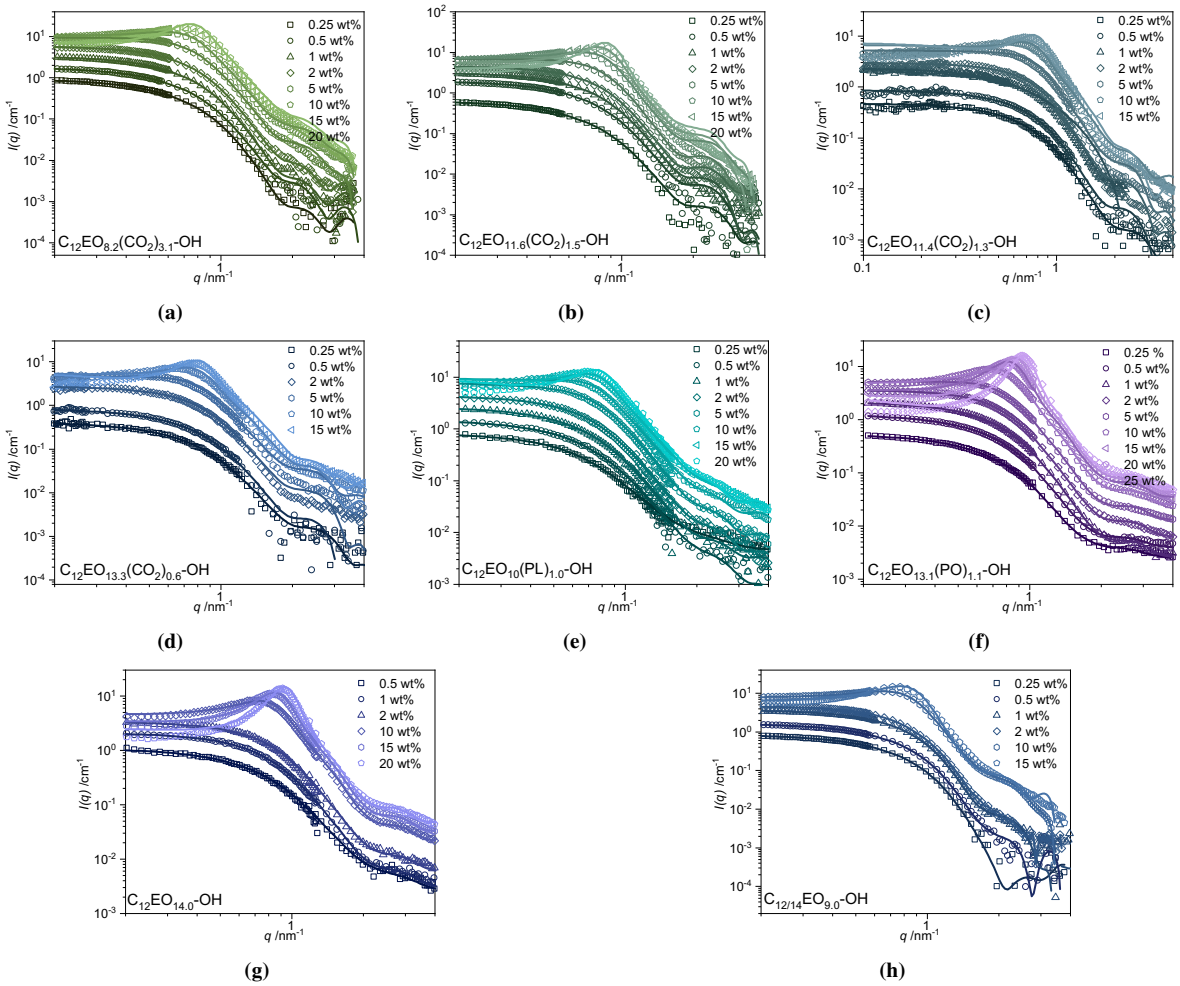

Figure 10.16: All SANS data in the concentration regime from 0.25 wt% up to 20 wt% for all surfactants with the fit model analysis.

Table 10.10: Summarized parameters obtained from the model analysis of the SANS data for all surfactants and concentrations at 25 °C. The parameters are: n_{por} is the porod exponent, f is the model fraction, ε is the ellipticity of the aggregates with the equatorial radius R_{eq} and the axial radius R_{ax}, the shell thickness T_{Shell}, the effective radius R_{eff}, the molecular weight M_w and the aggregation number N_{agg}.

ϕ_{dry}	n_{frac}	f	ε	R_{eq} /nm	R_{ax} /nm	T_{Shell} /nm	R_{eff} /nm	M_w /kDa	N_{agg}	H
$C_{12}EO_{8.2}(CO_2)_{3.1}-OH$										
0.003	7.54	0.94	1.8	15.9	28.5	18.1	37.8	64	94	73
0.007	7.71	1.00	1.8	15.7	28.5	19.8	39.3	62	91	85

0.012	7.16	0.93	1.8	16.1	28.7	18.7	38.6	66	96	76
0.024	3.87	0.79	1.8	16.3	29.5	19.0	39.2	69	101	76
0.061	3.93	0.56	2.1	16.0	32.9	19.9	40.8	74	109	79
0.119	3.61	0.41	2.3	16.2	37.0	20.2	42.3	85	126	77
0.182	3.96	0.38	2.5	16.4	40.9	19.9	43.1	97	142	72
0.241	3.63	0.48	2.8	16.4	45.5	19.3	43.5	107	158	66
$C_{12}EO_{11.6}(CO_2)_{1.5}-OH$										
0.003	7.16	1.00	2.0	13.2	25.9	19.5	36.5	45	59	105
0.010	7.89	1.00	1.9	13.5	26.0	19.9	37.1	47	61	106
0.017	3.44	1.00	2.0	13.6	26.6	19.7	37.1	48	63	102
0.028	2.42	1.00	1.8	14.1	25.4	19.7	37.2	50	65	100
0.062	3.18	0.88	1.8	14.4	26.3	19.8	37.8	54	71	96
0.125	3.28	0.63	1.9	14.9	28.2	20.0	38.9	62	82	91
0.187	3.23	0.51	1.9	15.5	29.3	20.0	39.6	70	92	86
0.247	3.48	0.44	2.0	15.9	31.4	19.7	40.2	78	103	80
$C_{12}EO_{11.4}(CO_2)_{1.3}-OH$										
0.006	1.96	1.00	1.9	12.2	23.6	20.0	35.6	34	46	125
0.003	1.57	1.00	2.2	12.0	26.6	18.0	38.8	37	50	102
0.011	2.00	0.00	4.1	10.2	41.3	12.0	29.7	41	56	60
0.022	3.16	1.00	2.1	12.7	26.2	19.7	37.0	41	55	111
0.055	2.65	1.00	2.3	12.9	30.0	19.3	38.3	49	65	100
0.111	2.00	1.00	3.0	13.0	38.5	18.2	40.4	63	85	82
0.166	2.28	1.00	3.2	13.4	42.9	18.2	41.0	74	99	77
0.274	2.23	1.00	3.7	13.4	49.9	17.2	40.6	87	117	68
$C_{12}EO_{13.3}(CO_2)_{0.6}-OH$										
0.006	3.61	1.00	2.0	11.9	23.5	18.9	34.2	34	43	125
0.003	1.34	1.00	2.1	11.5	24.4	18.1	36.9	33	42	120
0.011	7.38	0.00	3.5	10.4	36.4	12.0	28.9	40	51	64
0.022	1.97	1.00	2.1	12.1	25.8	18.7	35.5	39	49	115
0.055	1.50	1.00	2.3	12.6	29.0	18.9	38.0	48	60	106
0.111	1.22	1.00	2.7	12.8	35.2	17.9	39.6	59	75	90
0.166	1.26	1.00	3.1	12.9	40.1	17.3	40.3	69	87	81
0.274	1.76	1.00	3.6	12.9	46.3	16.5	39.7	79	100	72
$C_{12}EO_{10.3}(PL)_{1.0}-OH$										
0.004	1.58	0.00	2.4	12.5	30.3	20.0	44.9	42	61	107
0.006	0.52	0.77	2.4	13.1	31.6	18.2	36.5	48	71	85
0.012	1.60	0.99	2.5	13.2	32.7	18.0	36.6	51	74	82
0.023	1.54	0.94	2.5	13.3	33.1	18.3	37.1	52	76	84
0.053	1.93	0.95	2.6	13.6	35.0	18.4	37.9	58	84	80
0.100	1.64	0.89	2.9	13.9	39.8	18.4	40.1	69	100	75
0.163	1.13	0.83	3.1	14.3	44.4	18.7	41.3	81	118	72
0.217	1.09	0.90	3.3	14.5	48.4	18.5	41.8	91	132	68
$C_{12}EO_{13.2}(PO)_{1.1}-OH$										
0.003	0.38	0.44	1.8	12.7	22.4	17.9	33.5	38	46	100
0.006	0.39	0.62	1.9	12.6	24.2	17.2	34.1	41	50	92
0.011	1.29	0.74	2.2	12.3	27.1	16.4	36.9	44	53	83
0.023	1.13	0.72	2.2	12.4	27.6	16.7	38.4	46	55	84
0.048	0.84	0.77	2.4	12.4	29.8	16.5	39.3	49	60	80

0.112	1.35	0.77	2.6	12.7	32.9	16.2	40.1	56	69	74
0.168	1.51	0.77	2.6	12.9	33.8	16.1	39.9	60	73	71
0.210	1.53	0.78	2.7	13.0	34.7	16.1	39.7	63	77	70
0.274	1.62	0.84	2.8	13.0	36.9	16.0	39.1	67	81	68
$C_{12}EO_{14.0}-OH$										
0.005	0.69	0.39	2.4	11.3	27.1	15.4	31.2	36	45	85
0.012	0.71	0.72	2.4	11.6	27.7	15.4	35.8	39	49	82
0.022	0.46	0.69	2.3	11.6	27.2	15.2	33.5	38	48	80
0.105	0.76	0.79	2.6	12.1	32.0	15.2	38.2	49	61	73
0.161	0.96	0.78	2.6	12.4	32.6	15.3	38.0	52	65	71
0.215	0.74	0.74	2.4	12.8	31.2	15.4	37.2	53	67	70
$C_{12/14}EO_9-OH$										
0.003	3.25	1.00	1.7	16.0	27.3	14.9	29.7	56	90	55
0.006	7.51	0.49	1.0	18.4	18.4	18.0	36.0	50	81	74
0.013	7.65	0.00	1.1	18.2	20.0	18.1	36.1	53	86	73
0.020	4.17	0.30	1.0	18.5	18.7	19.0	38.0	51	83	80
0.109	3.50	0.14	1.6	16.8	26.2	19.3	38.6	59	96	77
0.161	3.66	0.19	1.1	19.3	21.2	19.1	38.2	64	103	72
0.261	4.31	0.28	1.9	16.7	32.5	18.1	36.2	73	118	65

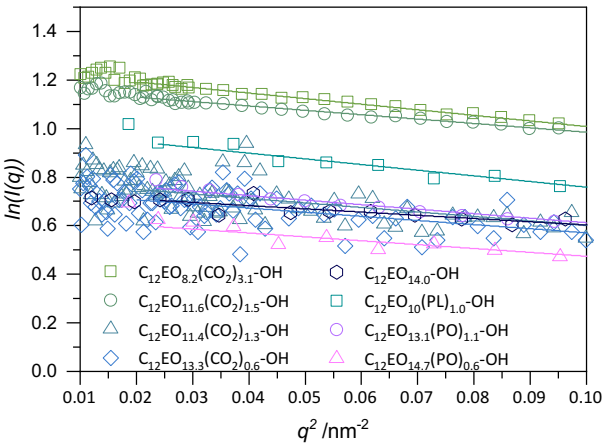

Figure 10.17: Guinier plot for spherical micelles (ln(I) vs. q^2) for all CO_2. Pl and PO surfactants and the reference surfactants $C_{12}EO_{14.0}-OH$ and $C_{12/14}EO_9-OH$ at 1 wt%.

A Guinier plot shows a linear regime for all the surfactants. The slope gives the radius of gyration which is listed for all measured surfactants in Table 5.4.

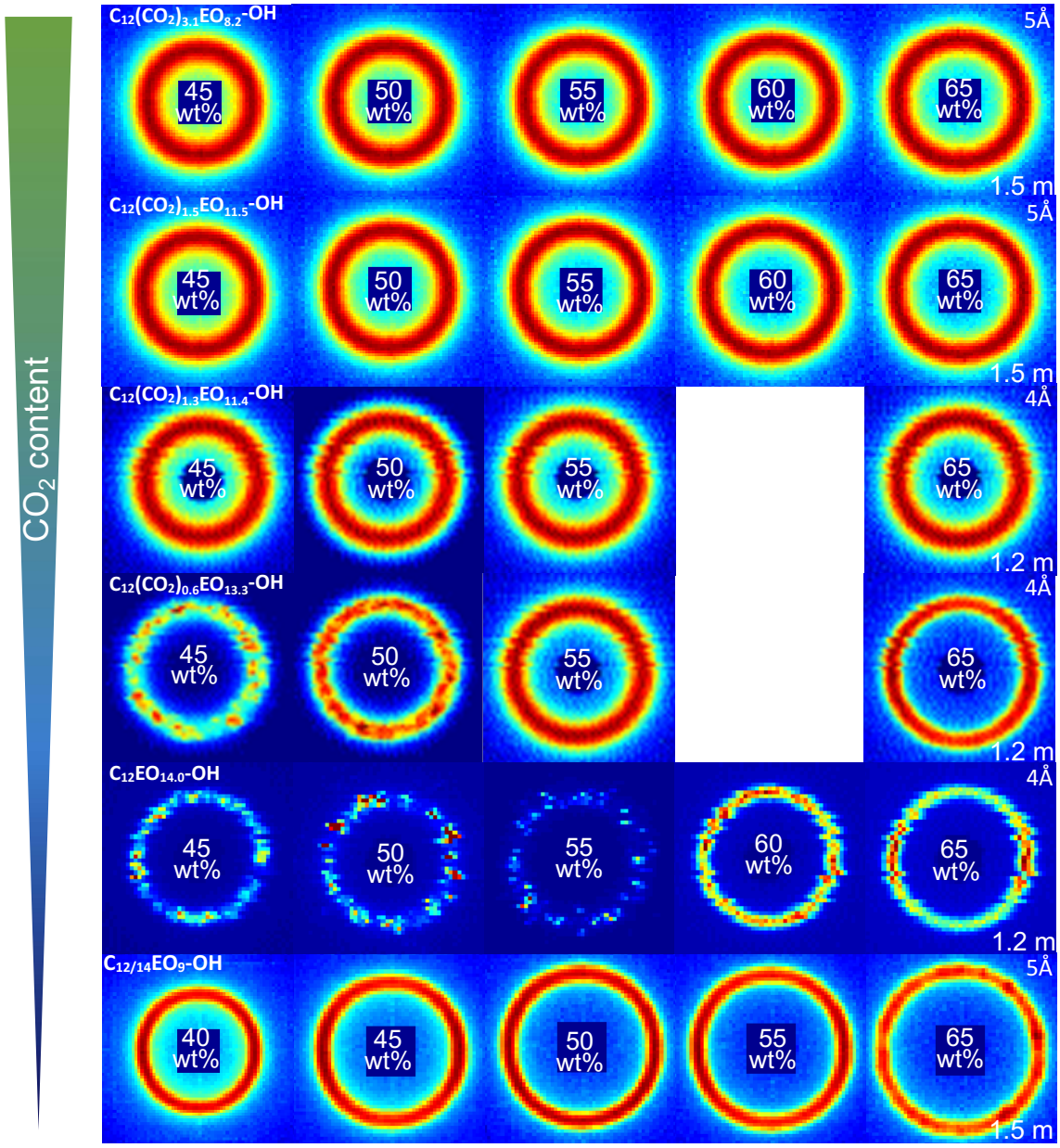

Figure 10.18: 2-D SANS intensities for all CO_2 surfactants and the reference sample $C_{12}EO_{14.0}-OH$; $C_{12/14}EO_9-OH$ for 50 wt% at 25°C for the concentration range from 45 up to 65 wt%. The scattering patterns were recorded with a wavelength of 5 Å and sample-to-detector distances of 1.5 m for KWS-1 for $C_{12}EO_{8.2}(CO_2)_{3.1}-OH$, $C_{12}EO_{11.6}(CO_2)_{1.5}-OH$, $C_{12/14}EO_9-OH$ and a wavelength of 4 Å and for $C_{12}EO_{11.4}(CO_2)_{1.3}-OH$, $C_{12}EO_{13.3}(CO_2)_{0.6}-OH$, $C_{12}EO_{14.0}-OH$ at a sample-to-detector distance of 1.2 m for PAXY.

Temperature Dependent SANS Data

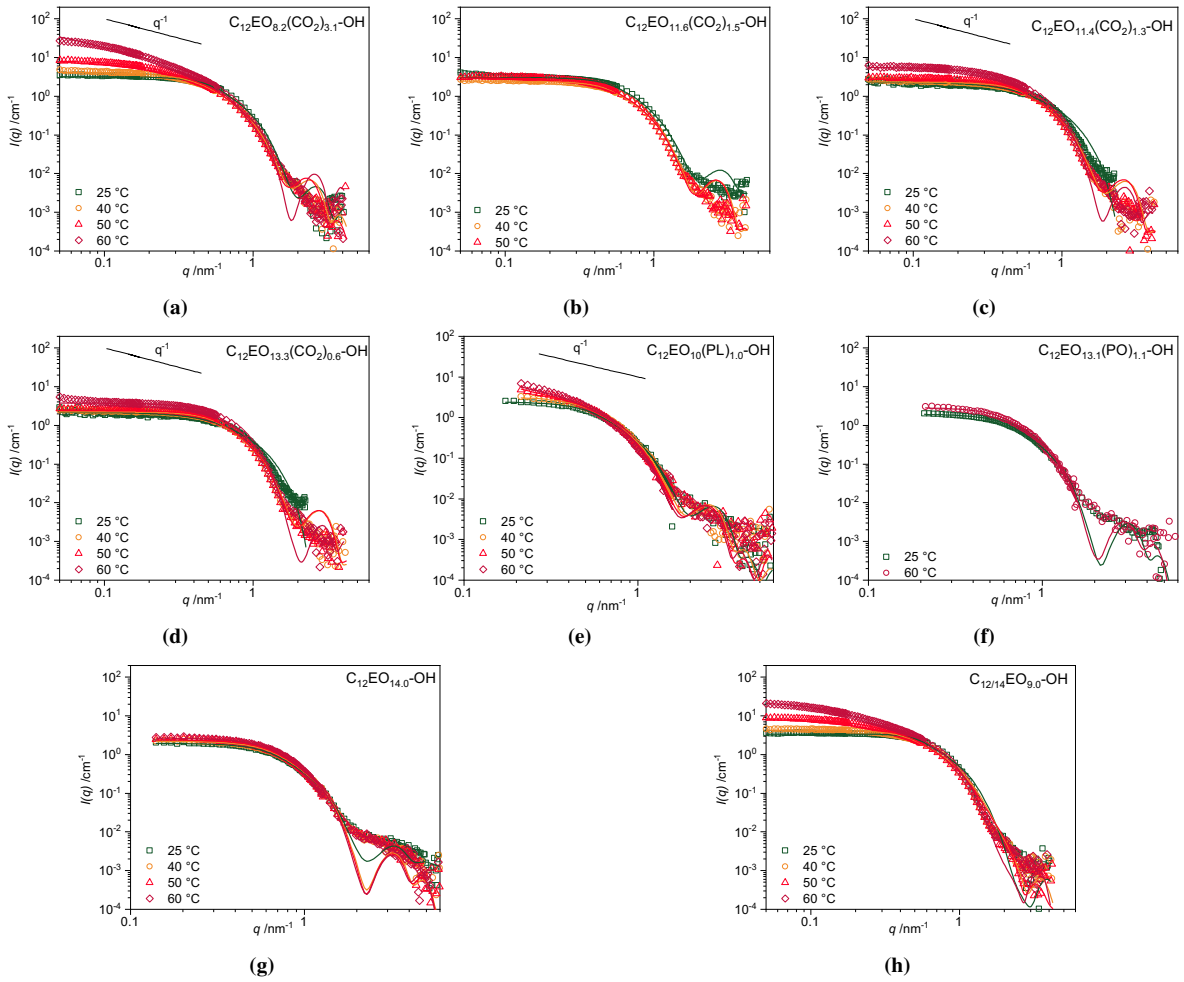

Figure 10.19: Temperature-dependent SANS curves for all CO2, PO and PL surfactants and the reference surfactant at 1 wt% at 25, 40, 50 and 60 °C with the fits from the cylinder model.

Table 10.12: Summarized parameters obtained from the model analysis with the cylinder model of the SANS data for all surfactants and temperatures.

T /K	R_{eq} /nm	R_{ax} /nm	T_{Shell} /nm	$L_{cylinder}$ /nm	M_w /kDa	N_{agg}
$C_{12}EO_{8.2}(CO_2)_{3.1}-OH$						
298.15	1.2	3.4	1.8	12.5	62	91
313.15	1.2	4.9	2.0	16.0	87	128
323.15	1.2	8.9	2.1	24.4	152	223
333.15	1.2	44.7	1.8	95.5	766	1126
$C_{12}EO_{11.6}(CO_2)_{1.5}-OH$						
298.15	0.9	4.1	1.9	13.8	49	65
313.15	1.0	3.5	1.9	12.8	51	68
323.15	1.0	4.0	2.0	13.9	60	79
$C_{12}EO_{11.4}(CO_2)_{1.3}-OH$						
298.15	0.9	3.6	1.2	11.3	38	51
313.15	1.0	3.5	1.9	12.8	49	66
323.15	1.0	4.0	2.0	13.8	58	77
333.15	1.2	5.0	1.8	16.0	97	130

$C_{12}EO_{13.3}(CO_2)_{0.6}-OH$						
298.15	0.8	3.3	1.2	10.8	36	45
313.15	0.9	3.4	1.9	12.3	45	56
323.15	0.9	3.4	1.9	12.5	48	60
333.15	1.2	3.0	1.6	11.5	67	84
$C_{12}EO_{10.3}(PL)_{1.0}-OH$						
298.15	1.0	3.7	1.9	13.1	47	68
313.15	1.1	4.1	1.9	14.2	61	89
323.15	1.0	10.7	2.0	27.4	135	197
333.15	1.1	13.2	2.1	32.6	179	261
$C_{12}EO_{13.2}(PO)_{1.1}-OH$						
298.15	0.9	2.6	1.6	10.3	38	47
333.15	1.1	2.5	1.7	10.4	50	61
$C_{12}EO_{14.0}-OH$						
298.15	0.9	2.7	1.5	10.2	34	43
313.15	0.9	2.6	1.5	10.1	38	47
323.15	1.0	2.6	1.5	10.2	41	51
333.15	1.0	2.5	1.5	10.1	44	55
$C_{12/14}EO_9-OH$						
298.15	1.2	3.3	1.8	12.4	56	90
313.15	1.1	5.0	2.3	16.8	77	125
323.15	1.2	9.2	2.6	25.8	137	221
333.15	1.3	16.0	2.2	38.9	271	438

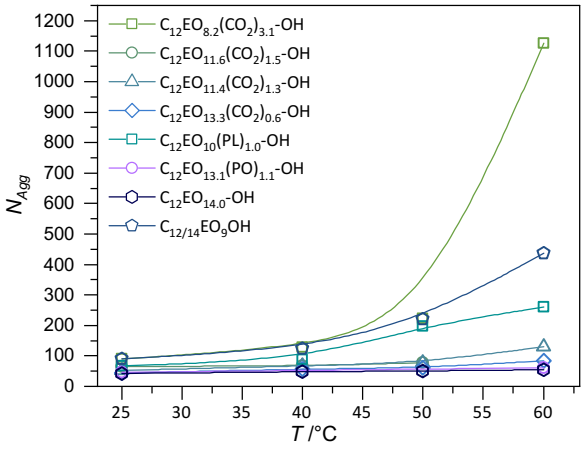

Figure 10.20: Temperature-dependent aggregation number of all CO_2 surfactants and the reference sample from SANS measurements.

E. Appendix Chapter 6

E.1. Calibration curves – UV-Vis measurements

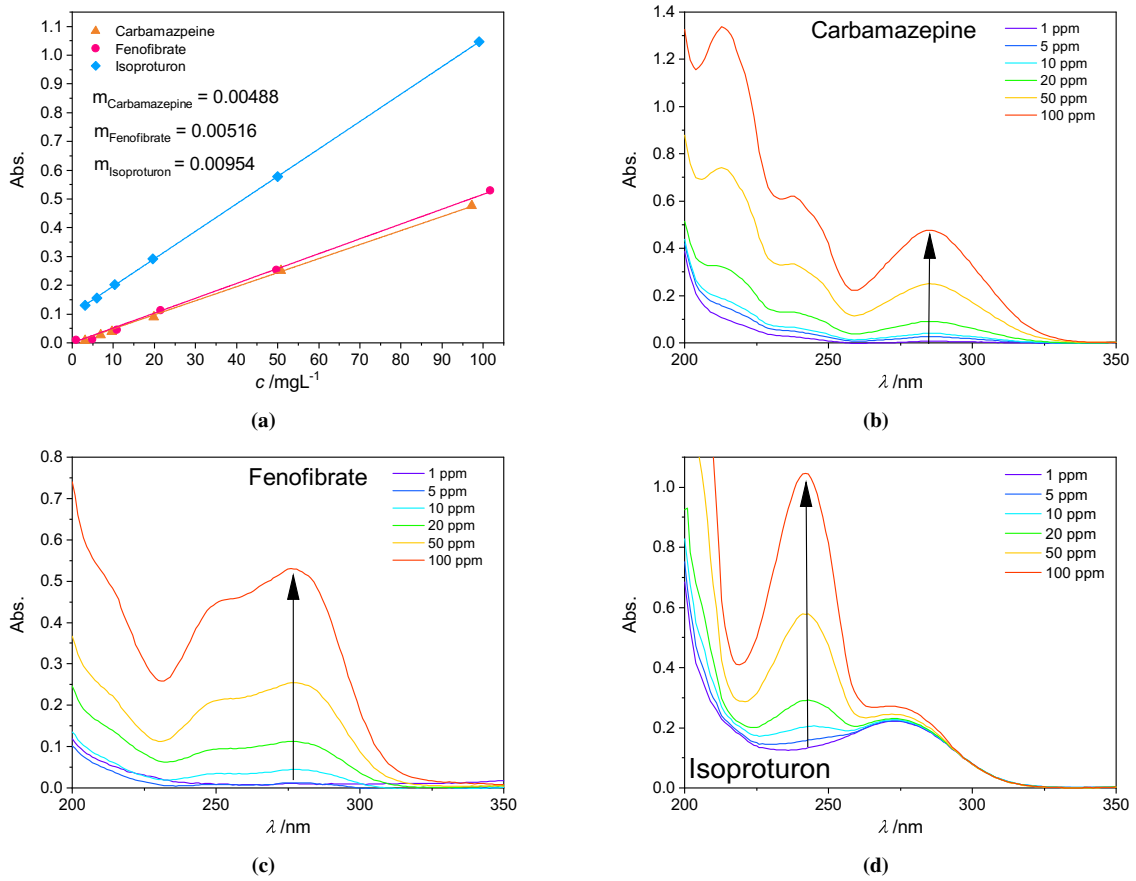

Figure 10.21: (a) calibration curve of all three hydrophobic compounds. The slope m is given in the diagram. (b) Calibration UV-Vis spectra of Carbamazepine at different concentrations in ethanol. (c) Calibration spectra of Fenofibrate and (d) of Isoproturon.

Table 10.14: Obtained concentrations S(tot) of isoproturon, fenofibrat, and carbamazepine solubilized by 1 wt% of surfactant solution at 25 and 40 °C.

Surfactants	**S(tot)$_{isoproturon}$ /mmol/L**	**S(tot)$_{fenofibrate}$ /mmol/L**	**S(tot)$_{carbamazepine}$ /mmol/L**
C_{12} surfactants 25 °C			
$C_{12}EO_{8.2}(CO_2)_{3.1}-OH$	0.878	0.172	1.458
$C_{12}EO_{14.0}-OH$	1.070	0.107	1.781
$C_{12/14}EO_9-OH$	1.092	0.137	1.724
C_{16} surfactants 25 °C			
$C_{16}EO_{7.8}(CO_2)_{2.8}-OH$	0.813	0.181	1.334
$C_{16}EO_{14.6}-OH$	1.145	0.202	1.657
$C_{16/18}EO_{13}-OH$	1.123	0.220	1.790
C_{12} surfactants 40 °C			
$C_{12}EO_{8.2}(CO_2)_{3.1}-OH$	1.244	0.166	1.804
$C_{12}EO_{14.0}-OH$	1.462	0.108	2.679
$C_{12/14}EO_9-OH$	1.347	0.135	3.304

C_{16} surfactants 40 °C			
$C_{16}EO_{7.8}(CO_2)_{2.8}-OH$	1.222	0.164	2.304
$C_{16}EO_{14.6}-OH$	1.441	0.187	2.273
$C_{16/18}EO_{13}-OH$	1.483	0.218	2.219
CO_2 triblock polymers 25 °C			
EO/CO_2-PO/CO_2-EO/CO_2	0.838	0.475	0.964
EO/CO_2-PO-EO/CO_2	0.432		0.872
EO-PO-EO	0.424	0.003	0.810
F38	0.025		0.833

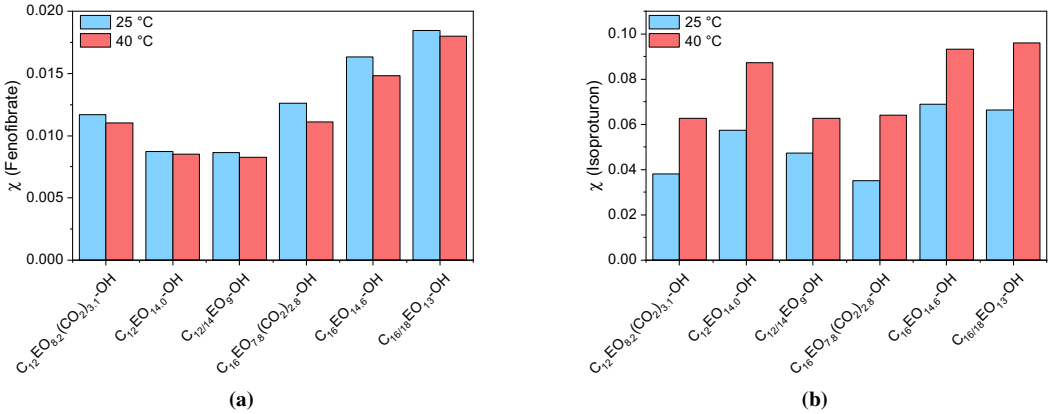

Figure 10.22: Temperature dependent solubilization capacity of fenofibrate (a) and isoproturon (b) by the C_{12} and C_{16} CO_2 surfactants.

E.2. SANS

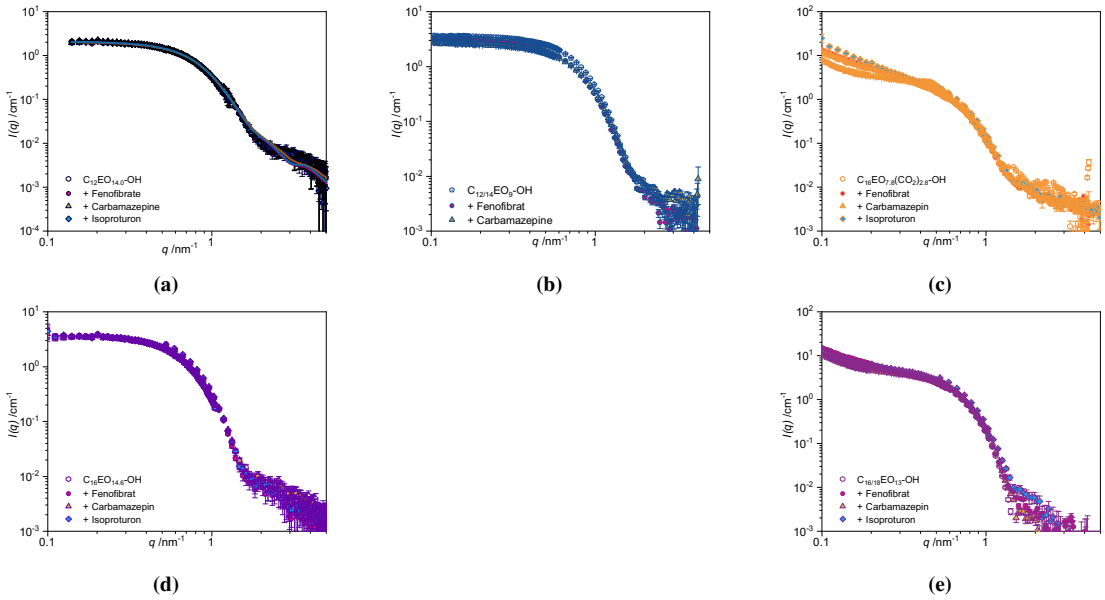

Figure 10.23: SANS spectra of all C_{12} and C_{16} surfactants with all three hydrophobic compounds.

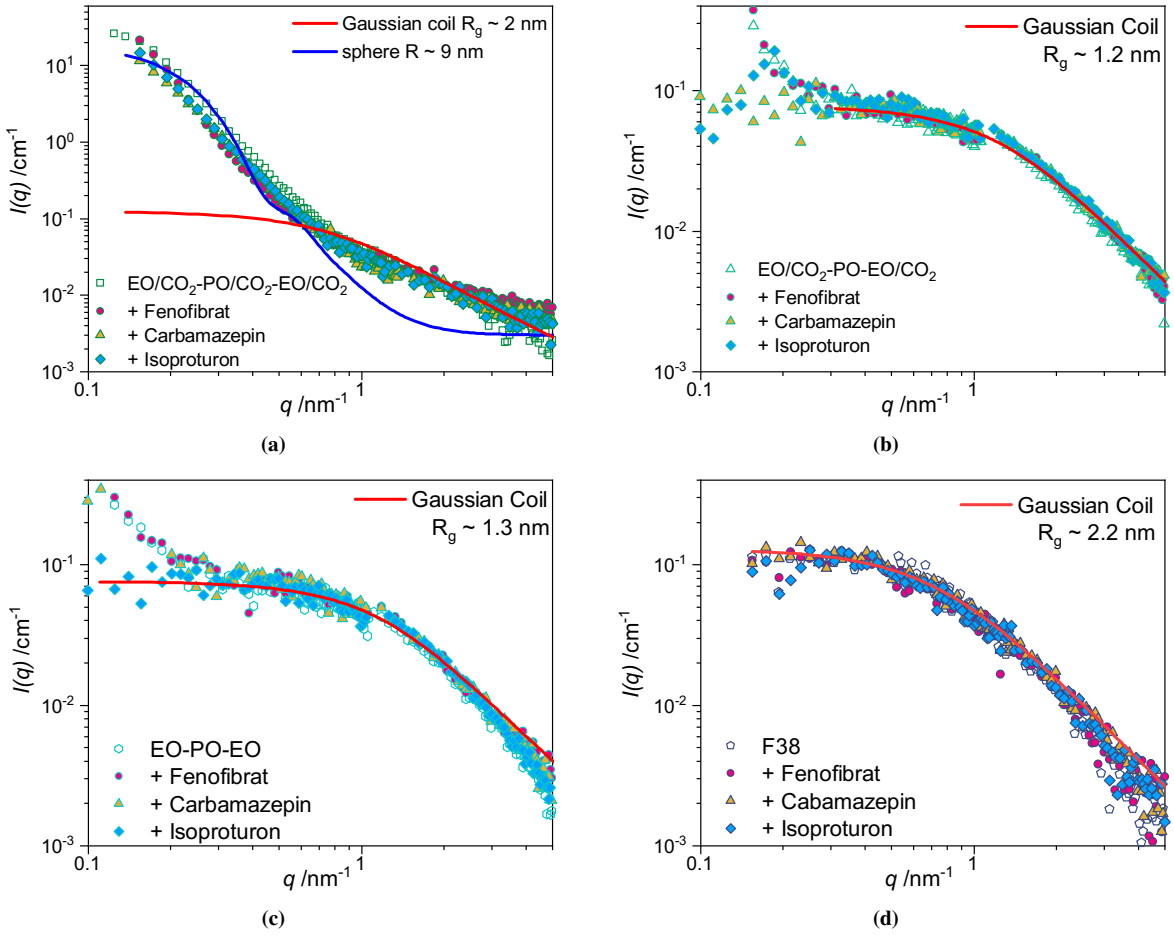

Figure 10.24: SANS spectra of all triblock polymers with all three hydrophobic compounds.

E.3. DOSY and NMR Data

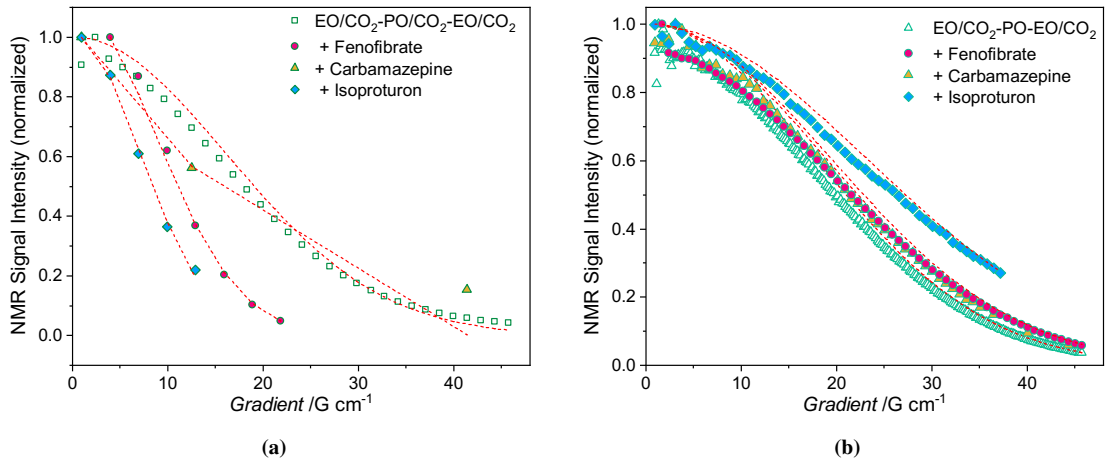

Figure 10.25: Normalizes NMR signal of all hydrophobic compounds in the presence of the polymer EO/CO_2-PO/CO_2-EO/CO_2 (left) and EO/CO_2-PO-EO/CO_2 (right) with all hydrophobic compounds in D_2O. Lines represent the fit of the NMR signal.

DOSY-NMR measurements allow the analysis of the dynamic behavior of the investigated molecules. In our case, we studied the dynamic behavior of the polymers with and without the hydrophobic compounds in D_2O. As shown in Fig. 10.25a we can observe a different

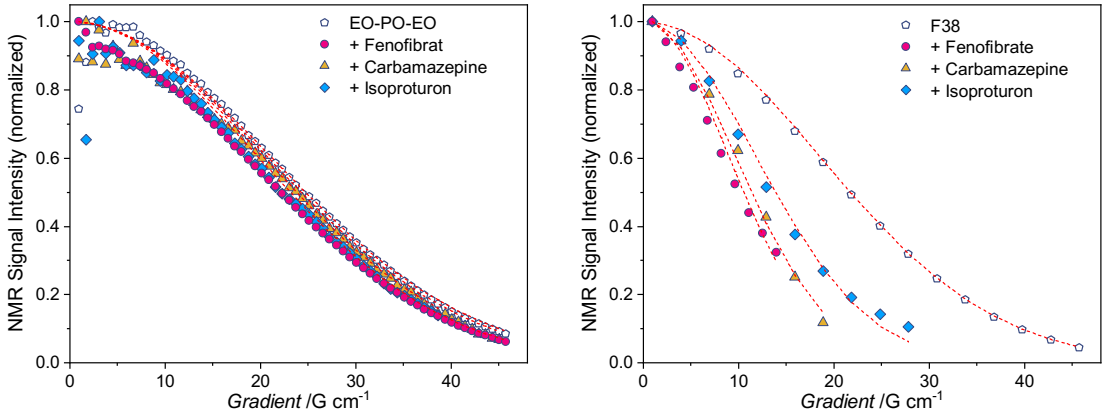

Figure 10.26: Normalizes NMR signal of all hydrophobic compounds in the presence of the polymer EO-PO-EO (a) and the reference F38 (b) with all hydrophobic compounds in D_2O.

dynamic behavior for fenofibrate, carbamazepine, and isoproturon in the presence of EO/CO_2-PO/CO_2-EO/CO_2 in comparison to the presence of EO/CO_2-PO-EO/CO_2 (Fig. 10.25b). For each hydrophobic compound and polymer, characteristic chemical shift signals were used to determine the characteristic diffusion of each hydrophobic compound in the presence of the polymer and its diffusion. In Table 6.4 the diffusion coefficient of all signals is listed with the characteristic signal positions.

From these measurements, we obtain the information, that the hydrophobic compound is in general freely diffusing and it is not influenced by the presence of the polymer. Moreover, the single polymer diffusion coefficient is for EO/CO_2-PO/CO_2-EO/CO_2 ~ $8.7 \cdot 10^{-11}$ m^2/s and for EO/CO_2-PO-EO/CO_2 ~ $1.2 \cdot 10^{-10}$ m^2/s, which indicates a somewhat larger size of the EO/CO_2-PO/CO_2-EO/CO_2 polymer. For the EO/CO_2-PO/CO_2-EO/CO_2 polymer one can observe that the different hydrophobic compounds have quite a larger diffusion coefficient (Fig. 10.25b). This indicates that the hydrophobic compounds diffusing freely with much smaller sizes and by that are permanently interacting with the polymer, that a collective diffusion could occur.

Table 10.16: Standard free energy of solubilization ΔG_s for all four triblock polyether carbonate polyols their reference samples as well as the commercial reference sample for all three hydrophobic compounds at 25 °C.

Surfactants	**Hydrophobic compound**	**ppm**	**D_1 /m²/s**	**$R_{H,1}$ /nm**	**ppm**	**D_2 /m²/s**	**$R_{H,2}$ /nm**
F38		3.713	$8.20 \cdot 10^{-11}$	2.99			
F38	Isoproturon	3.721	$8.14 \cdot 10^{-11}$	3.01	7.223	$1.55 \cdot 10^{-10}$	1.58
F38	Carbamazepine	3.717	$8.33 \cdot 10^{-11}$	2.94	7.119	$4.32 \cdot 10^{-10}$	0.57
F38	Fenofibrate	3.703	$8.40 \cdot 10^{-11}$	2.92	2.081	$5.02 \cdot 10^{-10}$	0.49
EO/CO_2-PO/CO_2-EO/CO_2		3.713	$8.60 \cdot 10^{-11}$	2.83			
EO/CO_2-PO/CO_2-EO/CO_2	Isoproturon	3.719	$9.62 \cdot 10^{-11}$	2.55	2.732	$6.99 \cdot 10^{-10}$	0.35
EO/CO_2-PO/CO_2-EO/CO_2	Carbamazepine	3.706	$9.48 \cdot 10^{-11}$	2.58	7.615	$2.90 \cdot 10^{-10}$	0.85
EO/CO_2-PO/CO_2-EO/CO_2	Fenofibrate	3.706	$1.06 \cdot 10^{-10}$	2.31	2.087	$6.94 \cdot 10^{-10}$	0.35
EO/CO_2-PO-EO/CO_2		3.704	$1.25 \cdot 10^{-10}$	1.95			
EO/CO_2-PO-EO/CO_2	Isoproturon	3.72	$1.40 \cdot 10^{-10}$	1.75	7.238	$3.49 \cdot 10^{-10}$	0.70
EO/CO_2-PO-EO/CO_2	Carbamazepine	3.709	$1.33 \cdot 10^{-10}$	1.84	7.111	$3.89 \cdot 10^{-10}$	0.63
EO/CO_2-PO-EO/CO_2	Fenofibrate	3.721	$1.22 \cdot 10^{-10}$	2.00			
EO-PO-EO		3.713	$1.20 \cdot 10^{-10}$	2.04			
EO-PO-EO	Isoproturon	3.719	$1.22 \cdot 10^{-10}$	2.00	7.228	$4.07 \cdot 10^{-10}$	0.60
EO-PO-EO	Carbamazepine	3.718	$1.22 \cdot 10^{-10}$	2.00	7.119	$4.26 \cdot 10^{-10}$	0.58
EO-PO-EO	Fenofibrate	3.719	$1.27 \cdot 10^{-10}$	1.94			

^{1}H NMR Spectra

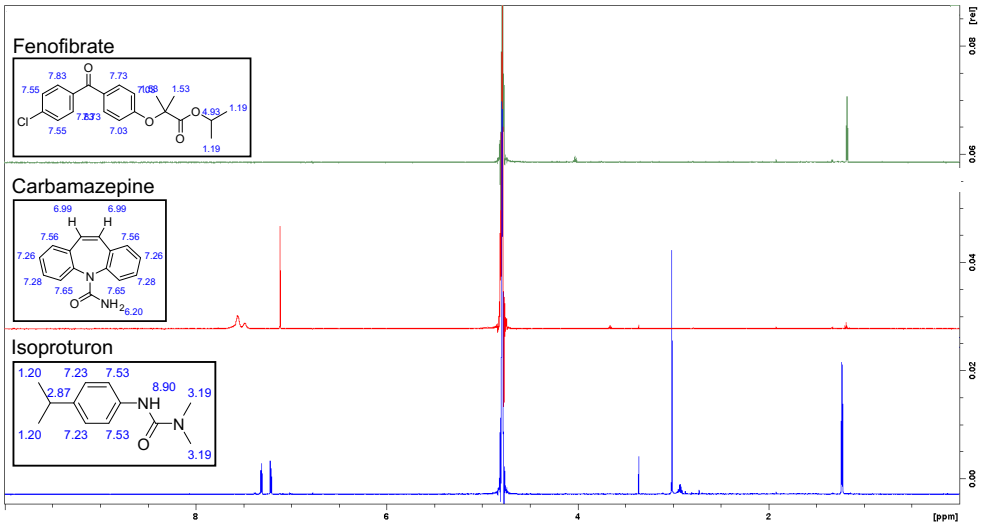

Figure 10.27: ^{1}H NMR Spectra of the three hydrophobic compounds.

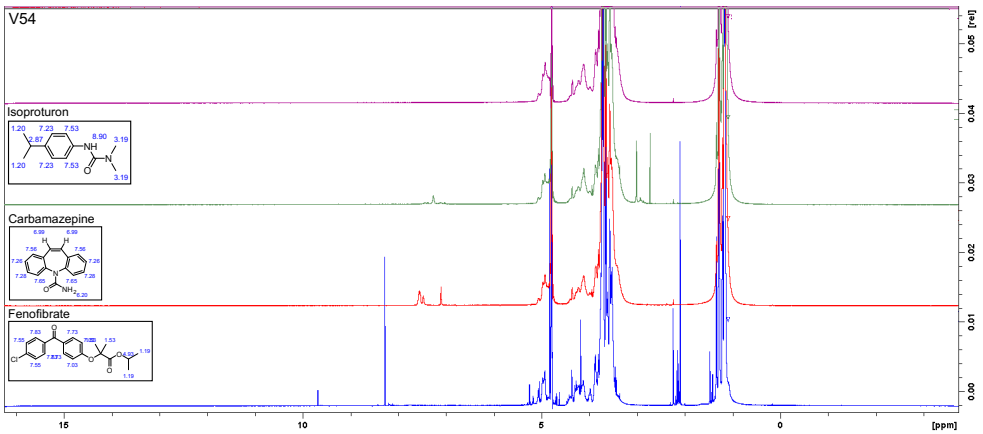

Figure 10.28: ^{1}H NMR Spectra of the polymer EO/CO_2-PO/CO_2-EO/CO_2 and the three hydrophobic compounds.

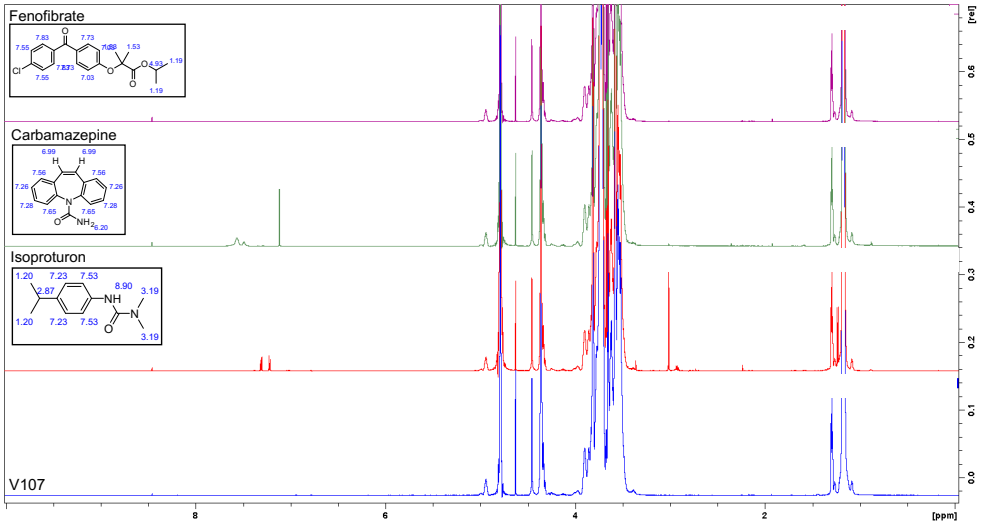

Figure 10.29: ^{1}H NMR Spectra of the polymer EO/CO_2-PO-EO/CO_2 and the three hydrophobic compounds.

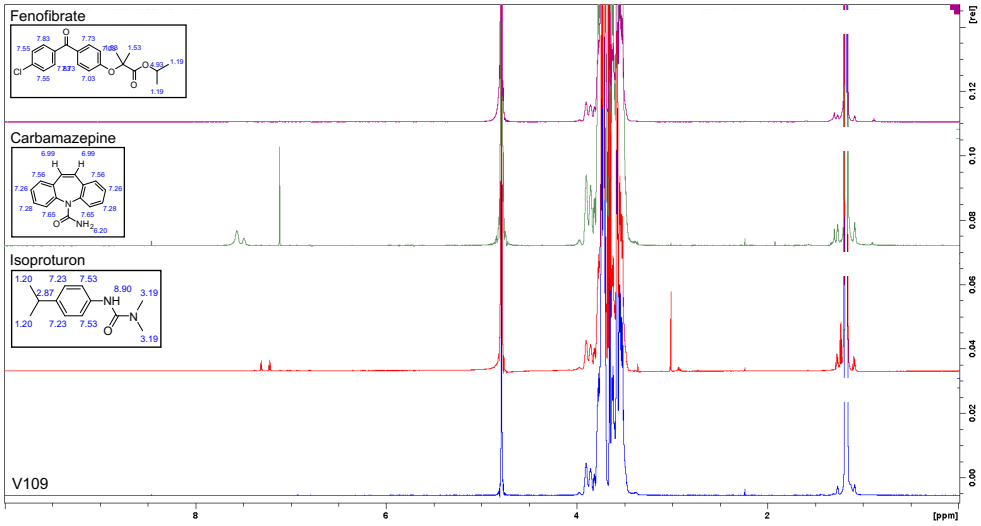

Figure 10.30: ^{1}H NMR Spectra of the polymer EO-PO-EO and the three hydrophobic compounds.

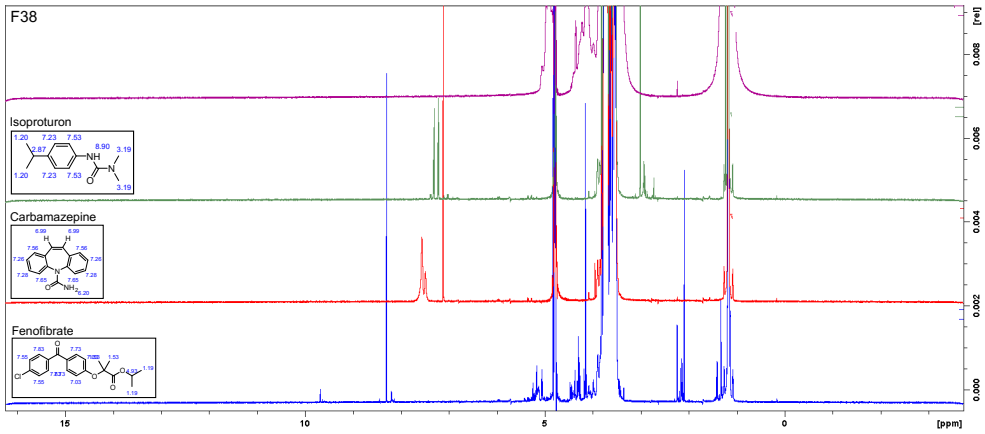

Figure 10.31: ^{1}H NMR Spectra of the polymer F38 and the three hydrophobic compounds.

F. Appendix Chapter 7

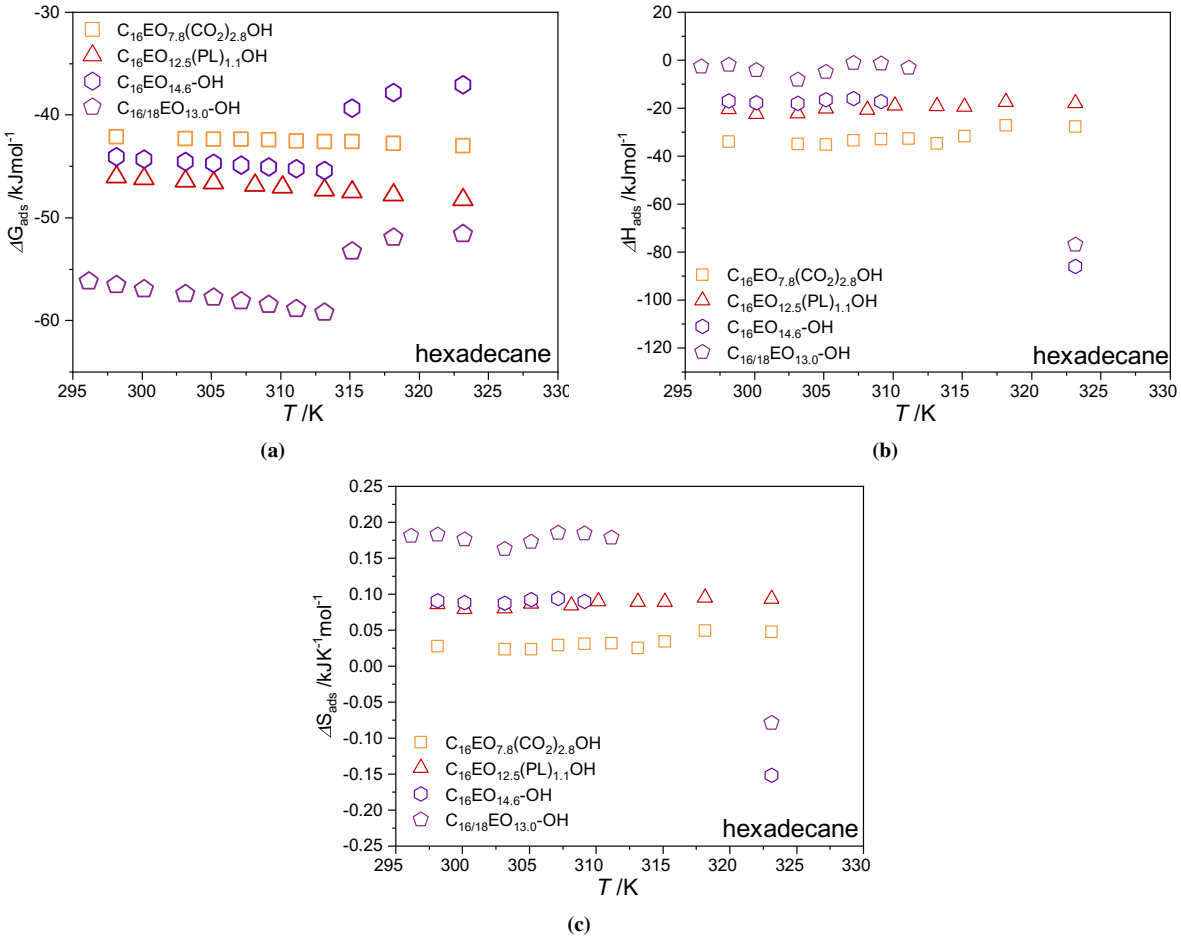

Figure 10.32: Gibbs energy ΔG_{ads} (a), Enthalpy ΔH_{ads} (b) and entropy ΔS_{ads} (c) of adsorption depending on the temperature for all C_{16} CO_2 surfactants in the temperature range from 20 up 50 °C obtained from interfacial tension measurements.